

**BATTELLE**

Report To

**National Aeronautics and Space Administration  
Marshall Space Flight Center Huntsville, Alabama**

**VOLUME II  
FINAL TECHNICAL REPORT  
on  
EVALUATION OF THE SPACE DISPOSAL  
OF DEFENSE NUCLEAR WASTE—PHASE II  
to  
NATIONAL AERONAUTICS AND  
SPACE ADMINISTRATION  
MARSHALL SPACE FLIGHT CENTER  
(Contract Number NAS8-32391)  
DPD No. 557, DR No. MA-04  
January 31, 1979**

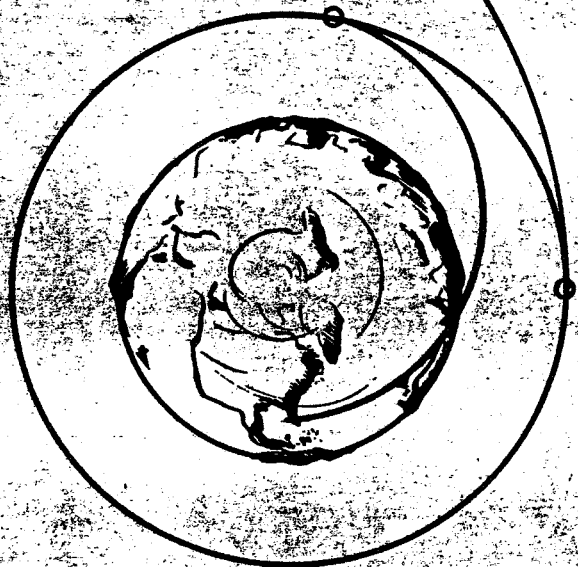
(NASA-CR-161103) EVALUATION OF THE SPACE  
DISPOSAL OF DEFENSE NUCLEAR WASTE, PHASE 2.  
VOLUME 2: TECHNICAL REPORT Final Report,  
Feb. 1978 - Jan. 1979 (Battelle Columbus  
Labs., Ohio.) 313 p

N79-74263

00/73 Unclas  
14355

**BATTELLE**

**Columbus Laboratories  
Columbus, Ohio 43201**



VOLUME II  
OF  
FINAL TECHNICAL REPORT  
ON  
EVALUATION OF THE SPACE DISPOSAL  
OF DEFENSE NUCLEAR WASTE--PHASE II

TO  
NATIONAL AERONAUTICS AND  
SPACE ADMINISTRATION  
MARSHALL SPACE FLIGHT CENTER  
(Contract Number NAS8-32391)  
DPD No. 557, DR No. MA-04

January 31, 1979

*D. S. Edgecombe*  
D. S. Edgecombe, Study Leader  
Battelle-Columbus Laboratories  
Columbus, Ohio

*C. C. Priest*  
C. C. Priest, COR  
NASA/Marshall Space Flight Center  
Huntsville, Alabama

BATTELLE  
Columbus Laboratories  
505 King Avenue  
Columbus, Ohio 43201

## FOREWORD

The study summarized in this report is a preliminary examination of the feasibility and preferred approaches for disposal of selected high-level defense nuclear wastes in space. The study is a continuation of previous NASA and NASA-sponsored study activities, but differs from these previous studies in the emphasis on defense wastes (a study ground rule specified jointly by the DOE and NASA). The study is an integral part of the ongoing NASA/DOE program for study of nuclear waste disposal in space, and was conducted in parallel with efforts at NASA Marshall Space Flight Center; Science Applications, Inc.; and the Jet Propulsion Laboratory. The research effort reported here was performed by Battelle-Columbus Laboratories under NASA Contract NAS8-32391 from February 1978 through January 1979. The major objective of the study was to conduct preliminary analyses of the nature and containment of defense nuclear waste, the safety of the space disposal approach, the environmental impact of selected credible accidents, and various program planning aspects.

The study made considerable use of existing documentation and direct visits to defense waste repositories. Despite these efforts, considerable uncertainty remains regarding the composition and possible concentration processes for defense waste. Similar data needs exist regarding Space Shuttle reliability and other systems safety. The development of such data will need to be a primary concern of a proposed NASA/DOE working group. Despite these needs, however, it is believed that the preliminary systems descriptions and safety and environmental impact analyses described in this report have scoped the fundamentals and likely approaches for space disposal of nuclear waste. Additional, more detailed studies are expected to build upon the data base reported here.

Inquiries regarding this study should be addressed to:

C. C. (Pete) Priest, COR  
NASA/Marshall Space Flight Center  
Attention: PS04  
Huntsville, Alabama 35812  
Telephone: (205) 453-2796

Donald S. Edgecombe, Study Leader  
Battelle-Columbus Laboratories  
505 King Avenue  
Columbus, Ohio 43201  
Telephone: (614) 424-5087

## ACKNOWLEDGMENTS

The principal authors, D. S. Edgecombe, E. E. Rice, R. J. Conlon, N. E. Miller, and K. R. Yates, acknowledge the generous assistance of the following individuals who provided significant contributions to the technical content of this report:

M. E. Balmert	W. E. Martin
S. G. Bloom	R. F. Porter
A. A. Boiarski	E. A. Ramlet
R. W. Earhart	A. E. Tischer
K. D. Kok	A. E. Weller
M. B. Kuhner	G. R. Whitacre

Acknowledgment is also made to the guidance by the NASA/MSFC study monitors, R. E. Austin and C. C. Priest, and by various members of the MSFC staff, particularly R. E. Burns, W. E. Galloway, and R. F. Nixon.



## TABLE OF CONTENTS

	Page
FOREWORD . . . . .	i
ACKNOWLEDGMENTS. . . . .	ii
1.0 INTRODUCTION. . . . .	1-1
2.0 BASELINE CONCEPT DEFINITION AND OPTIONS SUMMARY . . . . .	2-1
2.1 Concept Options . . . . .	2-2
2.2 Baseline Concept Summary. . . . .	2-3
2.3 Overall Baseline Mission Profile. . . . .	2-4
2.3.1 Nuclear Waste Payload Fabrication . . . . .	2-4
2.3.2 Nuclear Waste Ground Transport. . . . .	2-4
2.3.3 Payload Preparation at Launch Site. . . . .	2-6
2.3.4 Prelaunch Activities. . . . .	2-7
2.3.5 Booster Operations. . . . .	2-8
2.3.6 Upper Stage Operations. . . . .	2-9
2.4. Baseline Element Definitions and/or Requirements. . . . .	2-11
2.4.1 Waste Source. . . . .	2-11
2.4.2 Waste Mix. . . . .	2-12
2.4.3 Waste Form. . . . .	2-14
2.4.4 Waste Fabrication Facilities. . . . .	2-14
2.4.5 Payload Container, Shielding, and Reentry Systems . . . . .	2-14
2.4.6 Ground Transport Vehicles and Casks . . . . .	2-15
2.4.7 Launch Site Facilities. . . . .	2-16
2.4.8 Launch Vehicle. . . . .	2-16
2.4.9 Upper Stages. . . . .	2-17
2.4.10 Payload Ejection System. . . . .	2-18
2.4.11 Docking System . . . . .	2-18
2.4.12 Space Destination. . . . .	2-18
2.5 Accident and Malfunction Contingency Plans. . . . .	2-19
2.5.1 Ground Transportation . . . . .	2-19
2.5.2 Preflight Operations. . . . .	2-19
2.5.3 Launch Operations . . . . .	2-20
2.5.4 Orbital Operations. . . . .	2-21
2.6 Projected Traffic Model and Hardware Availability Requirements . . . . .	2-23
2.7 Unique System Design Requirements . . . . .	2-24
2.8 References. . . . .	2-25
3.0 CHARACTERIZATION OF DEFENSE HIGH-LEVEL WASTE PAYLOADS . . . . .	3-1
3.1 Defense Nuclear Waste Sources and Character . . . . .	3-2
3.1.1 Hanford Waste . . . . .	3-2
3.1.2 Savannah River Waste. . . . .	3-4
3.1.3 Idaho Waste . . . . .	3-7
3.1.4 Summary of Defense Waste Characteristics for Terrestrial Disposal. . . . .	3-7
3.2 Space Disposal Mixes. . . . .	3-9
3.2.1 Chemical Processing Recommended for Space Disposal. . . . .	3-9
3.2.1.1 Hanford Waste . . . . .	3-9
3.2.1.2 Savannah River Waste. . . . .	3-11
3.2.1.3 Idaho Waste . . . . .	3-13

**TABLE OF CONTENTS**  
(Continued)

	<b>Page</b>
3.2.2 Baseline Composition for Space Disposal . . . . .	3-14
3.2.2.1 Hanford Waste . . . . .	3-14
3.2.2.2 Savannah River Waste. . . . .	3-15
3.2.2.3 Idaho Waste . . . . .	3-17
3.3 Waste Forms for Space Disposal. . . . .	3-18
3.3.1 Chemical Processing . . . . .	3-18
3.3.2 Physical Properties and Characteristics . . . . .	3-19
3.4 Containerization Systems. . . . .	3-21
3.4.1 Shielding Analysis. . . . .	3-23
3.4.2 Thermal Analysis. . . . .	3-28
3.4.3 Accident Response Analysis. . . . .	3-33
3.4.3.1 Launch Pad Explosion. . . . .	3-34
3.4.3.2 Reentry . . . . .	3-43
3.4.4 Gamma Radiation Dose Calculations . . . . .	3-45
3.4.5 Concluding Remarks. . . . .	3-45
3.5 References. . . . .	3-48
4.0 MISSION ANALYSIS. . . . .	4-1
4.1 Low- and High-Speed Reentry System Stability and Impact Condition Analyses . . . . .	4-2
4.1.1 High-Speed Reentry System Stability Analysis. . . . .	4-2
4.1.2 Low-Speed Impact Analysis . . . . .	4-4
4.1.3 Conclusions . . . . .	4-6
4.2 Recovery of Nuclear Waste Payloads in Earth Orbit . . . . .	4-9
4.2.1 Details of Analysis . . . . .	4-9
4.2.2 Conclusions . . . . .	4-16
4.3 References. . . . .	4-17
5.0 SAFETY ASSESSMENT . . . . .	5-1
5.1 Major Accident Environment Characterization . . . . .	5-2
5.1.1 Space Shuttle Explosion and Fire. . . . .	5-2
5.1.1.1 Space Shuttle Hydrogen/Oxygen Fireball Environment . . . . .	5-4
5.1.1.2 Space Shuttle Solid Propellant Fire Environment . . . . .	5-15
5.1.1.3 Overpressure and Impulse Resulting from Space Shuttle External Tank Explosion. . . . .	5-20
5.1.1.4 Space Shuttle Fragment Environment . . . . .	5-24
5.1.1.5 Concluding Remarks . . . . .	5-33
5.1.2 Reentry of Container With/Without Reentry Protection. . . . .	5-39
5.1.3 Payload Entry Into Deep Ocean . . . . .	5-57
5.2 Preliminary Hazard Analysis . . . . .	5-59
5.2.1 Mission Phase Definition. . . . .	5-59
5.2.1.1 Phase 1: Payload Processing and Storage at Launch Site . . . . .	5-60
5.2.1.2 Phase 2: On-Pad, Prelaunch Operations . . . . .	5-60
5.2.1.3 Phase 3: Ignition to Clearing of Tower. . . . .	5-61

**TABLE OF CONTENTS**  
(Continued)

	<b>Page</b>
5.2.1.4 Phase 4: Clearing of Tower to SRB Burnout	5-61
5.2.1.5 Phase 5: SRB Burnout to ET Drop . . . . .	5-61
5.2.1.6 Phase 6: ET Drop to Achieving Orbit and Phase 7: Achieving Orbit to Rendezvous. . . . .	5-61
5.2.1.7 Phase 8: Rendezvous and Docking with OTV/SOIS. . . . .	5-62
5.2.1.8 Phase 9: OTV Ignition and Burn . . . . .	5-62
5.2.1.9 Phase 10: OTV Jettison to SOIS Ignition. . . . .	5-62
5.2.1.10 Phase 11: SOIS Burn. . . . .	5-63
5.2.1.11 Phase 12: Stay in Planned Orbit. . . . .	5-63
5.2.2 Failure Probability Data. . . . .	5-63
5.2.3 Fault Trees . . . . .	5-64
5.2.3.1 Phase 1 Fault Tree . . . . .	5-66
5.2.3.2 Phase 2 Fault Tree . . . . .	5-68
5.2.3.3 Phase 3 Fault Tree . . . . .	5-71
5.2.3.4 Phase 4 Fault Tree . . . . .	5-71
5.2.3.5 Phase 5 Fault Tree . . . . .	5-74
5.2.3.6 Phase 6 Fault Tree . . . . .	5-76
5.2.3.7 Phase 7 Fault Tree . . . . .	5-76
5.2.3.8 Phase 8 Fault Tree . . . . .	5-76
5.2.3.9 Phase 9 Fault Tree . . . . .	5-80
5.2.3.10 Phase 10 Fault Tree. . . . .	5-82
5.2.3.11 Phase 11 Fault Tree. . . . .	5-82
5.2.3.12 Phase 12 Fault Tree. . . . .	5-85
5.3 System Modification Requirements. . . . .	5-87
5.3.1 Ground Systems. . . . .	5-87
5.3.2 Payload Systems . . . . .	5-88
5.3.3 Space Shuttle Systems . . . . .	5-89
5.3.4 Upper Stage Systems . . . . .	5-90
5.4 References. . . . .	5-92
6.0 ENVIRONMENTAL IMPACT ASSESSMENT . . . . .	6-1
6.1 On- or Near-Pad Catastrophic Space Shuttle Failure with Release of Defense Nuclear Waste Material. . . . .	6-2
6.1.1 Model Descriptions. . . . .	6-3
6.1.1.1 The NASA/MSFC Multilayer Diffusion Model. . . . .	6-3
6.1.1.2 DACRIN Model and Dose Factors . . . . .	6-9
6.1.2 Results . . . . .	6-12
6.1.3 Conclusions . . . . .	6-23
6.2 Reentry Burnup of Defense Nuclear Waste Payload . . . . .	6-25
6.2.1 Model Description . . . . .	6-26
6.2.2 Results . . . . .	6-34
6.2.2.1 Maximum Doses to Individuals. . . . .	6-34
6.2.2.2 Worldwide Health Effects. . . . .	6-37
6.2.3 Conclusions . . . . .	6-38
6.3 References. . . . .	6-40
7.0 CONCLUSIONS . . . . .	7-1
8.0 RECOMMENDATIONS . . . . .	8-1

**TABLE OF CONTENTS**  
(Continued)

	Page
<b>APPENDICES</b>	
A. Acronyms and Abbreviations . . . . .	A-1
B. Metric/English Conversion Factors. . . . .	B-1
C. Waste Mix and Form Data Developed for Commercial Waste . .	C-1
D. Reentry Thermal Analysis Code (RETAC). . . . .	D-1
E. Calculation of the Space Shuttle External Tank Fireball Temperature and Heat Flux. . . . .	E-1
F. Population Dose Calculation Technique for On-Pad Space Shuttle Failures. . . . .	F-1
G. Dose Factor Model for High Altitude Burnup . . . . .	G-1

**LIST OF FIGURES**

Figure 2-1.	Major Options for Space Disposal of Nuclear Waste .	2-2
Figure 2-2.	Baseline Concept Summary for Initial Program to Dispose of Nuclear Waste in Space. . . . .	2-3
Figure 2-3.	Ground and Space Operation Profiles for Baseline Space Disposal Mission . . . . .	2-5
Figure 2-4.	Artist's Concept for Nuclear Waste Payload Shipping Cask for Terrestrial Transport . . . . .	2-6
Figure 2-5.	Artist's Concept of a Loaded Reentry/Docking Assembly. . . . .	2-7
Figure 3-1.	Hanford Radioactive Waste Management. . . . .	3-3
Figure 3-2.	Hanford Radionuclide Removal Process. . . . .	3-5
Figure 3-3.	Savannah River Salt Decontamination Process . . . .	3-6
Figure 3-4.	Total Number of Payloads as a Function of Defense Waste Concentration Factor (WCF). . . . .	3-22
Figure 3-5.	Shield Thickness Requirements as a Function of Waste Concentration Factor for Hanford Waste. . . .	3-26
Figure 3-6.	Baseline Shielded Container Design for Hanford Waste (WCF = 27). . . . .	3-27
Figure 3-7.	Waste and Maximum Deep Space Temperature Gradients as a Function of Waste Concentration Factor for Hanford High-Level Waste . . . . .	3-31

**LIST OF FIGURES**  
(Continued)

		<b>Page</b>
Figure 3-8.	Radiant Heat Flux vs Time for Launch Pad Fires. . .	3-36
Figure 3-9.	Thermal Response of Gamma Radiation Shielded Container to Solid Propellant Fires . . . . .	3-39
Figure 3-10.	Thermal Response of Reentry Protected and Shielded Container to Solid Propellant Fires . . . . .	3-41
Figure 3-11.	Thermal Response of Rotating Unprotected Waste Container During Shallow Unplanned Reentry. . . . .	3-44
Figure 3-12.	Gamma Radiation Dose Rate as a Function of Distance from Baseline Unshielded Hanford Waste Payload and Various Container Wall Thicknesses. . .	3-46
Figure 4-1.	Reentry Capsule Configuration . . . . .	4-3
Figure 4-2.	Reentry Capsule Aerodynamics and Hypersonic Stability Margin . . . . .	4-5
Figure 4-3.	Impact Conditions for Reentry Capsule Exhibiting High Degree of Subsonic Stability. . . . .	4-7
Figure 4-4.	Impact Conditions for Reentry Capsule Exhibiting Marginal Subsonic Stability. . . . .	4-8
Figure 4-5.	Definition of Angle Error Parameters. . . . .	4-10
Figure 4-6.	Effect of OTV Impulse Errors from Initial 333-km (180-n.mi.) Circular Orbit . . . . .	4-12
Figure 4-7.	Constraint Boundaries for Injecting Payload into Escape Trajectories. . . . .	4-14
Figure 4-8.	Circular Orbits Obtainable Using Second Orbit . . .	4-15
Figure 5-1.	Modeled Fireball Development. . . . .	5-5
Figure 5-2.	Hydrogen/Oxygen Fireball Enthalpy as a Function of Temperature. . . . .	5-9
Figure 5-3.	Temperature as a Function of Time for Space Shuttle Hydrogen/Oxygen Fireball Environment. . . .	5-12
Figure 5-4.	Radiant Heat Flux as a Function of Time for Space Shuttle Hydrogen/Oxygen Fireball Environment. . . .	5-13
Figure 5-5.	Fireball Diameter as a Function of Time for Space Shuttle Hydrogen/Oxygen Fireball Environment. . . .	5-14

**LIST OF FIGURES**  
(Continued)

		<b>Page</b>
Figure 5-6.	Fragment Model for Space Shuttle Solid Propellant Fire . . . . .	5-15
Figure 5-7.	Maximum Heat Flux at Time = 0 (Fragment Fire Model)	5-17
Figure 5-8.	Maximum Heat Flux as a Function of Time (Fragment Fire Model) . . . . .	5-18
Figure 5-9.	Split Motor Model for Space Shuttle Solid Propellant Fire . . . . .	5-19
Figure 5-10.	Maximum Heat Flux as a Function of Distance (Split Motor Fire Model) . . . . .	5-21
Figure 5-11.	Space Shuttle Vehicle with Assumed Center of Explosion and Location of Nuclear Waste Payload . .	5-23
Figure 5-12.	Overpressures as a Result of Space Shuttle ET Blast Wave . . . . .	5-25
Figure 5-13.	Reflected Impulse as a Result of Space Shuttle ET Blast Wave. . . . .	5-26
Figure 5-14.	Distribution of Fragment Sizes for Space Shuttle Fragment Environment. . . . .	5-28
Figure 5-15.	Distribution of Velocities of Mean Size Fragment for Space Shuttle Fragment Environment. . . . .	5-29
Figure 5-16.	Drag Correction Factors for Fragment Accelerations for Space Shuttle Fragment Environment. . . . .	5-31
Figure 5-17.	Fraction of Fragments Impacting Edge-On for Space Shuttle Fragment Environment. . . . .	5-34
Figure 5-18.	Effective Dimensions of Impacting Edge-On Fragments for Space Shuttle Fragment Environment. . . . .	5-35
Figure 5-19.	Fragment Velocity Distribution Assuming 1% Yield for Space Shuttle Fragment Environment. . . .	5-36
Figure 5-20.	Fragment Velocity Distribution Assuming 20% Yield for Space Shuttle Fragment Environment. . . .	5-37
Figure 5-21.	Fragment Velocity Distribution Assuming 160% Yield for Space Shuttle Fragment Environment. . . .	5-38
Figure 5-22.	Drag Coefficient for a Sphere as a Function of Mach Number. . . . .	5-40

**LIST OF FIGURES**  
(Continued)

		<b>Page</b>
Figure 5-23.	Drag Coefficient for Reentry System as a Function of Mach Number. . . . .	5-40
Figure 5-24.	Time as a Function of Altitude for Steep Reentry of Unprotected Container. . . . .	5-42
Figure 5-25.	Velocity as a Function of Altitude for Steep Reentry of Unprotected Container. . . . .	5-43
Figure 5-26.	Stagnation Point Heating Rate as a Function of Altitude for Steep Reentry of Unprotected Container	5-44
Figure 5-27.	Stagnation Pressure as a Function of Altitude for Steep Reentry of Unprotected Container. . . . .	5-45
Figure 5-28.	Stagnation Temperature as a Function of Altitude for Steep Reentry of Unprotected Container. . . . .	5-46
Figure 5-29.	Time as a Function of Altitude for Shallow Reentry of Unprotected Container. . . . .	5-47
Figure 5-30.	Velocity as a Function of Altitude for Shallow Reentry of Unprotected Container. . . . .	5-48
Figure 5-31.	Stagnation Point Heating Rate as a Function of Altitude for Shallow Reentry of Unprotected Container. . . . .	5-49
Figure 5-32.	Stagnation Pressure as a Function of Altitude for Shallow Reentry of Unprotected Container. . . . .	5-50
Figure 5-33.	Stagnation Temperature as a Function of Altitude for Shallow Reentry of Unprotected Container. . . . .	5-51
Figure 5-34.	Time as a Function of Altitude for Reentry of Reentry System . . . . .	5-52
Figure 5-35.	Velocity as a Function of Altitude for Reentry of Reentry System . . . . .	5-53
Figure 5-36.	Stagnation Point Heating Rate as a Function of Altitude for Reentry of Reentry System . . . . .	5-54
Figure 5-37.	Stagnation Pressure as a Function of Altitude for Reentry of Reentry System. . . . .	5-55
Figure 5-38.	Stagnation Temperature as a Function of Altitude for Reentry of Reentry System. . . . .	5-56



**LIST OF FIGURES**  
(Continued)

		<b>Page</b>
Figure 5-39.	Distribution of Ocean Depth (Pressure) for a 38° Inclination Space Disposal Orbit (1st Orbital Pass). . . . .	5-58
Figure 5-40.	Phase 1 Fault Tree (Payload Processing at Launch Site). . . . .	5-67
Figure 5-41.	Phase 2 Fault Tree (On-Pad, Prelaunch Operations) .	5-69
Figure 5-42.	Phase 3 Fault Tree (Ignition to Clearing of Tower). .	5-72
Figure 5-43.	Phase 4 Fault Tree (Clearing of Tower to SRB Burnout). . . . .	5-73
Figure 5-44.	Phase 5 Fault Tree (SRB Burnout to ET Drop) . . . .	5-75
Figure 5-45.	Phase 6 Fault Tree (ET Drop to Achieve Orbit) . . .	5-77
Figure 5-46.	Phase 7 Fault Tree (Achieving Orbit to Rendezvous). .	5-78
Figure 5-47.	Phase 8 Fault Tree (Rendezvous and Docking with OTV/SOIS). . . . .	5-79
Figure 5-48.	Phase 9 Fault Tree (OTV Ignition and Burn). . . . .	5-81
Figure 5-49.	Phase 10 Fault Tree (OTV Jettison to SOIS Ignition) . . . . .	5-83
Figure 5-50.	Phase 11 Fault Tree (SOIS Burn) . . . . .	5-84
Figure 5-51.	Phase 12 Fault Tree (Stay in Planned Orbit) . . . .	5-86
Figure 6-1.	Isopleths for Assumed 55-kg Release of Waste Payload During Spring Meteorological Condition. . .	6-6
Figure 6-2.	Isopleths for Assumed 55-kg Release of Waste Payload During Fall Meteorological Condition. . . .	6-7
Figure 6-3.	Isopleths for Assumed 55-kg Release of Waste Payload During Sea Breeze Meteorological Condition. .	6-8
Figure 6-4.	Schematic Diagram of the Task Group Lung Model. . .	6-10
Figure 6-5.	Individual Dose Commitments for Release of Savannah River Radioactive Waste as a Result of On- or Near-Pad Space Shuttle Catastrophic Accident. . . .	6-15

**LIST OF FIGURES**  
(Continued)

		<b>Page</b>
Figure 6-6.	Individual Dose Commitments for Release of Hanford Radioactive Waste as a Result of On- or Near-Pad Space Shuttle Catastrophic Accident. . . .	6-16
Figure 6-7.	Individual Lung Dose Commitments for Release of Radioactive Waste Resulting from On- or Near-Pad Space Shuttle Catastrophic Accident as a Function of AMAD, Waste Mix, and Meteorological Case . . . .	6-17
Figure 6-8.	Individual Bone Dose Commitments for Release of Radioactive Waste Resulting from On- or Near-Pad Space Shuttle Catastrophic Accident as a Function of AMAD, Waste Mix, and Meteorological Case . . . .	6-18
Figure 6-9.	Individual Total Body Dose Commitments for Release of Radioactive Waste Resulting from On- or Near-Pad Space Shuttle Catastrophic Accident as a Function of AMAD, Waste Mix, and Meteorological Case . . . .	6-19
Figure 6-10.	Deposition of Small Particles ( $< 4 \mu\text{m}$ ) Released at High Altitude as a Function of Injection Latitude .	6-30
Figure D-1.	General Layout of Reentry Thermal Analysis Code (RETAC) . . . . .	D-2
Figure F-1.	Population Distribution Surrounding KSC Launch Site . . . . .	F-2
Figure F-2.	Illustration of Interpolation Technique . . . . .	F-3
Figure G-1.	Krey-Krajewski Model. . . . .	G-2
Figure G-2.	Schematic Diagram of Atmospheric Transport. . . . .	G-3
Figure G-3.	Results from Atmospheric Transport Model. . . . .	G-6
Figure G-4.	Schematic Diagram of Task Group Lung Model. . . . .	G-9

## LIST OF TABLES

		Page
Table 2-1.	Current Volumetric Defense HLW Inventories . . . . .	2-12
Table 2-2.	Projected Mass Inventories of Defense HLW Proposed for Terrestrial Disposal. . . . .	2-12
Table 2-3.	Desired High and Desired Low Mass Inventories of Defense HLW Proposed for Space Disposal . . . . .	2-13
Table 2-4.	Space Shuttle Flights Required for Space Disposal. . . . .	2-13
Table 2-5.	Major Hardware Requirements Estimates for Defense Nuclear Waste Disposal in Space. . . . .	2-23
Table 3-1.	Characteristics of Defense HLW for Terrestrial Disposal . . . . .	3-8
Table 3-2.	Average Composition of Major Hanford Sludges . . . . .	3-10
Table 3-3.	Savannah River F- and H-Area High-Heat Sludge Composite Compositions. . . . .	3-12
Table 3-4.	Calcine Compositions for Idaho Waste . . . . .	3-13
Table 3-5.	Baseline Radionuclide Composition of Hanford Waste Payload (1990 Definition). . . . .	3-15
Table 3-6.	Baseline Radionuclide Composition of Savannah River Waste Payload (Fresh Waste). . . . .	3-16
Table 3-7.	Estimated Idaho Calcine Radionuclide Composition . . . . .	3-17
Table 3-8.	Baseline High-Level Defense Waste Payload Characteristics. . . . .	3-23
Table 3-9.	Photon Source Strength Spectrum for Hanford Waste (WCF = 27) . . . . .	3-24
Table 3-10.	Container and Shielding Masses for Various WCF Values, Assuming Hanford Waste . . . . .	3-25
Table 3-11.	Space Disposal Heat Transfer Input Property Data . . . . .	3-29
Table 3-12.	Payload Temperature Distributions for the Hanford Defense Waste as a Function of Waste Concentration Factor . . . . .	3-32
Table 3-13.	Launch Pad Explosion/Fragment Impact Data. . . . .	3-35

**LIST OF TABLES**  
(Continued)

		<b>Page</b>
Table 3-14.	Input Parameters for High-Level Hanford Waste Payload Thermal Response Analysis (Fire Environment)	3-37
Table 4-1.	Assumed System Parameters . . . . .	4-9
Table 5-1.	Identified Accidents Used to Select Most Severe Accidents for Further Consideration in Accident Environment Characterization . . . . .	5-3
Table 5-2.	Equilibrium Constant Data for Hydrogen/Oxygen Combustion . . . . .	5-8
Table 5-3.	Heat of Products and Composition Data as a Function of Temperature for Shuttle Hydrogen/Oxygen Fireball.	5-8
Table 5-4.	Input and Assumptions for the Reentry Environment Analysis . . . . .	5-41
Table 5-5.	Definition of Mission Phases . . . . .	5-60
Table 5-6.	Fault Tree Symbols . . . . .	5-65
Table 6-1.	Peak Downwind Instantaneous Concentrations of Nuclear Waste as a Function of Distance . . . . .	6-5
Table 6-2.	Peak Downwind Time-Integrated Concentrations of Nuclear Waste as a Function of Distance . . . . .	6-5
Table 6-3.	DACRIN Organ List. . . . .	6-9
Table 6-4.	Fraction of Inhaled Particles Deposited in the Respiratory System vs Particle Diameter, as Employed by DACRIN. . . . .	6-11
Table 6-5.	Dose Commitment Factors (rem/ $\mu$ g Waste) for Hanford Waste, with AMAD Value of 0.2 $\mu$ m). . . . .	6-13
Table 6-6.	Dose Commitment Factors (rem/ $\mu$ g Waste) for Hanford Waste, with AMAD Value of 1.0 $\mu$ m). . . . .	6-13
Table 6-7.	Dose Commitment Factors (rem/ $\mu$ g Waste) for Hanford Waste, with AMAD Value of 5.0 $\mu$ m). . . . .	6-13
Table 6-8.	Dose Commitment Factors (rem/ $\mu$ g Waste) for Savannah River Waste, with AMAD Value of 0.2 $\mu$ m) . . . . .	6-14

LIST OF TABLES  
(Continued)

		Page
Table 6-9.	Dose Commitment Factors (rem/ $\mu$ g Waste) for Savannah River Waste, with AMAD Value of 1.0 $\mu$ m) . .	6-14
Table 6-10.	Dose Commitment Factors (rem/ $\mu$ g Waste) for Savannah River Waste, with AMAD Value of 5.0 $\mu$ m) . .	6-14
Table 6-11.	Population Dose Commitments (70-Year) for Different Conditions as a Result of a 55-kg Release (1%) of Waste Payload, During On-Pad Space Shuttle Accident.	6-21
Table 6-12.	Health Effects Risk Factors. . . . .	6-22
Table 6-13.	Ranges of Expected Health Effects for On-Pad Shuttle Failure with Release of Defense Nuclear Waste Material. . . . .	6-22
Table 6-14.	Fraction ( $f_{ik}$ ) of Source ( $A_i$ ) Injected in Latitude Band $i$ Which Falls in Equal Area Latitude Band $k$ and Total Population ( $P_k$ ) of Band $k$ . . . . .	6-28
Table 6-15.	Summation of Population Factors for Each Injection Band. . . . .	6-29
Table 6-16.	Dose Factors (Rem/ $\mu$ Ci for Each Nuclide) for AMAD of 0.2 Microns . . . . .	6-31
Table 6-17.	Dose Factors (Rem/ $\mu$ Ci for Each Nuclide) for AMAD of 1.0 Microns . . . . .	6-32
Table 6-18.	Dose Factors (Rem/ $\mu$ Ci for Each Nuclide) for AMAD of 5.0 Microns . . . . .	6-33
Table 6-19.	World Population Dose Summary for Total Burnup of Savannah River Defense Waste Payload Above 21 km . .	6-35
Table 6-20.	World Population Dose Summary for Total Burnup of Hanford Defense Waste Payload Above 21 km . . . .	6-36
Table 6-21.	Ranges of Expected Health Effects for Payload Reentry Burnup . . . . .	6-38
Table C-1.	Mix 2 Optimization . . . . .	C-2
Table C-2.	Mix 2 Criticality Analysis . . . . .	C-3
Table C-3.	Mix 4 Composition. . . . .	C-4

**LIST OF TABLES**  
(Continued)

	<b>Page</b>
Table E-1. Enthalpy of Products for Various Values of Temperature for ET Fireball Case. . . . .	E-3
Table E-2. Results of Numerical Integration of Fireball Energy Equation Prior to Fireball Liftoff . . . . .	E-6
Table E-3. Results of Numerical Integration of Fireball Energy Equation Between the Times of Fireball and Stem Liftoff . . . . .	E-7
Table G-1. Fraction of Inhaled Particles Deposited in the Respiratory System vs Particle Diameter. . . . .	G-11
Table G-2. Clearance Parameter Values . . . . .	G-11
Table G-3. Pulmonary Clearance Classification of Inorganic Compounds . . . . .	G-12
Table G-4. Metabolic Parameters for Dose Factor Calculations. .	G-13

## 1.0 INTRODUCTION

This volume summarizes the technical data developed as a part of the 1978 Battelle study of space disposal of defense nuclear waste. The report is organized into five major technical sections. The first (Section 2, which follows this Introduction) summarizes the current baseline and primary alternatives for the waste disposal concept, and is based on data contained in the Concept Definition Document developed as a part of this study. The section describes the proposed mission profile from time of receipt of the nuclear waste payload at the Kennedy Space Center launch site to final solar orbit injection, required systems hardware elements, current accident and malfunction contingency plans, projected traffic and hardware availability requirements, and unique systems design responsibilities.

Section 3 summarizes all material developed on the defense nuclear waste and its containment.\* The sources and characteristics of the waste are presented, and chemical processes to reduce the mass of the waste are postulated. The physical forms in which the waste could be transported are also identified. A preliminary container design, including shielding, cooling, and structural considerations, is developed. Because of the uncertainties in the eventual degree of achievable waste concentration, certain aspects of the container design are presented parametrically as a function of a waste concentration factor, and a baseline payload configuration was selected for accident response analyses. The survivability of the baseline payload configuration under various accident environments is characterized, and some preliminary recommendations are made.

Section 4 presents the results of two special analyses conducted as a part of this study. Both relate to special aspects of the system safety problem. The first analysis examines the stability and likely impact conditions for a nuclear waste payload ejected from the Space Shuttle Orbiter cargo bay both near the ground and during high speed flight. The second analysis considers the problem of an incomplete and/or misdirected OTV Earth escape injection burn. The resultant Earth orbit is described as a function of angular error and  $\Delta V$ .

---

\*Some work on commercial waste mixes and forms was performed at the start of the study. That work is summarized in Appendix C.



imparted. The ability of a rescue OTV to either return the stranded payload to the Space Shuttle orbit or boost the payload into a heliocentric or higher Earth orbit is examined. This material complements the work done by Science Applications, Inc. (NASA Contract NAS8-33022, "Long-Term Risk Analysis Associated with Nuclear Waste Disposal in Space", January 1979), who have examined the OTV or SOIS failures that result in the payload being placed in a heliocentric orbit other than the desired 0.86 a.u. circular orbit.

Section 5 summarizes the material developed relative to accidents. The first part of the section describes the physical environment resulting from three specific accidents: an on- or near-pad Space Shuttle explosion and fire, Earth atmosphere reentry of the protected (reentry protection) and unprotected nuclear waste container, and payload entry into deep ocean. The first two accident environments form the basis for the preliminary payload survivability analyses described in Section 3. The environments are characterized in terms such as blast overpressures, fragment sizes and velocities, and ambient temperatures and heating rates.

The second portion of Section 5 presents the results of a preliminary fault tree analysis for the space disposal mission. The mission is defined in terms of twelve discrete phases, and a preliminary fault tree is presented for each phase. For each fault tree, the likely critical paths and potential workarounds or system modifications are described. These are then summarized as a set of possible modifications for the hardware elements (Shuttle, OTV, etc.) and for operational procedures.

The final technical section (Section 6) summarizes the results of a preliminary environmental impact assessment for accidents related to defense nuclear waste disposal in space. Two accidents were examined: (1) release of radionuclides into the troposphere following an on- or near-pad catastrophic failure of the Space Shuttle vehicle and (2) release of radioactive particles into the upper atmosphere due to the breach and burnup of an unprotected waste container during an inadvertent reentry. The two accidents are analyzed in terms of the health risks resulting from inhalation of radioactive particles.

Seven appendices are also contained in this volume. Appendix A provides definitions of acronyms and abbreviations used in the text. Appendix B contains appropriate metric to English unit conversion factors. Appendix C describes preliminary work done on commercial waste mixes and forms. Appendix

D summarizes the fire transient analysis that was done for payload systems response analyses (see Section 3.4). The details of the fireball analysis as described in Section 5.1.1.1 of the text are contained in Appendix E. Appendix F provides a description of the calculation technique used to estimate the population dose for an on- or near-pad catastrophic Space Shuttle failure. Finally, Appendix G describes the models used to develop world population doses for an upper atmospheric reentry and burnup accident.

References indicated in the text are found at the end of each major section.

## 2.0 BASELINE CONCEPT DEFINITION AND OPTIONS SUMMARY

The purpose of this section\* is to summarize the various options, definitions and/or requirements currently envisioned for the nuclear waste disposal in space mission.<sup>(2-1)</sup> Section 2.1 identifies all major mission options available for the space disposal of nuclear waste (from the waste payload fabrication facility to the final space destination), notes the baseline and primary alternatives, and identifies options that are no longer considered viable. Section 2.2 summarizes the baseline space option concept for nuclear waste management, i.e., outlining the "single thread" characteristics from waste source to space destination. Section 2.3 defines the baseline mission profile, giving emphasis to operational or procedural aspects. Definitions and/or requirements for specific baseline mission elements (e.g., waste payload characteristics, space systems and facilities) are provided in Section 2.4; emphasis is on hardware and facilities. Section 2.5 describes the major contingency plans, requirements, and developments that have been baselined to minimize effects caused by possible accidents and/or malfunctions. General space system hardware requirements for the early years of the waste disposal activity are identified in Section 2.6. Section 2.7 describes unique system design requirements.

---

\*Note: This section has been derived from the latest version of the Concept Definition Document, Reference 2-1.

## 2.1 Concept Options

The baseline concept for the initial space disposal of nuclear waste has been developed from a considerable number of options that are available at each step along the way from the military reactor to the ultimate space disposal destination. A summary of the various options available is shown in Figure 2-1. The baseline mission options are shown in the blocks; primary alternatives are indicated by an asterisk; and those options which are no longer considered viable have lines drawn through them. Discussions on many of these options are available in References 2-2 through 2-7.

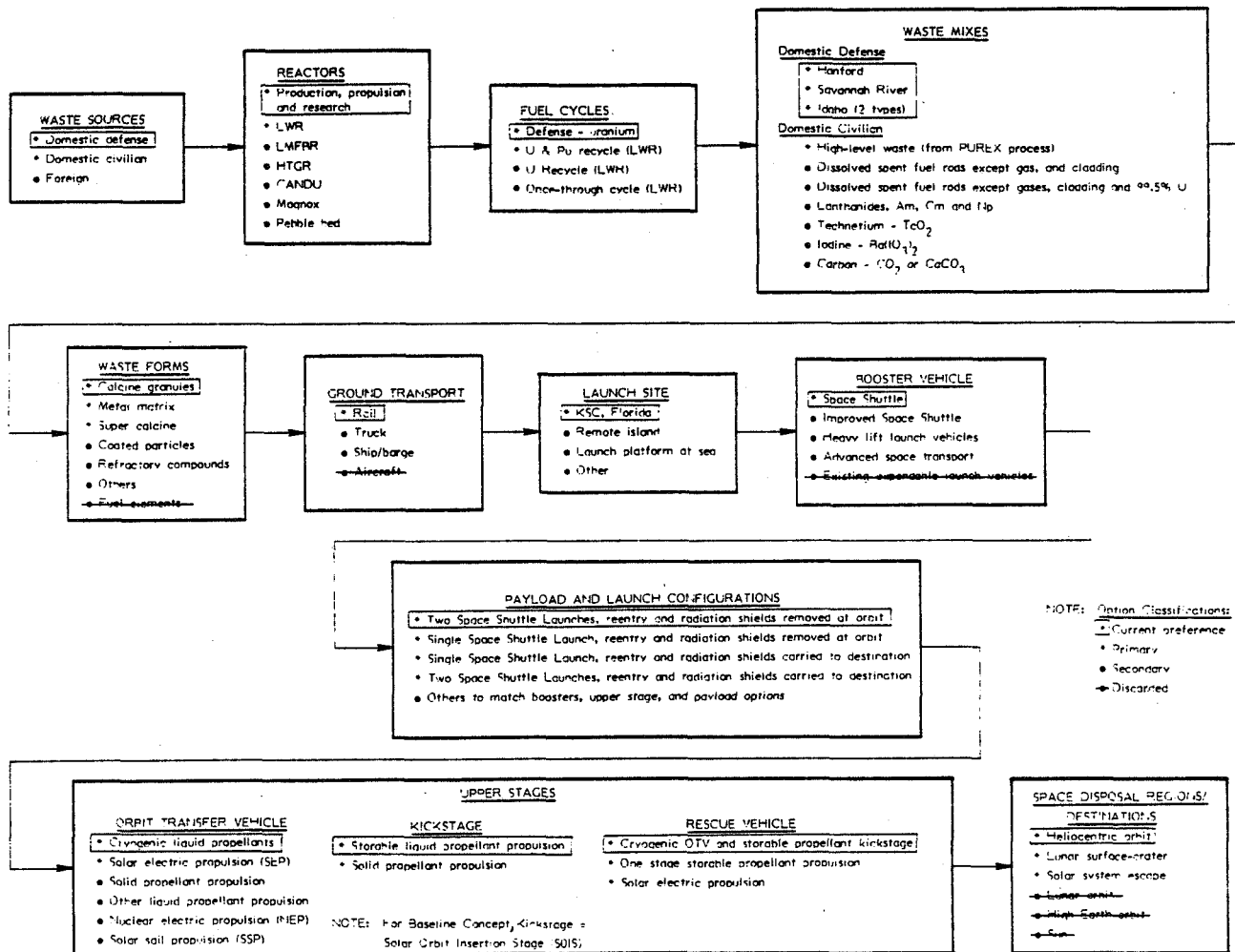


FIGURE 2-1. MAJOR OPTIONS FOR SPACE DISPOSAL OF NUCLEAR WASTE

## 2.2 Baseline Concept Summary

This section is intended to provide a brief overview of the baseline concept from the waste source to the final space destination. Elements of this concept are shown in Figure 2-2 and are described in subsequent sections.

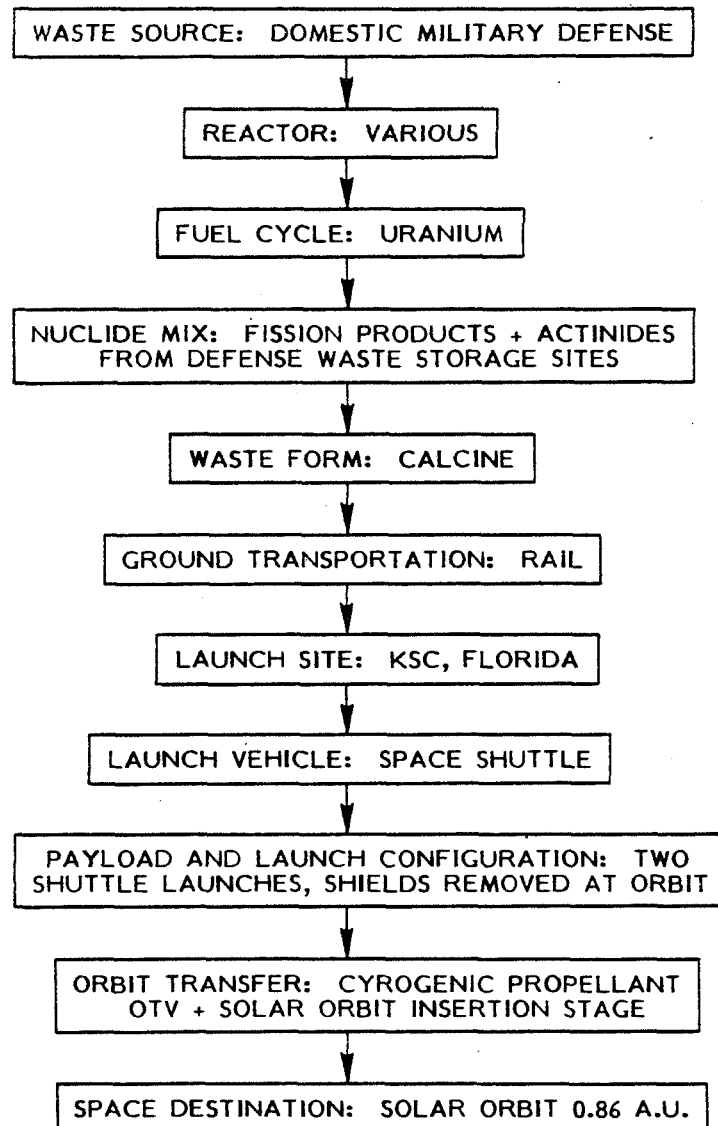


FIGURE 2-2. BASELINE CONCEPT SUMMARY FOR INITIAL PROGRAM TO DISPOSE OF NUCLEAR WASTE IN SPACE

## 2.3 Overall Baseline Mission Profile

The major aspects of the baseline mission profile are defined in this section. Figure 2-3 provides a pictorial view of this baseline mission profile. The baseline mission profile has been divided into six major categories. The first two activities are expected to be the responsibility of the Department of Energy (DOE) and the last four are expected to be NASA's. These are:

- (1) Nuclear Waste Payload Fabrication (DOE)
- (2) Nuclear Waste Ground Transport (DOE)
- (3) Payload Preparation at Launch Site (NASA)
- (4) Prelaunch Activities (NASA)
- (5) Booster Operations (NASA)
- (6) Upper Stage Operations (NASA).

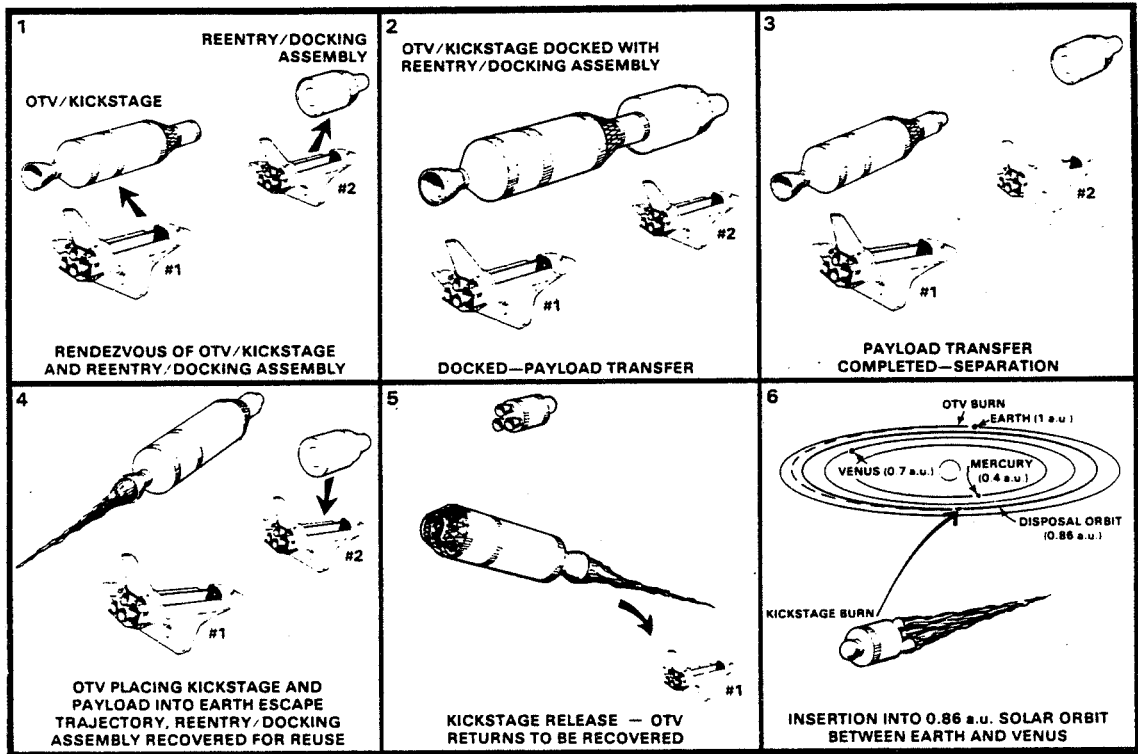
Consideration of rescue and recovery systems are discussed in Sections 2.4 and 2.5. Definitions and requirements for individual system elements are discussed in Section 2.4.

### 2.3.1 Nuclear Waste Payload Fabrication (DOE)

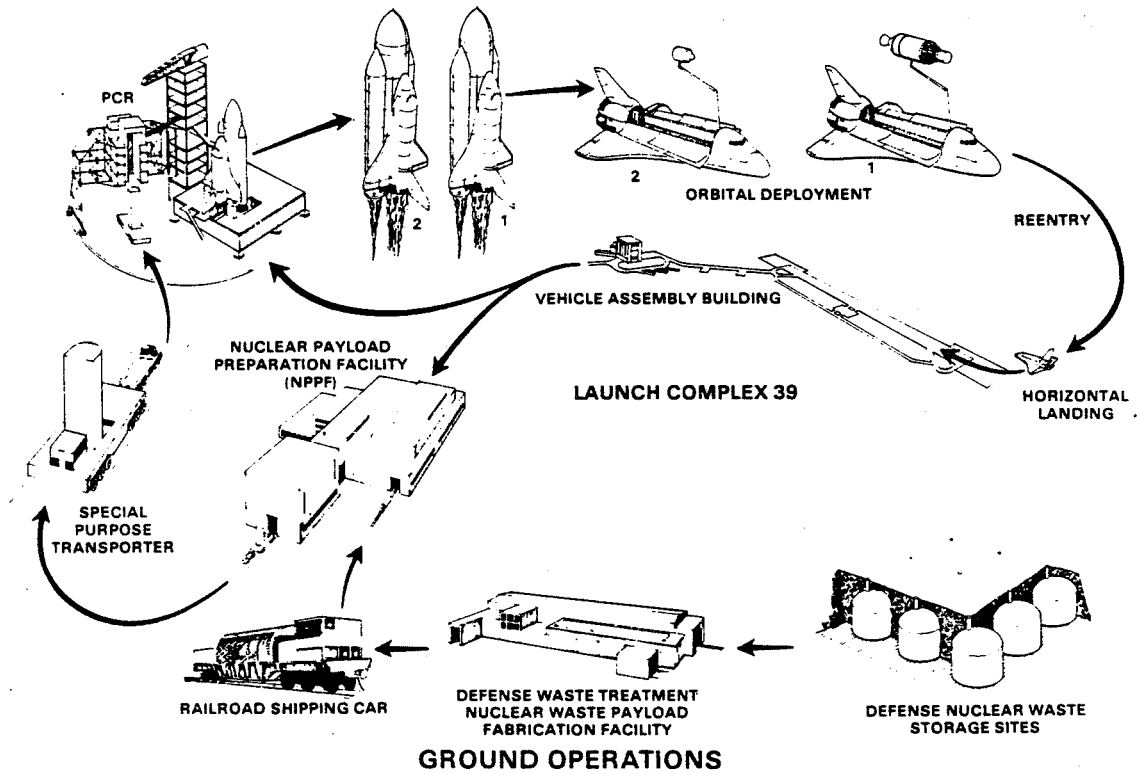
Defense nuclear waste contained at various storage sites (Hanford, Savannah River, and Idaho) would be packaged and transported to a nuclear waste payload fabrication facility. At this facility, the high-level waste, presently in various forms, would be appropriately treated. The current baseline waste form is a calcine. The treated waste would be packaged into the flight-weight container and placed into the space-mission, gamma-radiation-shield assembly.

### 2.3.2 Nuclear Waste Ground Transport (DOE)

The radiation shielded waste container would be loaded into a ground transportation shipping cask (see artist's concept in Figure 2-4). This cask, which provides additional shielding, and thermal and impact protection for the waste container to comply with the Nuclear Regulatory Commission/Department of Transportation regulations, would then be loaded onto a specially designed rail car for transporting the waste container from the waste payload fabrication site



**ORBITAL OPERATIONS**



**GROUND OPERATIONS**

FIGURE 2-3. GROUND AND SPACE OPERATION PROFILES FOR BASELINE SPACE DISPOSAL MISSION



to the Kennedy Space Center (KSC), Florida launch site. The rail car would be equipped with auxiliary cooling systems to provide continuous cooling for the waste package during transport. Once the cask reaches the launch site, the radiation shielded waste container would be unloaded in the Nuclear Payload Preparation Facility (NPPF).

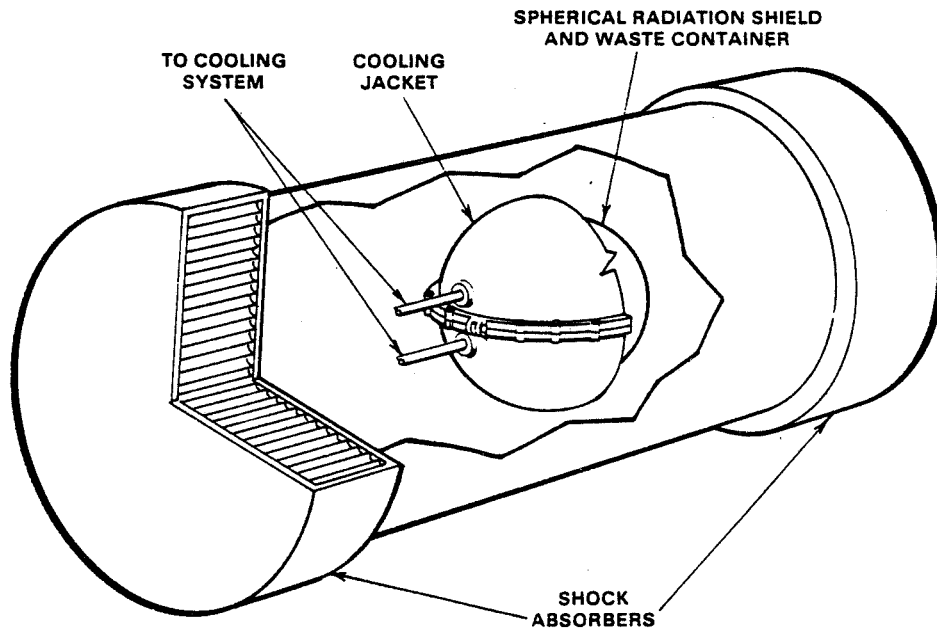


**FIGURE 2-4. ARTIST'S CONCEPT FOR NUCLEAR WASTE PAYLOAD SHIPPING CASK FOR TERRESTRIAL TRANSPORT**

### 2.3.3 Payload Preparation at Launch Site

The Nuclear Payload Preparation Facility (NPPF) would likely provide interim storage capability for up to three shielded waste containers, but storage of waste at the launch site should be limited to that which will afford efficient preparation for launching, plus capacity for delays. Upon receipt, the shielded waste container would be unloaded in the containment area of the NPPF. Depending on the shield assembly design, additional radiation shielding would be employed to further reduce personnel exposure for operations conducted close to the waste. Operations in the containment area of the NPPF would include: payload cooling, storage, inspection and monitoring of the waste containers, and incorporation of the radiation shielded waste container into the reentry system. In other areas of the NPPF, the reentry, docking and other auxiliary systems,

which comprise the payload reentry/docking assembly (see Figure 2-5), would be refurbished and checked out. Once the shielded nuclear waste container has been loaded into the reentry system, the reentry system would be moved to a second containment area. The reentry, docking, cooling, pallet, ejection and other systems would be mated. Propellant loading of the attitude control system would take place in a special area of the NPPF. Once the payload reentry/docking assembly, mounting structures (e.g., pallet) and supporting systems had passed the safety inspection they would be prepared for transfer to the Payload Changeout Room (PCR) at the launch pad.

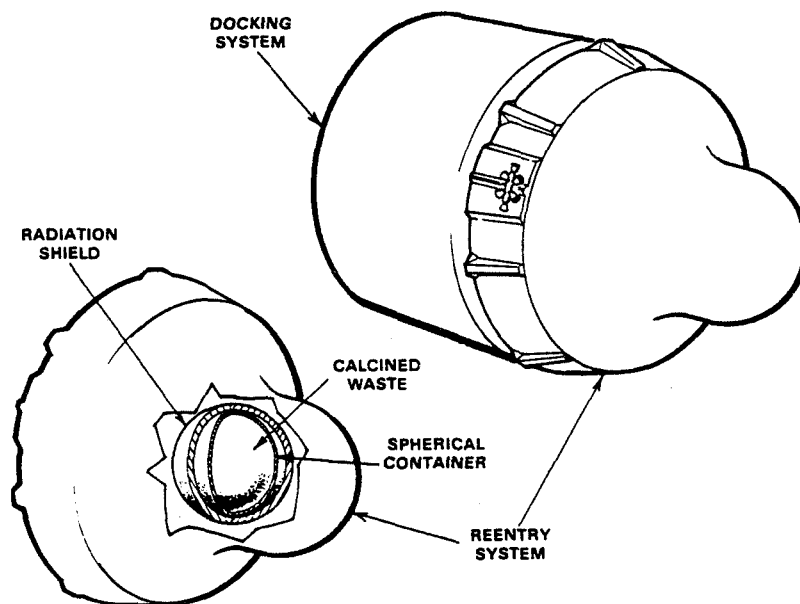


FIGURE 2-5. ARTIST'S CONCEPT OF A LOADED REENTRY/DOCKING ASSEMBLY

#### 2.3.4 Prelaunch Activities

After the nuclear waste payload assembly had been prepared for flight, it would be transferred from the NPPF to the Payload Changeout Room (PCR) at the launch pad by a dedicated special-purpose transporter. Once in the PCR, the loaded payload reentry/docking assembly would be attached to an auxiliary cooling system. The entire payload package would then be placed into the Space Shuttle cargo bay (see Figure 2-3), where final systems checkout begins.

After the initial checkout of the nuclear waste payload assembly in Shuttle number 2, Shuttle number 1, carrying the Orbit Transfer Vehicle/Solar

Orbit Insertion Stage (OTV/SOIS), would be launched. After about 2 hours, a launch decision for Shuttle number 2 would be made. A launch decision is expected to be based upon three major factors: (1) the OTV/SOIS is in the proper orbit and functioning properly; (2) Shuttle Orbiter number 2 and its payload have cleared checkout procedures, and (3) proper meteorological conditions (e.g., wind direction) are predicted for launch of the nuclear waste payload (a launch constraint which would avoid radiation exposure to the local population, should a payload breach occur as a result of a catastrophic Space Shuttle launch accident).

### 2.3.5 Booster Operations

Booster operations are those that are required of the Space Shuttle vehicle between the time of Space Shuttle Main Engine ignition and the return of the reusable Space Shuttle vehicle hardware to the launch site. As discussed in Section 2.3.4, two Shuttle vehicles would be readied for launch for a given disposal mission. For example, Pad A at KSC Launch Complex 39 could be used for launching the Shuttle carrying the reusable OTV and the 3-axis stabilized SOIS. Pad B would then be used to launch the Shuttle vehicle that carries the nuclear waste payload.

The OTV and SOIS would be launched by Shuttle number 1 at a 108 degree south azimuth to a 333 km (180 n.mi.) circular orbit inclined 38 degrees to the equator. Approximately 48 hours later, the nuclear waste payload would be launched by the second Shuttle into the same orbit as the first Shuttle. A small degree of yaw steering would be required for the second Shuttle launch, such that early land overflight of various populated land masses (West Indies and South Africa) is avoided. The first Shuttle Orbiter would remain on orbit in the vicinity of the OTV to control: (1) the docking of the OTV/SOIS to the payload reentry/docking assembly, (2) the remote removal of the waste container from the reentry system, (3) the attachment of the container to the OTV, and (4) OTV/SOIS orbital operations. The second Shuttle Orbiter would provide backup capability for OTV/SOIS operations. After the OTV delivers the nuclear waste payload and SOIS to the desired trajectory and returns to a low Earth orbit, the first Orbiter would rendezvous with the OTV and return it to the launch site for refurbishment for a later flight. As soon as it is determined that the waste

container is safely on its way to the proper space destination, the empty payload reentry/docking assembly would be recovered, stored and returned to KSC on board Orbiter number 2.

### 2.3.6 Upper Stage Operations

Upper stage operations are those that occur between the time the OTV/SOIS configuration is released from Orbiter number 1 and the time the OTV is recovered by the Orbiter and the SOIS has provided the velocity increment to the nuclear waste payload at the space destination (0.86 a.u. solar orbit).

After Shuttle Orbiter number 1 is on orbit with the OTV/SOIS, preliminary checkout would occur while the configuration is in the cargo bay. The Shuttle's manipulator arms would then be used to deploy the OTV/SOIS. The Orbiter would back away a short distance and begin further checkout procedures. Once the OTV/SOIS system and its docking mechanisms had passed checkout tests, the launch decision for Shuttle number 2 would be made.

When Orbiter number 2 reaches orbit, the nuclear waste payload reentry/docking assembly (see Figure 2-5) would be checked out, disconnected, removed, and released. Appropriate payload temperatures would be maintained by an auxiliary cooling system located on the reentry/docking assembly. The system would be designed to supply roughly 10 hours of active cooling. Passive cooling will be adequate after the container is removed from the reentry system.

The OTV/SOIS would then rendezvous and dock with the reentry/docking assembly. The mechanical locking system that releases the waste container from the reentry system would be manipulated by a remotely operated arm provided on the payload docking system; this arm would be used to: (1) remove the rear reentry shield wall, (2) remove the spherical container from the reentry system and attach it to the SOIS payload adapter, and (3) replace the rear reentry shield wall.

Once the container is attached to the OTV/SOIS, separation of the reentry/docking assembly occurs and the OTV/SOIS would back away with the container mounted on the payload adapter. The payload reentry/docking assembly would maintain a fixed attitude while the OTV/SOIS backs away. The OTV reaction control system then would place the OTV/SOIS into the proper attitude

for firing. The OTV propulsive burn for payload delivery would place the SOIS and its attached waste payload on the proper Earth escape trajectory. The SOIS and payload would then be released. In approximately 163 days the payload and the storable liquid propellant SOIS would travel to its perihelion at 0.86 a.u. about the Sun. The 3-axis stabilized SOIS would place the payload in its final space disposal destination by reducing the aphelion from 1.0 to 0.86 a.u. To aid in obtaining the desired orbital lifetimes, this orbit would be inclined to the ecliptic plane by at least 1 degree.

The recovery burns of the OTV would use the remaining OTV propellant to rendezvous with Shuttle number 1 for its subsequent recovery, refurbishment, and reuse on a later mission. The payload reentry/docking assembly would be recovered by Shuttle number 2 and returned to KSC for refurbishment and reuse.

## 2.4 Baseline Element Definitions and/or Requirements

The definitions and/or requirements for baseline mission elements are described below. Specific details not now available will be added at a later date. Twelve major system elements have been identified:

- (1) Waste Source
- (2) Waste Mix
- (3) Waste Form
- (4) Waste Fabrication Facilities
- (5) Payload Container, Shielding, and Reentry Systems
- (6) Ground Transport Vehicles and Casks
- (7) Launch Site Facilities
- (8) Launch Vehicle
- (9) Upper Stages
- (10) Payload Ejection System
- (11) Docking System
- (12) Space Destination.

Definitions and requirements for the baseline mission elements follow.

### 2.4.1 Waste Source

The primary waste source is the domestic military defense waste generated by the operation of plutonium production, test and naval reactors. Waste has been and will continue to be generated at three locations: (1) Hanford Site, Richland, Washington, (2) Idaho National Engineering Lab Site, Idaho Falls, Idaho; and (3) Savannah River Site, Aiken, South Carolina. Table 2-1 presents the volumetric inventories of high-level waste (HLW) as they presently exist. These wastes have, on the average, been cooled for periods exceeding ten years.

Additional quantities of waste will also be produced in the future. Hanford may resume waste production toward the end of the century. Savannah River will be producing more than 4,000 m<sup>3</sup> of waste annually. Idaho expects to have approximately 8500 m<sup>3</sup> of calcine waste by the year 2000.

TABLE 2-1. CURRENT VOLUMETRIC DEFENSE HLW INVENTORIES

Site	Waste Form (1000 m <sup>3</sup> )			
	Salt Cake	Sludge	Liquor	Calcine
Hanford	95	42	42	0
Savannah River	50	13	21	0
Idaho	0	0	0	1.5

#### 2.4.2 Waste Mix

Each waste generation site has its own peculiarities with respect to waste mix. Hanford waste is, in general, the oldest and has decayed the longest. Savannah River waste is similar to Hanford waste, but is newer on the average, and contains more total radioactivity. Idaho waste contains relatively different amounts of radionuclides than either Savannah River or Hanford because Idaho waste is generated by reprocessing naval reactor fuel rather than weapons production fuel. The exact radionuclide mix will vary substantially among the three sites. This is due to the different reprocessing techniques used to generate waste over the years and the cooling times of each batch.

To facilitate terrestrial disposal of defense nuclear waste, certain radionuclide concentration processes have been proposed at each site to reduce the amount of the inert material in the high-level waste. At Hanford and Savannah River, the salt cake and liquor would be decontaminated and the extracted radionuclides combined with the insoluble portions of the existing radioactive sludge. At Idaho, the calcine would be redissolved, to the extent possible, and the radionuclides combined with the insoluble portions of the calcine. Table 2-2 presents the approximate masses of high-level waste (HLW) remaining at each site after these concentration processes have occurred.

TABLE 2-2. PROJECTED MASS INVENTORIES OF DEFENSE HLW PROPOSED FOR TERRESTRIAL DISPOSAL

<u>Site</u>	<u>Amount, MT</u>
Hanford	16,400
Savannah River	3,750
Idaho	600



Additional inert removal, or radionuclide concentration, will be required to make the space disposal option more feasible. It may be possible to reduce the waste mass from between 1/10 to 1/100 of the original planned mass. Table 2-3 provides what is believed to be high and low mass inventory estimates for space disposal. The desired high scenario has been assumed here for the baseline.

**TABLE 2-3. DESIRED HIGH AND DESIRED LOW MASS INVENTORIES OF DEFENSE HLW PROPOSED FOR SPACE DISPOSAL**

Site	Desired High	Desired Low
	Metric Tons, MT	
Hanford	605	244
Savannah River	375	116
Idaho	<u>60</u>	<u>20</u>
TOTALS	1040	380

Table 2-4 shows the Space Shuttle flight requirements based on three levels: proposed for terrestrial; desired high; and desired low. The baseline is assumed to be at the desired high level, or 380 flights will be required for space disposal of defense high-level waste.

**TABLE 2-4. SPACE SHUTTLE FLIGHTS REQUIRED FOR SPACE DISPOSAL**

Site	Number of Shuttle Flights Required Based On -		
	Proposed Masses for Terrestrial Disposal	Desired High	Desired Low
Hanford	5960	220	90
Savannah River	1360	138	42
Idaho	<u>220</u>	<u>22</u>	<u>8</u>
TOTALS	7540	380	140

NOTE: Assumes a 5.5 MT payload and 2 Space Shuttles/payload.

As mentioned previously, the exact radionuclide composition will vary considerably from tank to tank, or batch to batch. Lists of typical radionuclide mixes are available in "Alternatives for Long-Term Management of Defense High-Level Radioactive Waste" from each of the three sites (References 2-8 through 2-10).

### **2.4.3 Waste Form**

As discussed in Sections 2.4.1 and 2.4.2, the existing and future defense wastes would be concentrated. The resulting wastes would be the insoluble sludge components, from Hanford and Savannah River, and the insoluble calcine components from Idaho. Wastes remaining after the Idaho concentration process can be converted to calcine again; however, it is not clear if high temperature treatment of Hanford and Savannah River wastes will actually yield oxides. For the purpose of defining a baseline, it is assumed that calcines can be produced following the presently proposed radionuclide concentration processes and also after any additional treatment occurs to remove portions of remaining inert materials.

Final waste forms may be calcine, compartmented calcine, metal matrix, supercalcine, or coated particles. Hanford is also developing a sintered clay ceramic waste form which may have waste loadings comparable to metal matrix forms. High waste loading, thermal stability, and low dispersibility will be the primary requirements for a suitable waste form. The baseline waste form, at this time, is calcine.

### **2.4.4 Waste Fabrication Facilities**

The defense waste mixes would undergo additional chemical treatment, as necessary, to produce the desired waste form at facilities located at each of the three waste generation sites. The waste payload fabrication facilities would provide a series of interconnected, shielded cells for loading the waste into containers, closing, sealing, inspecting, decontaminating the container, and ultimate insertion into the gamma flight radiation shield assembly. Each cell would have provisions to connect the waste container to an auxiliary cooling system as necessary. Each site would provide interim storage facilities for a number of shielded waste packages and facilities for cask handling and rail car loading in closed, restricted areas.

### **2.4.5 Payload Container, Shielding, and Reentry Systems**

The primary containment for the radioactive waste would be a spherically shaped metal container (see Figure 2-5). This container must provide

high integrity containment for the waste during the various defined mechanical and thermal loads to which it is subjected in anticipated normal and accident conditions. These loads would be mitigated in varying degrees by the gamma radiation shield assembly, by the shipping cask which provides additional gamma radiation shielding for ground transportation, and by the reentry system during the prelaunch and boost phase. The container would be housed in a radiation shield assembly for the period prior to leaving the waste fabrication facility for the launch site. This flight-weight shielding would be designed to limit the radiation level to 2 rem/hr at 1 meter from its surface; additional shielding would be provided by temporary shielding at the NPPF and PCR, and possibly a shadow shield in the Shuttle Orbiter for the crew. The container would be designed to provide the conductivity and surface emissivity for dissipating the heat generated within the waste by passive cooling to the space environment. During launch and orbital operations the maximum temperature of the waste will not exceed the normal limiting temperature of 700 C (as defined in Section 3.4.2). Prior to removal of the container from the reentry system, the temperature would be controlled with assistance of various auxiliary cooling systems located on the Space Shuttle and the reentry system. If an accident should occur, the temperature of the waste might exceed the normal limit, but must not exceed that which will cause loss of containment. The shielded waste container would be enclosed in a protective payload reentry system prior to launch and during the boost phase (see Figure 2-5). This system would be designed to minimize the probability of containment breach as a result of accidents or malfunctions which could occur during the prelaunch, launch, suborbital, or orbital phases of the mission. Specific design requirements would be developed as the possible health hazards and other consequences of various release scenarios are assessed.

#### 2.4.6 Ground Transport Vehicles and Casks

For transport from the waste fabrication facility to the launch site, the waste containers and associated flight-weight shielding would be housed in a shipping cask which would afford additional shielding, thermal and impact protection to meet the Nuclear Regulatory Commission/Department of Transportation regulations. The cask (see Figure 2-4) would be licensed by the Nuclear Regulatory Commission and would be transported on a specially designed

rail car which would adequately support and distribute the weight of the cask and provide acceptable tiedowns. In addition, the rail car would carry an auxiliary cooling system to reliably cool the waste package.

#### 2.4.7 Launch Site Facilities

The baseline launch site for launching nuclear waste payloads during the early phase of the program (late-1980's to early-1990's) is Launch Complex 39 at Kennedy Space Center (KSC), Florida. The following new facility construction and equipment, at least, is projected:

- (1) A secure, sealed, environmentally controlled, Nuclear Payload Preparation Facility (NPPF) to store, cool, monitor, assemble, and checkout the waste payload systems from the time the nuclear waste container and gamma radiation shield arrive at KSC until the time the loaded payload reentry/docking assemblies are moved to the launch pad.
- (2) A dedicated, special-purpose transporter to move the nuclear waste payload assembly from the NPPF to the Payload Changeout Room (PCR) at the launch pad. This includes construction of a roadway or tracks to accommodate the transporter.

The currently planned Shuttle launch facilities may or may not be adequate to support the additional Shuttle launches required by a nuclear waste disposal program. Further analysis of the nuclear waste disposal traffic model coupled with the baseline Shuttle traffic model and current turnaround timelines is needed. Also, it will take further analysis to determine where SOIS processing, OTV refurbishment and processing and upper stage mating and checkout can be performed and what new supporting systems and facilities would be required. As the study of space disposal options progresses, these and other launch facility requirements will be identified and addressed.

#### 2.4.8 Launch Vehicle

The launch vehicle chosen as the baseline is the Space Shuttle system (see Figure 2-3). The Space Shuttle consists of a piloted reusable orbiting

vehicle (the Orbiter) mounted on an expendable External Tank (ET) containing hydrogen/oxygen propellants and two recoverable and reusable Solid Rocket Boosters (SRBs). The Orbiter will have three main hydrogen/oxygen liquid rocket engines and a cargo bay 18.29 m long and 4.57 m in diameter. At launch, both the SRBs and the Orbiter's three liquid rocket engines will burn simultaneously. When the Space Shuttle vehicle attains an altitude of approximately 43 km, the SRBs will be separated and subsequently recovered from the ocean. The ET is jettisoned before the Orbiter goes into orbit. The Orbital Maneuvering System (OMS) will then be used to propel the Orbiter into the desired Earth orbit. The Orbiter with its crew and payload will remain in orbit to carry out its mission, normally from 1 to 7 days, but, when required, as long as 30 days. When the mission is completed, the Orbiter is deorbited and piloted back to the launch site for an unpowered landing on a runway. The Orbiter and SRBs will subsequently be refurbished and reflown on other space missions. References 2-11, 2-12 and 2-13 provide additional information about the Space Shuttle and its capabilities.

#### 2.4.9 Upper Stages

Two different upper stages have been defined for use for the nuclear waste disposal mission: (1) an Orbit Transfer Vehicle (OTV), and (2) a storable propellant Solar Orbit Insertion Stage (SOIS). The OTV is a completely reusable and recoverable stage, whereas the SOIS is expendable. Orbital rescue capability would be performed by the OTV and SOIS systems.

The OTV is defined as a reusable  $\text{LO}_2/\text{LH}_2$  chemical propulsion stage similar to the cryogenic OTV defined in the last few years for possible development and use with the Space Shuttle. This vehicle would have separate propellant tanks, an oxidizer to fuel mixture ratio of 6 and a delivered specific impulse of 470 seconds. It would also have an advanced, redundant, avionics and attitude control system. Other unique features are expected to be defined later.

The storable propellant pressure-fed SOIS is expected to be sized to provide a specific impulse of 289 sec. This stage would have three off-the-shelf (Space Shuttle-Reaction Control System) pressure-fed engines at a thrust level of 3870 N (870 lb) each,  $\text{MMH}/\text{N}_2\text{O}_4$  propellants, a guidance and control system, and a payload docking adapter system compatible with the docking system. The

stage would be designed to withstand adequately the adverse nuclear radiation, and space environments experienced while coasting 163 days before firing.

The rescue vehicle would be a Shuttle launched OTV/SOIS system. It would include appropriate provisions for targeting and docking with the nuclear waste container attached to an OTV/SOIS, the nuclear waste container attached to a SOIS only, a payload reentry/docking assembly, or an unshielded, separated waste container. It would be reusable or expendable depending upon the rescue mission. This vehicle would be required to have a suitable on-orbit stay time. Depending upon the type of rescue mission, the rescue vehicle may be returned to Earth by the Shuttle for refurbishment.

#### **2.4.10 Payload Ejection System**

A payload ejection system is planned to be incorporated into the pallet which supports the reentry/docking assembly. This system would employ four small solid propellant rocket motors which would be ignited to eject the loaded reentry system from the Orbiter cargo bay in the event of a critical on-pad or ascent failure. The reentry system would be designed to withstand the impact environment.

#### **2.4.11 Docking System**

The payload docking system would be launched into orbit attached to the payload reentry system. This configuration is known as the payload reentry/docking assembly (see Figure 2-5). The docking system would be used to transfer the waste payload container from the reentry system to the SOIS payload adapter. It would also be designed to jettison with the nuclear payload during the very low probability occurrence of a critically inaccurate OTV propulsive burn. This action could prevent reentry and allow subsequent recovery by a Shuttle or OTV rescue vehicle.

#### **2.4.12 Space Destination**

The baseline space destination for the nuclear waste disposal mission is defined as an orbital region between the orbits of the Earth and Venus. The nominal circular orbit is defined as 0.86 a.u. The orbital inclination about the Sun is defined as 1 degree from the ecliptic plane.

## 2.5 Accident and Malfunction Contingency Plans

There are four general mission phases which require development of accident and malfunction contingency plans:

- Ground transportation from the payload fabrication sites to KSC
- Preflight operations at KSC prior to ignition of the Shuttle's engines
- Launch operations from the launch pad to achieving parking orbit
- Orbital operations.

Preliminary baseline contingency plans for each of these operational phases are addressed below.

### 2.5.1 Ground Transportation

Ground transport (via rail) of the shipping cask is expected to be the responsibility of the Department of Energy (DOE). DOE will supply the necessary accident recovery plans and systems for ground transport. At least two types of incidents must be considered: loss of cooling to the waste container and possible breach of the waste container with a loss of radioactive material.

In the case of loss of cooling, provisions must be made to have self-contained, auxiliary cooling units available. Monitoring equipment for both container temperature and radiation would be required during all ground transport operations.

A continuous capability to cope with a container breach will be necessary. A specially trained decontamination crew would always need to be ready to act, if necessary.

### 2.5.2 Preflight Operations

Contingency plans must be provided for potential malfunctions and accidents that could occur while the waste payload is in the NPPF, being transported to the launch pad, being transferred from the pad PCR to the Shuttle cargo bay, and awaiting liftoff in the Shuttle. Accidents and contingency plans would be similar to those discussed above.

### 2.5.3 Launch Operations

Certain major failures could result in a catastrophic on- or near-pad Shuttle failure (e.g., SRB failure to ignite, and External Tank rupture). As a result, the payload could be subjected to severe blast wave, high velocity fragments, fire, and high velocity impact. Contingency plans, procedures and systems envisioned to minimize the short-term risk caused by these failures are as follows:

- A system to eject the loaded reentry system (contains nuclear waste) from the Orbiter's cargo bay and ensuing adverse environments
- A destruct system on the External Tank and SRBs to reduce the explosive yield of the hydrogen/oxygen propellants, thus reducing the effect of the accident environment on the containment systems
- Stringent containment systems designs (e.g., container, shielding and reentry systems) to maximize the probability of surviving possible hostile environments. The reentry system would contain flotation gear and locator beacons to assist in the recovery of the payload.
- The use of a waste form that is not easily dispersed or leached
- The application of appropriate launch constraints (e.g., wind direction) to reduce human radiological exposure resulting from a containment breach.

Subsystem failures (e.g., one Shuttle main engine shuts down) that occur later in the boost phase may also endanger the payload. Systems and procedures in addition to some of those mentioned above which would minimize the short-term risk caused by these subsystem failures are:

- The capability for intact aborts. These abort procedures can be implemented after about 120 seconds into the flight (the time when the SRBs are jettisoned). Three types of intact aborts are planned for the Space Shuttle. These are: the return to launch site (RTL), abort-to-once-around (ATOA) and abort-to-orbit (ATO).
- The capability for contingency aborts. Such an abort could lead to either a return to land or to ditching at sea.



- Designing the boost trajectory to avoid land overflight (e.g., 38 degree inclination orbit).

#### 2.5.4 Orbital Operations

The OTV propulsion phase provides for transportation from low Earth orbit to either the final or intermediate destination. In the initial years of the disposal mission the OTV could be a relatively high-thrust, chemical propulsion stage. Later on, low-thrust technology (SEP, NEP, solar sail) might be used. With low-thrust systems, both the probability and magnitude of an explosion are decreased. In addition, there is a much longer decision time available in case of a malfunction of the low-thrust propulsion systems. For the baseline concept (see Section 2.3.6) the OTV would be a liquid hydrogen/liquid oxygen system. Certain low probability failures (e.g., guidance system, propulsion system, etc.) could result in abnormal trajectories which might result in Earth reencounter and subsequent reentry of the unprotected waste container. Systems, procedures and design requirements envisioned to minimize the short-term risk are given below:

- The capability to detect a critically inaccurate OTV propulsive burn and command OTV engine shutdown or OTV destruction to terminate the burn
- The capability to separate the SOIS and attached payload from the OTV and use of the SOIS to place the payload in a safe orbit for eventual recovery by a rescue vehicle or Shuttle Orbiter
- A jettison system to separate the payload from the OTV/SOIS configuration when necessary to preclude a possible reentry
- The use of a rescue vehicle to retrieve a payload stranded in any given orbit
- The use of redundant systems where feasible to ensure high reliability
- Prime and backup on-orbit OTV launch crews (i.e., crews onboard two Orbiters to obtain instantaneous visual and telemetric status of the OTV propulsive burn
- The proper design of trajectories and propulsive burns of the OTV to reduce the chance for reentry if a failure occurs.

The SOIS provides for transportation from an intermediate to the final destination. For the baseline concept, the SOIS would be used to reduce the aphelion from 1.0 to 0.86 a.u. (see Section 2.3.6). If a system failure should occur prior to or during the SOIS propulsive burn, the payload might have a finite probability of eventually reencountering the Earth, resulting in a reentry and possible burnup of the waste in the atmosphere. Systems, procedures and design requirements envisioned to minimize the risk are given as:

- The use of a rescue vehicle to retrieve a payload stranded in any orbit in heliocentric space
- The use of redundant systems where feasible to ensure high reliability
- The proper design of trajectories (e.g., orbits inclined to the ecliptic plane and also those which exhibit long-term orbital stability)
- The use of systems onboard the SOIS to aid in tracking and rescue operations.

## 2.6 Projected Traffic Model and Hardware Availability Requirements

The projected traffic model and hardware availability requirements for all major mission elements have been estimated and are documented here for reference. For the baseline mission definition a total of 380 Space Shuttle flights (see Table 2-4) would be required to dispose of all of the high-level defense nuclear wastes (two Shuttle flights would be required for each disposal mission). Consideration of development flights and aborted missions would be expected to increase this number somewhat. Table 2-5 shows the major mission elements, the hardware use factor assumed, and the total hardware requirements. No consideration has been given to a traffic schedule at this time. Disposal missions could occur over a 10 to 30-year period. Little impact is expected on the Space Shuttle traffic model for the decade of the 1980's (see Reference 2-14), as the nuclear waste disposal activity is not expected to be operational until the late 1980's to early 1990's.

**TABLE 2-5. MAJOR HARDWARE REQUIREMENTS ESTIMATES FOR DEFENSE NUCLEAR WASTE DISPOSAL IN SPACE**

Hardware Element	Use Factor	Number Required
Space Shuttle Hardware		
- Orbiters	100	4
- ETs	1	380
- SRBs (2 SRBs Per Flight)	20	38
Upper Stage Hardware		
- OTVs	20	10
- SOISs	1	190
Waste Payload Systems		
- Containers	1	190
- Gamma Radiation Shields	20	10
- Payload Reentry/Docking Assemblies	20	10
- Crew Shields	100	2
- Cooling Systems	100	2
- Rail cars and casks	100	2

NOTE: Table assumes 380 Space Shuttle flights to dispose of defense nuclear waste, 2 Shuttle flights per mission.

## 2.7 Unique System Design Requirements

To serve as a guideline to a realistic program development, various unique system design requirements have been identified which will insure viability of the space option for nuclear waste disposal. The requirements are listed below with the assigned agency responsibility:

- Waste treatment/inerts removal (DOE)
- Waste form production (DOE)
- Waste form environmental response (DOE)
- Payload fabrication techniques (DOE)
- Materials compatibility (NASA/DOE)
- Containment system accident environment response (NASA/DOE)
- Radiation shielding (NASA/DOE)
- Docking system mechanisms (NASA)
- Deep space rescue techniques (NASA).

Design/safety experiments and testing that are expected to be conducted during the Concept Definition Phase of the R&D Program (see Appendix B, Volume III of this report) will play the vital role in the evaluation of concepts/systems that are proposed for the nuclear waste disposal in space mission. These experiments and tests have not been defined fully at present.

Actual technology demonstrations required for the nuclear waste disposal in space mission are geared to the initiation of the development schedule. Should serious unresolved technology issues exist at the end of the 3-year Concept Definition Phase (milestone for development decision) the development program would likely be delayed until they have been resolved.

2.8 References

- 2-1. Austin, R. E., Edgecombe, D. S., et al., "Concept Definition Document for Defense Nuclear Waste Disposal in Space", NASA/Marshall Space Flight Center, Huntsville, Alabama, and Battelle-Columbus Laboratories, Columbus, Ohio, A Working Paper (October 23, 1978).
- 2-2. Burns, R. E., et al., "Nuclear Waste Disposal in Space", NASA-TP-1225, NASA/MSFC, Huntsville, Alabama (May, 1978).
- 2-3. Pardue, W. M., et al., "Preliminary Evaluation of the Space Disposal of Nuclear Waste", 8-32391(100), Battelle Memorial Institute, Columbus, Ohio (August 1977).
- 2-4. Brown, B. G., "Nuclear Waste Disposal Mission Analysis", TR-223-1874, Northrop Services, Inc., Huntsville, Alabama (November 1977).
- 2-5. Friedlander, A. L., et al., "Analysis of Long-Term Safety Associated with Space Disposal of Hazardous Material", SAI-1-120-676-T11, Science Applications, Inc., Schaumburg, Illinois (December 1977).
- 2-6. Friedlander, A. L., et al., "Aborted Space Disposal of Hazardous Material: The Long-Term Risk of Earth Reencounter", SAI-1-120-676-T8, Science Applications, Inc., Rolling Meadows, Illinois (February 1977).
- 2-7. "Feasibility of Space Disposal of Radioactive Nuclear Waste", NASA-TM-X-2911, NASA/LeRC, Cleveland, Ohio (December 1973).
- 2-8. "Alternatives for Long-Term Management of Defense High-Level Radioactive Waste, Hanford Reservation," ERDA 77-44, Richland, Washington (September 1977).
- 2-9. "Alternatives for Long-Term Management of Defense High-Level Radioactive Waste, Savannah River Plant," ERDA 77-42/1, Aiken, South Carolina (May 1977).
- 2-10. "Alternatives for Long-Term Management of Defense High-Level Radioactive Waste, Idaho Chemical Processing Plant," ERDA 77-43, Idaho Falls, Idaho (September 1977).
- 2-11. "Final Environmental Impact Statement for the Space Shuttle Program," NASA Headquarters, Washington, D.C. (April 1978).
- 2-12. "Space Shuttle", NASA SP407, NASA Headquarters, Washington, D.C. (1976).
- 2-13. "Space Shuttle System Payload Accommodations", NASA/JSC 07700, Volume XIV, NASA/JSC, Houston, Texas (1977).
- 2-14. "NASA Payload Model", JSC 13829, NASA/JSC, Houston, Texas (January 1978).

### 3.0 CHARACTERIZATION OF DEFENSE HIGH-LEVEL WASTE PAYLOADS

Examination of high-level defense waste as a candidate for disposal in space was initiated during this study period. This necessitated a study to determine the relative quantities of this waste which would be available for disposal, and to identify the characteristics of the present waste types and the possibilities of modifying the wastes to be more attractive for disposal in space. This study is complicated by the fact that much desired information, if available, cannot be disclosed openly because of the sensitive nature of the military programs which produced the wastes.

In general, all defense high-level wastes originate as acidic solutions containing fission products and actinide elements from the reprocessing of reactor fuel. At the Hanford and Savannah River sites these solutions have been neutralized and stored in large subsurface storage tanks. At the Idaho site the solutions have been partially separated and the bulk converted to dry oxide powders which are stored in bins.

Section 3.1 discusses the present and possible characteristics of the defense wastes. Section 3.2 deals with the possible modifications for optimization for space disposal, and presents waste compositions used in space disposal. Section 3.3 discusses possible waste forms. Section 3.4 presents the results of preliminary structural, thermal, nuclear shielding, and accident response analyses.

Data generated during the early part of this study which relate to commercial nuclear waste are given in Appendix C.

### 3.1 Defense Nuclear Waste Sources and Character

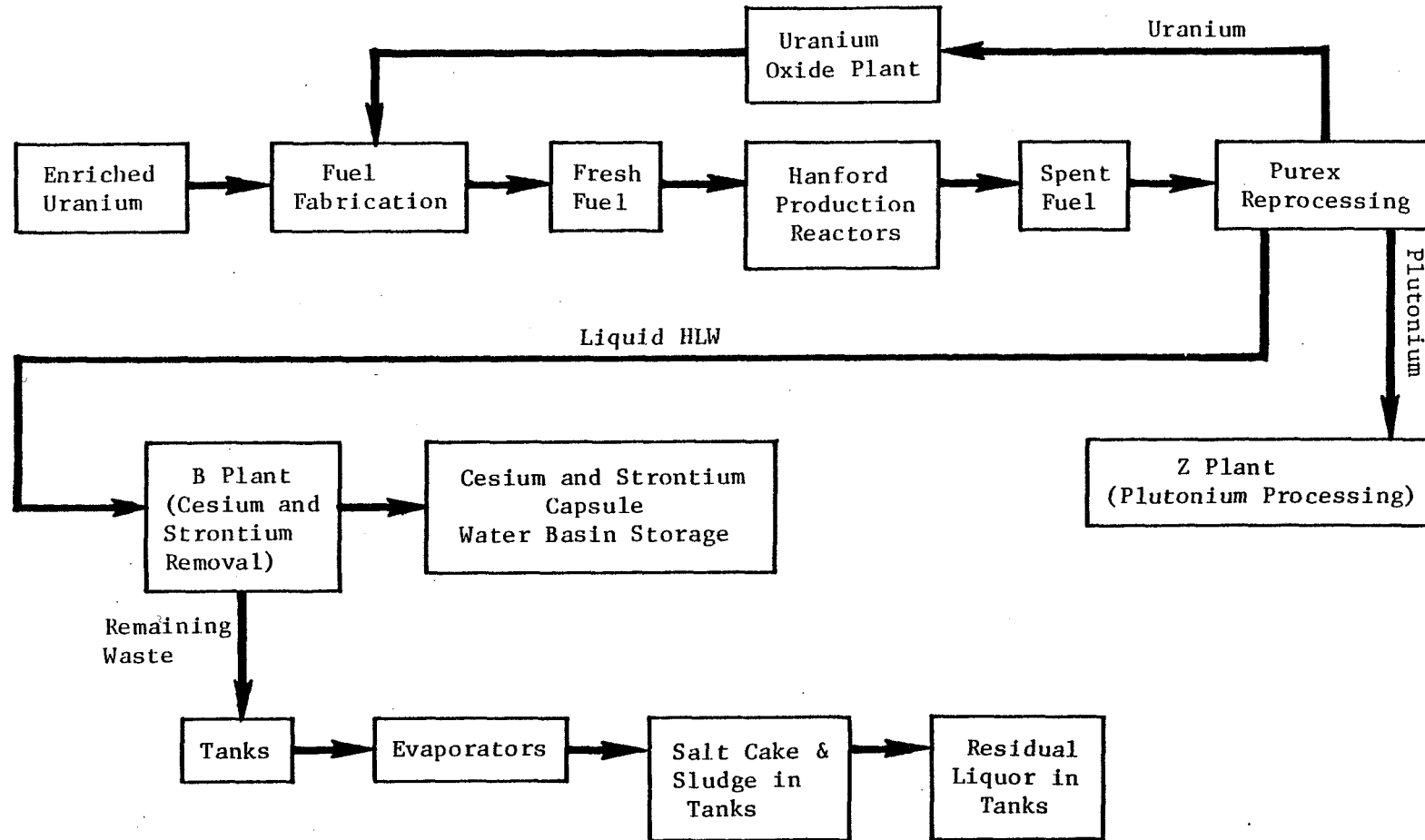
Defense high-level waste (HLW) has been accumulating since the 1940's. This waste results from the reprocessing of plutonium production reactor fuel at the Hanford and Savannah River sites and from the reprocessing of submarine and research reactor fuel at the Idaho site. At the Hanford and Savannah River sites liquid HLW has been neutralized and stored in large in-ground tanks. The result is a waste consisting of sludge, salt cake, and residual liquor. At the Idaho site the liquid HLW is calcined to a powder and stored in in-ground bins as a solid. In general, defense HLW will not generate as much heat or radiation as commercial HLW because of dilution with inert materials and relatively long decay periods.

#### 3.1.1 Hanford Waste

The Hanford site, located near Richland, Washington, has been producing plutonium and other special nuclear materials since 1944. As a result of the reprocessing of irradiated reactor fuels, HLW consisting of fission products, actinides, cladding components and inert chemical additives has been and will continue to be generated and accumulated (see Figure 3-1). Although Purex reprocessing is currently in use, other reprocessing methods have been used in the past. They include the Bismuth Phosphate, Redox, and Tributyl Phosphate processes. Slightly different wastes have been generated by each process. (3-1)

Approximately 55% of the  $^{90}\text{Sr}$  and 70% of the  $^{137}\text{Cs}$ , both high heat-emitting nuclides, have been removed by a fractionization process. These nuclides are subsequently converted to solid strontium fluoride and cesium chloride, and encapsulated in double walled capsules. The remaining waste is stored in tanks as damp salt cake, sludge, and residual liquor. Presently, the defense HLW inventory at the Hanford site consists of:

- $25 \times 10^6$  gallons (bulk) of damp salt cake
- $11 \times 10^6$  gallons (bulk) of damp sludge
- $11 \times 10^6$  gallons of residual liquor
- $3 \times 10^6$  gallons of liquid waste in active processing
- 2900 capsules of  $^{90}\text{Sr}$  or  $^{137}\text{Cs}$ .



3-3

Source: Reference 3-1.

FIGURE 3-1. HANFORD RADIOACTIVE WASTE MANAGEMENT



By 1990, an additional  $1.3 \times 10^6$  gallons of salt cake,  $2 \times 10^5$  gallons of sludge, and  $1 \times 10^6$  gallons of residual liquor will be generated as well as 1080 capsules of Cs or Sr.<sup>(3-1)</sup>

Because of the extremely large amounts of inert materials contained in the HLW, a radionuclide removal process has been proposed with the objective of removing all long-lived nuclides from the salt cake and residual liquor. A considerably smaller quantity of HLW would result plus a large volume of low-level chemical waste which could be disposed of inexpensively. Figure 3-2 shows the radionuclide removal process. The product consists of the washed and dried sludge, technetium concentrate, strontium sludge, and cesium carbonate with a total mass of approximately 16,400 MT, having a total heat output of about 460 kW.<sup>(3-1)</sup>

### 3.1.2 Savannah River Waste

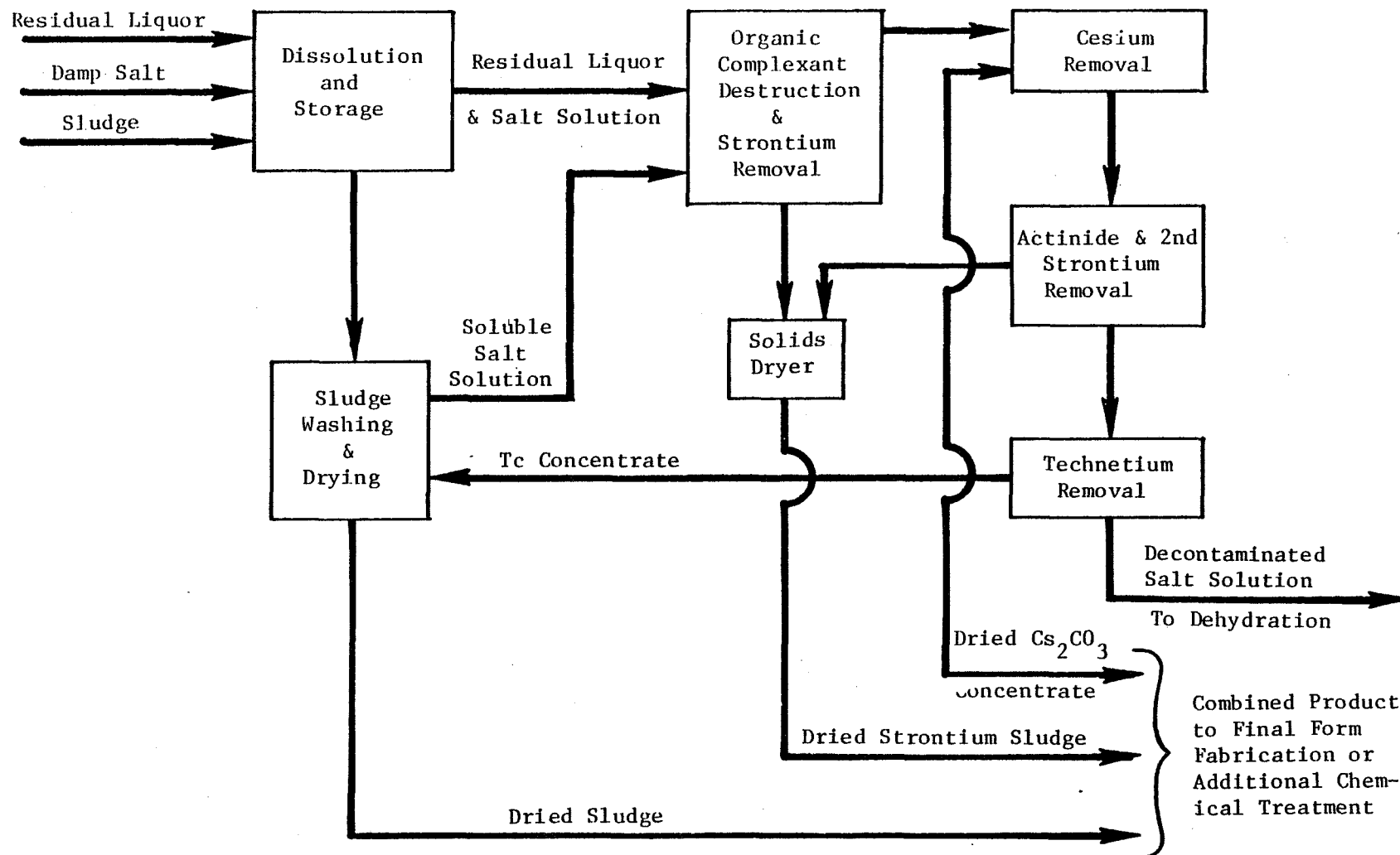
The Savannah River Plant, near Aiken, South Carolina, has been producing special nuclear materials for defense purposes since 1953. Products are mainly plutonium and tritium. HLW, consisting of fission products, actinides, cladding components and inert chemical additives has been and will continue to be generated and accumulated by the reprocessing of spent reactor fuels. In contrast to the Hanford operations, which used several reprocessing methods, all the Savannah River waste is generated by Purex reprocessing. This waste is stored as an alkaline liquid with a precipitated sludge in large underground tanks. After the decay heating has been reduced by the decay of short half-life nuclides, the supernate is converted to salt cake.

By 1985, the Savannah River HLW inventory is expected to consist of:

- $13.3 \times 10^6$  gallons of damp salt cake
- $3.4 \times 10^6$  gallons of sludge
- $5.6 \times 10^6$  gallons of residual liquor.

Additional HLW is expected to be generated annually after that time at a rate of  $1.0 \times 10^6$  gallons/year.<sup>(3-2)</sup>

As in the case of Hanford HLW, the extremely large quantities of inert materials in the Savannah River HLW have encouraged the use of a proposed salt decontamination process (see Figure 3-3). This process is quite similar to the Hanford radionuclide removal process. The product consists of



3-5

Source: Reference 3-1.

FIGURE 3-2. HANFORD RADIONUCLIDE REMOVAL PROCESS

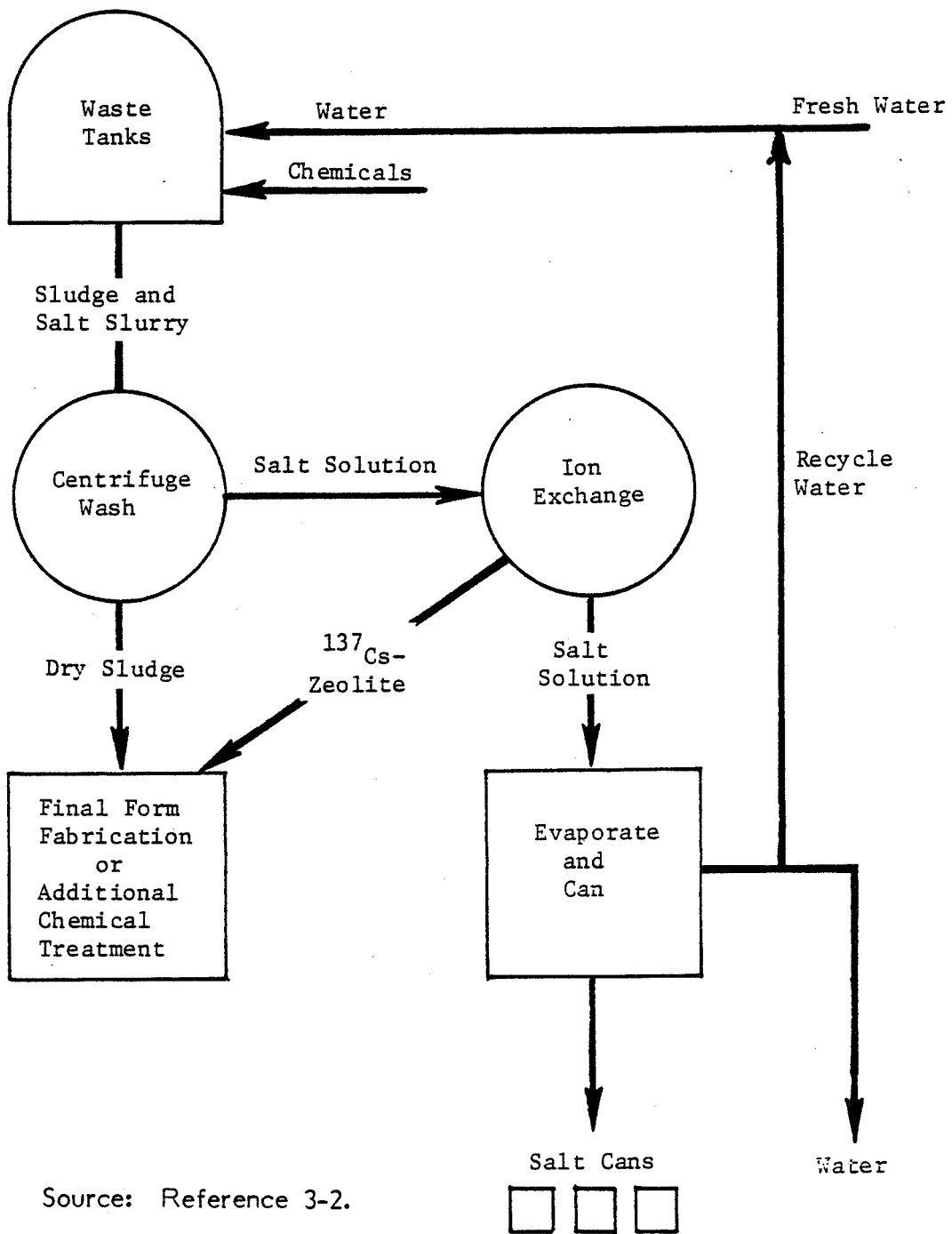


FIGURE 3-3. SAVANNAH RIVER SALT DECONTAMINATION PROCESS

washed and dried sludge, precipitates of plutonium and strontium, and cesium zeolite. The total mass of this product would be 3750 MT, having a total heat output of 1725 kW<sup>(3-2)</sup>. Although this mass is smaller than that produced using the Hanford radionuclide removal process mass, it is nevertheless quite large.

### 3.1.3 Idaho Waste

In contrast to Hanford and Savannah River, the Idaho Chemical Reprocessing Plant near Idaho Falls, Idaho, has been converting liquid HLW to calcine. Calcining is the high temperature treatment of liquid HLW to produce granular solid waste oxides and other solid compounds. Idaho HLW contains fission products, actinides, cladding components, and inert chemical additives, and is produced by several processes.

At the present time, approximately 1500 m<sup>3</sup> of calcine have been produced. As reprocessing and calcine production continue, a total of 8500 m<sup>3</sup> or 11,900 MT of calcine, having a range of heat output (non-decayed) of approximately 1700-4200 kW, is expected by the year 2000.<sup>(3-3)</sup> It is believed this mass can be reduced by a proposed calcine dissolution process to approximately 600 MT. Nitric acid would be used as the solvent to dissolve about 95 percent of the calcine.

### 3.1.4 Summary of Defense Waste Characteristics for Terrestrial Disposal

In summary, defense HLW from the three sites have been characterized for terrestrial disposal in References 3-1, 3-2 and 3-3. The authors of these documents have performed analyses based upon different baseline availability dates (e.g., 1990 for Hanford, 1985 for Savannah River, and 2000 (assuming no decay) for Idaho). These differences must be considered when defining data for detailed container designs for space disposal; however, for this preliminary analysis given here, these data are appropriate. Table 3-1 provides the characteristics of defense HLW for terrestrial disposal of the Hanford, Savannah River and Idaho wastes. Total mass, activity, heating rate, as well as density and specific activity data are given.

TABLE 3-1. CHARACTERISTICS OF DEFENSE HLW  
FOR TERRESTRIAL DISPOSAL

Waste Characteristics	Waste Source		
	Hanford (1990)	Savannah River (1985)	Idaho (2000) <sup>(a)</sup>
Total Mass, MT	16,400	3750	600
Total Activity, Ci	$7.8 \times 10^7$	$3.2 \times 10^8$	$1.3 \times 10^8$ - $1.2 \times 10^9$ <sup>(b)</sup>
Total Heat Generation Rate, kW	460 <sup>(c)</sup>	1725	1700-4200 <sup>(b)</sup>
Density, g/cc	0.7-1.6	0.7-1.6	1.1-1.6
Specific Activity, Ci/kg	4.8	85	216-2000 <sup>(b)</sup>
References	3-1	3-2	3-3

- NOTES: (a) Assuming 8500 m<sup>3</sup> of calcine by the year 2000.  
 (b) Assuming no decay for all calcine. Although no data are available for decayed calcine, it can be expected that the actual radiation and heat levels, by the year 2000, will be approximately 1/10 to 1/20 of those given above for Idaho waste.  
 (c) Assuming that approximately 2/3 of the high heat-emitting elements (Cs and Sr) have been removed from this waste.

## 3.2 Space Disposal Mixes

The previous section illustrated that the mass of defense HLW for space disposal at each of the three sites is quite large. For space disposal, various additional chemical processes could be applied to reduce the combined total mass of waste at the three sites to a more manageable level. This section describes the proposed additional waste processing and the baseline waste mix compositions.

### 3.2.1 Chemical Processing Recommended for Space Disposal

This section describes the postulated chemical processes, generally based on laboratory experiments, which can further reduce the mass of defense HLW.

#### 3.2.1.1 Hanford Waste

As described in Section 3.1.1, the majority of the Hanford waste, after radionuclide removal, is in the form of sludge. The composition of the sludge component of the Hanford waste varies, depending upon the method of chemical processing from which it was derived. There are five major sludges; these are: (1) bismuth phosphate sludge, (2) Redox sludge, (3) nickel-ferrocyanide-strontium sludge, (4) Purex sludge, and (5) zirconium sludge. The average composition of the combined sludges resulting from radionuclide removal processing is shown in Table 3-2. <sup>(3-4)</sup>

TABLE 3-2. AVERAGE COMPOSITION OF MAJOR HANFORD SLUDGES

Component	Mass%	Component	Mass %
H <sub>2</sub> O	1.2	Cr(OH) <sub>3</sub>	1.2
NaNO <sub>3</sub>	14.1	Fe(OH) <sub>3</sub>	7.3
NaNO <sub>2</sub>	0.6	Sr(OH) <sub>2</sub>	0.3
Na <sub>2</sub> CO <sub>3</sub>	10.8	BiPO <sub>4</sub>	2.5
NaOH	0.9	CaCO <sub>3</sub>	2.1
NaAlO <sub>2</sub>	0.3	Na <sub>2</sub> UO <sub>4</sub>	7.9
Na <sub>2</sub> SO <sub>4</sub>	0.1	MnO <sub>2</sub>	1.2
Na <sub>3</sub> PO <sub>4</sub>	2.3	Ni <sub>2</sub> Fe(CN) <sub>6</sub>	2.8
NaF	0.7	P <sub>2</sub> O <sub>5</sub> · 24WO <sub>2</sub> · 44H <sub>2</sub> O	0.1
Cancrinite	16.6	ZrO <sub>2</sub> · 2H <sub>2</sub> O	2.5
Al(OH) <sub>3</sub>	14.2	Sr <sub>3</sub> (PO <sub>4</sub> ) <sub>2</sub>	6.2
Ce(OH) <sub>3</sub>	2.1	NaTi <sub>2</sub> O <sub>5</sub> H (Resin)	0.5

Based on laboratory tests, it may be possible to dissolve the first four sludges in molten caustic followed by treatment with nitric acid.<sup>(3-5)</sup> Such a dissolution would make additional waste concentration possible by removing inert materials from the radionuclide mix.

The gross composition of the first four sludges follows.

Total Mass of Inerts:	15,400 MT
Total Mass of Fission Products:	56 MT
Total Mass of Thorium:	15 MT
Total Mass of Uranium:	908 MT

If these four sludges can be put into solution, Hanford has estimated that 99% of the inert material could be removed. Also, since uranium and thorium do not cause problems for terrestrial disposal, it may be possible, using conventional separation techniques, to remove 95-98% of these elements.

The zirconium sludge, which weighs 318 MT, is insoluble in molten caustic and will require the development of new treatment methods to achieve significant inert removal.<sup>(3-5)</sup>

The total mass of Hanford waste to be carried to space, assuming the application of the chemistry described above, is as follows:

154 MT	Inert material
66 MT	Fission product oxides of the form $M_2O_3$ at an average molecular mass of 130
0.3-0.8 MT	Thorium at 95-98% removal
21-52 MT	Uranium at 95-98% removal
3-14 MT	Isolated products from salt cake and liquor
<u>?-318 MT</u>	Part or all of zirconium sludge.
244 MT (+ Zr fraction) - 605 MT	

605 MT is the baseline for Hanford space waste disposal. As suggested by Hanford personnel, the above reductions depend on the development of acid-based separation chemistry. (3-5)

### 3.2.1.2 Savannah River Waste

As shown in Section 3.1.2, the major component of Savannah River waste, after salt decontamination, is sludge. The sludge has been produced by the Purex process; however, two major types exist: high iron and high aluminum sludge. Table 3-3 shows the composition of these two types of sludge. (3-6)



TABLE 3-3. SAVANNAH RIVER F- AND H-AREA HIGH-HEAT SLUDGE COMPOSITE COMPOSITIONS

	F Area Composite	H Area Composite	Overall Composite
Sludge Sampled, gal	317,000	1,049,000	1,366,000
Total Sludge, percent	73.0	80.1	78.4
Sludge Sampled, percent	23.2	76.8	100.0
Principal Elements, mass %			
Fe	15.3	13.62	14.0
Al	2.34	19.50	15.5
Mn	2.96	4.50	4.14
U	5.54	2.58	3.27
Na	3.22	2.03	2.31
Ca	1.06	1.59	1.47
Hg	0.163	1.83	1.44
Ni	3.25	0.507	1.14
C	11.9	-	2.76
Si	2.29	0.221	0.701
Principal Anions, mass %			
NO <sub>3</sub>	1.14	1.08	1.09
NO <sub>2</sub>	0.079	0.09	0.087
SO <sub>2</sub>	14.31	1.72	4.64
PO <sub>2</sub>	0.134	1.22	0.97

Source: Reference 3-6.

Personnel contacted at Savannah River have indicated that inert removal from the sludge is possible.<sup>(3-7)</sup> This could be accomplished by successive washing with caustic, to remove aluminum, and with oxalic acid, to remove iron. Estimates indicate that a 90% reduction in sludge mass may be achievable. This process is not designed to dissolve the sludge as is the case for the Hanford process. This would result in 360 MT of sludge plus 15 MT from the concentration of cesium zeolite from salt decontamination, or a total of 375 MT as a baseline for space disposal.

Since washing of the sludge with caustic and oxalic acid actually constitutes sludge dissolution, the wash would have to be decontaminated and the dissolved radionuclides returned to the sludge radionuclide inventory. If total sludge dissolution and cesium zeolite concentration are possible for the Savannah River waste, perhaps additional mass reduction could be achieved.

### 3.2.1.3 Idaho Waste

The Idaho waste volume will total 8500 m<sup>3</sup> of calcine powder granules, with a mass of approximately 11,900 MT by the year 2000. Five major types of calcine exist based on the nature of reprocessing used for HLW generation; they are:<sup>(3-8)</sup>

Type	Volume (Year 2000)
1. Alumina	500 m <sup>3</sup>
2. Zirconia	1000 m <sup>3</sup>
3. Zirconia-Sodium Blend	1300 m <sup>3</sup>
4. Fluorinel	5500 m <sup>3</sup>
5. Electrolytic	200 m <sup>3</sup>
Total	8500 m <sup>3</sup>

Typical calcine compositions are given in Table 3-4.<sup>(3-8)</sup>

**TABLE 3-4. CALCINE COMPOSITIONS FOR IDAHO WASTE**

Component	Calcine Type, percent				
	Alumina	Zirconia	Zirconia-Na Blend (3:1)	Fluorinel	Electrolytic
Al <sub>2</sub> O <sub>3</sub>	89	20	20	17	65
Fe <sub>2</sub> O <sub>3</sub>	-	-	-	-	10
Na <sub>2</sub> O	2	-	5	-	1
ZrO <sub>3</sub>	-	21	17	15	-
NO <sub>3</sub>	1-3	1-3	7-10	1-4	3-5
CaF <sub>2</sub>	-	50-55	37	55	1
B <sub>2</sub> O <sub>3</sub>	1-2	1-2	1	3	1
SO <sub>2</sub>	-	-	-	-	-
PO <sub>4</sub>	-	-	2	-	-
SO <sub>4</sub>	-	-	6	4	10
CdO	-	-	-	-	-
Gd <sub>2</sub> O <sub>3</sub>	-	-	-	-	6
Fission Products and Actinides	0.6	0.6	0.4	0.5	0.5
Other	1-3	1-3	3	-	3

Source: Reference 3-8.

To concentrate these calcined wastes to the point where they could be disposed of in space, they must be dissolved. Dissolution chemistry is not difficult and has been under development as part of the Idaho actinide and lanthanide partitioning scheme.<sup>(3-8)</sup> Approximately 95% of the calcine can be dissolved with 8M  $\text{HNO}_3$ . The residual material can be almost completely dissolved in molten  $\text{NaHSO}_4$ .<sup>(3-9)</sup>

The mass of remaining radionuclides would be approximately 60 MT plus a small amount of residual inert material. If actinide and lanthanide partitioning is considered feasible and necessary, the quantity of radionuclides may be reduced to 20 MT or less. At this time, 60 MT is considered as the baseline for Idaho waste for space disposal; however, since this material is essentially 100% radionuclides, it will generate considerably more heat and radiation than the Hanford or Savannah River baseline waste compositions. The Idaho mix could be tailored to about the same composition as Hanford and Savannah River waste by leaving a portion of inert material in the waste. Separate shielding and cooling packages must be designed if the 100% radionuclide waste mix is chosen for Idaho. Work cannot proceed on this option, however, until detailed radionuclide compositions are available from Idaho.

### 3.2.2 Baseline Composition for Space Disposal

This section describes the radionuclide and chemical composition of the defense HLW, for each of the three sites, as baselined for space disposal (see Section 2.4.2).

#### 3.2.2.1 Hanford Waste

After the chemical treatment postulated in Section 3.2.1.1, the Hanford HLW would consist of: insoluble compounds of Al, Fe, Cr, and Zr; U and Th compounds remaining after separation of the majority of these elements; fission products; and actinides. The radionuclide composition of Hanford HLW, based on a 5500-kg waste payload, and decayed to the year 1990, is shown in Table 3-5.

TABLE 3-5. BASELINE RADIONUCLIDE COMPOSITION OF HANFORD WASTE PAYLOAD (1990 DEFINITION)

Nuclide	Activity, Ci	Mass, kg	Nuclide	Activity, Ci	Mass, kg
<sup>90</sup> Sr	4.1 E+05	3.0 E+00	<sup>147</sup> Pm	9.5 E+03	9.8 E-03
<sup>93</sup> Zr	6.5 E+01	1.6 E+01	<sup>151</sup> Sm	1.3 E+04	5.1 E-01
<sup>99</sup> Tc	3.0 E+02	1.7 E+01	<sup>152</sup> Eu	1.4 E+01	7.9 E-05
<sup>106</sup> Ru	7.0 E-01	2.1 E-07	<sup>154</sup> Eu	7.0 E+02	4.6 E-03
<sup>107</sup> Pd	5.4 E-01	1.1 E+00	<sup>155</sup> Eu	7.3 E+02	5.1 E-04
<sup>113m</sup> Cd	4.9 E+01	2.1 E-04	<sup>233</sup> U	1.9 E-01	2.0 E-02
<sup>121m</sup> Sn	1.0 E+00	1.7 E-06	<sup>235</sup> U	6.0 E-03	2.8 E+00
<sup>126</sup> Sn	6.2 E-01	2.2 E-02	<sup>238</sup> U	1.4 E-01	4.2 E+02
<sup>125</sup> Sb	1.9 E+02	1.3 E-04	<sup>237</sup> Np	9.5 E-01	1.4 E+00
<sup>129</sup> I	4.3 E-01	2.7 E+00	<sup>238</sup> Pu	3.8 E+00	2.2 E-04
<sup>134</sup> Cs	6.2 E+00	5.1 E-06	<sup>239</sup> Pu	2.0 E+02	3.3 E+00
<sup>135</sup> Cs	2.3 E+00	1.8 E+00	<sup>240</sup> Pu	4.9 E+01	2.1 E-01
<sup>137</sup> Cs	2.6 E+05	3.0 E+00	<sup>241</sup> Pu	5.4 E+02	4.9 E-03
<sup>144</sup> Ce	8.1 E-02	2.7 E-08	<sup>241</sup> Am	4.6 E+02	1.4 E-01
			Total	7.0 E+05	4.7 E+02

NOTE: Based on a 5500-kg waste payload (the remaining mass is inert material).

### 3.2.2.2 Savannah River Waste

Assuming the chemical treatment given in Section 3.2.1.2, the Savannah River HLW would consist of: insoluble compounds of Al, Fe, and Mn; uranium compounds; fission products; and actinides. The baseline radionuclide composition of fresh Savannah River HLW, as based on a 5500-kg waste payload, is shown in Table 3-6. The radionuclide composition of the Savannah River HLW, based on an initial quantity of  $22.3 \times 10^6$  gal of salt cake, sludge, and liquor before chemical treatment, and on a 5500-kg waste payload is shown in Table 3-6 for fresh waste. It should be noted that several of the nuclides listed in Table 3-6 will have decayed to insignificant levels by the 1985-1990 time period. These include: <sup>89</sup>Sr, <sup>91</sup>Y, <sup>95</sup>Zr, <sup>95</sup>Nb, <sup>103</sup>Ru, <sup>127</sup>Te, <sup>129</sup>Te, and <sup>141</sup>Ce. A partial radionuclides list for Savannah River HLW indicates that actual payload

activities at that time may be approximately 1/15 of that for fresh waste as listed in Table 3-6. A more complete radionuclide composition table showing activities decayed to 1985 will need to be incorporated into subsequent space waste disposal studies as that information becomes available.

TABLE 3-6. BASELINE RADIONUCLIDE COMPOSITION OF SAVANNAH RIVER WASTE PAYLOAD (FRESH WASTE)

Nuclide	Activity, Ci	Mass, kg	Nuclide	Activity, Ci	Mass, kg
<sup>79</sup> Se	3.3 E-00	5.1 E-02	<sup>144</sup> Ce	3.2 E+05	1.0 E-01
<sup>89</sup> Sr	5.8 E+04	4.1 E-01	<sup>144</sup> Ce - <sup>144</sup> Pc	2.3 E+07	7.1 E+00
<sup>90</sup> Sr	9.9 E-05	7.0 E+00	<sup>147</sup> Pm	4.0 E+06	4.1 E+00
<sup>91</sup> Y	1.5 E+07	6.2 E-01	<sup>151</sup> Sm	2.5 E+04	1.0 E+00
<sup>93</sup> Zr	3.3 E+01	8.2 E+00	<sup>152</sup> Eu	6.7 E-02	3.7 E-07
<sup>95</sup> Zr	2.0 E+07	9.4 E-01	<sup>154</sup> Eu	3.3 E+01	2.3 E-04
<sup>95</sup> Nb	5.1 E+05	1.3 E-01	<sup>158</sup> Tb	2.0 E-02	8.8 E-06
<sup>99</sup> Tc	1.7 E+02	9.6 E+00	<sup>233</sup> U	6.6 E-01	7.0 E-02
<sup>103</sup> Ru	3.2 E+06	1.0 E-01	<sup>235</sup> U	9.8 E-03	4.6 E+00
<sup>106</sup> Ru	1.3 E+06	3.9 E-01	<sup>238</sup> U	2.0 E-01	5.9 E+02
<sup>107</sup> Pd	1.7 E-01	3.5 E-01	<sup>237</sup> Np	1.3 E-01	1.9 E-01
<sup>126</sup> Sn - <sup>126</sup> Sb	3.4 E+00	1.2 E-01	<sup>238</sup> Pu	3.4 E+03	2.0 E-01
<sup>127</sup> Te	6.6 E+05	2.5 E-04	<sup>239</sup> Pu	9.8 E+01	1.6 E+00
<sup>129</sup> Te	6.7 E+05	3.1 E-05	<sup>240</sup> Pu	2.0 E+01	8.8 E-02
<sup>129</sup> I	3.2 E-01	2.0 E+00	<sup>241</sup> Pu	6.6 E+02	5.8 E-03
<sup>135</sup> Cs	1.3 E+01	1.0 E+01	<sup>242</sup> Pu	2.0 E-02	5.1 E-03
<sup>137</sup> Cs	9.6 E+05	1.1 E+01	<sup>241</sup> Am	3.2 E+02	1.0 E-01
<sup>141</sup> Ce	4.0 E+06	1.4 E-01	<sup>244</sup> Cm	3.3 E+02	4.0 E-03
			Total	7.9 E+07	6.6 E+02

NOTE: Based on a 5500-kg waste payload (the remaining mass is inert material).

### 3.2.2.3 Idaho Waste

If the chemical processing given in Section 3.2.1.3 is assumed, the Idaho HLW will consist primarily of fission products and actinides with small quantities of inert materials. The radionuclide composition of Idaho HLW is not well known at this time. Sampling and analysis is presently underway but results are not expected for some time. There is only fair agreement between Idaho sources of information on radionuclide composition. <sup>(3-3,3-8)</sup> Table 3-7 presents limited radionuclide composition data for the Idaho waste.

**TABLE 3-7. ESTIMATED IDAHO CALCINE RADIONUCLIDE COMPOSITION**

Radionuclide	Specific Activity, Ci/kg	Maximum Quantity of Radionuclide, kg
<sup>90</sup> Sr	3-15	1250
<sup>137</sup> Cs	3-18	2450
<sup>144</sup> Ce	1-38	140
<sup>106</sup> Ru	0.1-1	35
Others	4-25	?
Total Transuranics	$2 \times 10^{-2}$	?
<sup>239</sup> Pu	$4 \times 10^{-4}$	?

Source: Reference 3-8.

### 3.3 Waste Forms for Space Disposal

Final waste forms acceptable for space disposal must have high waste loadings to make efficient use of each flight. This requirement practically eliminates the consideration of several final forms (e.g., glass), which have relatively low waste loadings. Final waste forms suitable for space disposal of defense HLW include calcine, compartmented calcine, and metal matrix forms. Other possible forms include coated particles, supercalcine, calcined clay ceramics, and sintered glass ceramics. The following sections discuss the processes required to fabricate the final forms mentioned above and the properties of each waste form.

#### 3.3.1 Chemical Processing

The previous study, "Preliminary Evaluation of the Space Disposal of Nuclear Waste",<sup>(3-10)</sup> describes the four main processes for producing calcine, and the processes required to produce supercalcine, coated particles, and metal matrix. Detailed descriptions of these processes are not given in this report; however, a few comments are in order. Calcine production is well proven and reasonably simple. Supercalcine and metal matrix production are more complex than calcine production. Coated particle production is very complex in comparison to calcine production and should not be considered unless all other processes appear untenable.

Compartmented calcine is the term used to describe calcine enclosed in small stacked metal containers or in metal "egg crate" spacers which would be sealed on each end. Although no experience exists in fabricating such a waste form, it seems relatively straightforward using conventional metalworking and automated container loading equipment.

Calcined clay ceramics are formed by mixing the dried powdered product of chemical separations postulated in Section 3.2.1 with clay and water and firing at high temperature.<sup>(3-1)</sup> Waste loadings of 50-70% appear possible based on laboratory experience.

Sintered glass ceramics are produced by sintering a mixture of calcine and flux or frit. In this process, calcine, flux and water are fed to a mixer-feeder. Water acts as a binder and lubricant and minimizes dusting. The

mix is then pressed into a thin-walled container at low pressure in the shape of a thin disk and sintered at 1000<sup>o</sup> C for 4 to 6 hr. Sintering causes additional densification. After cooling, disks can be stacked in a storage container.<sup>(3-3)</sup>

### 3.3.2 Physical Properties and Characteristics

High waste loading, low dispersibility, and thermal stability are the primary requirements for a suitable waste form. Each waste form listed above has advantages and disadvantages peculiar to itself.

Calcine has the highest waste loading. Since high waste loading is of prime importance for efficient space disposal, calcine rates highest in this area. Calcine powder can be pressed into pellets or other shapes to decrease dispersibility; however, dispersibility will always be a problem. Leach rates (dissolution rates) of calcine will be higher than for any other waste form. Dispersibility and solubility can be lessened to a large extent by carefully engineered safety features such as impact absorbers, thermal shielding, flotation devices, etc. Ground transportation can be accomplished safely by the use of heavy walled shipping casks. Although calcine is a desirable waste form because of its high waste loading, it does have problems (such as high dispersibility and poor thermal stability) which should not be underestimated. Calcine is the waste form baseline at this time.

The compartmented calcine waste form has been postulated as a means of providing additional safety when using a calcine. Calcine encased in small stacked metal containers or "egg crate" spacers sealed on each end may possibly provide leach resistance and low dispersability sufficient to mitigate the effects of most credible accidents. While such a concept sounds useful, it is important to note that fabrication and testing of compartmented calcines have never been attempted. A major consideration is the weight penalty associated with the use of metal compartments.

Metal matrix waste forms possess several attractive characteristics: waste loading is relatively high (60-70%); leach rate is low; thermal conductivity is excellent; and the dispersibility potential is low. Although metal matrix waste forms are not currently in vogue in the United States, a great deal of work on this type of waste form has been done in Belgium, Germany and France. As in the case of compartmented calcine, the weight penalty associated with metal may be a problem.



Supercalcine has a lower leach rate than calcine, but is still dispersible. Waste loading is relatively high, approximately 70%. Supercalcine offers better thermal stability than calcine but the waste loading is lower than calcine.

Calcined clay ceramics and sintered glass ceramics are fairly similar. Both forms have relatively high waste loadings (50 to 70%) and produce a solid with much lower leach rate and dispersibility than calcine. Both processes require further development. Based on the scant data available, it appears that sintered glass ceramics may be somewhat less dispersible and more leach resistant than calcined clay ceramics. Neither one of these forms appears to be as good as metal matrix forms.

### 3.4 Containerization Systems

The space disposal of high-level nuclear waste requires that the payload primary container maintain its integrity during both the expected normal and the defined accident environments. Unlike the transportation regulations for terrestrial shipment of nuclear materials, there are no definitions of either the normal, or accident conditions of space disposal. Consequently, before the containerization analysis began, it was necessary to have the various payload environments defined. (Section 5.1 identifies and characterizes the various accident environments that might be expected during the space portion of the disposal mission.) In this preliminary study, the emphasis of the analytical effort was placed upon the payload response to the various accident environments, although the effects of normal environments were used to initially define the payload container package.

No quantitative assessment of accident risks and probabilities is feasible at this stage of development. However, several accident conditions covering a range of probabilities have been considered (see Section 5.1). Of these, the most severe chosen for analysis here were:

- Explosion and fire on launch pad
- Reentry of an unprotected payload container.

The primary container design is dominated by the character of its contents, the high-level waste. Table 3-8 lists the baseline high-level waste payload characteristics for each of the three waste mixes. Most of the data shown in this table are based upon Tables 3-5, 3-6 and 3-7. The actual density of the defense waste form is still speculative. The value of 2.8 g/cc, as indicated in Table 3-8, was computed based upon the theoretical densities of the component oxides from two compositions of synthetic sludges.<sup>(3-11)</sup> Typically, a value of two-thirds the theoretical density is attainable, resulting in 2.8 g/cc as a best estimate. Figure 3-4 provides the definition of waste concentration factor (WCF) for each of the three defense waste sites. The number of 5500-kg payloads required to dispose of waste from each of the sites is given as a function of WCF. The baseline "desired high model" (see Table 2-3) is given by the circles; the more optimistic case, the "desired low model" is given by the squares.

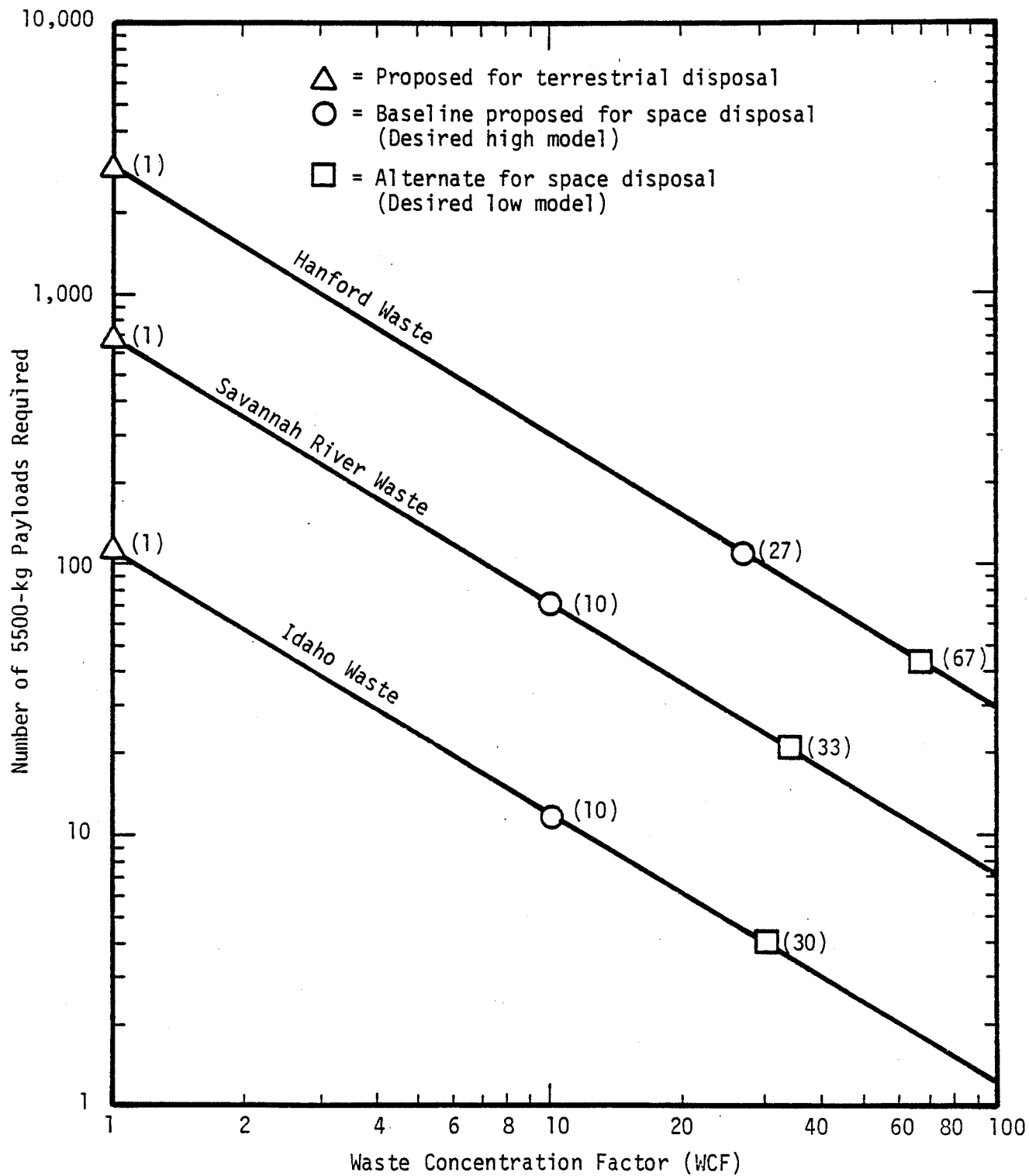


FIGURE 3-4. TOTAL NUMBER OF PAYLOADS AS A FUNCTION OF DEFENSE WASTE CONCENTRATION FACTOR (WCF)

Most of the analyses performed in the following sections are based upon Hanford waste. Although both Savannah River and Idaho baseline waste compositions have higher internal heat generation than does Hanford, the analyses in this section are based on Hanford waste because of its greater mass.

**TABLE 3-8. BASELINE HIGH-LEVEL DEFENSE WASTE PAYLOAD CHARACTERISTICS**

Parameter	Hanford	Savannah River	Idaho
Disposal Reference Date	1990	1985	2000
Waste Density, g/cc	2.8	2.8	2.8
Waste Radius, cm	78	78	78
Waste Activity, Ci	$7 \times 10^5$	$7.9 \times 10^7$	-
Radionuclide Mass, kg	470	660	-
Inert Mass, kg	5030	4840	-
Waste Concentration Factor (WCF) <sup>(a)</sup>	27	10	10
Specific activity, Ci/kg	$1.5 \times 10^3$	$1.2 \times 10^5$	-
Heat Generation, kW	4.34 <sup>(b)</sup>	25 <sup>(c)</sup>	-

- NOTES: (a) The waste concentration factor is defined as the ratio of the masses given for each defense waste site, as recommended for terrestrial disposal, to the mass of the waste for space disposal after further chemical concentration (see Figure 3-4).
- (b) Based upon ORIGEN computer calculations using data in Table 3-5.
- (c) Based on mass reduction (WCF = 10) and heat generation rate for Savannah River waste in Table 3-1.

#### 3.4.1 Shielding Analysis

This section presents the results of the shielding analysis performed for the baseline container. This analysis was performed by first obtaining the radiation source strength using the ORIGEN<sup>(3-12)</sup> computer code. This code

predicts the generation of fission products and the transmutation of isotopes through neutron reactions and decay. The input nuclide quantities were taken from Table 3-5. The Savannah River and Idaho waste were not considered in this preliminary analysis because of their smaller quantity. The resulting gamma source strength for Hanford is shown in Table 3-9.

TABLE 3-9. PHOTON SOURCE STRENGTH SPECTRUM FOR HANFORD WASTE (WCF = 27)

Mean Group Energy MeV	Source Strength, photons/sec per MT of Waste
0.30	8.93 E14
0.63	9.22 E15
1.10	5.26 E13
1.55	6.72 E12
1.99	2.01 E11
2.38	7.91 E7
2.75	6.23 E6
3.25	1.98 E5
Total	1.02 E16

The neutron source strength for defense waste as predicted by the ORIGEN code is several hundred to several thousand times smaller than the typical commercial reactor waste source. Since the neutron dose is a secondary contributor for even commercial high-level waste designs, it was ignored for defense waste.

The ANISN<sup>(3-13)</sup> shielding code was used to compute the gamma dose from the waste container (using the ORIGEN output), and thereby determine the shielding requirements.

ANISN is a computer program written in FORTRAN IV. It solves the one-dimensional Boltzmann transport equation with general anisotropic scattering for slab, cylindrical, and spherical geometries using discrete ordinates and the diamond difference solution technique. ANISN is well suited for solving problems of deep penetration of both gamma radiation and neutrons such as encountered in shield design.

The shielding thicknesses required, assuming a uranium only shield, a steel only shield, and a uranium shield including 2.54 cm of steel (represents the

baseline case), were determined as a function of source strength. Figure 3-5 shows the relationship between the thickness of a particular shield required to maintain the dose of 2 rems per hour at one meter from the shield surface and the concentration factor for Hanford defense waste. For the baseline case (Hanford waste, WCF = 27), the uranium shielding thickness is 2.85 cm. The baseline shielded container design is shown in Figure 3-6. The steel wall thicknesses shown were chosen as typical values. For purposes of steady-state thermal and shielding analysis, the amount of steel present is not a major factor. Detailed structural analyses are necessary to determine more realistic wall geometry.

The significance of the shield thickness (other than to minimize exposure) is in its effect on the payload launch mass. The expected masses of the waste payload, less the reentry system and other supporting systems, are given in Table 3-10 for various waste concentration factors.

**TABLE 3-10. CONTAINER AND SHIELDING MASSES FOR VARIOUS WCF VALUES, ASSUMING HANFORD WASTE\***

Payload Component	Waste Concentration Factor (WCF)	Mass, kg
Waste	-	5500
Container	-	770
Shielding		
Steel Cladding	1	819
	27	836
	67	842
Uranium	1	1742
	27	4448
	67	5376
Total (waste, container, and shield)	1	8831
	27	11,554
	67	12,488

\*NOTE: Excludes reentry system.

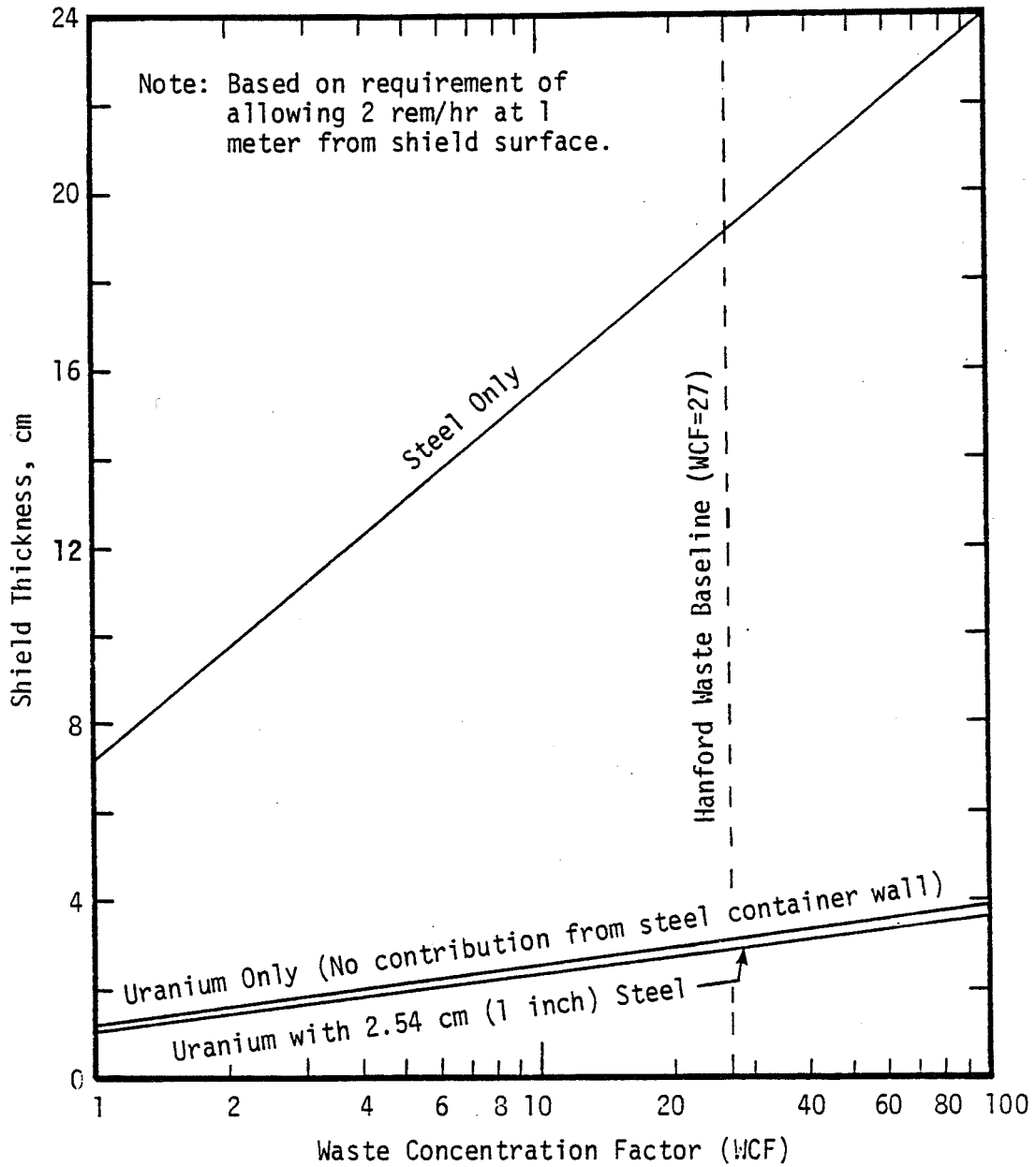


FIGURE 3-5. SHIELD THICKNESS REQUIREMENTS AS A FUNCTION OF WASTE CONCENTRATION FACTOR FOR HANFORD WASTE

For the baseline mission, Table 3-10 shows that the mass of the waste, shielding, and container, is about 11,500 kg. Since the Space Shuttle capability for the baseline disposal mission is expected to be 29,500 kg (65,000 lb),<sup>(3-14)</sup> the total mass of the reentry system, pallet, ejection system, cooling system and other systems would be limited to 18,000 kg (39,700 lb), assuming no landing limit constraint. With a landing limit of 14,500 kg (32,000 lb), these systems would be limited to 9,200 kg (20,300 lb). If the appropriate limit could not be met, then the size of the waste payload, given WCF = 27, would have to be reduced.

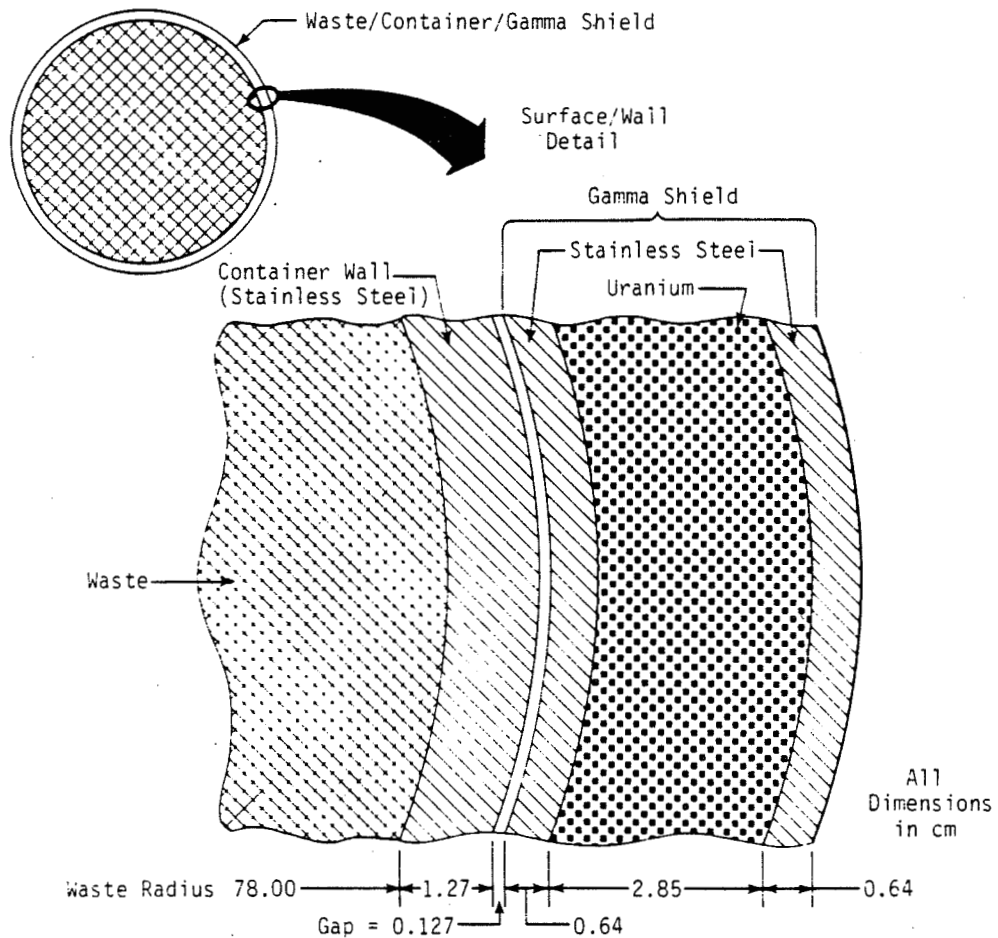


FIGURE 3-6. BASELINE SHIELDED CONTAINER DESIGN FOR HANFORD WASTE (WCF = 27)



### 3.4.2 Thermal Analysis

In an earlier study for commercial nuclear waste disposal in space,<sup>(3-10)</sup> the long-term deep space environment was identified as the principal factor in determining the design characteristics of the primary payload container (see Figure 3-6). All other normal conditions were of short duration, relative to final disposal, so as to be handled by additional design features (e.g., auxiliary cooling and shielding, and reentry protection.) Therefore, the payload performance must remain within design limits based upon the deep-space environment. Prior to launch, some of these limits can be exceeded for other normal conditions of short duration.

A one-dimensional thermal analysis of the high-level waste container design was applied to the more critical environmental conditions. The analysis was parametric with the Hanford waste concentration factor as the major variable. A spherical geometry was chosen for the container, as it is the current baseline (see Figure 3-6), and since temperatures are not strongly dependent upon wall construction.

Before analyses were completed, several candidate materials were considered for the container, gamma shield, and reentry system design. The waste form is discussed more fully in Section 3.3. The waste container must provide protection during high stress and corrosive environments. Consequently, typical pressure vessel steels including stainless were considered along with materials such as niobium and titanium. Stainless steel was selected for preliminary designs.

Shielding materials available are lead, steel, and depleted uranium. The most efficient, on a weight basis, is uranium.

No materials development is expected to be necessary for the selection of reentry system materials. Typical designs include stainless steel shell, Min-K insulation, and ATJ-graphite material as the heat shield. The addition of a steel honeycomb as an impact absorbing device was also considered.

The materials assumed for waste, container and shielding systems and the reentry system are listed below:

- Calcined Waste - maximum density of 2.8 g/cc for all processed defense wastes
- Stainless Steel Container
- Depleted Uranium Gamma Shield

- Reentry System - including stainless steel shells, steel honeycomb, insulation, and ablative material.

The maximum allowable temperature of the waste form is a critical parameter in the thermal analysis. For calcined waste, the selected baseline waste form, the allowable temperature should be limited to less than the temperature at which the calcine is formed. Calcines are formed at temperatures up to 900 C.<sup>(3-10)</sup> However, for conservatism, a temperature limit of 700 C was assumed to maintain a stable product. Similar limits for other waste forms are listed below:

Metal matrix (aluminum base)	300-600 C
Supercalcine	900 C
Coated particles	900-1100 C
Glass	350-550 C

The TRUMP<sup>(3-15)</sup> computer program, a recognized code for both steady-state and transient thermal analysis, was used to determine steady state temperature distributions. In earlier studies<sup>(3-10)</sup>, the effects of variation of thermal input properties were examined. For the final waste form and concentration, most of the thermal data can be considered constant for preliminary analysis. Table 3-11 lists the input data used for the thermal analyses.

TABLE 3-11. SPACE DISPOSAL HEAT TRANSFER INPUT PROPERTY DATA

	Waste	Container	Gamma Shield	Reentry System		
				Insulation	Ablation	Impact
Material	Calcine-HLW	304 SS	Depleted Uranium	Min-K	ATJ Graphite	Steel Honeycomb
Specific heat, W-hr/kg- C	0.20	0.13	0.03	0.21	0.17	0.13
Conductivity, W/m- C	0.52*	16.2	24.2	0.052	70.6	16.2
Density, g/cc	2.8	7.8	11.3	0.32	1.9	0.78
Surface Emissivity	-	0.7	-	-	0.7	-

\*NOTE: This is an estimated value for compacted calcine based on values for powder of 0.2 to 0.3 W/m-C (Reference 3-16).

The initial analysis examined the influence of the waste concentration factor upon payload temperature gradient ( $\Delta T$ ).  $\Delta T$  is defined as the difference in temperature between the center and outer surface of the spherical waste payload. A graphical representation of waste  $\Delta T$  versus waste concentration factor is shown in Figure 3-7. The straight line indicates the temperature gradient for Hanford waste. The curved line marked "Deep Space" intersecting the  $\Delta T$ -line for the payload represents the limiting condition for the waste based on the assumed maximum allowable temperature of 700 C. The intersection of this curve with the  $\Delta T$ -line indicates the limiting condition for Hanford waste with no auxiliary cooling or internal cooling fins. The intersection occurs at a waste concentration factor (WCF) of 35 for Hanford waste. For WCF values greater than 35, this limit would be exceeded. Auxiliary passive cooling, a higher waste thermal conductivity (including consideration of a metal matrix waste form), cooling fins, or the consideration of a higher allowable maximum temperature are examples of design options that would be required for this case.

Similar curves could be plotted based on the launch pad environment. However, since the long-term environment of deep space was assumed to have the major influence on the waste container design, the launch pad conditions were examined only insofar as they make further demands on the container design. Obviously, without auxiliary cooling, a container design optimized to maintain waste temperatures in deep space will not do so in an Earth environment. However, as is shown in Table 3-12, any design suitable for deep space environment can be actively maintained on Earth.

The actual temperature distributions for the waste payload and reentry system for both "deep space" and "launch pad" environments are shown in Table 3-12 for various Hanford WCF values. The auxiliary cooling requirements are included whenever the waste center temperature limit is exceeded. A nominal gap  $\Delta T$  is included to represent the interface between the waste container and radiation shield. However, with the typical values listed, the auxiliary cooling required can adequately maintain the waste and container wall temperatures below their limits while cooling the shield surface. At higher heat generation rates (WCF > 40), it may be necessary to cool the container wall directly because of the poor conductance of the gap.

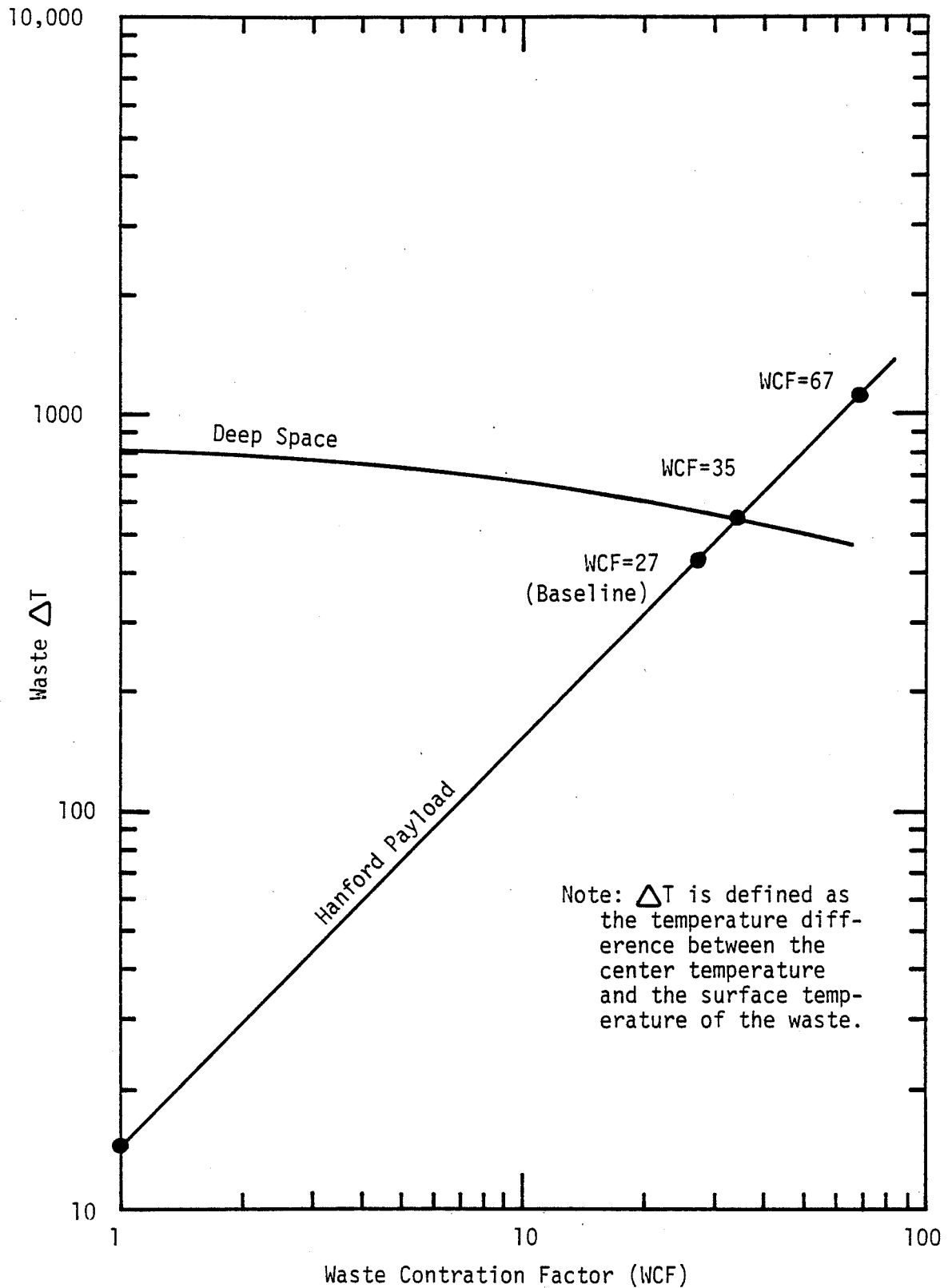


FIGURE 3-7. WASTE AND MAXIMUM "DEEP SPACE" TEMPERATURE GRADIENTS AS A FUNCTION OF WASTE CONCENTRATION FACTOR FOR HANFORD HIGH-LEVEL WASTE

TABLE 3-12. PAYLOAD TEMPERATURE DISTRIBUTIONS FOR THE HANFORD DEFENSE WASTE AS A FUNCTION OF WASTE CONCENTRATION FACTOR

Defense Waste Concentration Factor(WCF)	Payload Heat Generation, kW	Shielding Auxiliary Cooling Required, kW	Payload System Element Temperature, C			
			Waste Center	Container	Shield	Reentry System
Launch Environment at 21 C						
1	0.16	0.0	59	44	43	23
27 (Baseline)	4.34	2.64	700 <sup>(b)</sup>	277	248	48
40 <sup>(a)</sup>	6.51	6.51	700	64	21	21
Deep Space Environment at -273 C						
1	0.16	-	-176	-191	-	-
27 (Baseline)	4.34	-	544	118	-	-
67	10.85	-	1286 <sup>(c)</sup>	218	-	-

- NOTES: (a) For greater WCF values, auxiliary cooling requirements equal heat generation, but waste requires direct cooling.  
 (b) Assumed maximum normal operating limit achieved by auxiliary cooling.  
 (c) This condition would be unacceptable; cooling fins, metal matrix waste form or a smaller payload would be required to reduce this temperature to the acceptable level.

The following paragraphs discuss the effects of temperature limits on the waste container design for the various mission phases.

Assuming the waste fabrication process temperature is greater than the container wall operating temperature limit, at the payload fabrication plant the limiting thermal condition will be the container wall. For the type 304 stainless steel, a conservative allowable temperature would be 427 C, based on the creep limit of the ASME<sup>(3-17)</sup> code. A material such as niobium would have a higher limit but would also require oxidation protection. The fabrication condition was not analyzed for defense waste, but, for commercial reactor waste, the results<sup>(3-10)</sup> indicated that the post-fabrication container would not require auxiliary cooling for several hours after fabrication.

During ground transportation, auxiliary cooling will be required for shipments lasting more than several hours. The limiting parameter for this condition would be the waste temperature.

During handling at KSC and while inside the Shuttle, auxiliary cooling will be required for highly concentrated defense waste (minimum waste concentration factor of 18 for Hanford). For commercial waste, auxiliary cooling is required, in conjunction with a high conductivity waste material and/or internal fins.

In deep space, the unprotected, unshielded payload container should be designed to be within all temperature limits assuming only passive cooling by radiation to space. The thermal distribution for the baseline Hanford waste payload design (see Table 3-12) was made assuming a bare container and no internal cooling fins, or solar radiation. For waste concentration factors greater than 35 (see Figure 3-7), the waste center exceeds the assumed temperature limit.

Compared to commercial reactor waste, defense high-level waste will not have as many thermal restrictions. Depending on the optimum degree of concentration, it may be possible to design a container without internal fins, that requires infrequent auxiliary cooling during ground operations, and will remain within allowable temperatures in the deep space environment.

### 3.4.3 Accident Response Analysis

The container system designs were analyzed for their response to various accident environment conditions (see Section 5.1). As a preliminary evaluation, two major accidents were chosen to represent the worst-case extreme abnormal environments. The first accident is defined as an explosion of the Space Shuttle vehicle on the launch pad. This accident entails the effects of a shock wave, liquid propellant fireball, a solid propellant fire, and fragment impact. The second accident concerns the payload response to an unplanned reentry of the unprotected container under various reentry conditions. This analysis does not include the consequences of an Earth impact of the waste and container following reentry.

### 3.4.3.1 Launch Pad Explosion

The payload container is assumed to be in the Space Shuttle cargo bay in preparation for launch. As such, it will be housed within a gamma radiation shield and the reentry system. One of the important design trade-offs which has a bearing on the response of the container during this accident scenario is the concept of a "front-end" reentry protection design versus a completely enclosed package (see Figure 2-5). The ramifications of this design option were considered in this analysis.

The reentry system is entirely within the Shuttle cargo bay. Realistically, for a launch pad fire involving the External Tank (ET) and Solid Rocket Boosters (SRB), the Shuttle itself would provide some degree of protection from the direct fire/explosion environment. As a means of simplification and yet remaining conservative, the mitigating effects of the Shuttle body will be neglected.

The thermal property data for the various components of the payload waste container and reentry system are shown in Table 3-11.

**Shock Wave.** The shock wave parameters are described in Section 5.1.1.3. The stress analysis of the container response to the shock wave<sup>(3-18)</sup> took into account the inertia of the loading and material strain rate effects.<sup>(3-19)</sup> In addition, the compressive strength of the waste<sup>(3-20)</sup> and effects of multiple shells were included. Together, these modeling assumptions led to the conclusion that the conceptual primary container design is adequate to resist the shock wave conditions for a 20% explosive yield of the ET (e.g., a pressure of  $4300 \text{ N/cm}^2$  and an impulse of  $5700 \text{ (N/cm}^2) \cdot (\text{msec})$ ). It should be noted that, with all the assumptions made, the analysis is conservative in many areas. The significant point is that the conceptual container will sustain the accident overpressure without the shield, reentry system, or Shuttle structure available for protection.

**Fragment Impact.** The fragment environment is described in Section 5.1.1.4. Table 3-13 lists the input parameters which define this condition.

TABLE 3-13. LAUNCH PAD EXPLOSION/FRAGMENT IMPACT DATA

---

20% Explosive Yield
93% of Fragments @ $V \leq 4000$ m/sec
Edge-On Impact Orientation
Fragment Diameter = 1.2 - 1.7 cm
Fragment Mass = 5 - 20 g

---

Using dynamic material strengths, the maximum energy absorption capacity of the container design was calculated including contributions from wall shear, waste compression, and shell bending. This analysis showed that for the fragment mass and impact velocity assumed, the present design is capable of absorbing only about 5% of the impact energy. In addition, the impact force is estimated to be greater than the forces required to deform the container system.<sup>(3-21)</sup>

Consequently, for the container, shield, and reentry system models assumed, the high velocity fragments are capable of penetrating the waste container barrier.

Further analyses indicates that, for the assumed impact data, the fragment velocity which corresponds to an impact energy equivalent to the energy absorption capability of the payload package is about 870 m/s. From a statistical viewpoint, for a 20% yield, about 45% of all fragments will be at a velocity less than 870 m/s. The full effect of the fragment impact upon the container and associated system's designs must be based on a statistical evaluation of the design fragment environment.

**Fire.** There are two types of launch pad fires of specific interest (see Sections 5.1.1.1 and 5.1.1.2): (1) a solid propellant fragment fire, and (2) a split solid propellant rocket motor fire. Essentially, the first fire environment is characterized by the External Tank (ET) fire (hydrogen/oxygen) for the first 5 seconds, followed by the solid propellant fire extending for an additional 450 seconds. Residual fires remaining after this time have been neglected. The time history of the radiant heat flux resulting from this fire is shown in Figure 3-8. The second fire, the split motor fire, is characterized by the ET fire plus the contribution from the split motor. The radiant heat flux is also shown in Figure



3-8. For the second fire, the flux is assumed to remain at approximately 3000 kW/m<sup>2</sup> for 15 minutes (not including the 5-second contribution of the ET fire) before complete burnout (see Figure 5-10). Note that the total heat,  $Q_T$ , radiated from the split motor fire is approximately eight times that of the solid propellant fragment fire.

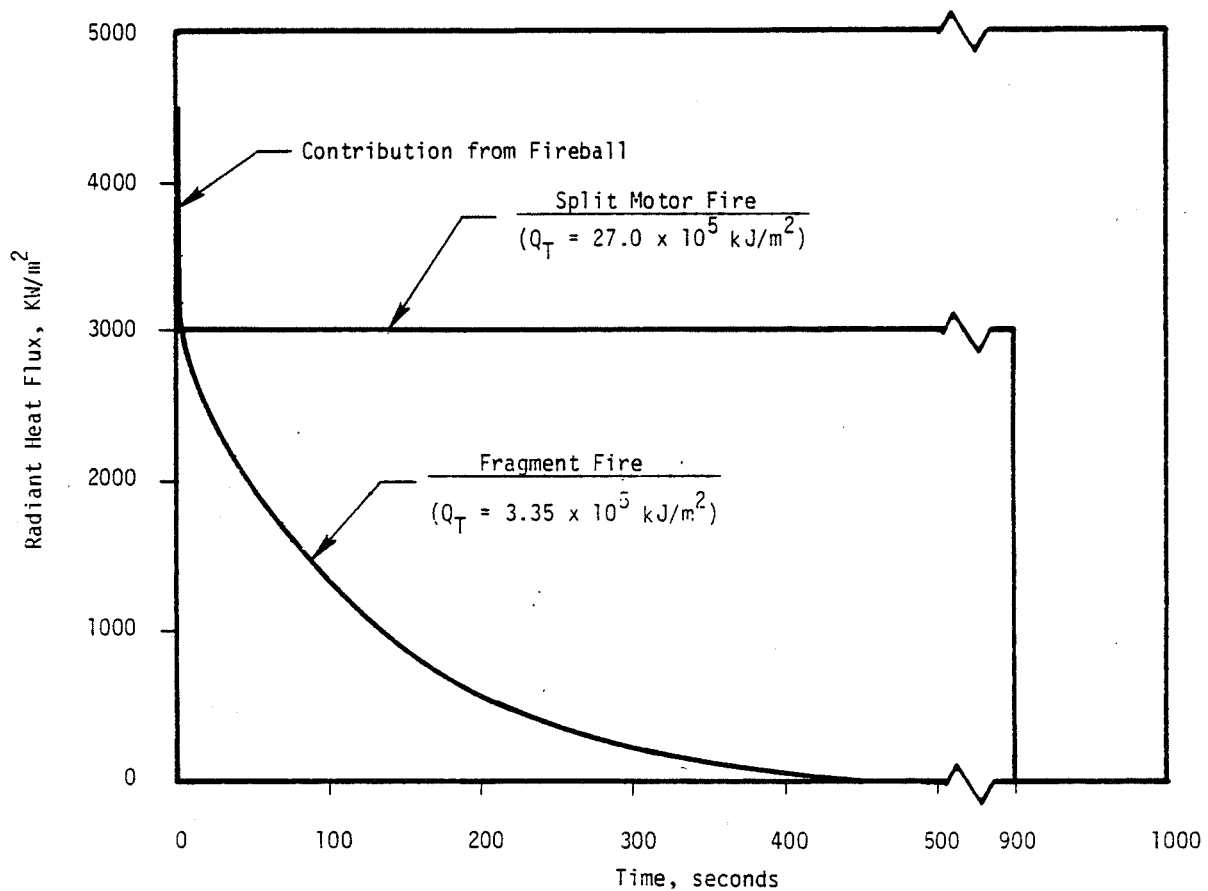


FIGURE 3-8. RADIANT HEAT FLUX VS TIME FOR LAUNCH PAD FIRES

Two configurations were examined for the response of a container for the Hanford waste to both fires. The first included the waste container and

radiation shield and neglected the reentry protection and Shuttle structure. This configuration being exposed to the two defined fires represents a conservative, worst case scenario, reflecting the design option of not completely surrounding the shielded waste within the reentry system. The second configuration is identical to the first except that reentry protection is assumed to completely enclose the container and gamma radiation shield. This configuration represents the case where reentry protection is uniform around the container.

Additional input parameters for the fire response analyses are listed in Table 3-14. As a design basis, an accident limiting waste temperature of 900 C was assumed. This is selected as a level at which some decomposition or melting of the complex waste form may occur (assumed equal to the formation temperature). Definition for the assumed limiting temperatures ( $T_l$ ) for the various other payload materials are given in Table 3-14.

**TABLE 3-14. INPUT PARAMETERS FOR HIGH-LEVEL HANFORD WASTE PAYLOAD THERMAL RESPONSE ANALYSIS (FIRE ENVIRONMENT)**

		Temperatures, C	
<u>Region</u>	<u>Material</u>	<u>Initial</u>	<u>Limiting</u>
Waste Source - - - - - Hanford (Baseline concentration, WCF = 27)			
Container/Shield Gap, cm - - - - - 0.127			
Waste, Center	Calcine Waste	700	900 (a)
Waste, Average	Calcine Waste	533	900 (a)
Container	Stainless Steel	277	1450 (b)
Radiation Shield	Uranium	248	1130 (b)
Impact Absorber	Steel Honeycomb	170	1450 (b)
Reentry System Insulation, Average	Min-K	109	980 (c)
Reentry System Ablative Shield	ATJ Graphite	48	3300 (d)

NOTES: (a) Decomposition temperature.  
 (b) Melt temperature.  
 (c) Maximum steady state service temperature (much higher temperatures are allowed for transient conditions).  
 (d) Sublimation temperature.

The transient material response to both fires was analyzed by the RETAC computer code (described in Appendix D). The principal simplifying assumption was that the effect of the melting or sublimation of material was neglected. Thus, the material was assumed to continue to absorb heat as if it remained in place as a pseudo-solid. The effect of this assumption was twofold. First, when the outer shell actually reaches the melting or sublimation temperature, the heat flux into the adjacent material region will be reduced by the latent heat of fusion. The effect of this heat sink mechanism is to reduce the temperature, at any given time, of the inner regions. Second, the outer shell would actually be removed once it has left the solid state, and the resultant heat flux acting on the inner regions may be increased due to the absence of the heat capacity effect of the outer shell. This will tend to raise the temperatures of inner regions. Consequently, the effects of the modeling assumptions are somewhat offsetting, implying the need for more detailed analysis.

In the present computations, the nominal values of specific heat, conductivity, and density from Table 3-11 were utilized. Surface emissivity was conservatively taken as 0.7 for all material types. Note that in Table 3-11, the density of the steel honeycomb material was taken to be 10% of the solid metal value. However, the conductivity and heat capacity were assumed to remain identical to that of a solid metal. In the actual computation, the variation of these parameters with temperature was taken into account.

In the context of the above discussion, the results of the launch pad fire analysis indicate that, for the waste container and gamma radiation shield assembly, with no reentry protection, the following occurs:

For a solid propellant fragment fire environment, the outer regions of the unprotected shield walls reach melting temperatures in the first 15 seconds of the fire and the uranium shield is expected to start to melt within the first minute of the fire (see Figure 3-9a). But, due primarily to the reduced conductivity of the gamma radiation shield/waste container interface gap, the container wall is not predicted to melt. In actuality, once the radiation shield fails (i.e., melts), the insulating effect of the container/shield gap is no longer present. Consequently, once the shield has exceeded melt temperatures, the temperatures within the waste and container are underestimated, and some waste exposure could occur.

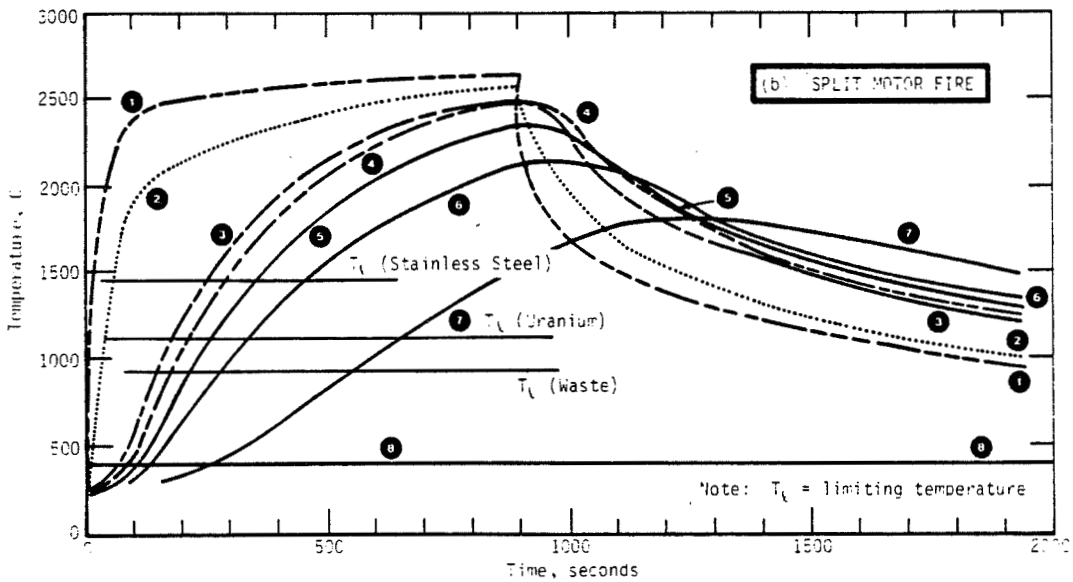
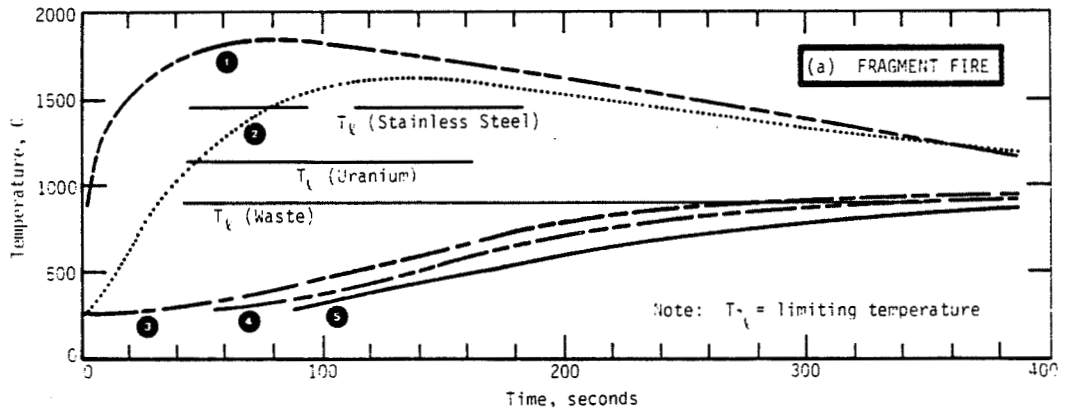
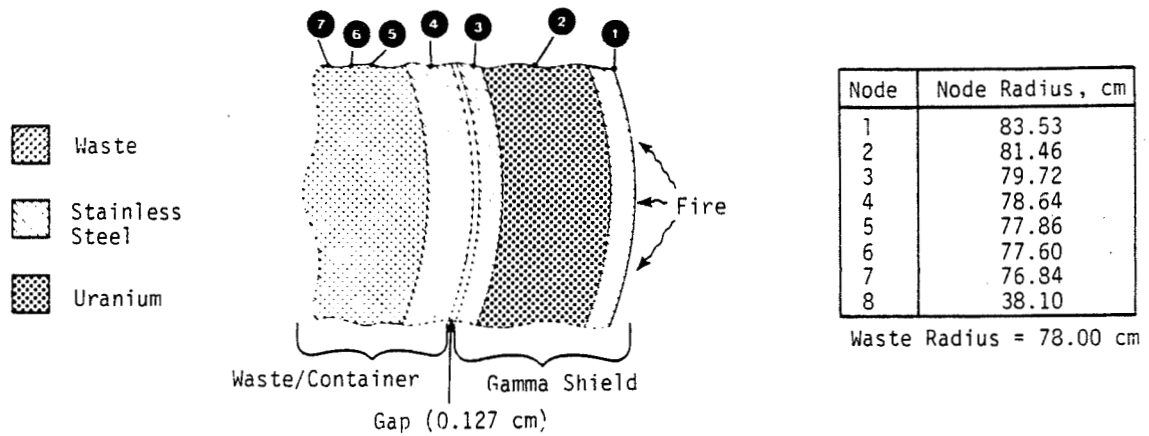


FIGURE 3-9. THERMAL RESPONSE OF GAMMA RADIATION SHIELDED CONTAINER TO SOLID PROPELLANT FIRES

In the case of a split motor fire, the temperatures of various layers of the waste container and shield are as shown in Figure 3-9b as a function of time. Note that temperatures of the outer and inner stainless steel cladding and the uranium shield all exceeded their melting points for an extended period of time. Therefore, approximately 300 to 500 seconds after start of the fire, the waste could be exposed directly to the radiant heat flux. Even though the bulk temperature of the waste will probably not reach the decomposition temperature (see Figure 3-9b), certainly the surface temperature will exceed the decomposition value and some waste will be dislodged from the primary mass.

For the configuration which included the reentry shield, the solid propellant fragment fire analysis shows that the temperatures remained below decomposition limits for all materials (see Figure 3-10a). A small portion of the outer edge of the MIN-K insulation may exceed the limit temperature during the fire. However, these phenomena are not extensive enough to cause temperature limits to be exceeded in interior regions of the payload. Consequently, the reentry system with fire protection on the rear side should withstand a solid propellant fragment fire.

For the case of a split motor fire, much more heat impinges on the loaded reentry system. In this case the ATJ material reaches a surface temperature of approximately 2700 C within 3 minutes of the start of the fire and remains at this temperature until the fire stops (see Figure 3-10b). Essentially, re-radiation of heat by the heat shield material itself tends to balance the heat input from the fire at this temperature value. The outer regions of the MIN-K insulation will exceed the limit temperature as specified in Table 3-14. However, as noted in the table, the maximum limit for MIN-K during transients is much higher. Additional detailed analyses are necessary to ascertain whether MIN-K insulation temperatures exceed actual limits. Nevertheless, the MIN-K insulation prevents heat from entering the body so the temperatures of various material components again remain below limits for all inner regions of the payload. These calculations are based upon a constant flux heat transfer model. This model is not appropriate at the higher payload surface temperatures. As a result, the calculated surface temperature exceeded the highest temperature physically possible (about 2430 C). For those cases where the predicted surface temperature approaches or exceeds this limit, reexamination is necessary using a variable heat flux model in future efforts.

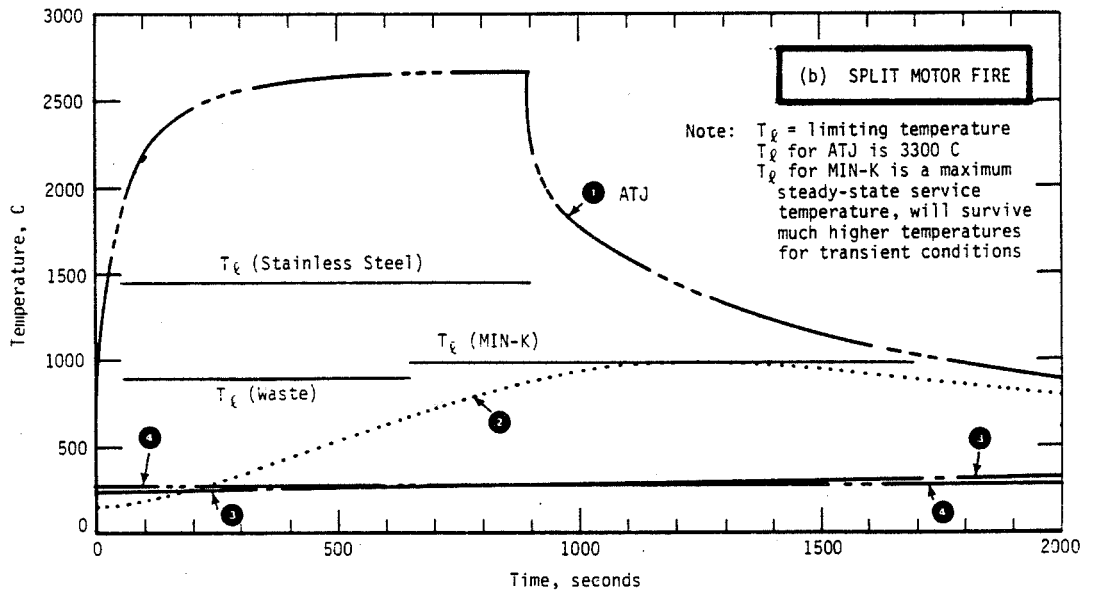
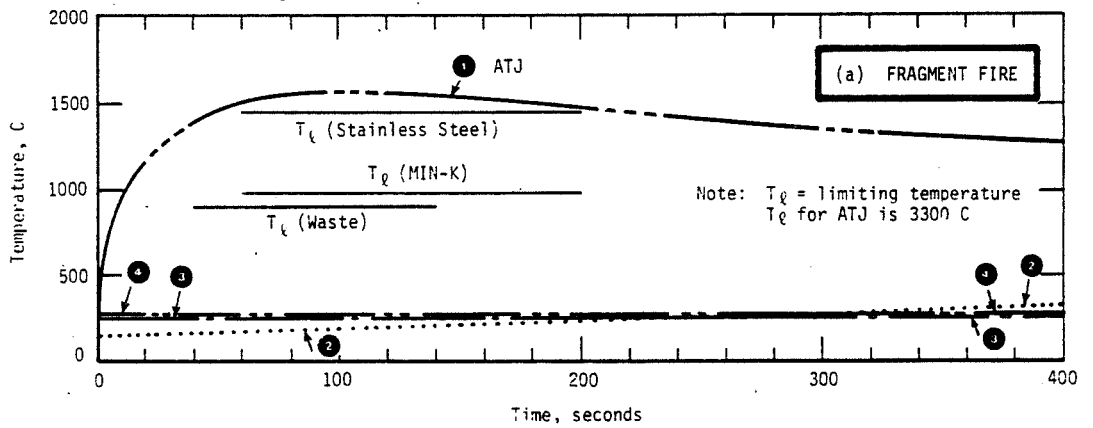
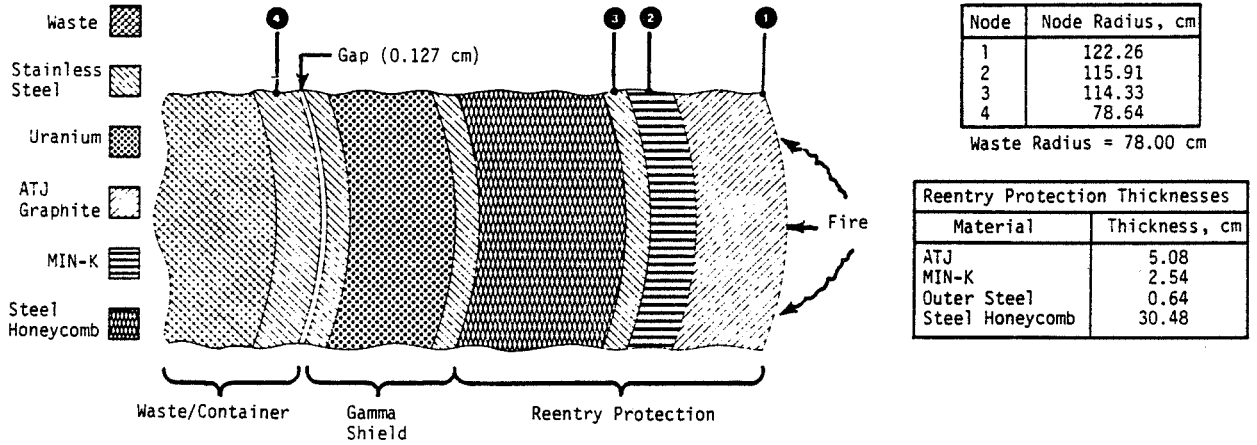


FIGURE 3-10. THERMAL RESPONSE OF REENTRY PROTECTED AND SHIELDED CONTAINER TO SOLID PROPELLANT FIRES

In summary, for the launch pad fires, it appears feasible to design the payload to survive by designing a reentry system that completely encloses the payload container and radiation shield. Without this assumed insulation, the primary container is likely to be breached if exposed directly to the split-motor fire. For the solid propellant fragment fire, a more detailed analysis may show that the primary container will not be breached. It must be kept in mind, however, that metal fragments from the ET explosion may likely damage the outer insulating surface, such that the payload would respond differently to a fire condition. More analysis is required to couple these effects. Also, an improved analytical model should include nonlinear effects such as material loss due to melting and subsequent changes in thermal properties due to latent heat of vaporization and loss in heat capacity.

The effects of internal heat generation are very minor when compared to the magnitude of the radiant heat flux from the fire. The major effect of the waste heat generation is in determining the steady state pre-accident temperatures. However, variations in these values (due to changes in waste concentration) result in shifts of the temperature - time curves of only a few seconds; they do not affect peak fire temperatures. Consequently, the response of Savannah River and Idaho defense waste mixes will be similar to that of Hanford compositions.

**Summary of Launch Pad Explosion.** The conceptual design of the high-level waste payload design, including container, gamma shield, and reentry system, appears to be a good approach toward one that is capable of surviving the assumed accident environment. To further improve the container design, the areas which need further development include a statistical definition of the fragment impact parameters, and performance of a more realistic analysis of the thermal behavior.

The results indicate that the shock wave presents no problem for the container design. Further definitive analysis and possible design modifications are needed to assure lack of penetration due to high velocity fragments. The reentry system is expected to survive the postulated fires with temperatures remaining under the melting limits. However, if no thermal protection exists at the rear of the reentry system for the split motor fire, damage to the shield and/or container is expected to occur. The response to this environment requires more detailed analysis.

### 3.4.3.2 Reentry

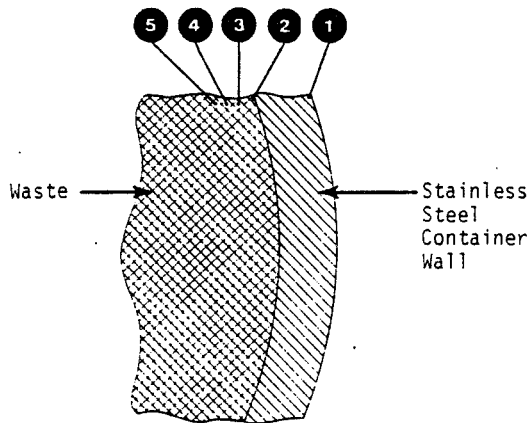
The conditions postulated for an unplanned reentry of the baseline waste payload (5500-kg Hanford waste) are defined in Section 5.1.2. Reentry analyses were performed for the thermal response of the payload for two cases: (1) the unprotected container on a steep entry, and (2) the unprotected container on a shallow entry. It is assumed that the reentry system would be designed to withstand the possible reentry environments. The basic assumptions and input parameters are listed in Table 5-4.

The stagnation point heating rates as a function of time experienced by the reentry of the base container are derived from Section 5.1.2. The heating rates for the two reentry cases were calculated by using the CONTEMP computer code and were input to the RETAC computer program (see Appendix D). The analytical model was similar to the one used for the launch pad fire, in that no melting or ablation was included. The assumption of a spherical rotating body during reentry simplified the analysis by making the external heating coefficient a function of time only (i.e., one-dimensional analysis). The temperature-time history for a two-dimensional stable body trajectory could be included at a later date, but this detail was not warranted at the present time.

The results for the steep reentry indicate that the container should survive atmosphere reentry intact until ground impact (at a velocity of 340 m/s). The maximum temperature calculated for the container wall was about 500 C, well below the melt temperature of 1450 C.

For the shallow reentry, the analysis indicates that the container will not survive atmospheric reentry. The results indicate (see Figure 3-11) that the container wall is expected to begin to melt about 1830 seconds into the reentry (or at an altitude of about 45 km). The waste will begin to decompose at a lower temperature than the container wall, at about 1820 seconds after reentry begins. Figure 3-11 illustrates the progressive "melt front" through the waste. Less than 1 cm of waste (about 3% of the mass) in the outer regions of payload (at container wall interface) is expected to decompose. At an altitude of about 40 km the entire container wall is predicted to melt away, thus exposing the calcine powder waste form to the reentry environment. The waste would then be available for dispersion in the upper atmosphere prior to Earth impact. Future analysis should include the effects of material loss and aerodynamic influences on the waste. Waste forms with better mechanical properties will have a better





Node	Node Radius, cm
1	79.27
2	78.90
3	77.88
4	77.62
5	77.24

waste Radius = 78.00 cm

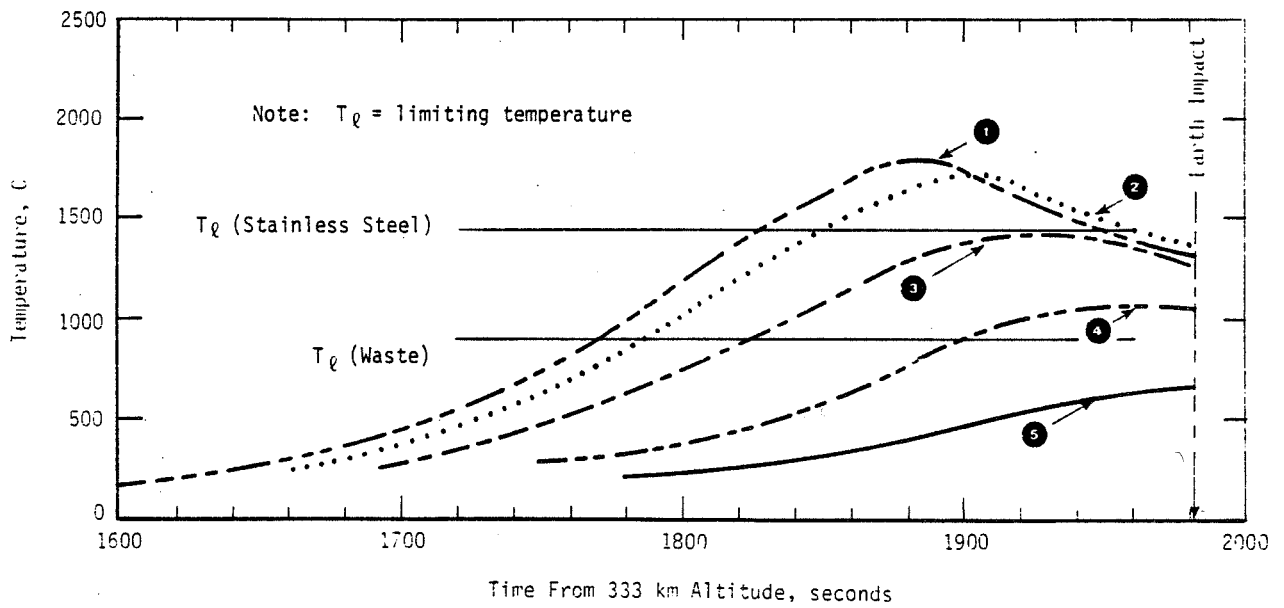


FIGURE 3-11. THERMAL RESPONSE OF ROTATING UNPROTECTED WASTE CONTAINER DURING SHALLOW UNPLANNED REENTRY

chance of not being dispersed in the upper atmosphere (see Section 3.3.2 for a discussion of various waste form characteristics).

In summary, these results indicate that without reentry protection and assuming a shallow reentry, the waste container wall is expected to melt away and expose the waste to the reentry environment in the upper atmosphere. More detailed analyses are required to determine how much waste material would be deposited in the atmosphere prior to Earth impact. The environmental impact consequences of waste burnup as a result of an unplanned reentry of an unprotected container are described in Section 6.2.

#### 3.4.4 Gamma Radiation Dose Calculations

To predict the radiation exposure to workers, crew, and principal components of the disposal system, gamma radiation dose rate calculations were performed with the ANISN<sup>(3-13)</sup> computer code using the baseline concentration (WCF = 27) for the Hanford waste composition. Figure 3-12 provides the dose for given thicknesses of the steel container wall as a function of distance from the primary container. These relationships can be used with acceptable dose criteria to derive conceptual designs of shielding protection for the crew and various hardware components.

#### 3.4.5 Concluding Remarks

The purpose of the analyses in Sections 3.4.1 through 3.4.4 is to provide a preliminary assessment of the high-level waste container response to a variety of expected normal and possible extreme environments. Obviously, the container design is dependent on the waste form and character. These analyses have attempted to bound the problem by using the best available data on defense waste.

Given the variation in waste form, the baseline waste mix composition is the Hanford waste at a waste concentration factor of 27. The amount of gamma shielding required appears to be feasible within the constraints of dose and mass limits, but is only conceptual, given the uncertainty of the overall design requirements.

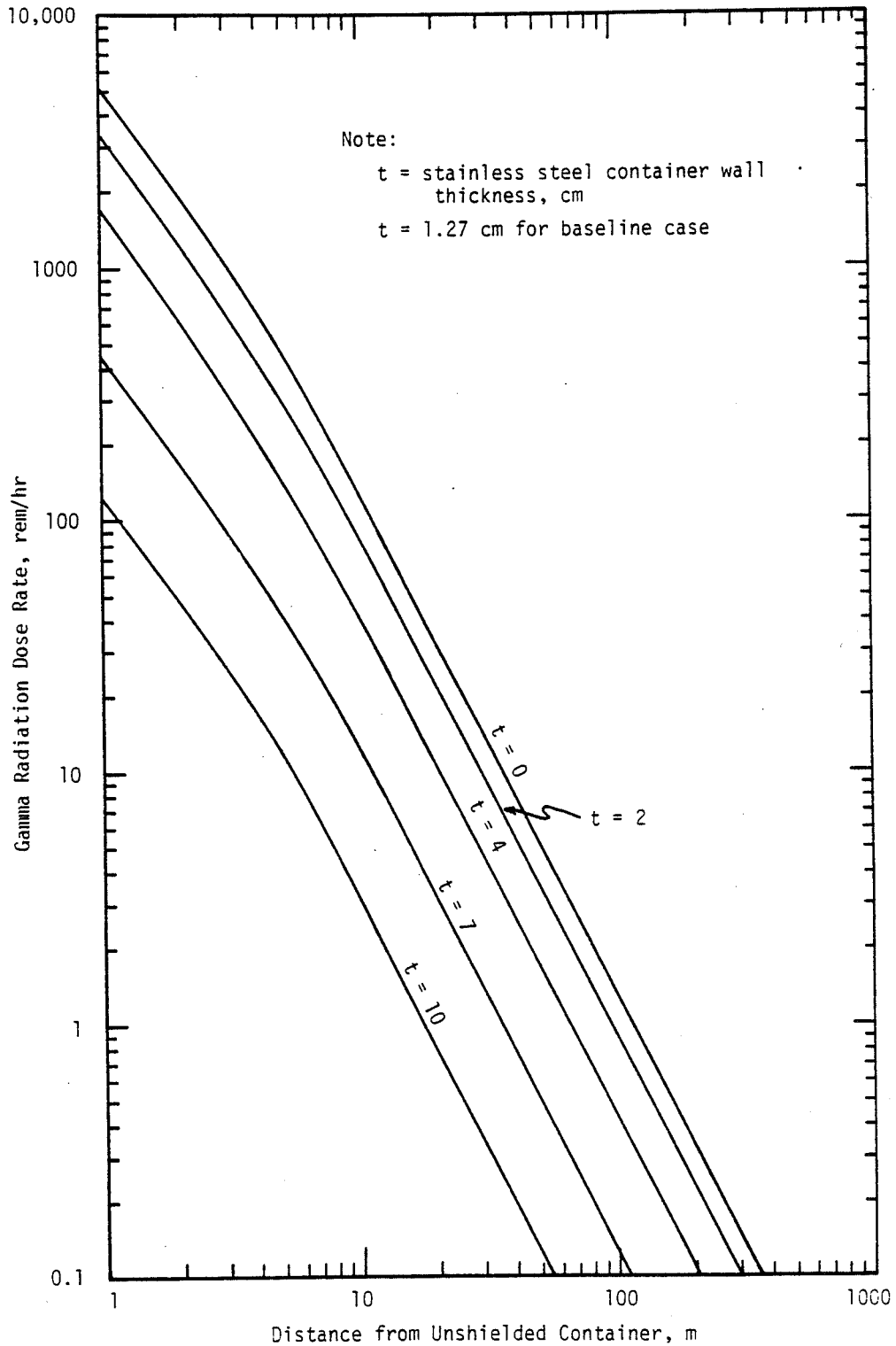


FIGURE 3-12. GAMMA RADIATION DOSE RATE AS A FUNCTION OF DISTANCE FROM BASELINE UNSHIELDED HANFORD WASTE PAYLOAD AND VARIOUS CONTAINER WALL THICKNESSES

Another key factor which will affect the container design is the thermal constraints which the payload must meet. Analyses indicate that, for the Hanford waste baseline composition (WCF = 27), the normal thermal environments do not severely limit the design. Consequently, the container and waste temperatures can be passively controlled in an environment such as deep space. However, the waste package must include provisions for auxiliary cooling whenever the container is placed into enclosures such as the reentry system and shipping cask. Obviously, for waste concentration factors significantly greater than the baseline, the waste package must include provisions for internal heat removal (e.g., fins or metal matrix waste form).

Of greater consequence, however, will be the response of the container design to accident environments. As is shown in the previous analyses, the baseline design concept responds to the accident situations in a variety of ways. It is not possible at this time to determine the acceptability of a given container design during a postulated accident, since so little data are available and more concept definition remains to be performed. Rather, the utility of this analysis lies in the determination of the direction in which design improvements should proceed. As described in other sections, the final safety assessment must include an evaluation of not only the consequence of failure, but the probability as well, in order that the determination can be made of what is or is not an acceptable risk. Once this is accomplished, the container design can be tailored to match the safety requirements for the accident conditions.

The analysis here was based almost entirely on the data describing the baseline Hanford waste composition. The Savannah River and Idaho waste components are similar to Hanford's, with Idaho having the highest thermal output of the three, but still below the thermal output expected for commercial waste. The container designs given here appear feasible. As the waste gets hotter (e.g., WCF increases beyond the baseline), improved cooling methods will be required, up to those evaluated for commercial waste. Differences among the three types of defense wastes are not expected to significantly alter the results of the accident analyses performed.

In summary, the defense high-level waste container system has been analyzed parametrically for various normal and accident environments. Further design improvements await the development of more detailed design criteria and analyses.

### 3.5 References

- 3-1. "Alternatives for Long-Term Management of Defense High-Level Radioactive Waste - Hanford Reservations", ERDA 77-44, Richland, Washington (September 1977).
- 3-2. "Alternatives for Long-Term Management of Defense High-Level Radioactive Waste - Savannah River Plant", ERDA 77-42/1, Aiken, South Carolina (May 1977).
- 3-3. "Alternatives for Long-Term Management of Defense High-Level Radioactive Waste - Idaho Chemical Processing Plant", ERDA 77-43, Idaho Falls, Idaho (September 1977).
- 3-4. Letter No. R78-1338, D. D. Wadrich (Rockwell Hanford) to K. R. Yates, Battelle-Columbus (July 17, 1978).
- 3-5. Telephone conversation(s): W. Schultz and R. Watrous (Rockwell Hanford) to K. R. Yates (Battelle-Columbus) and R. Burns (NASA/MSFC) (June-September 1978).
- 3-6. Material supplied by L. Hyder (Savannah River) to K. R. Yates (Battelle-Columbus) (June 1978).
- 3-7. Meeting at Savannah River: L Hyder et al. (Savannah River) with K. R. Yates (Battelle-Columbus) and R. Burns (NASA/MSFC) (September 1978).
- 3-8. Letter: J. P. Hamric (Idaho) to R. Burns (NASA/MSFC) (May 18, 1978).
- 3-9. Telephone conversation, Wally Hendricks (Idaho) to R. Burns (NASA/MSFC) (May 1978).
- 3-10. Pardue, W. M., et al., "Preliminary Evaluation of the Space Disposal of Nuclear Waste", 8-32391(100), Battelle Memorial Institute, Columbus, Ohio (August 30, 1977).
- 3-11. Counts, J. S., "Quarterly Report, Technical Development for Long Term Management of Hanford High Level Waste (January - March, 1976)", ARH-ST-132C, Atlantic-Richfield Hanford Company, Richland, Washington (June 1976).
- 3-12. Bell, M. J., "ORIGEN - The ORNL Isotope Generation and Depletion Code", ORNL-4628, Oak Ridge National Laboratory, Tennessee (May 1973).
- 3-13. Soltesz, R. G., "Revised WANL ANISN Program User's Manual", WANL-TMI-1967, Westinghouse Astronuclear Laboratory (April 1969).
- 3-14. "Space Shuttle System Payload Accommodations", NASA/JSC 07700, Volume XIV, NASA/JSC, Houston, Texas (1977).

- 3-15. Edwards, A. L., "TRUMP: A Computer Program for Transient and Steady-State Temperature Distributions in Multidimensional Systems", UCRL-14754, Rev. 3, Lawrence Livermore Laboratory (September 1, 1972).
- 3-16. "Alternatives for Managing Wastes from Reactors and Post-Fission Operations in the LWR Fuel Cycle", ERDA-76-43, Volume 2, Battelle Pacific Northwest Laboratories, Richland, Washington (May 1976).
- 3-17. ASME Boiler and Pressure Vessel Code, Section III, Nuclear Power Plant Components (1974 Ed.).
- 3-18. Kinney, G. F., Explosive Shocks in Air, MacMillan, New York, New York (1962).
- 3-19. Albertini, C., and Montagnani, M., "Testing Techniques Based on Split Hopkinson Bar", Proc. Conf. Mech. Prop. of Materials at High Rates of Strain, Oxford (April 2-4, 1974).
- 3-20. McElroy, J. L., "Quarterly Progress Report Research and Development Activities Waste Fixation Program - January Through March 1977", PNL-2265-1, UC-70, Battelle Northwest Laboratories, Richland, Washington (November 1977).
- 3-21. Clark, D. S., "The Influence of Impact Velocity on the Tensile Characteristics of Some Aircraft Metals and Alloys", NACA Technical Note No. 868 (October 1942).

#### 4.0 MISSION ANALYSIS

As a part of this study, two special analyses considering specific mission aspects that strongly influence system safety were conducted. The first analysis considers the stability and range of impact conditions (attitude, impact velocity) of a nuclear waste payload (container plus reentry system) ejected from the Orbiter cargo bay under emergency conditions. The payload is considered to be ejected both under near-pad and high-speed flight conditions. The results of the analysis have implications regarding design impact loads for the payload, particularly for impact on the aft end structure.

The second special analysis considers the rescue and return of a payload following an incomplete and/or misdirected OTV Earth-escape insertion burn. The characteristics of the resulting trajectory and the regions where return to the Shuttle orbit by a second OTV is feasible are identified. For those regions where return is not feasible, boosting to Earth escape or to a higher Earth orbit is considered.

#### 4.1 Low- and High-Speed Reentry System Stability and Impact Condition Analyses

The purpose of this assessment was to briefly evaluate two of the proposed nuclear waste package reentry systems for positive static stability in both the subsonic and hypersonic flight regions. This action was deemed desirable in view of proposed abort scenarios which specify ejection of the nuclear waste package and reentry system from the Space Shuttle cargo bay. The hypersonic stability analysis is valid for aborts in the final phases of the Shuttle flight profile and for inadvertent reentry of the payload once orbit has been achieved. Stability is of particular importance at high speed to ensure that the reentry shroud thermal protection system is aligned with the free-stream flow direction. The subsonic calculations were designed to identify potential impact angles and velocities for low-speed ejection. The intent was to categorize the conditions for which the aft structure of the reentry system should be designed since landing on the forward hemispherical end may not occur in certain situations. Each of these analyses is described in greater detail in the following sections.

##### 4.1.1 High-Speed Reentry System Stability Analysis

The procedures used to evaluate the high-speed static stability for a representative proposed reentry system configuration are outlined here. The physical dimensions and location of the center of gravity (c.g.) for this version is shown in Figure 4-1. All reentry capsule data were supplied by NASA/Marshall Space Flight Center.

Calculations of the aerodynamic forces and moments acting on these bodies were based on the technique of Reference 4-1. The equations contained therein employ Newtonian impact theory and are thus applicable only to high-supersonic and hypersonic Mach numbers. A small computer program was developed to perform the required computations. Output from the program consisted of normal force, axial force, and pitching moment coefficients as a function of angle of attack.

One measure of the static stability of a body is the distance that the center of pressure lies behind the overall center of gravity. The greater the distance, the more statically stable the configuration. The center of pressure is, however, known to shift forward with increasing angle of attack. Care must be



exercised to ensure that an adequate static stability margin exists for the entire range of angles of attack likely to be encountered.

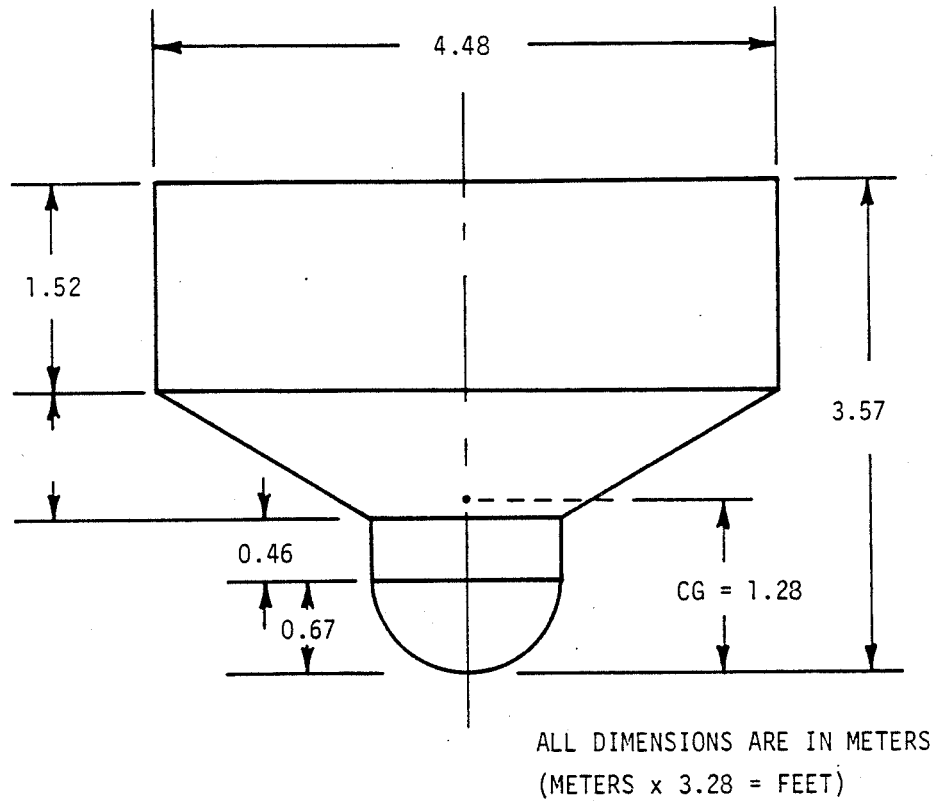


FIGURE 4-1. REENTRY CAPSULE CONFIGURATION

The force and moment coefficients previously mentioned were calculated with respect to the center of gravity of the body. Center of pressure is defined as the point at which the aerodynamic moment is zero and can thus be found by the following transformation:

$$X_{CP} = X_{CG} - \frac{C_M L_{REF}}{C_N} ,$$

where:

$X_{CP}$  = distance to center of pressure from forward end of capsule

$X_{CG}$  = distance to center of gravity from forward end of capsule

$C_M$  = moment coefficient

$C_N$  = normal force coefficient

$L_{REF}$  = reference length, taken to be the diameter of aft end of capsule.

Figure 4-2 shows the aerodynamic coefficients and center of pressure locations for the reentry capsule. The angle of attack has been varied from 0 to 90 degrees to investigate all likely flight path angles.

These data indicate that the reentry capsule would be statically stable in the hypersonic flight regime. The values displayed are also reasonably consistent with similar numbers generated by NASA/Marshall Space Flight Center. Investigation of the dynamic stability of the capsule was beyond the scope of this preliminary analysis.

#### 4.1.2 Low-Speed Impact Analysis

A comparable computational technique for determining the subsonic static stability margin for the reentry capsules is not known to exist. The normal procedure involves construction of instrumented models which are subsequently given extensive wind tunnel or free flight testing. Such activities were beyond the scope of this study and it was necessary to concentrate the efforts toward quantifying the potential impact conditions. Capsule orientation and velocity at the instant of impact were the primary items of interest.

The first step in calculating the previously mentioned values was to estimate low-speed drag and lift coefficients for the bodies. The drag coefficient was assumed to have a value approximately 0.94 times the hypersonic number as obtained from the work described in Section 4.1.1. This multiplier was selected from consideration of the information contained in Figure 5-23. Examination of aerodynamic data suggested that the slope of the hypersonic lift coefficient versus angle of attack decreases in the subsonic flight environment. A correction to the lift data obtained from Section 4.1.1 was made in view of this observation.

A second assumption dealt with the period of the body oscillations and the damping of the motion. To bound the situation, two cases were developed for further analysis. The period of the motion was held constant in both instances and was estimated at a value of 5 seconds. A time to half amplitude of 10 seconds was selected for what may be considered a highly stable design with a corresponding half-amplitude time of infinity (no damping) for the marginally stable body.

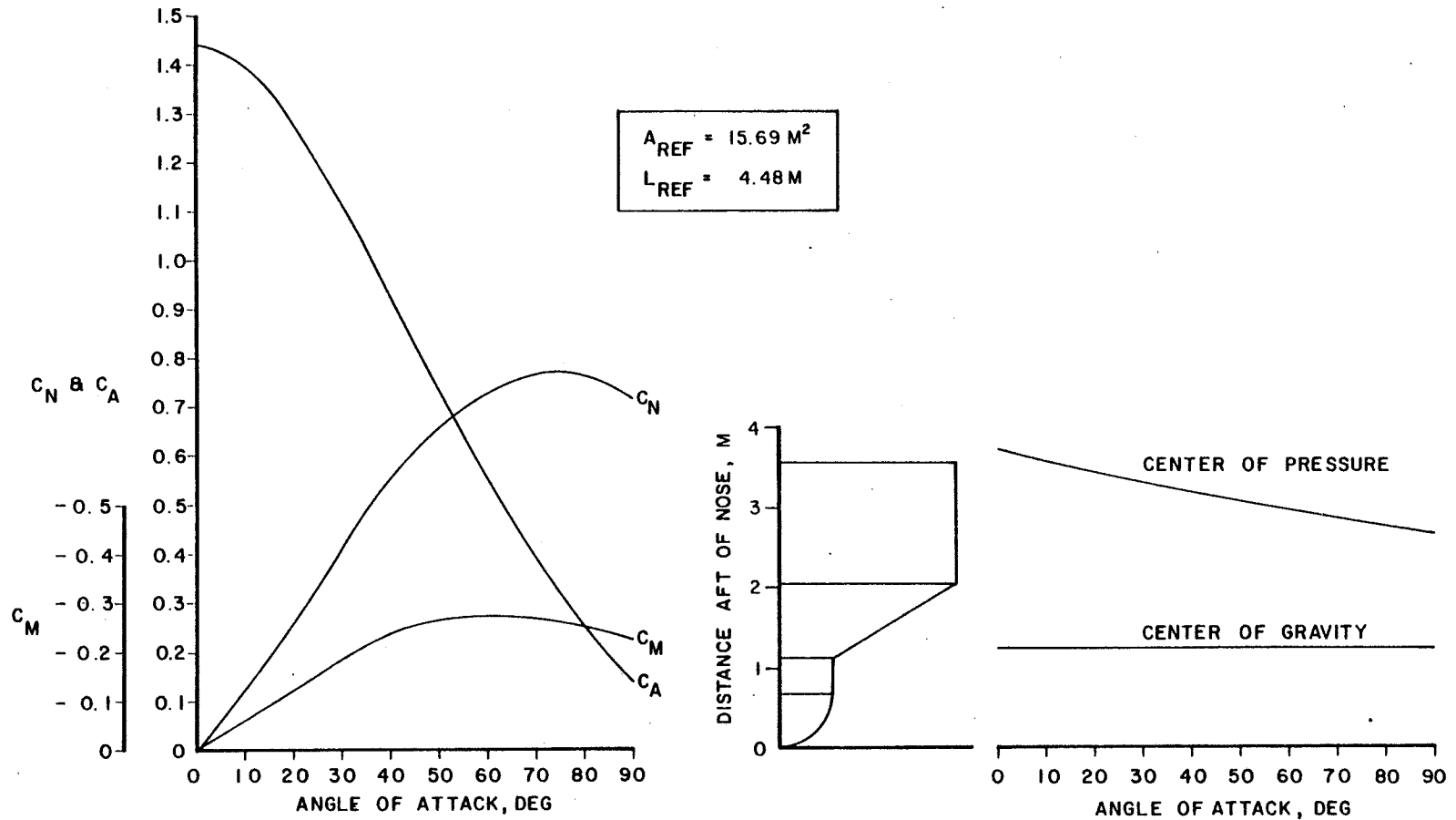


FIGURE 4-2. REENTRY CAPSULE AERODYNAMICS AND HYPERSONIC STABILITY MARGIN

All of the above items were incorporated into a computer program which integrated the equations of motion to determine the impact angle, velocity, and downrange distance. The calculations were performed for ejection on the pad, at 16 seconds into the flight, and at 39 seconds into the Shuttle flight profile for both highly and marginally stable reentry systems. For the purpose of determining initial flight velocities and angles of attack, the payload ejection system was specified to impart a velocity of 45.7 m/sec perpendicular to the cargo bay centerline to the reentry package.

The results of this phase are shown in Figures 4-3 and 4-4. The impact displayed in Figure 4-4 for the on-pad abort was generated by holding the capsule angle of attack at a fixed value of 90 degrees to the velocity vector. This condition was imposed to determine the likely worst case landing condition since impact on the aft structure is probable only during the very early seconds of Shuttle flight.

The analysis described above is preliminary in nature and is intended solely as an initial cut for early design purposes. Further work is required in this area if future abort planning retains the on-pad ejection concept.

#### 4.1.3 Conclusions

Based on the above analyses, the reentry system would need to be capable of withstanding impacts of up to approximately 100 m/s on the hemispherical nose cap. Because of the possibility of early ejection at low dynamic pressure, the reentry system may not necessarily impact in a "nose-on" configuration. To cover this possibility, the reentry system also would need to be able to withstand an impact of 30-40 m/s on the side or rear structure.

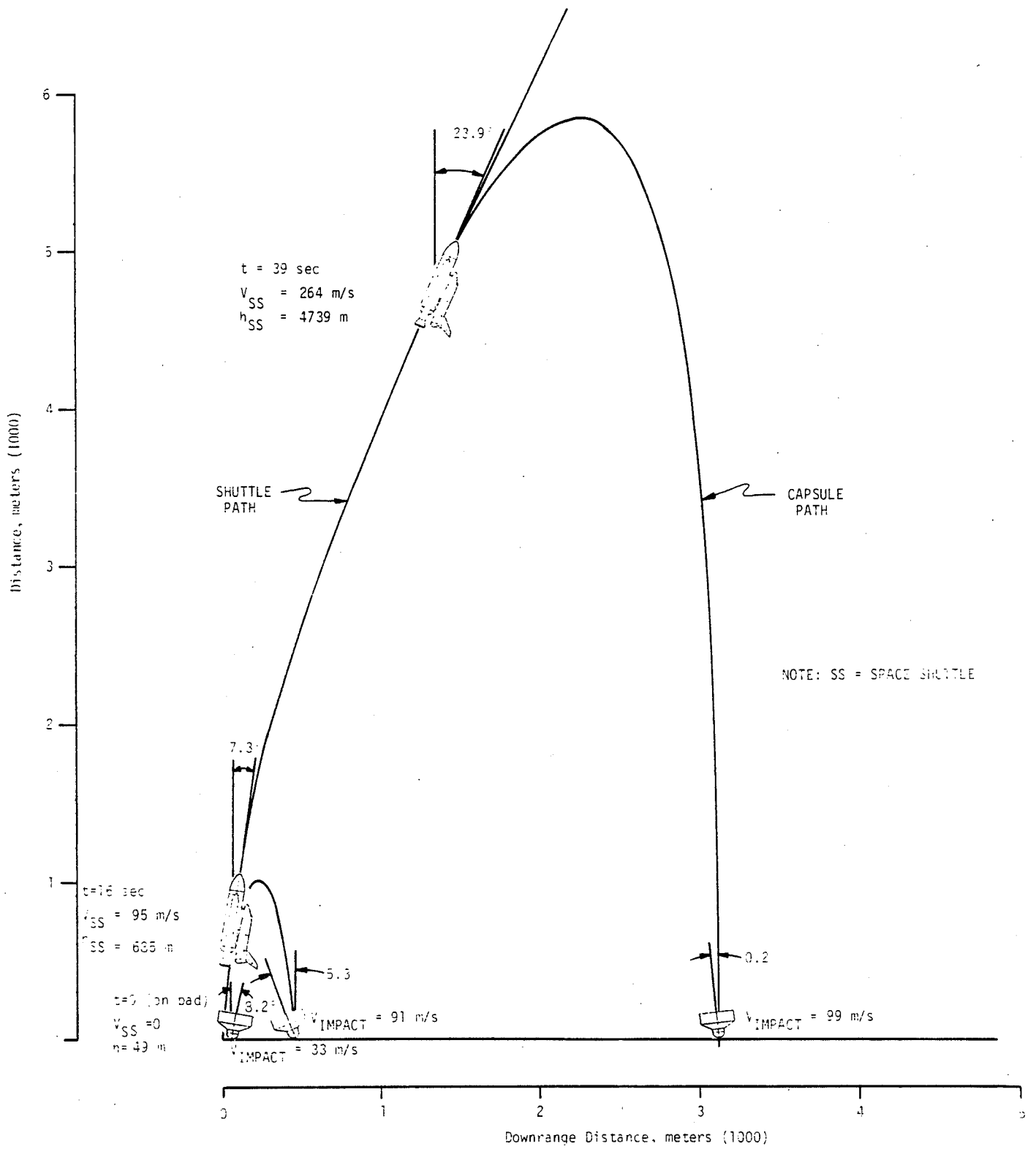


FIGURE 4-3. IMPACT CONDITIONS FOR REENTRY CAPSULE EXHIBITING HIGH DEGREE OF SUBSONIC STABILITY

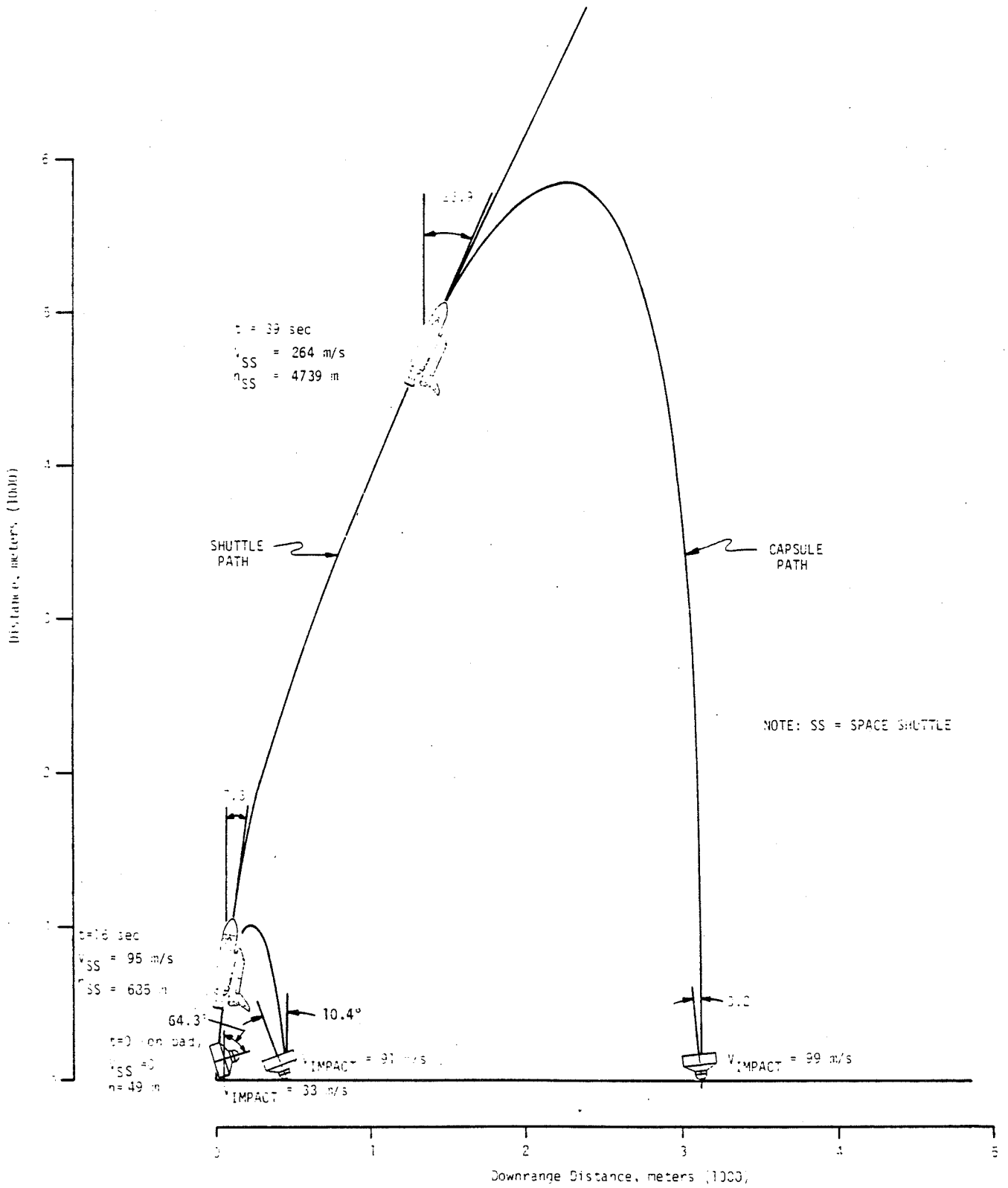


FIGURE 4-4. IMPACT CONDITIONS FOR REENTRY CAPSULE EXHIBITING MARGINAL SUBSONIC STABILITY

## 4.2 Recovery of Nuclear Waste Payloads in Earth Orbit

A brief analysis was conducted to examine the consequences of possible gross errors in the magnitude and/or direction of the OTV Earth-escape injection impulse, with emphasis on the recovery of payload/kickstage packages which remain in Earth orbit. The recovery vehicle would be a second OTV.

The assumed characteristics of the system are given in Table 4-1, with deployment from a 333 km (180 n.mi.) circular Shuttle orbit.

**TABLE 4-1. ASSUMED SYSTEM PARAMETERS**

	OTV	SOIS Kickstage	Payload
Gross Stage Mass, kg	24,950	5420	4760*
Inert Mass, kg	2890	1300	-
Specific Impulse, sec	470	289	-

\*NOTE: Because of the parallel nature of many of the study analyses, this analysis was conducted using an earlier value for payload mass. The current baseline payload mass is 5500 kg. This change in baseline payload would shift some of the curves of Figure 4-6, but would not alter the general conclusions.

In keeping with the preliminary nature of this calculation, no allowance was made for velocity losses or phasing and maneuvering impulse requirements during the recovery operations.

### 4.2.1 Details of Analysis

The most benign consequence of an OTV impulse error would be the injection of the SOIS kickstage/payload package into an erroneous, but safe, Earth-escape trajectory. Contingency operations in this event are not considered in this analysis. At the other extreme of severity, the package may impact the Earth directly or be placed in an Earth orbit with insufficient lifetime to effect a recovery. To delineate these latter cases, an arbitrary, but reasonable, criterion was used which requires a minimum perigee altitude of 185 km (100 n.mi.) for recovery to be considered.

The correct OTV velocity increment is aligned with the instantaneous Shuttle orbit velocity vector. The direction of the erroneous OTV velocity increment is represented by two angles, as shown in Figure 4-5. The angular error is denoted by  $\epsilon$ , measured in the plane containing the intended OTV velocity increment vector and the actual OTV vector. This plane is inclined at the angle  $\delta$  with respect to the local horizontal plane.

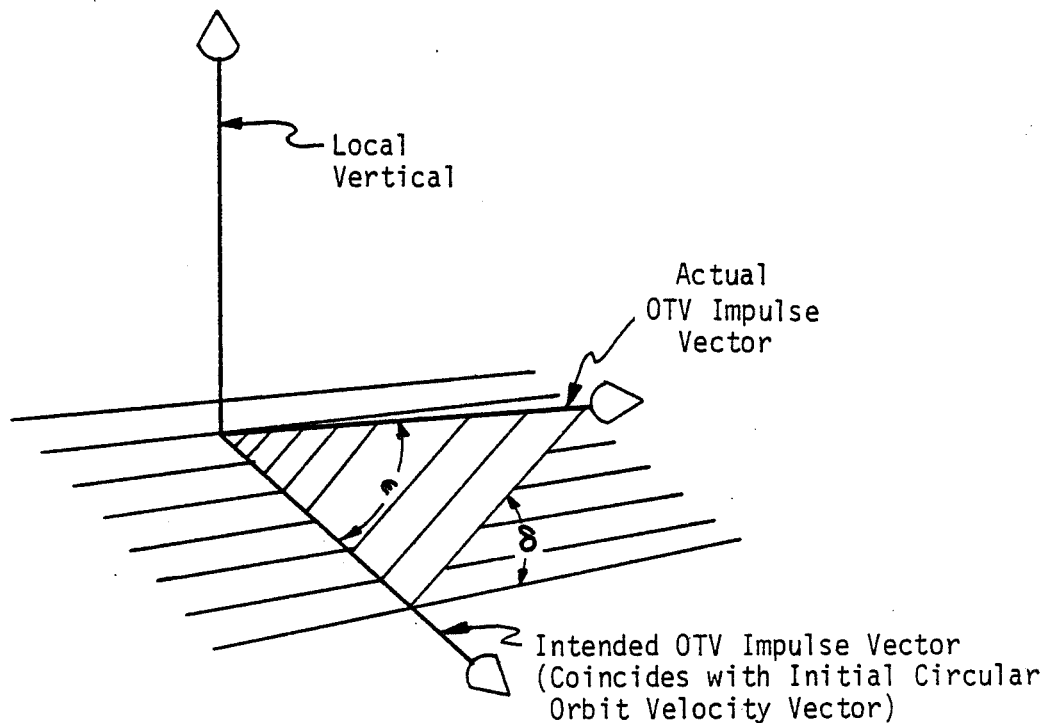


FIGURE 4-5. DEFINITION OF ANGLE ERROR PARAMETERS

The magnitude of the final velocity, given by the magnitude of the vector sum of the Shuttle orbit velocity and the OTV impulse, is independent of  $\delta$ . Consequently, from the vis-viva relationship, the final orbit energy and semi-major axis are dependent only upon  $\epsilon$  for a given OTV impulse magnitude. The angle  $\delta$ , on the other hand, determines the flight path angle from the horizontal and, consequently, the perigee and apogee altitudes consistent with the semi-major axis. By virtue of symmetry, it is not necessary to consider values of  $\delta$  beyond  $\pm 90$  degrees.



Figure 4-6 is a map of the  $\epsilon$ ,  $\Delta V$  domain and summarizes the results of this analysis. If the OTV pointing error were constrained to the horizontal plane ( $\delta = 0^\circ$ ), the permissible angular error ( $\epsilon$ ) could be in excess of 95 degrees before an unacceptably low perigee would be produced. At the other extreme, if the OTV impulse lies in the vertical plane ( $\delta = \pm 90^\circ$ ), the permissible pointing error is reduced considerably. Furthermore, if the value of  $\delta$  is random, half of all cases will have an absolute magnitude between 45 and 90 degrees; and, from Figure 4-6, the perigee constraint boundary for  $\delta = \pm 45^\circ$  is seen to be very near the vertical plane boundary ( $\delta = \pm 90^\circ$ ).

In the region below the  $\delta = \pm 90^\circ$  line, the nuclear waste payload always will either enter a heliocentric orbit or remain in an Earth orbit from which it can be recovered, regardless of the magnitude of the erroneous OTV impulse.

For those packages remaining in Earth orbit, the recovery operation is assumed to be a simple two-impulse maneuver in which a second OTV is placed into an identical orbit with the errant payload, attaches itself to the original vehicle assembly (with negligible expenditure of propellants), and then re-establishes a circular 333 km (180 n.mi.) orbit for recovery by a Shuttle Orbiter. With this simple two-impulse model, the mass which can be recovered by the second OTV is uniquely determined by the magnitude of the erroneous impulse of the first vehicle.

As indicated in Figure 4-6, if the original impulse magnitude is less than about 1.9 km/sec, and if the perigee altitude is satisfactory as determined by  $\epsilon$  and  $\delta$ , the second OTV can recover the entire package without venting propellants from the first OTV or the kickstage. For initial error impulses from 1.9 to 2.9 km/sec, it would be necessary to vent the propellants from the original stages to reduce the recovered mass. If the initial OTV stage is discarded, the vented kickstage and payload package could be recovered up to initial error impulses of 3.29 km/sec; whereas only the payload itself could be recovered for error impulses from 3.29 to about 3.51 km/sec (if the value of  $\delta$  were sufficiently large to cause the payload to remain in Earth orbit).

If the magnitude of the first OTV impulse exceeds 3.5 km/sec, recovery by a second OTV is not possible. For error angles ( $\epsilon$ ) less than about 26 degrees, the nuclear payload would escape into a heliocentric orbit. For greater  $\epsilon$  magnitudes, up to the hyperbolic path boundary of Figure 4-6, the

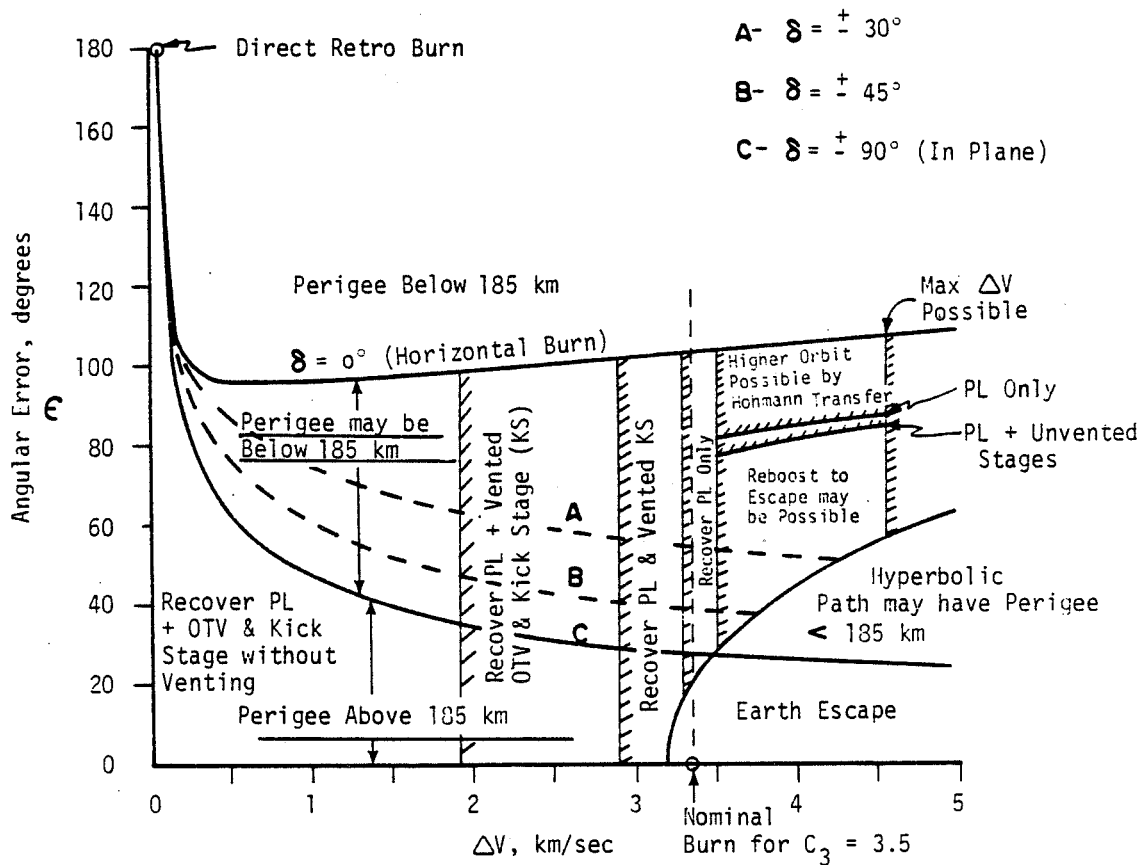


FIGURE 4-6. EFFECT OF OTV IMPULSE ERRORS FROM INITIAL 333-KM (180-N.MI) CIRCULAR ORBIT

payload would either escape or be placed in a hyperbolic orbit with a perigee below 185 km (100 n.mi.), depending on the magnitude and sign of  $\delta$ . If  $\delta$  were positive (ascending flight path angle), the payload would not pass perigee before escape; but negative values of  $\delta$  introduce the possibility of direct impact or a velocity loss at perigee which could convert the hyperbolic orbit into an elliptical orbit with an unacceptably low perigee.

As indicated in Figure 4-6, a region for high-velocity impulse errors exists above the hyperbolic path boundary, where the payload would be injected into an elliptical Earth orbit from which it could not be recovered by a second OTV. In the unlikely event that the erroneous  $\Delta V$  and  $\epsilon$  were sufficiently large to enter this region, it may be possible, as an alternative, to re-boost the payload to escape velocity with the second OTV.

Figure 4-7 shows the relationships between  $\epsilon$ ,  $\delta$ , perigee altitude and the available impulse from the second OTV for three values of erroneous impulse in this region. For a given  $\Delta V$ ,  $\delta$ , and  $\epsilon$ , the perigee altitude and velocity are uniquely determined, from which the perigee impulse required to escape can be readily computed. Furthermore, the propellant mass available in the second OTV for the escape impulse is fixed by the initial error impulse magnitude. Performing these parametric calculations, the three carpet plots of Figure 4-7 were obtained, and the upper re-boost boundaries shown in Figure 4-6 were generated.

As indicated in the carpet plots of Figure 4-7, very large values of  $\epsilon$  combined with small values of  $\delta$  can produce elliptic orbits with acceptable perigees but which require perigee impulses for escape in excess of the capability of the second OTV. Even in this region, however, it is possible to convert these eccentric orbits into circular orbits with sufficient altitude for extended lifetimes. This can be accomplished by using the second OTV to provide a Hohmann transfer to the higher circular orbit. A portion of the available OTV propellant is expended to provide a perigee impulse to raise apogee; then, the remaining impulse is applied at the new apogee to circularize the final orbit.

Figure 4-8 displays the circular orbit altitude which is obtainable as a function of  $\epsilon$  and  $\delta$  for fixed value of velocity impulse error. At worst, a circular orbit at over 2000 km altitude above the Earth appears to be achievable.

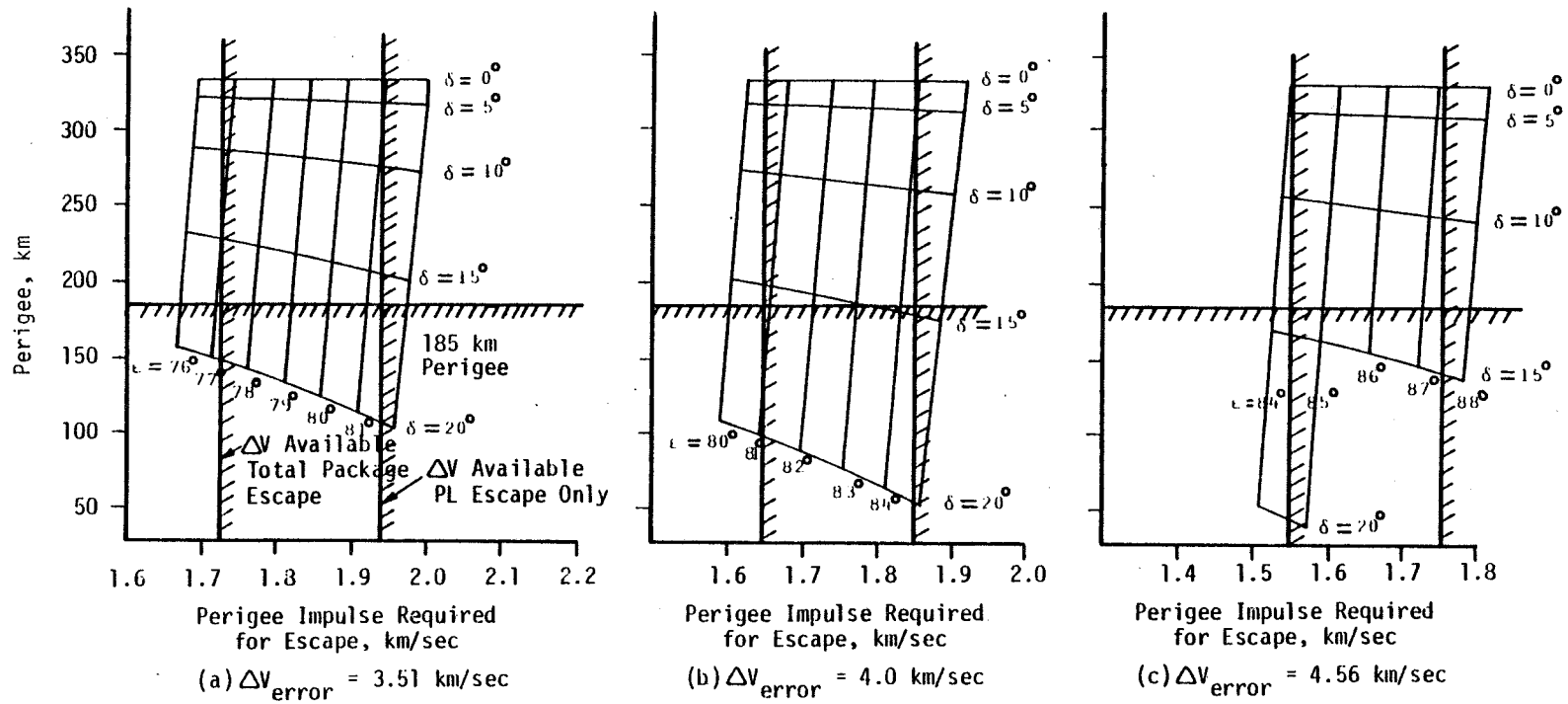
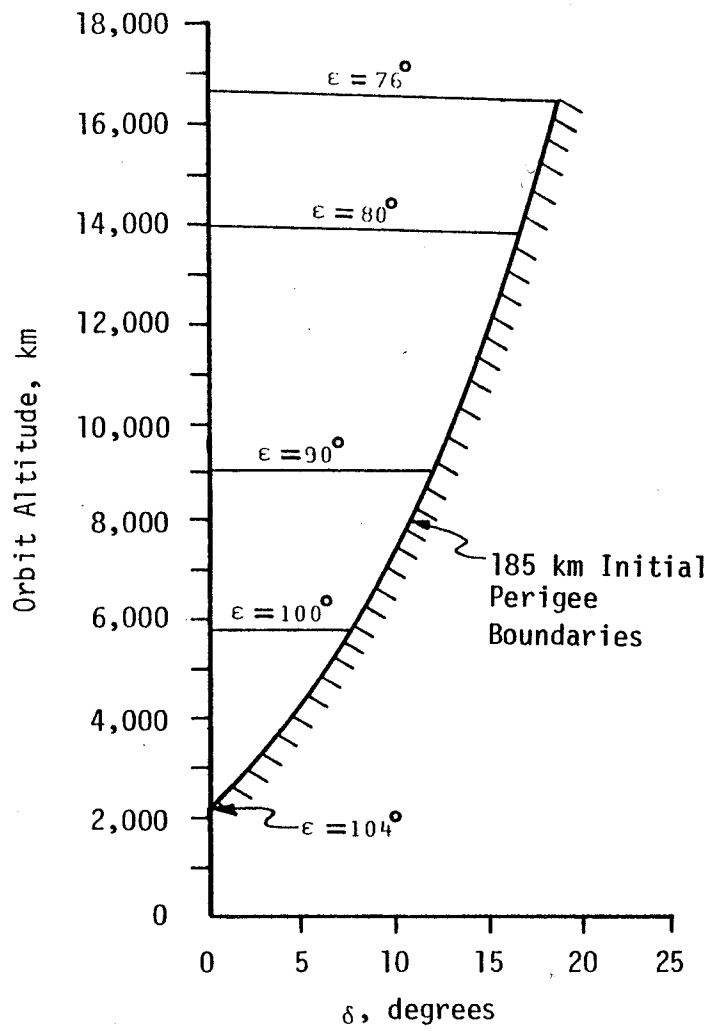
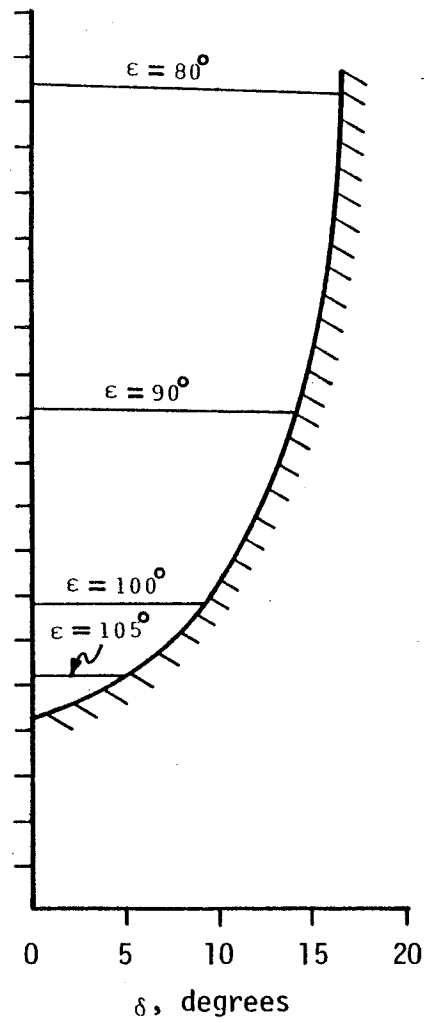


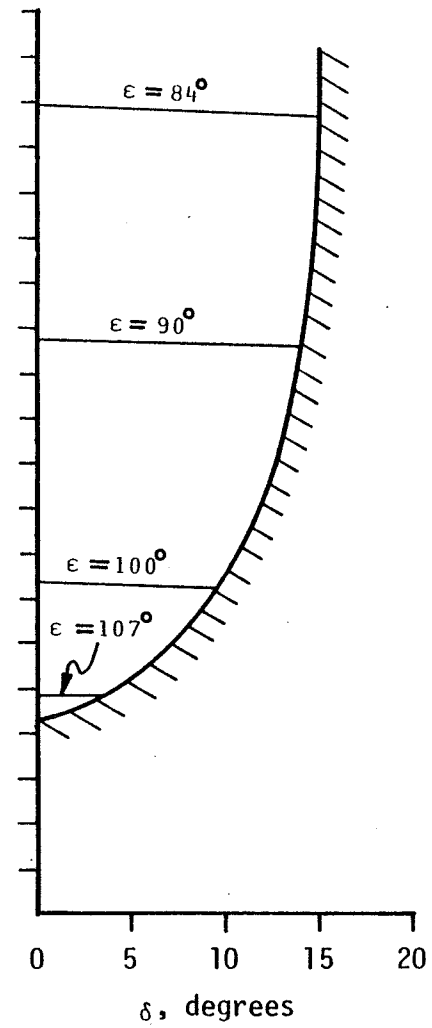
FIGURE 4-7. CONSTRAINT BOUNDARIES FOR INJECTING PAYLOAD INTO ESCAPE TRAJECTORIES



(a)  $\Delta V_{\text{error}} = 3.51 \text{ km/sec}$



(b)  $\Delta V_{\text{error}} = 4.0 \text{ km/sec}$



(c)  $\Delta V_{\text{error}} = 4.56 \text{ km/sec}$

FIGURE 4-8. CIRCULAR ORBITS OBTAINABLE USING SECOND ORBIT

### 4.2.2 Conclusions

Based on the data summarized in Figure 4-6, the following conclusions have been reached. Rescue of a failed payload in Earth orbit can be conducted by a second OTV under a wide range of impulse errors provided that the magnitude of the angular error can be held to under 30 degrees from the nominal. If the misdirected OTV burn can be detected and terminated early enough, the second OTV can recover the payload, the failed OTV and the SOIS. If the burn proceeds further, it may be possible to recover the payload, the vented OTV and SOIS; the payload and vented SOIS; or the payload alone, depending upon the velocity increment imparted by the first OTV. If the angular error cannot be held to  $\sim 30$  degrees or less, then a misdirected burn must be terminated almost immediately or else run the risk of possibly injecting into an Earth orbit trajectory with a perigee low enough to result in an early Earth reentry.

### 4.3 References

- 4-1. Margolis, K., "Theoretical Evaluation of the Pressures, Forces, and Moments at Hypersonic Speeds Acting on Arbitrary Bodies of Revolution Undergoing Separate and Combined Angle-of-Attack and Pitching Motions", NASA TN D-652, NASA/Langley Research Center, Langley, Virginia (June 1961).

## 5.0 SAFETY ASSESSMENT

In any potential engineering project involving the safety of human beings, it is customary (and, usually, required legally) to perform analyses to show that the project will not compromise human safety beyond an acceptable level. In the disposal of nuclear waste products in space, large amounts of high-level waste would be placed near very large amounts of potentially explosive propellants and oxidizers, be accelerated to very high velocities, and be subject to the possibility of encountering very high temperatures in the case of reentry or propellant fire. Due to the extreme, if highly unlikely, potential consequences of accidents, exhaustive analyses of dangerous environments and methods of safely coping with these events and conditions must be accomplished. This can only be done over a long period of time as the system concept and design evolves. The work reported here represents the first step in such a sequence.

Section 5.1 describes those accident environments that are expected to produce the most severe conditions experienced by the nuclear waste payloads. The results of this section were then used in Section 3.4.3 to determine the effects of these severe accident environments on the design of the payload container (see Section 3.4) and in Section 6.0 to estimate the resultant environmental impacts.

Section 5.2 is a first step in defining systematically all possible accidents or combinations of events that could lead to release of the nuclear waste, no matter how small the chance. Fault tree methodology was used in this section, but probabilities were not assigned to individual events because of the lack of credible data. Subjective estimates were made for the most likely failure paths and possible "workarounds" that could lessen their likelihood.

Section 5.3 deals with some suggested changes to the baseline mission and hardware that could produce a higher degree of safety. Section 5.4 contains a listing of the documents referred to in the previous three sections.



## 5.1 Major Accident Environment Characterization

The proper design of containment systems for nuclear waste disposal has to include considerations for the occurrence of all likely accidents. The preliminary container design effort, as discussed in Section 3.4 of this report, required the definition of the more significant accident environments for the space disposal missions. The severity of an accident and the consideration of what could happen as a result of a particular event also has a direct bearing on the work described in the safety and environmental impact analysis sections of this report (Sections 5.0 and 6.0).

The first step in defining accident environments was to identify the more severe accidents. A preliminary screening of possible events that could occur during ground handling, prelaunch, launch, and orbital operations led to the identification of accidents that are shown in Table 5-1. It should be noted that this list is not exhaustive, as is indicated later in Section 5.2. As identified in Table 5-1, three severe accident types were chosen for further study. It was believed that these accidents would be the major containment design drivers. The three major accident environments that were chosen to be evaluated were: (1) Space Shuttle vehicle explosion and fire, (2) reentry of the payload, both protected and unprotected, and (3) payload sinking to the bottom of the ocean. The environments that the payload would be expected to experience due to these three events are discussed in the following sections.

Accident environments which have not been treated here, but which are believed to be important in future work are those associated with: (1) the OTV/SOIS explosion in a vacuum, (2) orbital collisions with other objects, (3) abnormal reentry after an accident or malfunction during ascent, and (4) ground and water impact environments.

### 5.1.1 Space Shuttle Explosion and Fire

Various types of accidents can occur with the Space Shuttle vehicle, which lead to a catastrophic explosion and fire (see Section 5.2). For example, the vehicle could, during the early phase of the launch (liftoff), tip over, fall back or collide with the launch tower, resulting in a moderate (10-20%) explosive yield. The capability of employing a destruct system is planned where

**TABLE 5-1. IDENTIFIED ACCIDENTS USED TO SELECT MOST SEVERE ACCIDENTS FOR FURTHER CONSIDERATION IN ACCIDENT ENVIRONMENT CHARACTERIZATION**

GROUND HANDLING ACCIDENTS

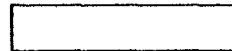
- Reentry System Propellant Fire
- Drop Loaded Container in NPPF
- Drop Loaded Reentry System in NPPF
- Outside Intrusion (Flying Vehicles, Natural)
- Transporter Accident
- Drop Loaded Reentry System at/in PCR
- Accidental SRM Ignition at Pad
- Accidental On-Pad Vehicle Explosion/Fire During/After Propellant Loading
- Accidental Ignition of Ejection Motor(s)
- Loss of Container Cooling

VEHICLE ON-PAD AND ASCENT ACCIDENTS

- Vehicle Fallback/Tipover/Tower Collision
- High Velocity Vehicle Impact on Land/Water
- Orbiter Crashes on Land/Water
- Payload Descends to Ocean Floor After System Failure
- Vehicle or Orbiter Collides with Another Aircraft
- Vehicle Explodes at Altitude W/O Command Destruct
- Abnormal Reentry of Reentry System
- Reentry System Impacts on Land/Water Surfaces After Ejection From Orbiter
- Accidental Ignition of Ejection Motor(s)
- Loss of Container Cooling

ORBITAL OPERATIONS ACCIDENTS

- Accidental Ignition of Ejection Motor(s)
- Collisions Between Payload and Another Object
  - OIV/Kickstage (KS)
  - Orbiter
  - Spacecraft
  - Space Debris
  - Meteors
- Critically Inaccurate OIV Burn (Direction/Duration) Resulting in Reentry
- Communications Failure Resulting in Reentry
- Lunar Collision
- Loss of Container Cooling
- Rescue Failure



Major Accident Environments Selected for Evaluation

hazardous payloads are flown in the Shuttle. When it would be used, the explosive yield (Y) would be quite low (1%). A high velocity surface impact of the vehicle could lead to a high explosive yield (20% Y 160%) if the destruct system either would not be used or would fail. The specific thermal and mechanical environments generated by these postulated events can be categorized into four areas: (1) a hydrogen-oxygen fireball, (2) a blast wave (shock wave) caused by the detonation of the hydrogen-oxygen propellants, (3) high velocity fragments from the External Tank skin resulting from the detonation, and (4) a ground-based solid propellant fire. The following subsections present preliminary data relating to these specific environments.

#### 5.1.1.1 Space Shuttle Hydrogen/Oxygen Fireball Environment

If the fully loaded (liquid hydrogen/liquid oxygen) Space Shuttle External Tank (ET) were to explode on the launch pad, the nuclear waste payload could be exposed to a short-term severe thermal environment. This section describes the model used and the results of calculations dealing with this thermal environment. The basic fireball model is that of Bader, et al.<sup>(5-1)</sup> The results presented provide estimates of fireball temperature and radiant heat flux as a function of time after the explosion.

Fireball Model and Assumptions. The Liquid-Propellant Rocket Abort Fire Model, developed by Bader<sup>(5-1)</sup> was used to calculate the thermal environment of the fireball resulting from an on-pad Space Shuttle ET explosion. The first analytical work on rocket abort models was done by Van Nice and Carpenter in 1965.<sup>(5-2)</sup> Various experimental data concerning rocket launch aborts have also been reported.<sup>(5-3 through 5-7)</sup> In 1966, Kite and Bader developed a fireball model<sup>(5-8)</sup> from the analytical results of Reference 5-2; in 1971 Bader revised<sup>(5-1)</sup> this earlier work. Analysis here has employed Bader's recent model and developed it further for the Space Shuttle case.

The general assumptions of the model used here are as follows:

- The rate of liquid hydrogen/liquid oxygen addition to the ET fireball is constant (this is justified by experimental data shown in Reference 5-1).

- Air entrainment into the fireball is ignored, providing the worst case condition. Inclusion of it would lead to lower temperatures and radiant heat fluxes.
- Complete burnup of the Shuttle LH<sub>2</sub>/LO<sub>2</sub> propellants is assumed, thus providing a worst case condition.
- The fireball is an isothermal, homogeneous body which is spherical at all times. The isothermal, homogeneous characteristic is based on the high degree of turbulence existing during the fireball formation. Reference 5-2 concluded that this assumption is reasonable.
- The fireball radiates as a blackbody with an emissivity of 1.0.
- The time until the fireball lifts off the ground and the time when all the propellant is consumed are identical.
- Chemical equilibrium exists within the fireball.

Figure 5-1 presents a schematic that defines the assumed fireball features and fireball development with time. Time  $t = 0$  is when the explosion begins. All propellant is assumed to be consumed by  $t = t_{\text{liftoff}}$ . The features of the modeled fireball stem and possible residual fire are also shown.

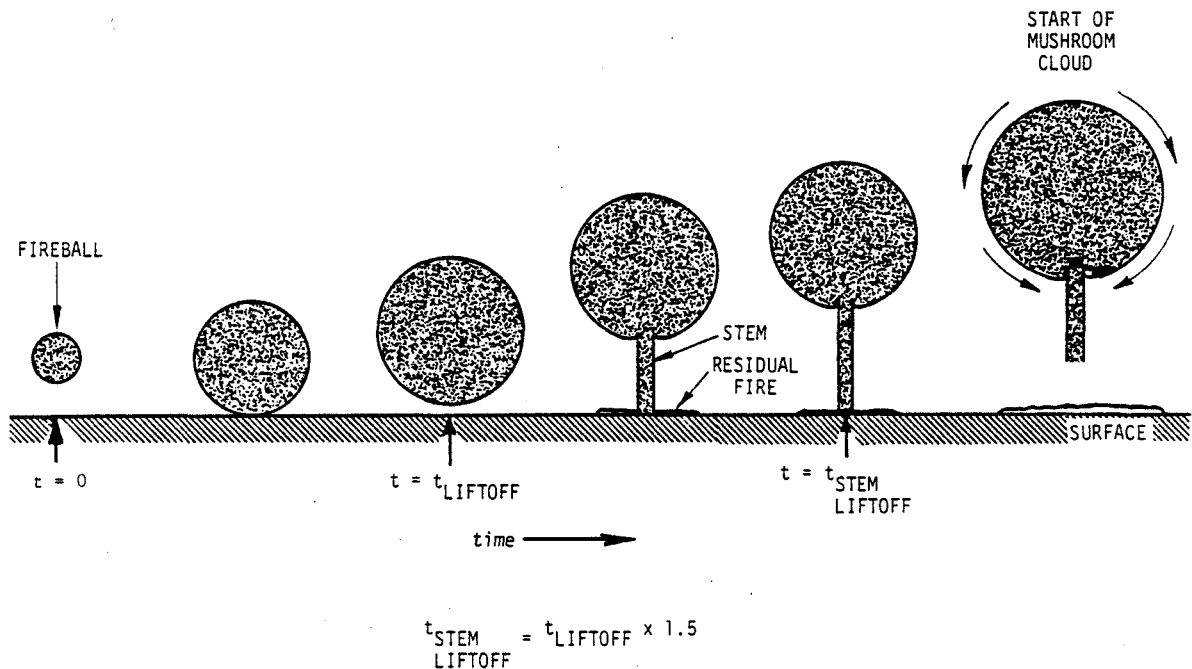


FIGURE 5-1. MODELED FIREBALL DEVELOPMENT

**Thermochemical Analysis.** The procedure used to calculate the internal equilibrium conditions of the  $H_2/O_2$  fireball are described below. Before the equilibrium composition of a gas mixture can be determined the elemental composition must be defined. The Space Shuttle External Tank holds approximately 609,600 kg of liquid oxygen and 102,500 kg of liquid hydrogen at liftoff, providing an oxygen to hydrogen elemental mole ratio of 0.3747. By assuming that the propellants were at their normal boiling point temperatures, and assuming values of heat of formation as found in Reference 5-9, the initial heat of reactants was calculated to be -213 kcal per kg of total propellant.

For the reaction of oxygen and hydrogen there are six species that are expected in the reacted mixture, namely,  $H_2O$ ,  $H_2$ ,  $O_2$ ,  $OH$ ,  $H$ , and  $O$ . If the reactions are assumed to occur at constant pressure (free volume combustion), then there are six unknown species and an unknown equilibrium temperature to calculate. Therefore, seven equations are needed to solve for the seven unknowns. Relationships involving mass, energy and state conditions provide the basis for the calculation.

Since the elemental mole ratio (A) of oxygen to hydrogen has been calculated to be 0.3747 for the Space Shuttle, and the total pressure, P, is 1 atmosphere, two relationships relating partial pressures of the species can be written as follows:

$$\frac{P_{H_2O} + 2P_{O_2} + P_{OH} + P_O}{2P_{H_2O} + 2P_{H_2} + P_H + P_{OH}} = 0.3747 = A \quad (1)$$

and

$$P = 1.0 = P_{H_2O} + P_{H_2} + P_{O_2} + P_{OH} + P_O + P_H \quad (2)$$

Four more relationships relating temperature (equilibrium constants) and partial pressures, given the equilibrium chemical reaction, can be written as follows:

$$K_p(T)^{H_2O} = \frac{P_{H_2O}}{P_{H_2} P_{O_2}^{1/2}} \text{ for } H_2 + \frac{1}{2} O_2 \rightleftharpoons H_2O \quad (3)$$

$$K_p(T)^{H_2} = \frac{P_{H_2}}{P_H^2} \text{ for } H + H \rightleftharpoons H_2 \quad (4)$$

$$K_p(T)^{O_2} = \frac{P_{O_2}}{P_O^2} \text{ for } O + O \rightleftharpoons O_2 \quad (5)$$

$$K_p(T)^{OH} = \frac{P_{OH}}{P_H P_O} \text{ for } O + H \rightleftharpoons OH \quad (6)$$

where:

$K_p(T)$  = the temperature dependent equilibrium constant for the defined chemical reactions.

Finally, the heat of reactants must equal the heat of products to satisfy the equilibrium requirement, thus, we can write:

$$0 = h_{\text{reactants}} - h_{\text{products}} \quad (7)$$

Since  $h_{\text{reactants}} = -213 \text{ kcal/kg}$ , the case where  $h_{\text{products}} = -213 \text{ kcal/kg}$  needs to be solved. This is accomplished as follows. Equations 1 through 6 can be rearranged to form the following relationship:

$$P_H = \frac{-1 + \sqrt{1 - 4 \left[ K_p^{H_2(A+1)} + A K_p^{H_2} K_p^{H_2O} K_p^{O_2^{1/2}} P_O \right] \left[ (A-1) - A P_O - K_p^{O_2(A+1)} P_O^2 \right]}}{2 \left[ K_p^{H_2(A+1)} + A K_p^{H_2} K_p^{H_2O} K_p^{O_2^{1/2}} P_O \right]} \quad (8)$$

For a given value of  $T$  and  $P_O$ , the value of  $P_H$  can be calculated by employing data in Table 5-2 which determines the equilibrium constants. Once a value of  $P_H$  and  $P_O$  have been established, the partial pressures of the four other species can be calculated by using Equations 3 through 6. This calculation is performed for various values of  $P_O$  until Equation 2 is satisfied. Once this is accomplished, then the heat of products can be calculated for the given value of  $T$ . A computer program was written to accomplish this tedious procedure. Figure 5-2 provides the results of these calculations. Equation 7 is satisfied for the equilibrium condition where  $T = 2989^\circ\text{K}$ . Table 5-3 provides the heat of products data and species compositions as a function of temperature for the  $H_2/O_2$  fireball.

TABLE 5-2. EQUILIBRIUM CONSTANT DATA FOR HYDROGEN/OXYGEN COMBUSTION

Ti, °K	$\log_{10} K_p^{H_2}$	$\log_{10} K_p^{H_2O}$	$\log_{10} K_p^{O_2}$	$\log_{10} K_p^{OH}$
2100	5.0162	3.2277	5.7202	5.1744
2200	4.5021	2.9428	5.1423	4.6696
2300	4.0317	2.6830	4.6143	4.2079
2400	3.6004	2.4441	4.1300	3.7842
2500	3.2027	2.2246	3.6842	3.3939
2600	2.8354	2.0217	3.2725	3.0331
2700	2.4946	1.8341	2.8910	2.6986
2800	2.1781	1.6594	2.5367	2.3876
2900	1.8830	1.4969	2.2066	2.0978
3000	1.6069	1.3455	1.8984	1.8269
3100	1.3488	1.2033	1.6100	1.5733
3200	1.1066	1.0701	1.3395	1.3352

Source: Reference 5-10.

TABLE 5-3. HEAT OF PRODUCTS AND COMPOSITION DATA AS A FUNCTION OF TEMPERATURE FOR SHUTTLE HYDROGEN/OXYGEN FIREBALL

T °K	h, cal/g*	P <sub>O</sub>	P <sub>H</sub>	P <sub>OH</sub>	P <sub>O<sub>2</sub></sub>	P <sub>H<sub>2</sub></sub>	P <sub>H<sub>2</sub>O</sub>
-----Atmospheres-----							
2100	-1844	2.5 E-6	1.5 E-3	5.6 E-4	3.2 E-6	2.50 E-1	7.48 E-1
2200	-1752	9.2 E-6	2.8 E-3	1.2 E-3	1.2 E-5	2.49 E-1	7.47 E-1
2300	-1653	3.1 E-5	4.8 E-3	2.4 E-3	4.0 E-5	2.48 E-1	7.44 E-1
2400	-1542	1.0 E-4	7.9 E-3	4.5 E-3	1.0 E-4	2.47 E-1	7.40 E-1
2500	-1414	3.0 E-4	1.2 E-2	7.9 E-3	3.0 E-4	2.46 E-1	7.33 E-1
2600	-1261	6.5 E-4	1.9 E-2	1.3 E-2	8.0 E-4	2.46 E-1	7.21 E-1
2700	-1073	1.5 E-3	2.8 E-2	2.1 E-2	1.8 E-3	2.45 E-1	7.02 E-1
2800	-836.4	3.3 E-3	4.0 E-2	3.2 E-2	3.6 E-3	2.46 E-1	6.75 E-1
2900	-540.4	6.4 E-3	5.7 E-2	4.6 E-2	6.6 E-3	2.48 E-1	6.35 E-1
3000	-178.8	1.2 E-2	7.9 E-2	6.2 E-2	1.1 E-2	2.52 E-1	5.84 E-1
3100	251.9	2.0 E-2	1.1 E-1	8.0 E-2	1.6 E-2	2.57 E-1	5.20 E-1
3200	739.6	3.2 E-2	1.4 E-1	9.7 E-2	2.2 E-2	2.59 E-1	4.49 E-1

\*NOTE: The average molecular weight is 14.006 g.

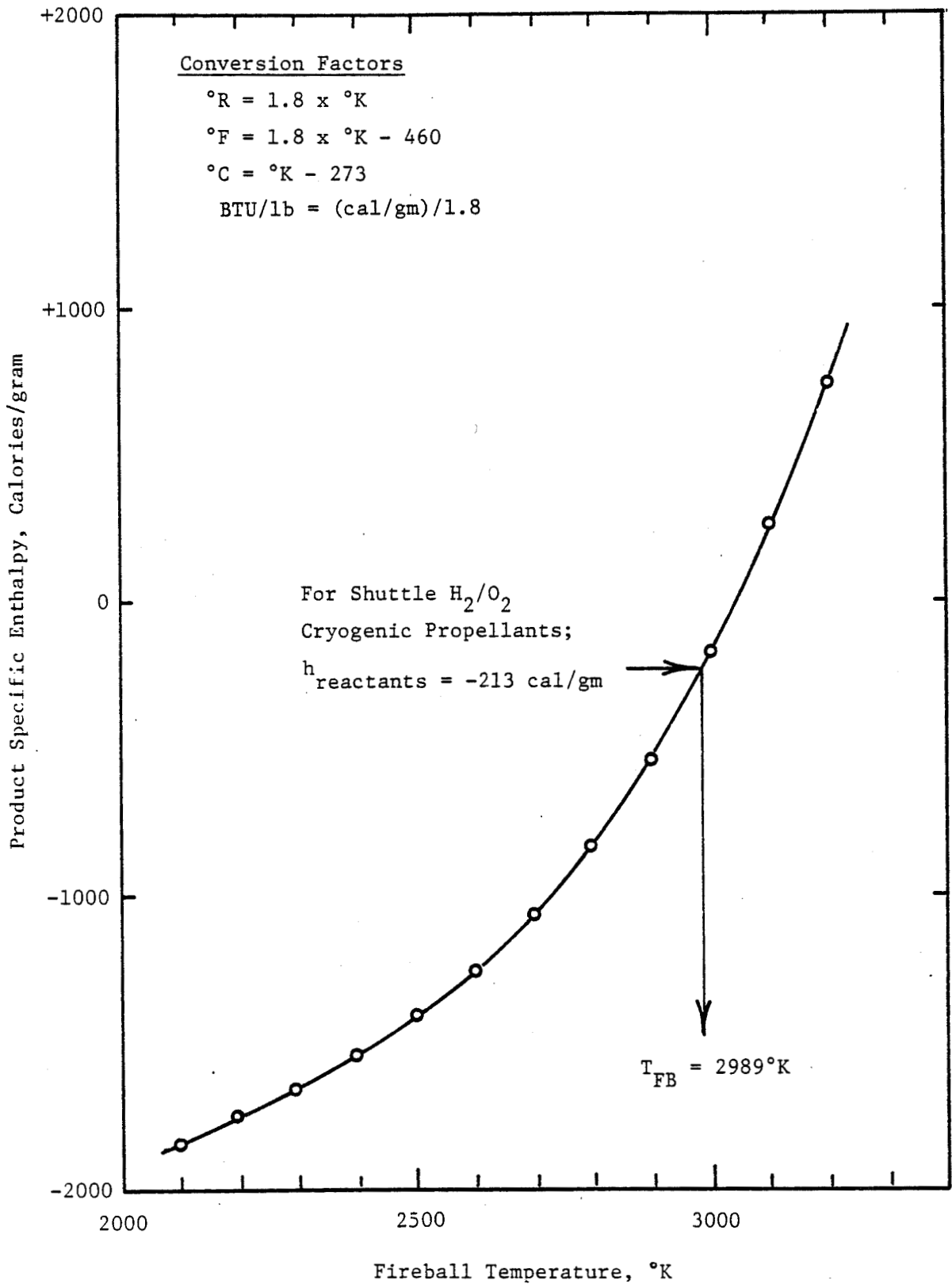


FIGURE 5-2. HYDROGEN/OXYGEN FIREBALL ENTHALPY AS A FUNCTION OF TEMPERATURE



**Calculations Employing Bader Model.** As indicated in Reference 5-1, the temperature relationship with time needs to be determined for two time,  $t$ , regions:

- (1)  $0 < t \leq t_{\text{fireball liftoff}}$ ,
- (2)  $t_{\text{fireball liftoff}} < t \leq t_{\text{stem liftoff}}$ .

While heat is still being added to the fireball ( $0 < t \leq t_{\text{fireball liftoff}}$ ), the change in internal enthalpy is equal to the rate change of chemical heat energy less radiation losses (see Equation 9). After all the fuel is consumed, the change in internal enthalpy is due to radiation losses only (see Equation 10).

$$R \cdot h_r - \epsilon \sigma A T^4 = \frac{d(W h_p)}{dt} \quad (9)$$

$$- \epsilon \sigma A T^4 = (W - W_b) \frac{d(h_p)}{dt} \quad (10)$$

where:

- R = Constant Rate of Fuel Addition
- $\epsilon$  = Emissivity
- $\sigma$  = Stephen-Boltzman Constant
- T = Temperature
- W = Weight of Fireball ( $W_b$  = Total Weight of Shuttle ET Propellants)
- t = Time
- $h_r$  = Enthalpy/Unit Mass of Reactants
- $h_p$  = Enthalpy/Unit Mass of Products

Appendix E provides a more in-depth discussion of the model used here. From Appendix E, the following equations for  $dT/dt$  were developed:

$$\frac{dT}{dt} = \left[ h_r - h_p - \frac{\epsilon \sigma 4\pi}{R} \left( \frac{3R\dot{R}}{4\pi P} \right)^{2/3} t^{2/3} T^{14/3} \right] \left[ \frac{1}{t} \right] \left[ \frac{1}{dT} \right] \quad (11)$$

$$\frac{dT}{dt} = \left[ - \frac{\epsilon \sigma 4\pi}{W_b} \left( \frac{2R\dot{R}}{4\pi P} \right)^{2/3} \right] \left[ T^{14/3} \right] \left[ t \right] \left[ \frac{1}{dT} \right] \quad (12)$$

where:

$R$  = Gas Constant

$P$  = Pressure

A computer program was written to integrate these equations by employing the 4th order Runge-Kutta-Gill Method. The resulting relationships between temperature and time as well as heat flux and time are provided in Figures 5-3 and 5-4, respectively. These figures indicate that the extreme thermal environment is expected to last less than 10 seconds. During actual conditions air entrainment would be expected to lower the temperature and flux values. A residual fire is assumed to occur. It is not clear, however, how long this fire will continue. The postulated solid propellant fire (see Section 5.1.1.2) may last from 7 to 15 minutes and would provide higher temperatures and fluxes than the "residual fire".

The predicted fireball diameter is a function of time, as shown in Figure 5-5. See Appendix E for further details.

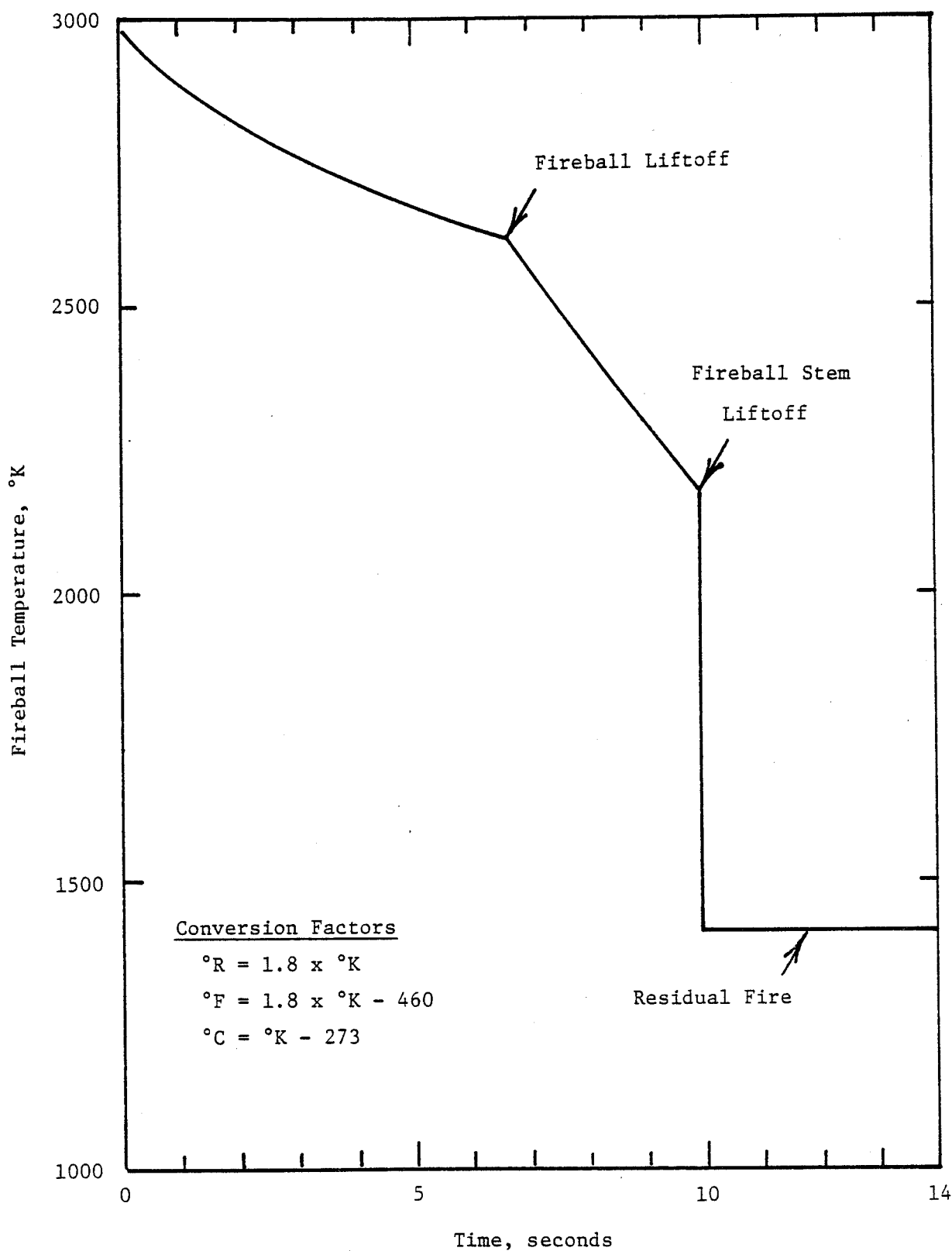


FIGURE 5-3. TEMPERATURE AS A FUNCTION OF TIME FOR SPACE SHUTTLE HYDROGEN/OXYGEN FIREBALL ENVIRONMENT

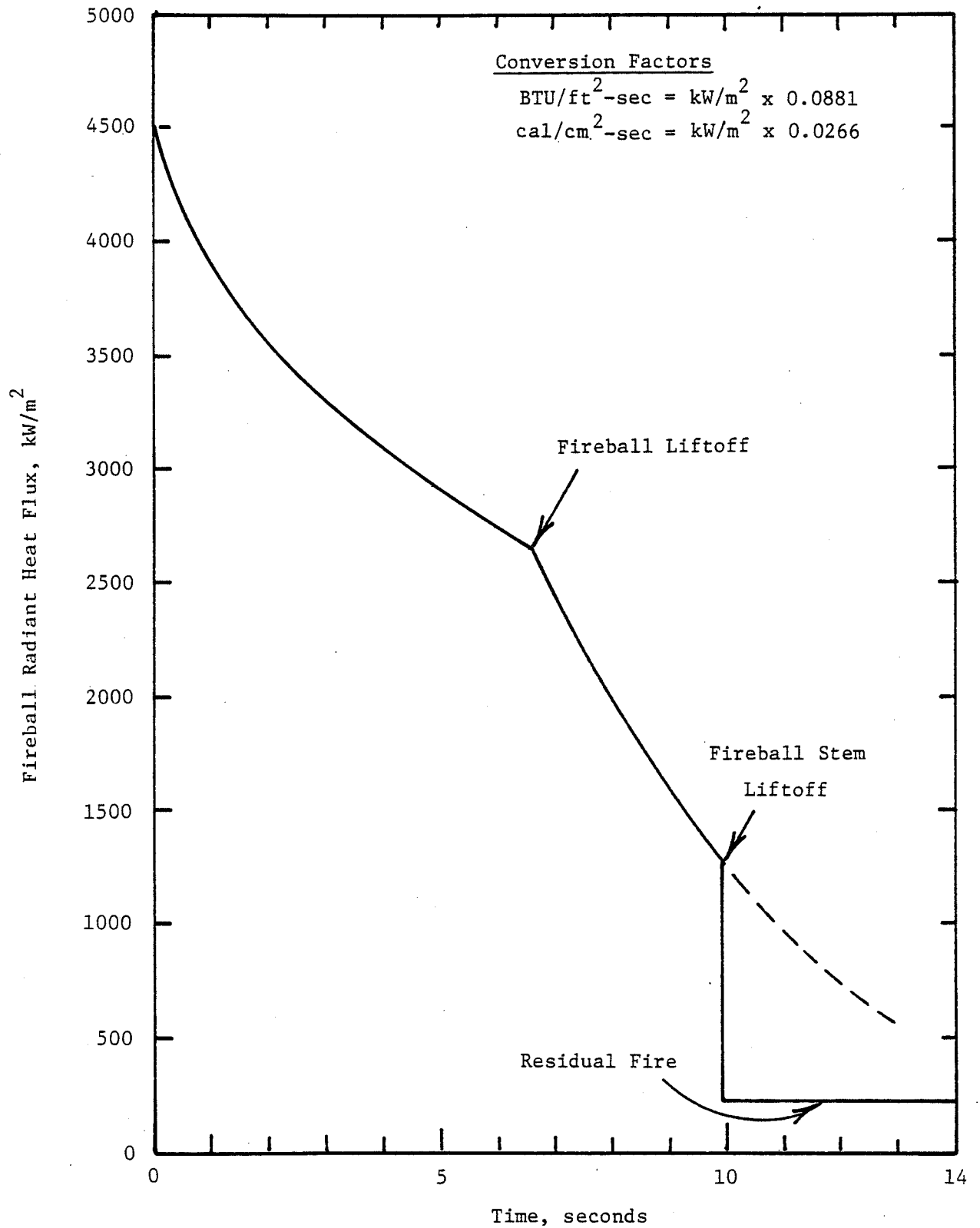


FIGURE 5-4. RADIANT HEAT FLUX AS A FUNCTION OF TIME FOR SPACE SHUTTLE HYDROGEN/OXYGEN FIREBALL ENVIRONMENT

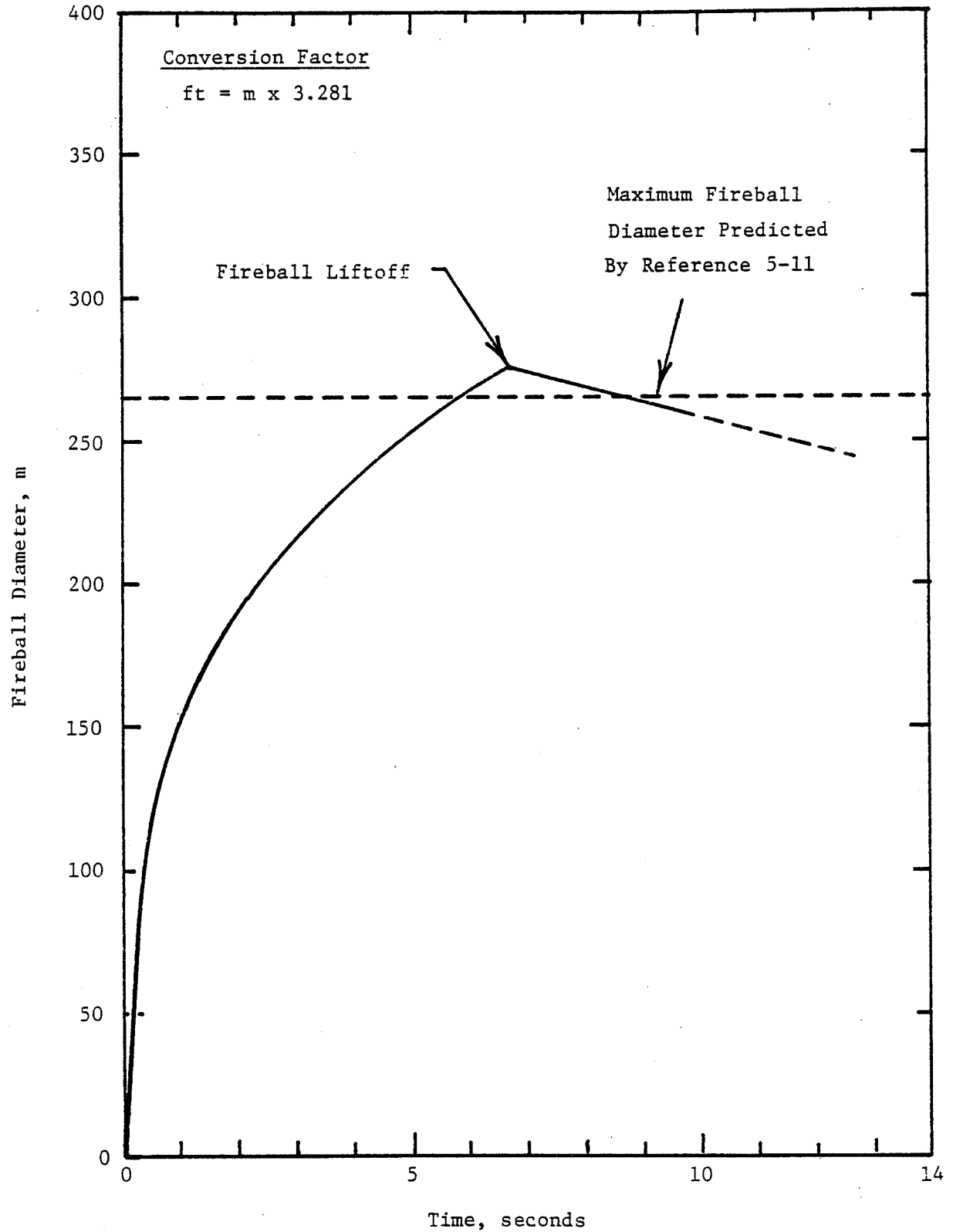
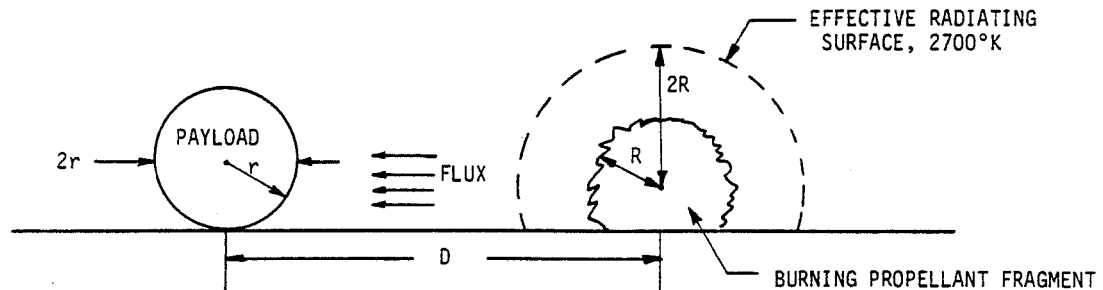


FIGURE 5-5. FIREBALL DIAMETER AS A FUNCTION OF TIME FOR SPACE SHUTTLE HYDROGEN/OXYGEN FIREBALL ENVIRONMENT

### 5.1.1.2 Space Shuttle Solid Propellant Fire Environment

Some on-pad or early flight failure mode sequences may result in the payload separating from the Space Shuttle Orbiter and falling to the launch pad. It is possible that the payload will then be subjected to a fire involving solid propellant from the Solid Rocket Boosters (SRBs). Two cases have been examined: one in which the SRBs have disintegrated and fragments of unconfined burning propellant are scattered on the launch pad, and a second case where the SRB has been split lengthwise by the destruct charge but is otherwise intact.

**Solid Propellant Fragment Fire.** This case is modeled as shown in Figure 5-6. The parameters associated with the burning propellant fragment are to some degree uncertain. The parameters chosen here, an effective radiating temperature of 2700 K and an effective radiating surface approximating a hemisphere with a radius of  $2R$ , where  $R$  is the "radius" of the propellant fragment, were taken from the tests and analyses made in connection with the multihundred watt radioisotope thermal generators used in the Lincoln Experimental Satellites 8 and 9.



**FIGURE 5-6. FRAGMENT MODEL FOR SPACE SHUTTLE SOLID PROPELLANT FIRE**

Heating of the payload is considered to be dominated by radiation from the burning propellant. This is justified by the high radiant flux corresponding to the high effective temperature and the near unity emissivity of the flame. Convective heating fluxes would be relatively low because of the low

velocities and would occur only when the separation of the payload and propellant fragment is small.

View factors\* between the radiating flame and the nearest point on the payload surface (considered to be a sphere or cylinder oriented perpendicular to the line joining it with the propellant fragment) were determined graphically. To a good approximation, these view factors were a function only of the normalized separation,  $(D - 2R - r)/(2R)$ , where  $D$  is the separation distance of the propellant fragment and payload centers,  $R$  is the propellant fragment radius, and  $r$  is the radius of the payload. As this view factor applies to the point in the payload surface closest to the burning propellant, it represents a worst case. However, no correction has been applied for reflection or re-radiation from the pad surface, and in this sense, the view factors are somewhat smaller than the true value. The correction should not be large, and should be compensated by the use of the view factor for the worst case point on the payload surface. Generally, the results of the following analysis are believed to be conservative.

Typical values of the view factor follow:

$\frac{D - 2R - r}{2R}$	View Factor*
0.0	0.95
0.25	0.47
0.50	0.27
0.75	0.175
1.0	0.123
1.5	0.077
2.0	0.055

The resulting fluxes are plotted in Figure 5-7.  $R_0$  in the figure represents the "radius" of the burning fragment at time zero, and  $\alpha = (D - 2R_0 - r)/(2R_0)$  is the value of the normalized separation at time zero. The figure applies generally for any value of time if the appropriate value of  $R$  is substituted for  $R_0$ . However, the parameter  $\alpha$  is normally restricted to the value of the initial normalized separation.

\*NOTE: A view factor is defined as the fraction of the radiation leaving a black surface A in all directions which is intercepted by surface B.

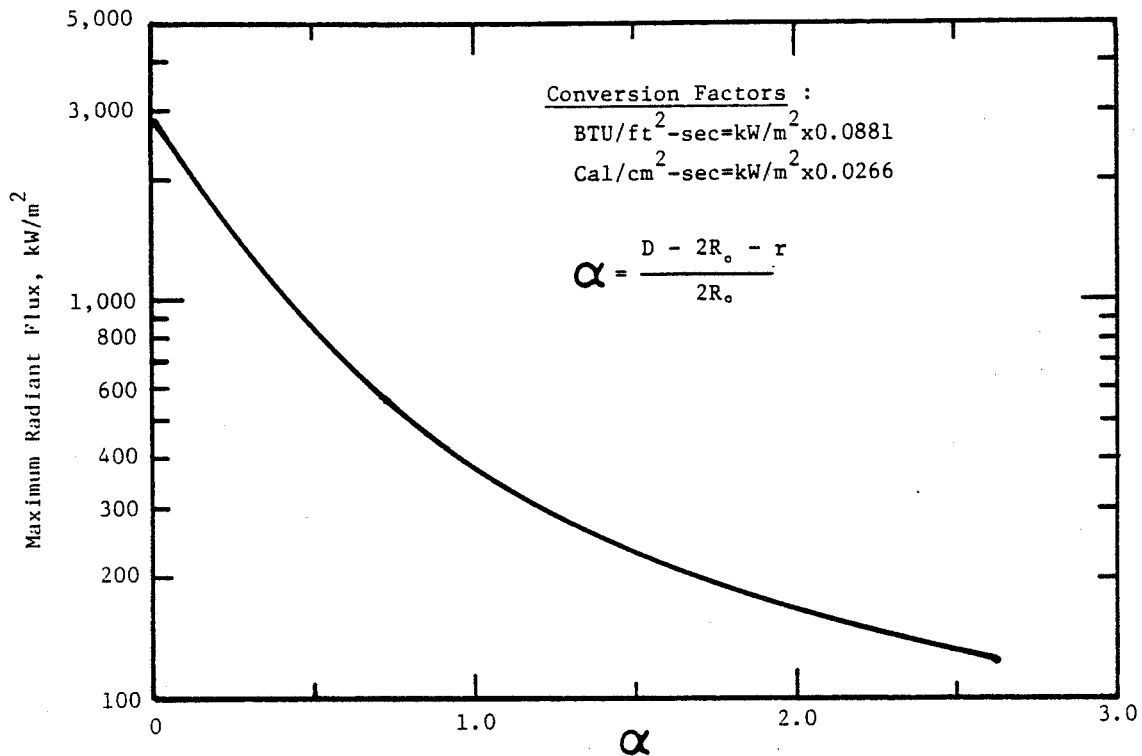


FIGURE 5-7. MAXIMUM HEAT FLUX AT TIME = 0  
(FRAGMENT FIRE MODEL)

As the propellant fragment burns, its size decreases and the normalized separation increases. The view factor and heat flux thus decrease with time. Figure 5-8 shows how the heat flux varies with dimensionless time for a range of  $\alpha$  values. The time is normalized by the burning time of the fragment,  $\tau = R_o/B.R.$ , where B.R. is the propellant burning rate at atmospheric pressure, 0.00115 m/s.

With Figure 5-8 and initial conditions of  $R$ ,  $r$ , and  $D$ , the time history of the radiant flux at the payload surface may be determined.

Since the maximum web thickness of the SRB propellant grain is 1.04 m,  $R_o = 1.04/2$ , and the maximum duration of a solid propellant fragment fire will be  $\tau = (1.04/2)/(0.0115) = 452$  seconds or about 7.5 minutes.

**Split Motor Fire.** The destruct system for the SRBs is a linear-shaped charge which splits the motor casing lengthwise. If the case should fall back to the launch pad after the destruct system was activated without further breakup, it would be possible for the payload, assumed to have been



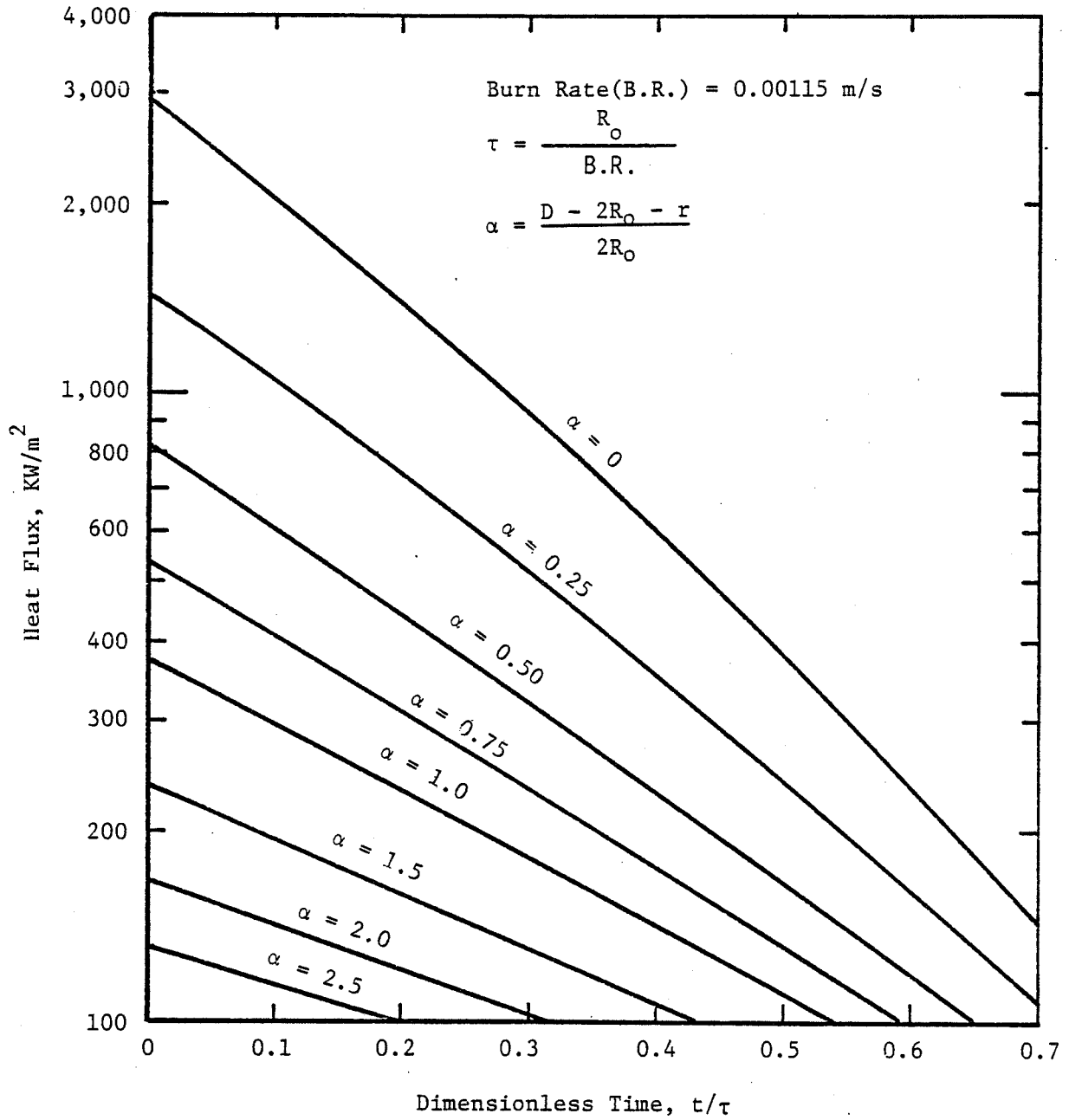
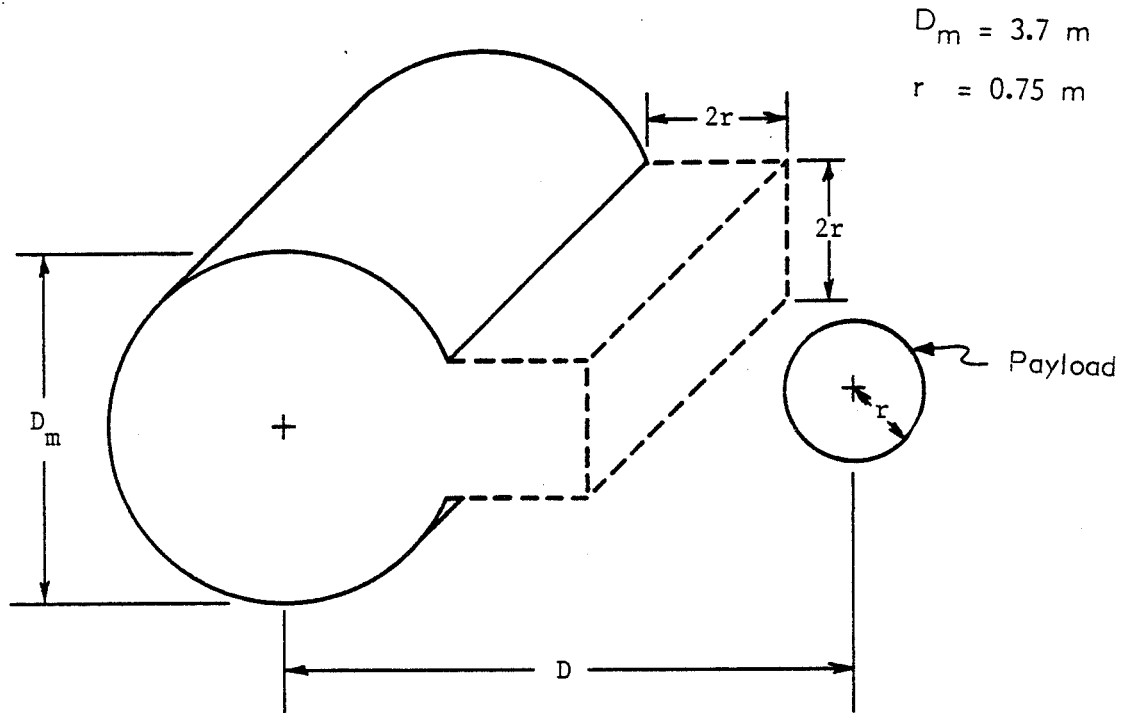


FIGURE 5-8. MAXIMUM HEAT FLUX AS A FUNCTION OF TIME (FRAGMENT FIRE MODEL)

freed from the Orbiter and to have fallen back to the launch pad, to be exposed to heating from burning solid propellant in the split casing.

Figure 5-9 illustrates this configuration. The dimension of the opening in the casing was chosen equal to twice the payload radius, assumed to be 0.75 m, to simplify the analysis. This should represent a conservative choice, as the opening seems unlikely to be this large.



**FIGURE 5-9. SPLIT MOTOR MODEL FOR SPACE SHUTTLE SOLID PROPELLANT FIRE**

The payload was assumed to be a cylinder lying parallel to the motor casing; however, the calculated heat fluxes are not strongly influenced by this assumption. As in the case of the propellant fragment fire, the effective radiating surface was assumed to extend to a distance equal to the width of the opening in the case.

For analysis, the radiating surface and the payload were replaced by parallel rectangles, with the length of the payload small compared to the length of the split motor casing.

The view factor for radiation between the effective flame surface and the payload can be calculated from relations given in standard texts.<sup>(5-12)</sup> The

calculated view factors as a function of the smallest distance between the SRB and the payload center line are as follow.

<u>Distance, m</u>	<u>View Factor</u>
1.5	1.0
1.5	1.0
2.3	0.59
3.0	0.38
3.8	0.24
4.6	0.15
7.6	0.06

The resulting heat fluxes to the payload are shown in Figure 5-10. Because the geometry does not change with time, the heat flux remains constant until the propellant within the casing is consumed. With a maximum web thickness of 1.04 m, this will be  $(1.04/0.00115) = 904$  seconds or about 15 minutes.

#### 5.1.1.3 Overpressure and Impulse Resulting from Space Shuttle External Tank Explosion

This section discusses the overpressure and impulse payload environments produced by an explosion of the hydrogen and oxygen contained in the Space Shuttle External Tank (ET). The possible contribution due to an explosion of the solid propellant contained in the Solid Rocket Boosters is ignored, as it is small compared to the ET contribution. The ET could explode as a result of various on-pad or ascent accidents or malfunctions. Also, the ET can be destructed deliberately by the linear-shaped charge that is placed along the ET on the side opposite to the Orbiter, should flight controllers determine that an off-course vehicle would endanger the local population or ground features. Depending upon the event, varying degrees of explosive yield can result. The explosive yield is defined as percentage of TNT equivalent. For example, if a given ET explosion would produce a 100% yield, that means that the total weight of propellants would produce the same effect as the same weight of TNT. Reference 5-13 suggests that the following explosive yields be considered for the Space Shuttle ET blast hazard analysis:

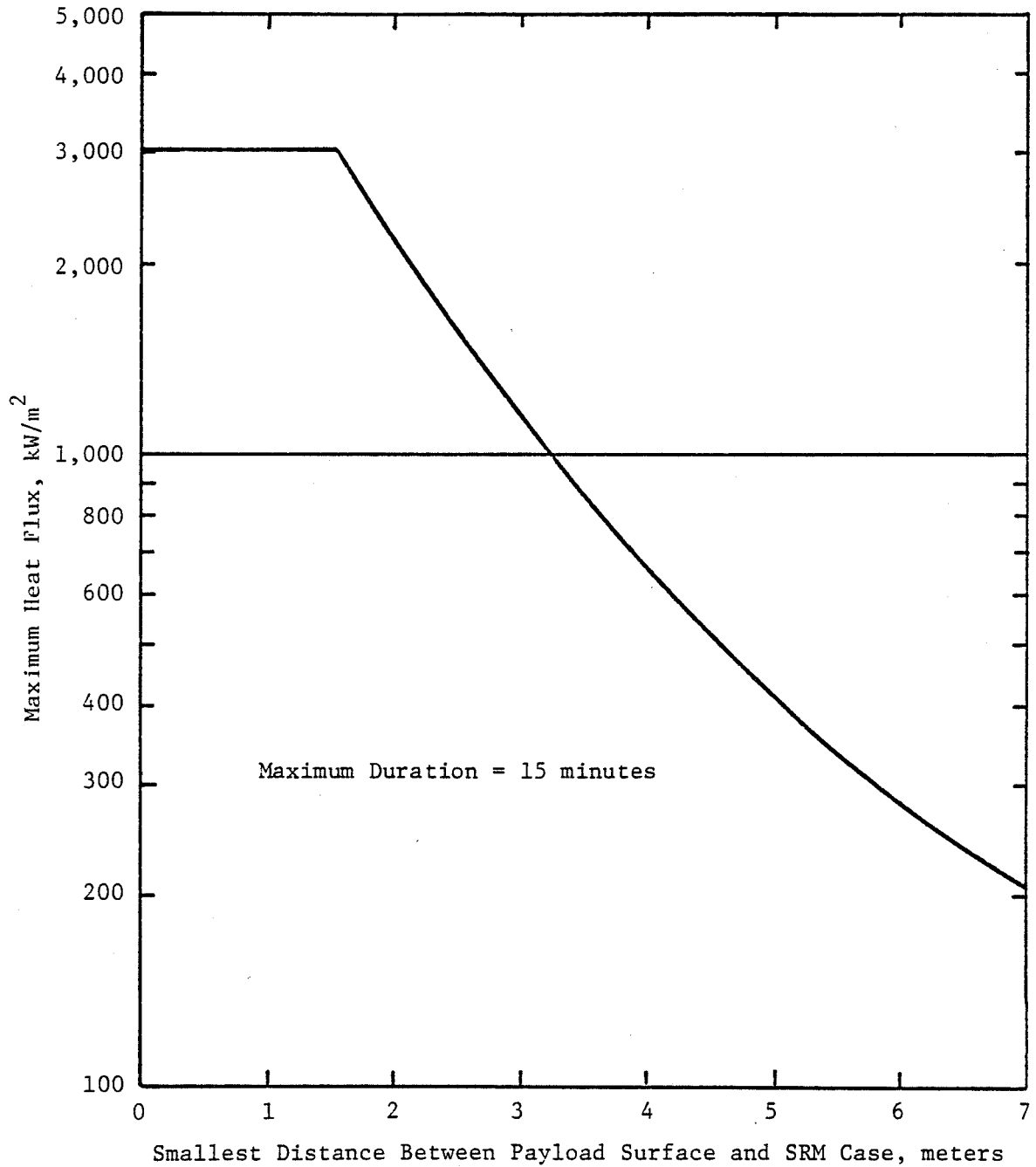


FIGURE 5-10. MAXIMUM HEAT FLUX AS A FUNCTION OF DISTANCE (SPLIT MOTOR FIRE MODEL)

<u>Explosion Event</u>	<u>Percent Explosive Yield</u>
Destruct	1
On-pad, no destruct	20
Fallback 30 m	50
High velocity impacts:	
350 m/s	100
550 m/s	160

Explosions of the ET are expected to produce mechanical environments that pose a hazard to payloads. For the nuclear waste payload, in particular, a shock blast wave could damage the containment vessel such that it might not survive a possible fire environment (see Sections 5.1.1.1 and 5.1.1.2). Also, and probably more critically, the blast wave will create high-velocity fragments which could cause a breach of the nuclear waste containment (see Section 5.1.1.4 for discussion of fragment environment).

This section provides estimates of the blast environment a payload might experience by calculating the incident (static) and reflected blast wave overpressures as a function of explosive yield. Also, the reflected blast impulses are calculated and presented as required for the fragment environment analysis (see Section 5.1.1.4).

It was assumed that all the ET propellant (609,600 kg of liquid oxygen, and 102,500 kg of liquid hydrogen) would be available for the explosion, giving a total of  $7.12 \times 10^5$  kg ( $1.57 \times 10^6$  lb) of available propellant.

Previous studies of explosion hazards for launch vehicles, carrying radioactive material, have assumed the center of explosion (COE) to be at the point (or points) of first potential liquid fuel/liquid oxidizer contact with each other. Figure 5-11 provides a scale drawing of the Space Shuttle Vehicle.<sup>(5-14)</sup> The center of explosion (COE) for the Space Shuttle case is taken to be the center of the intertank structure, between the liquid hydrogen and liquid oxygen tank of the ET. The position of this assumed COE and the position of the nuclear waste payload are shown. The position of the payload was obtained from Reference 5-15. The distance from the COE to the payload surface was calculated to be 21.6 m (70.8 ft). This distance has been used for all of the following calculations.

Procedures outlined in the CPIA-194 Hazards of Chemical Rockets and Propellants Handbook (Volume 1)<sup>(5-16)</sup> were used to calculate the overpressures

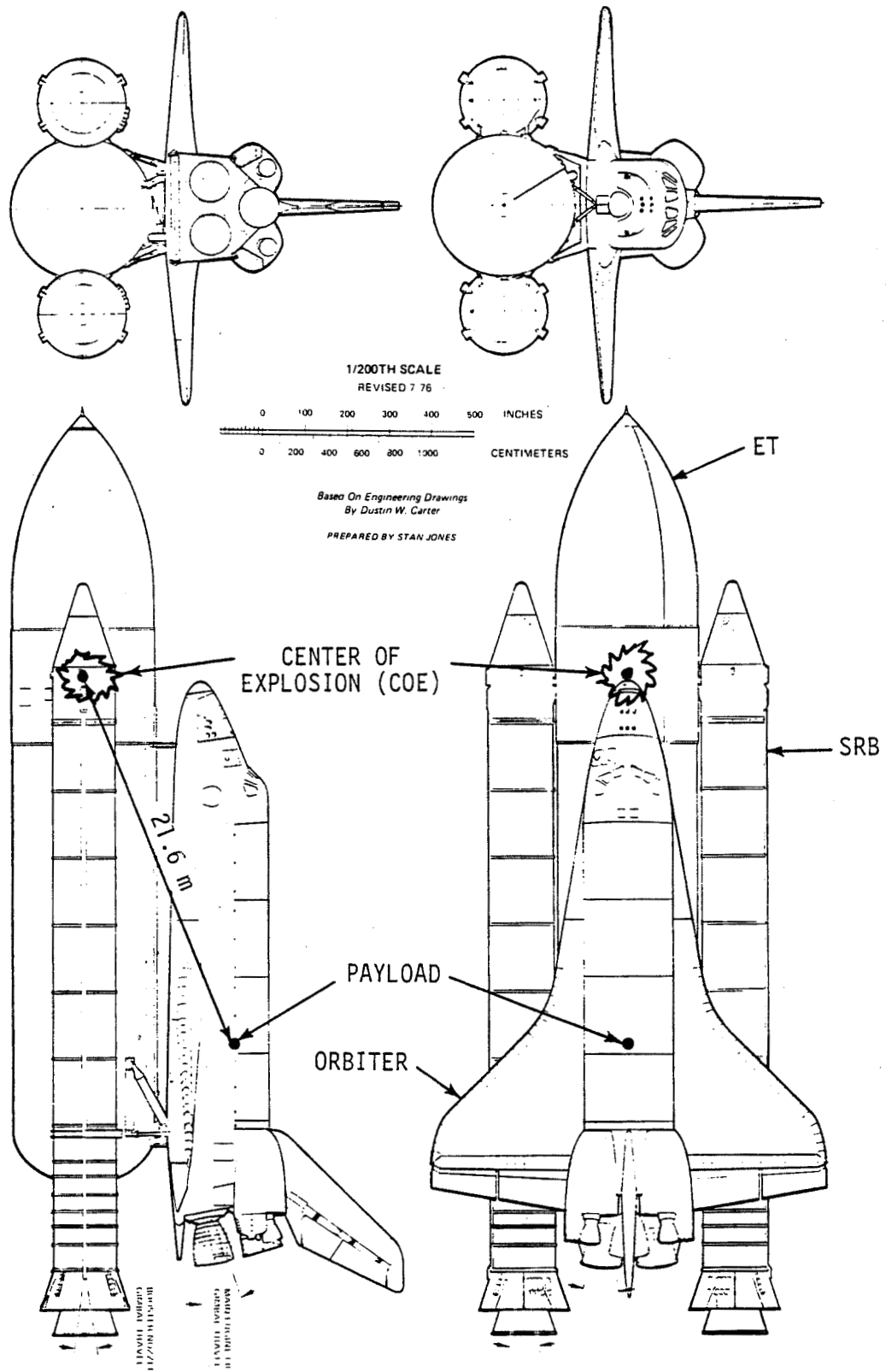


FIGURE 5-11. SPACE SHUTTLE VEHICLE WITH ASSUMED CENTER OF EXPLOSION AND LOCATION OF NUCLEAR WASTE PAYLOAD

that would result from the incident shock wave. Reflected pressures were calculated by using the relationship<sup>(5-16)</sup>:

$$\Delta P_R = 2 \Delta P_S \left[ \frac{7P_0 + 4\Delta P_S}{7P_0 + \Delta P_S} \right] \quad (13)$$

where:

$$\begin{aligned} \Delta P_S &= \text{Static (or Incident) Blast Wave Pressure} \\ P_0 &= \text{Ambient Pressure (1 atm)} \end{aligned}$$

The results are presented in Figure 5-12 for the five different explosive yields assumed.

The CPIA Handbook<sup>(5-16)</sup> was also used to calculate the reflected impulse,  $I_R$ , that is required for the analysis in Section 5.1.1.4. The relationship,

$$I_R = 2I_S \left[ \frac{7P_0 + 4\Delta P_S}{7P_0 + \Delta P_S} \right] \quad (14)$$

where:

$$\begin{aligned} I_S &= \text{Static Impulse} \\ P_0 &= \text{Ambient Pressure (1 atm)} \\ \Delta P_S &= \text{Static Blastwave Pressure} \end{aligned}$$

was used to calculate the curve shown in Figure 5-13.

#### 5.1.1.4 Space Shuttle Fragment Environment

An explosion of the External Tank (see Section 5.1.1.3) could result in the payload being impacted by fragments of the External Tank. The flux of fragments by velocity and size was calculated for explosive yields (based on the mass of hydrogen and oxygen in the External Tank) of 1, 20 and 160 percent TNT equivalent. These yields correspond to hypothesized possible failure sequences, with the highest yield occurring from a high-velocity impact of the Space Shuttle onto an unyielding surface.

The method of analysis was basically that used by Teledyne Energy Systems.<sup>(5-17)</sup> This approach uses as inputs fragment size distributions from Reference 5-18 and fragment velocity distributions from Reference 5-19.

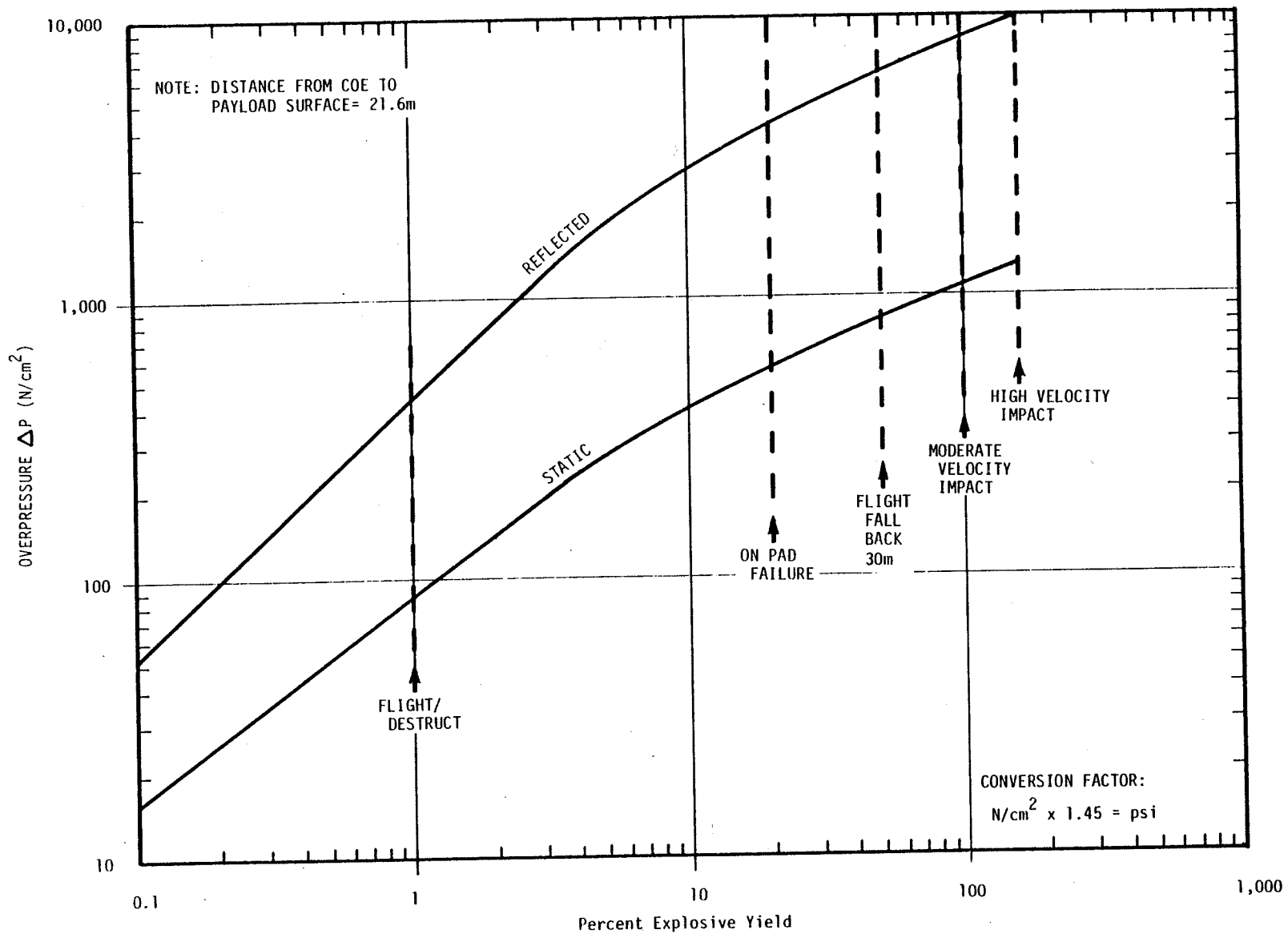


FIGURE 5-12. OVERPRESSURES AS A RESULT OF SPACE SHUTTLE ET BLAST WAVE



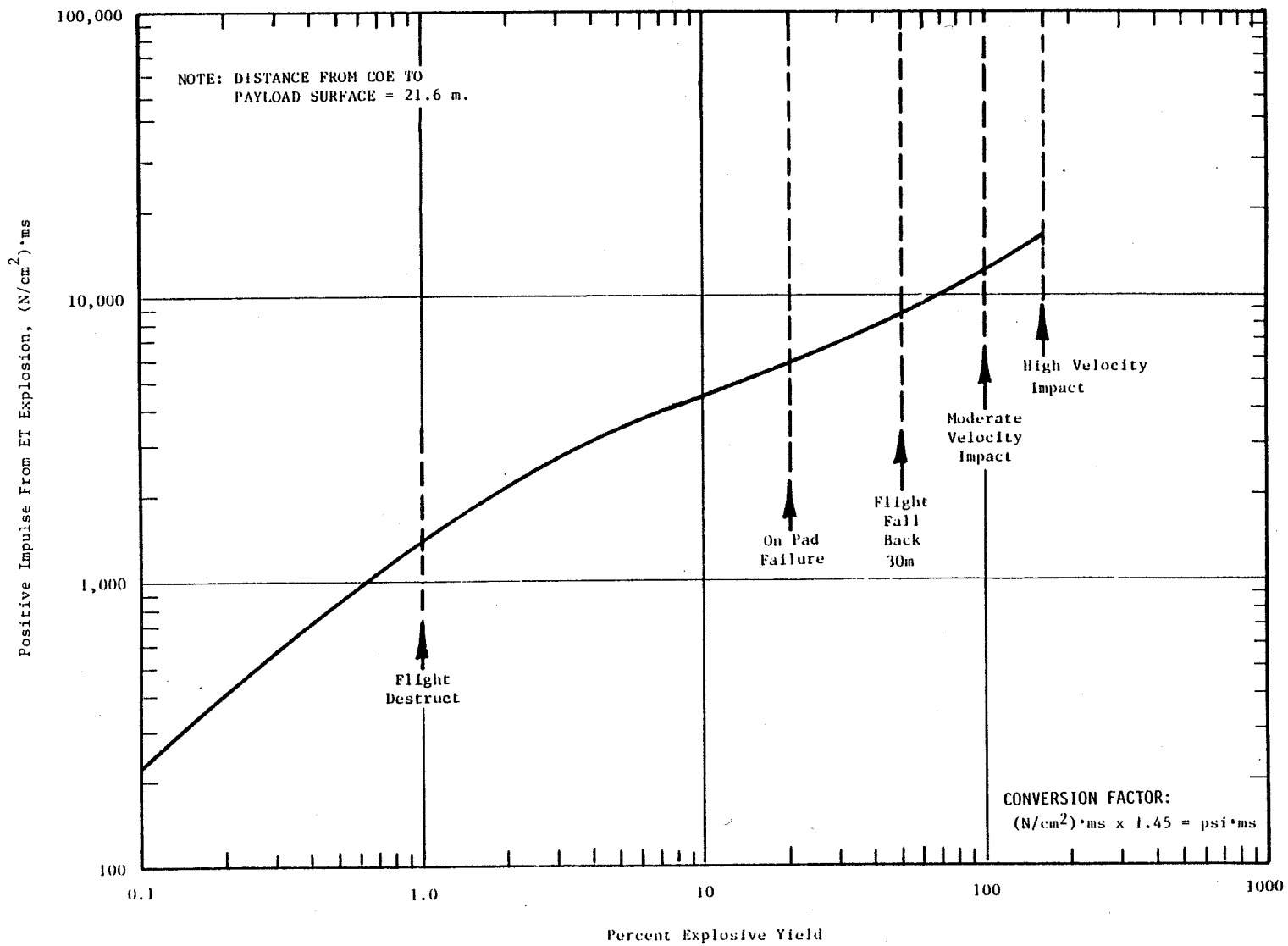


FIGURE 5-13. REFLECTED IMPULSE AS A RESULT OF SPACE SHUTTLE ET BLAST WAVE

The mean fragment size for a given yield,  $\bar{D}$ , is calculated from the equation

$$\bar{D} = D_o + 99.78 (I_r)^{0.882} \text{ cm}, \quad (15)$$

where  $D_o$  is the minimum fragment size, determined here by the External Tank skin thickness, and  $I_r$  is the reflected impulse in  $\text{N-s/cm}^2$  at the distance of the tank skin from the center of explosion (taken to be the midway between the bulkheads on the ET centerline - see Figure 5-11). The standard deviation is 2.3.

Figure 5-14 shows the resulting fragment size distributions for a series of explosive yields, where fragment size is expressed as the average diameter of the tank skin fragment. The minimum fragment size is taken as equal to the External Tank skin thickness. Fragments larger than 10 cm have been ignored, as they have a low probability of impacting the payload in an orientation favorable for penetration and relatively few large fragments are generated.

The mean velocity of the mean size fragment,  $\bar{V}$ , is calculated as

$$\bar{V} = \left[ 80.47 - 110.95 e^{-0.51(\bar{D}/D_o)} \right] I_r \text{ m/sec} \quad (16)$$

with a standard deviation of 2.5.

Figure 5-15 shows the resulting velocity distribution for the mean size fragment for various explosive yields. The upper velocity has been limited to 4000 m/sec, which is in the range of the expected detonation velocity of  $\text{H}_2/\text{O}_2$  mixtures.

The velocities of fragments larger and smaller than the mean size were calculated by applying a drag correction; that is, the fragments were assumed to be accelerated by an aerodynamic drag mechanism, so that the velocity attained is proportional to the drag coefficient. As a conservative assumption, all fragments were assumed to be accelerated in a high drag orientation (maximum dimensions perpendicular to blast wave motion). The drag coefficients were assumed to vary with fragment size as:

$$C_D = 1.17 (1 - 1.379 e^{-0.911D}). \quad (17)$$

The smallest fragments, with a size of 0.56 cm, thus have a drag coefficient of 0.2, equivalent to a sphere, while the largest fragments have a drag coefficient

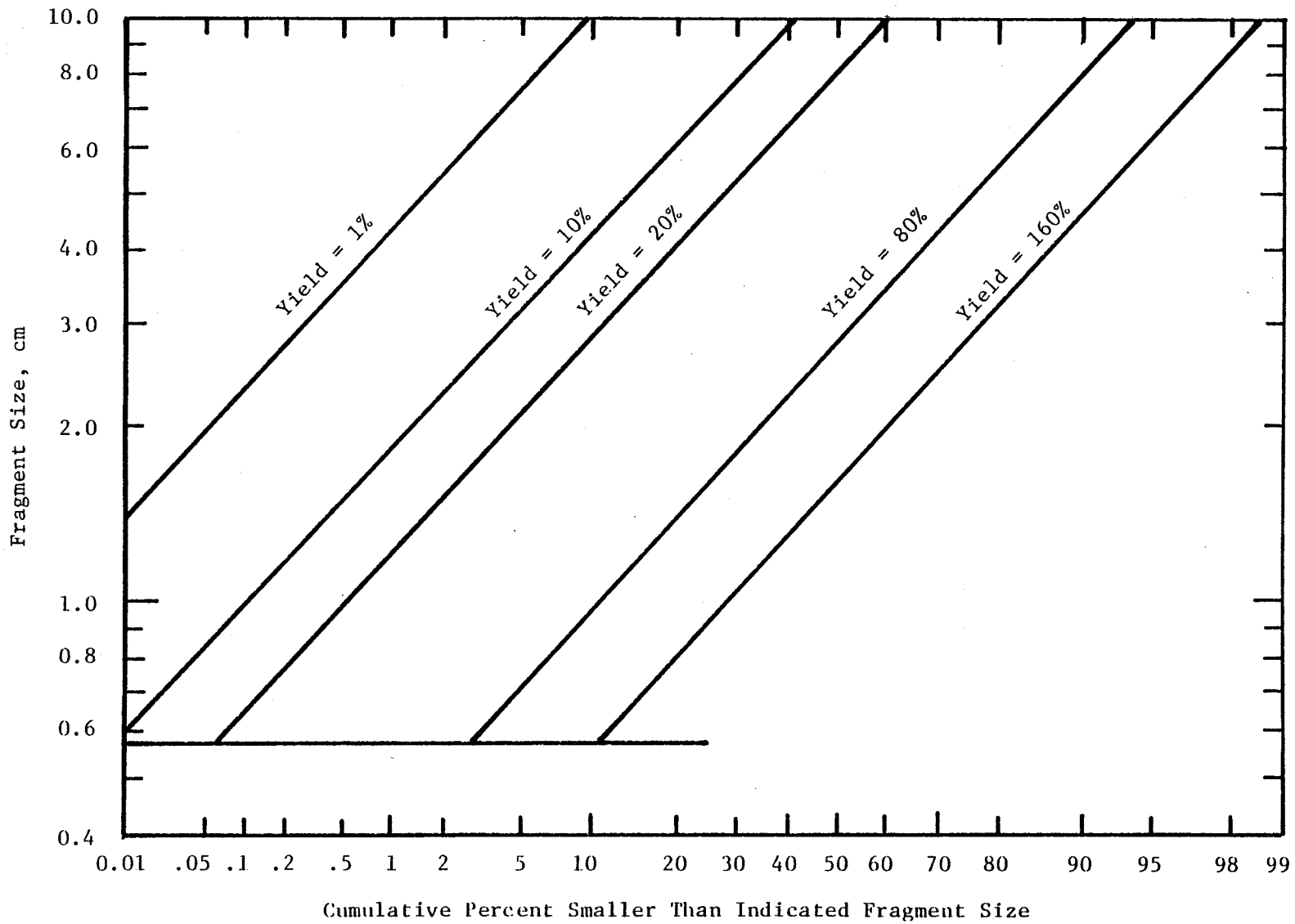


FIGURE 5-14. DISTRIBUTION OF FRAGMENT SIZES FOR SPACE SHUTTLE FRAGMENT ENVIRONMENT

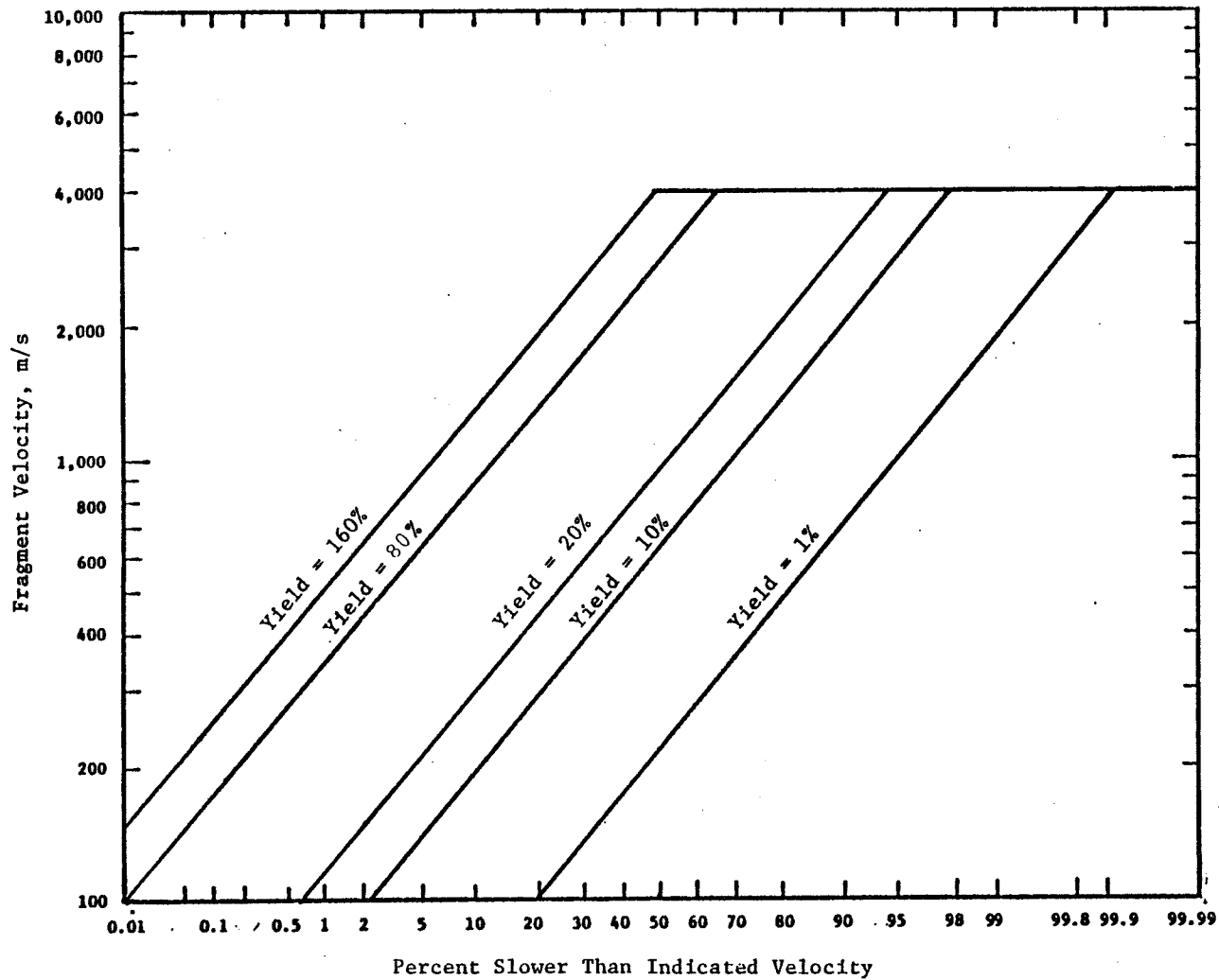


FIGURE 5-15. DISTRIBUTION OF VELOCITIES OF MEAN SIZE FRAGMENT FOR SPACE SHUTTLE FRAGMENT ENVIRONMENT

of 1.17, equivalent to a flat plate at normal incidence. Expressed as a correction factor, i.e.,

$$F = (1 - 1.379 e^{-0.911D}), \quad (18)$$

this relation is plotted in Figure 5-16. Mean velocities for various fragment sizes are calculated by multiplying the mean velocity of the mean size fragment by the ratio of the convection factors:

$$V_D = \frac{\bar{V} F_D}{\bar{F}}, \quad (19)$$

where  $V_D$  is the mean velocity of fragments of size  $D$ ,  $\bar{V}$  is the mean velocity of the mean size fragment, and  $F_D$  and  $\bar{F}$  are the correction factors for the fragment of size  $D$  and of the mean size fragment.

The distance between the hypothesized location of the explosion and the center of the payload is 23 meters, so that a solid angle of

$$\Omega = \frac{1}{(23)^2} = 0.00189 \text{ str} \quad (20)$$

is subtended per square meter of projected payload cross section. The area of External Tank skin intercepted by this solid angle is

$$A_s = (\ell)^2 \Omega \csc \phi, \quad (21)$$

where  $\ell$  is the distance from the center of explosion to the tank skin and  $\phi$  is the angle between the axis of the External Tank and the line joining the center of explosion and the payload. By measurement from Space Shuttle drawings,  $\ell = 11.00$  m and  $\phi = 22^\circ$ . Hence, the area of External Tank skin intercepted per unit area of projected payload cross section is

$$\frac{A_s}{A_p} = (11.00)^2 \times 0.00189 \times \csc 22^\circ = 0.610. \quad (22)$$

It is assumed that all fragments for this intercepted tank skin area impact on the payload.

The number of such fragments is calculated by dividing the intercepted tank skin area by the mean area of all fragments, which is given by

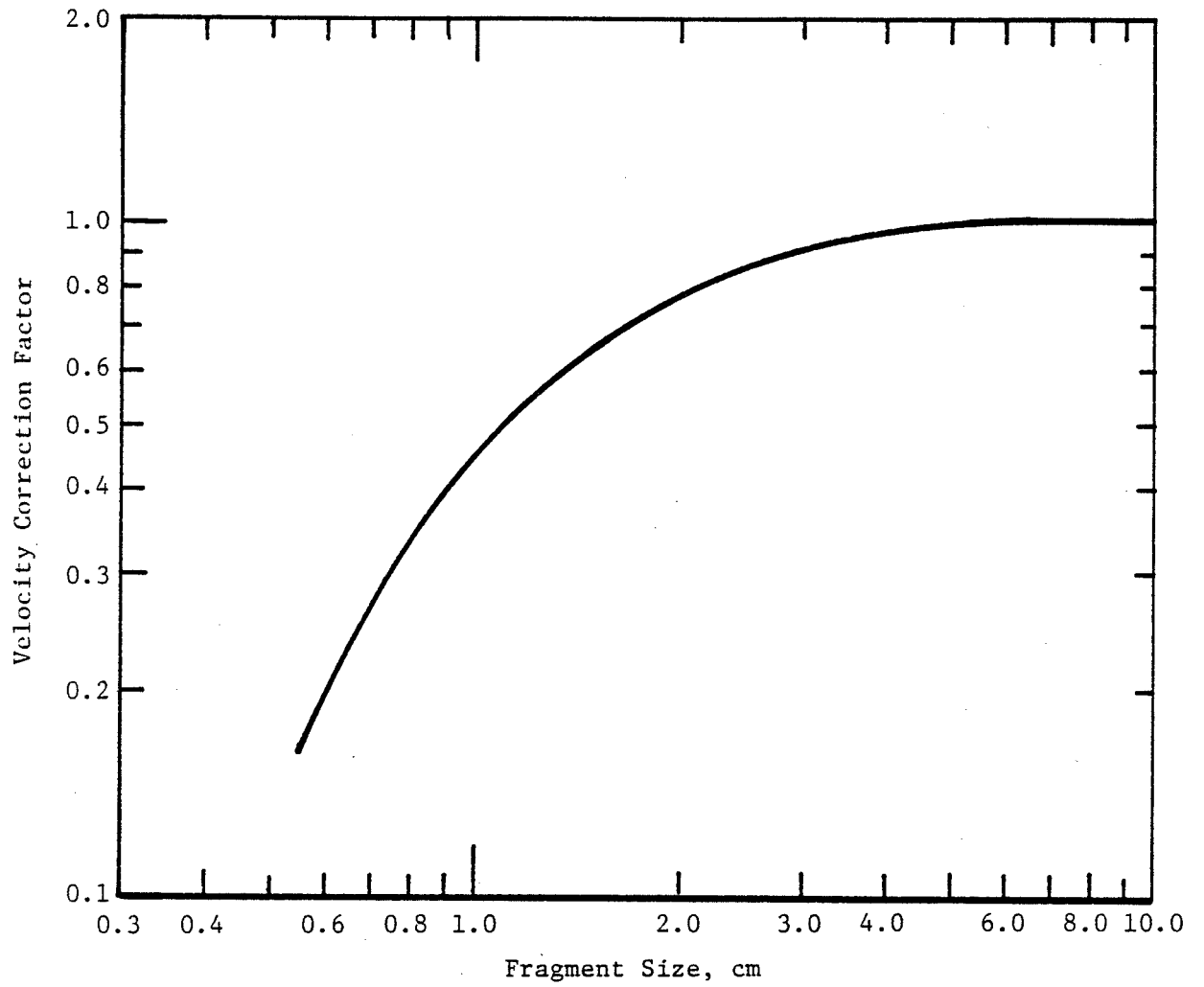


FIGURE 5-16. DRAG CORRECTION FACTORS FOR FRAGMENT ACCELERATIONS FOR SPACE SHUTTLE FRAGMENT ENVIRONMENT

$$\bar{A} = \frac{\pi}{4} \bar{D}^2 e^{2(\ln \sigma)^2}, \quad (23)$$

where  $\sigma$  is the standard deviation for the fragment size distribution. Thus, the number of impacting particles per unit area of projected payload surface is

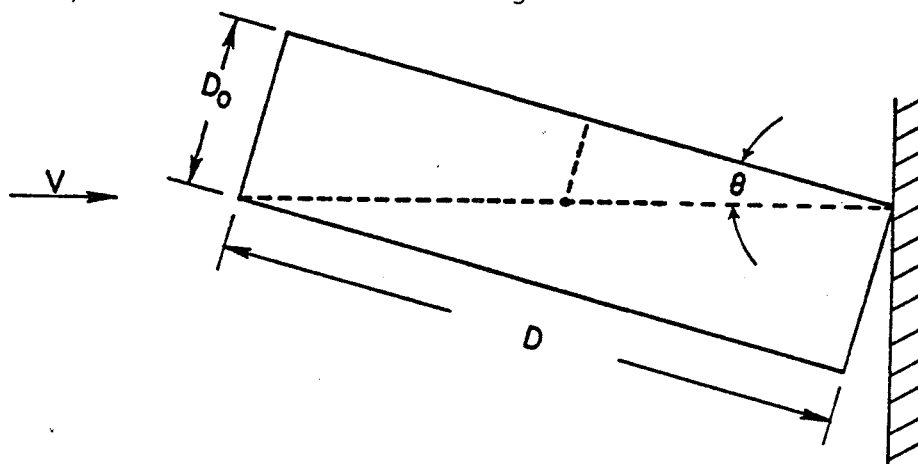
$$N = \frac{4 \times 0.610 \times 10^4}{\pi \bar{D}^2 e^{2(\ln \sigma)^2}} = \frac{1939}{\bar{D}^2} \text{ m}^{-2}, \quad (24)$$

where the mean fragmented size is given in cm.

Impacted fragments of the same size can have widely differing penetrating abilities, depending on their orientation, with those fragments impacting edge-on having the greatest penetrating potential. As a first approximation, only those fragments "edge-on" are considered, with "edge-on" being defined as impacting at such an angle that the center of mass is within 0.28 cm (one-half of the fragment thickness) of the initial contact point when the fragment is viewed edge-on, a condition given by

$$\tan \theta \leq \frac{D_0}{D}. \quad (25)$$

The geometry is illustrated in the following sketch:



Assuming that the fragments are randomly distributed in orientation, the fraction,  $f$ , that is "edge-on" will be

$$f = \frac{2}{\pi} \tan^{-1} \left( \frac{D_0}{D} \right). \quad (26)$$

The value of this parameter is shown in Figure 5-17.

The effective size of the "edge-on" fragments is estimated by assuming a projected cross-sectional area of  $D D_o$  and a total volume of  $\frac{\pi}{4} D^2 D_o$  (the fragments are assumed to be approximated by a disk). Hence the effective diameter is

$$D' = \sqrt{\frac{4}{\pi} D D_o}, \quad (27)$$

and the effective length,

$$L' = \frac{\pi D^2 D_o}{4} \times \frac{1}{D D_o} = \frac{\pi D}{4}. \quad (28)$$

Thus, the fragment is transformed into a rod-like projectile with the same volume (or mass) and having a cross section equal to the projected cross section of the actual edge-on ( $\theta = 0$ ) fragment. Values for the effective diameter and effective length are shown in Figure 5-18.

Using the preceding figures and calculations, the fragment flux of "edge-on" fragments at the payload projected cross section can be determined. Figures 5-19, 5-20 and 5-21 show the results for three explosive yields, 1, 20 and 160 percent. The fragments have been grouped into size ranges to permit a single presentation of the results.

#### 5.1.1.5 Concluding Remarks

Sections 5.1.1.1 through 5.1.1.4 have characterized what is believed to be the worst-case accident environments that are expected for an on-pad explosion and fire. The environments defined here for the Space Shuttle are much more severe than those that have previously been defined for the Titan III launch vehicle.<sup>(5-13)</sup> The use of a destruct system, when flying nuclear waste payloads, or other hazardous payloads, would greatly reduce the severity of the accident environments. The data developed in this section have been used in Section 3.4.3.1 to evaluate the response of the reentry system to the on-pad Shuttle explosion and fire.



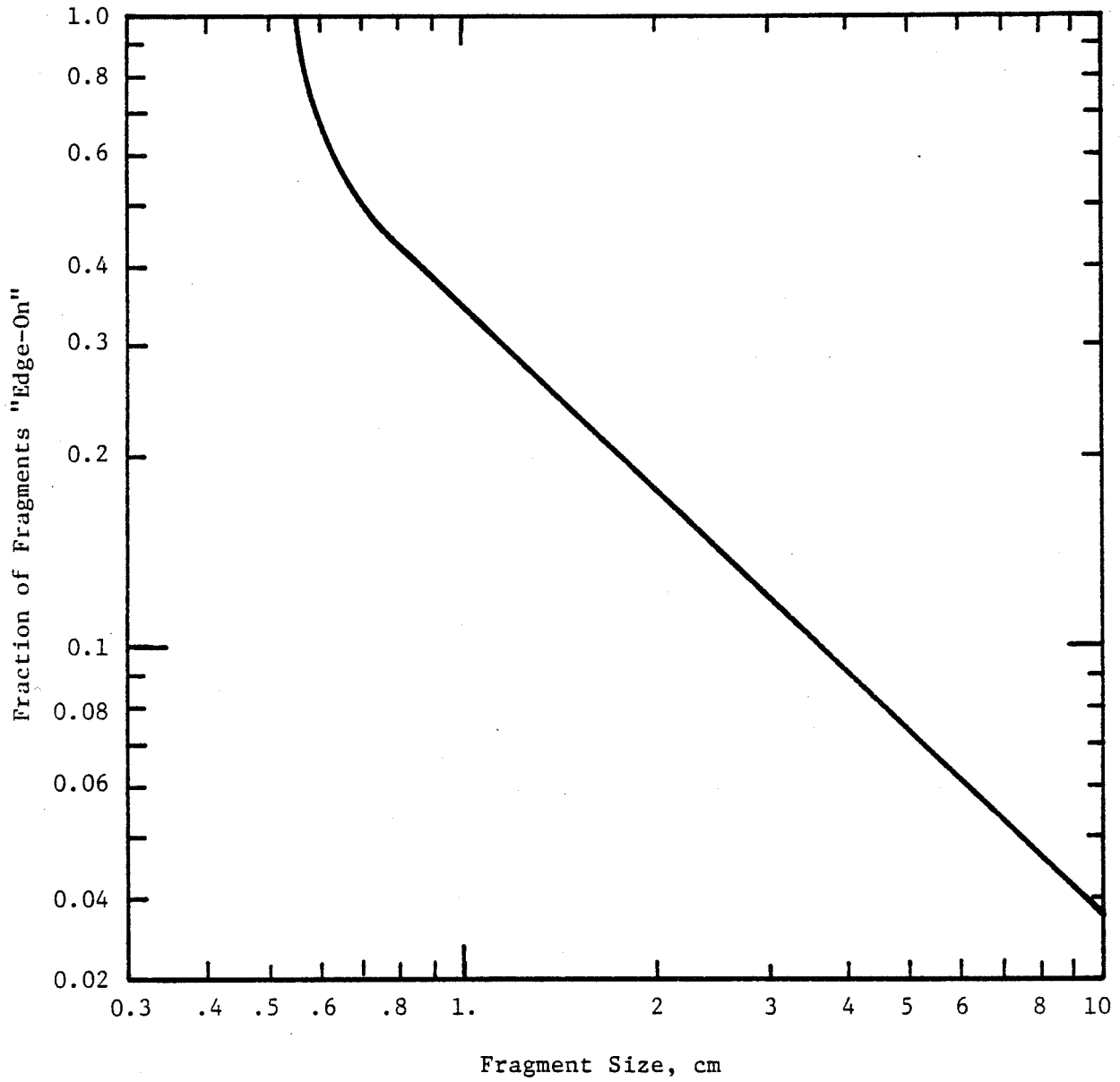


FIGURE 5-17. FRACTION OF FRAGMENTS IMPACTING EDGE-ON FOR SPACE SHUTTLE FRAGMENT ENVIRONMENT

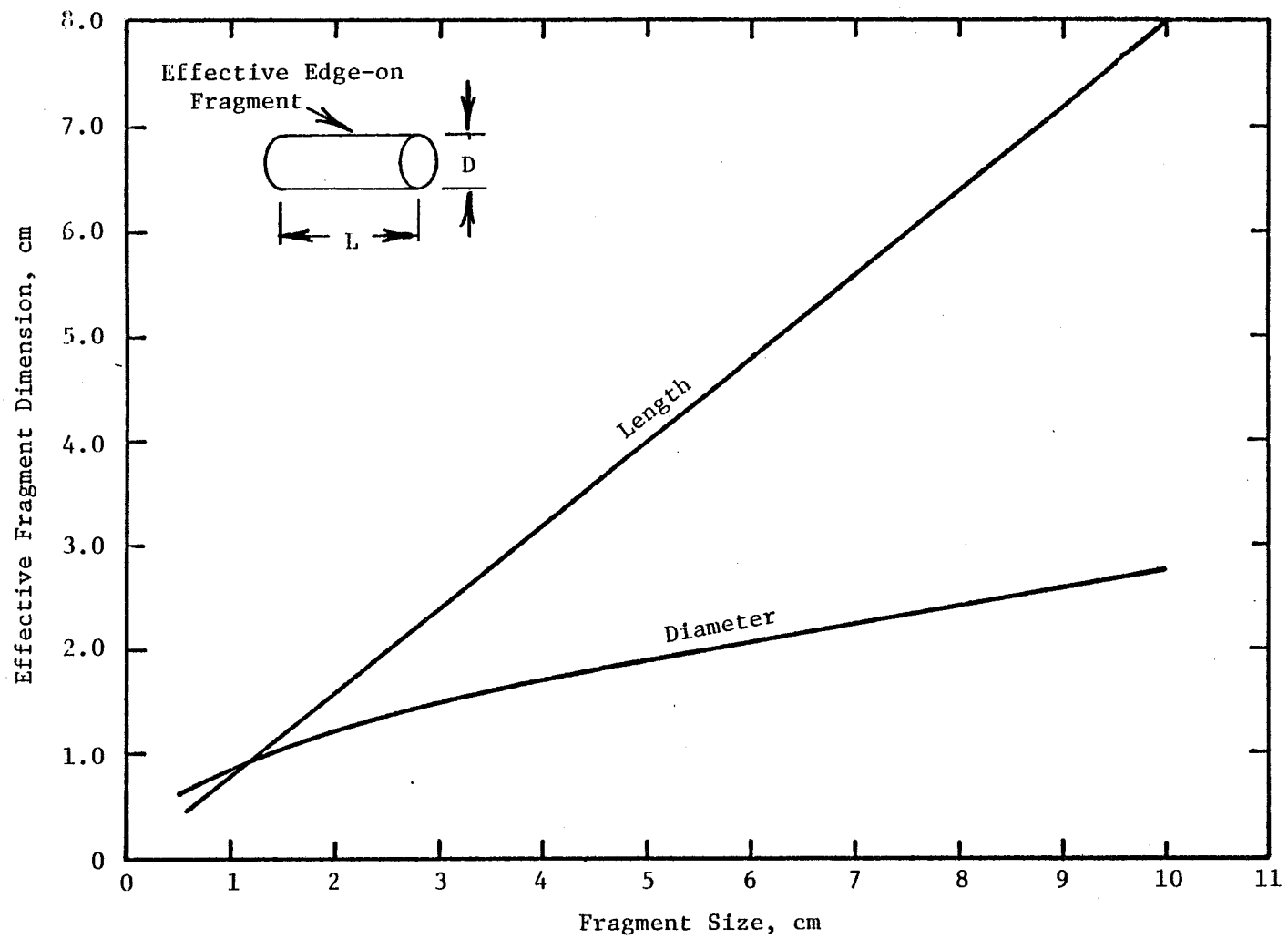


FIGURE 5-18. EFFECTIVE DIMENSIONS OF IMPACTING EDGE-ON FRAGMENTS FOR SPACE SHUTTLE FRAGMENT ENVIRONMENT

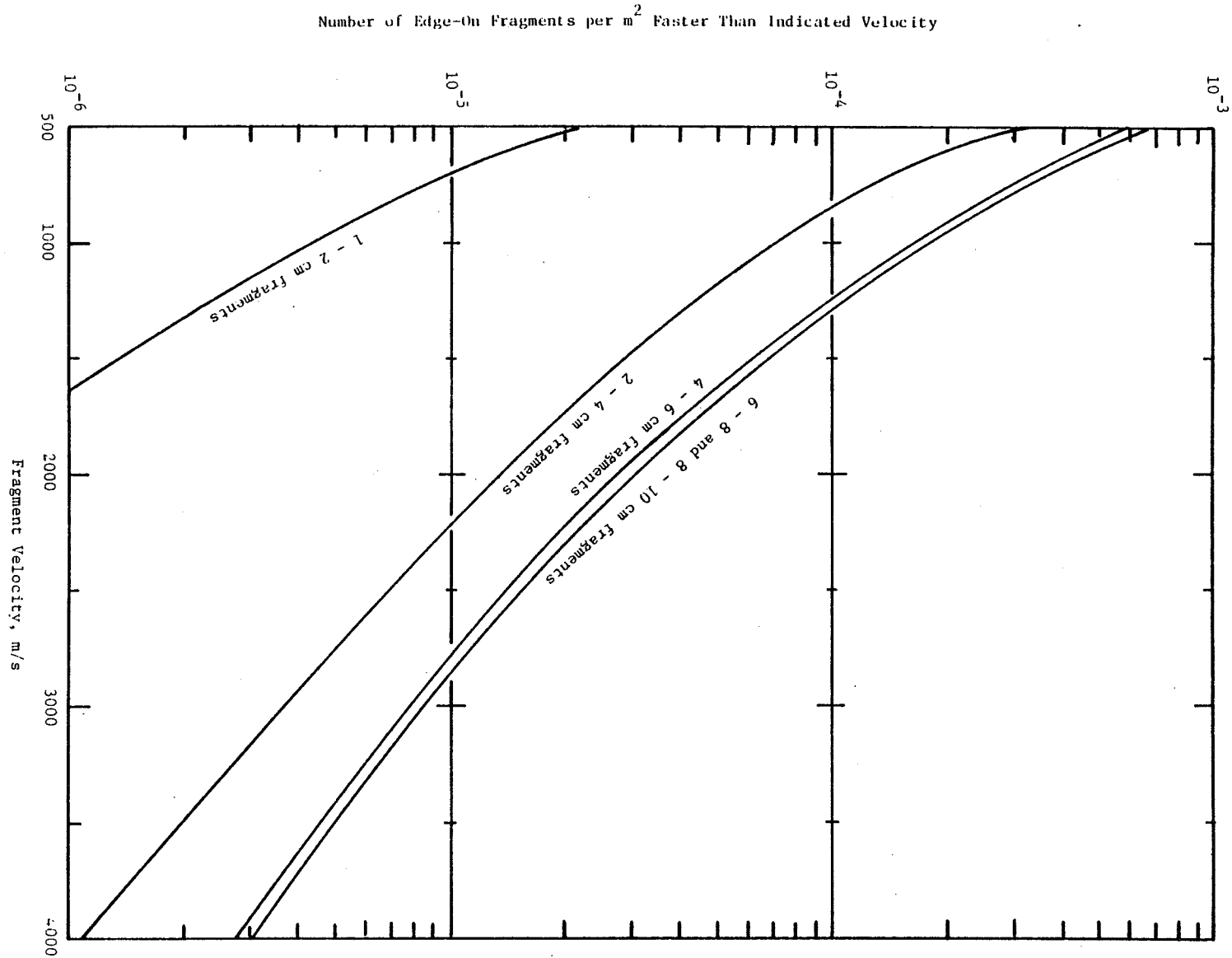


FIGURE 5-19. FRAGMENT VELOCITY DISTRIBUTION ASSUMING 1% YIELD FOR SPACE SHUTTLE FRAGMENT ENVIRONMENT

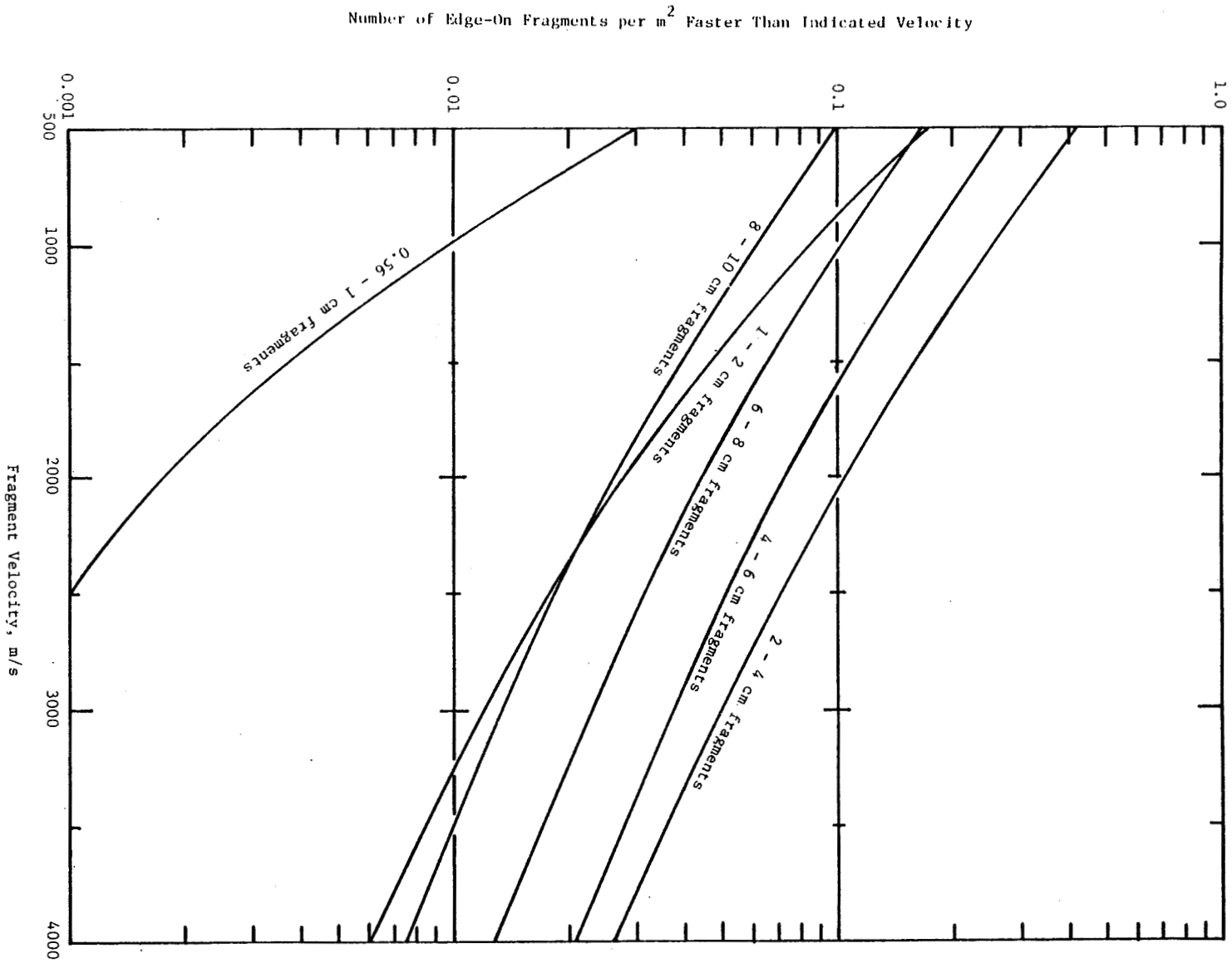


FIGURE 5-20. FRAGMENT VELOCITY DISTRIBUTION ASSUMING 20% YIELD FOR SPACE SHUTTLE FRAGMENT ENVIRONMENT

Number of Edge-On Fragments per m<sup>2</sup> Faster Than Indicated Velocity

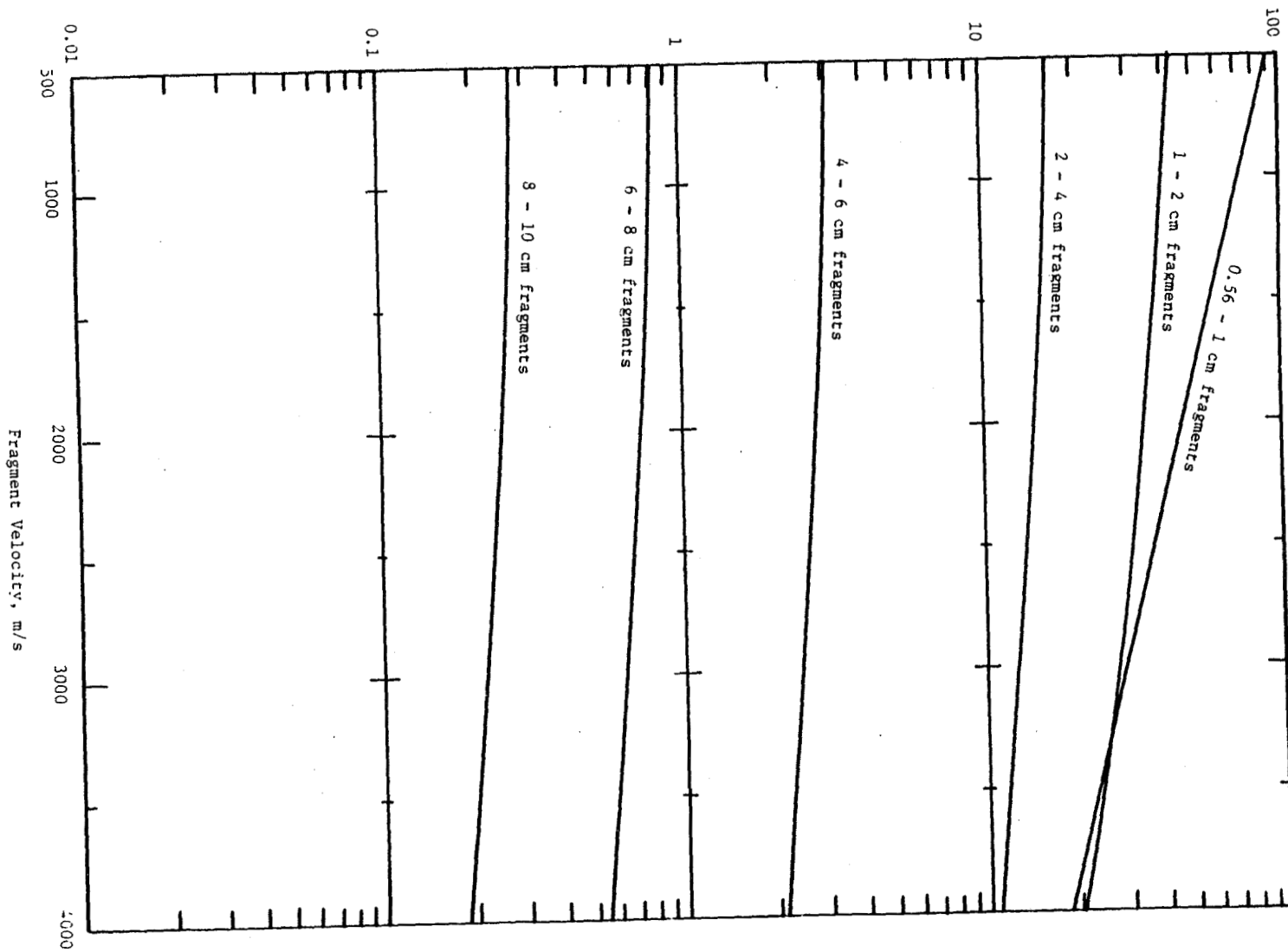


FIGURE 5-21. FRAGMENT VELOCITY DISTRIBUTION ASSUMING 160% YIELD FOR SPACE SHUTTLE FRAGMENT ENVIRONMENT

### 5.1.2 Reentry of Container With/Without Reentry Protection

Various types of low probability malfunctions could occur which might lead to the atmospheric reentry of the loaded reentry system or the baseline unprotected nuclear waste container. The protected spherical container (positioned in the reentry system - see Figure 2-5) may reenter after an emergency ejection from the Space Shuttle cargo bay just prior to achieving orbit, or the unprotected container (having been removed and attached to the payload adapter of the OTV/SOIS configuration) may reenter after a critically inaccurate OTV burn coupled with other malfunctions. These reentry environments were characterized by using a Battelle developed reentry computer code called CONTEMP. The code assumes that there is no mass loss from the payload, there is no heat transfer to or from the reentry body (cold wall), and equilibrium conditions exist in the fluid flow. Specific data used for the reentry cases assumed here are given in Table 5-4. Data related to the reentry system were obtained from the in-house NASA/MSFC study effort. The loaded reentry system was assumed to reenter at a velocity of 7818 m/s, having a zero flight path angle, at an altitude of 91.4 km (just before the ET is dropped). Two reentry conditions for the unprotected container were used; one steep and one shallow. The steep reentry represents the case where the OTV burns in the wrong direction (opposite) for an extended period of time. The shallow reentry represents the case where the OTV has provided a small velocity change, but just enough to cause reentry in the first orbit. These two cases should provide the bounds for the reentry environment. The assumed drag curves for the two configurations are shown in Figures 5-22 and 5-23.

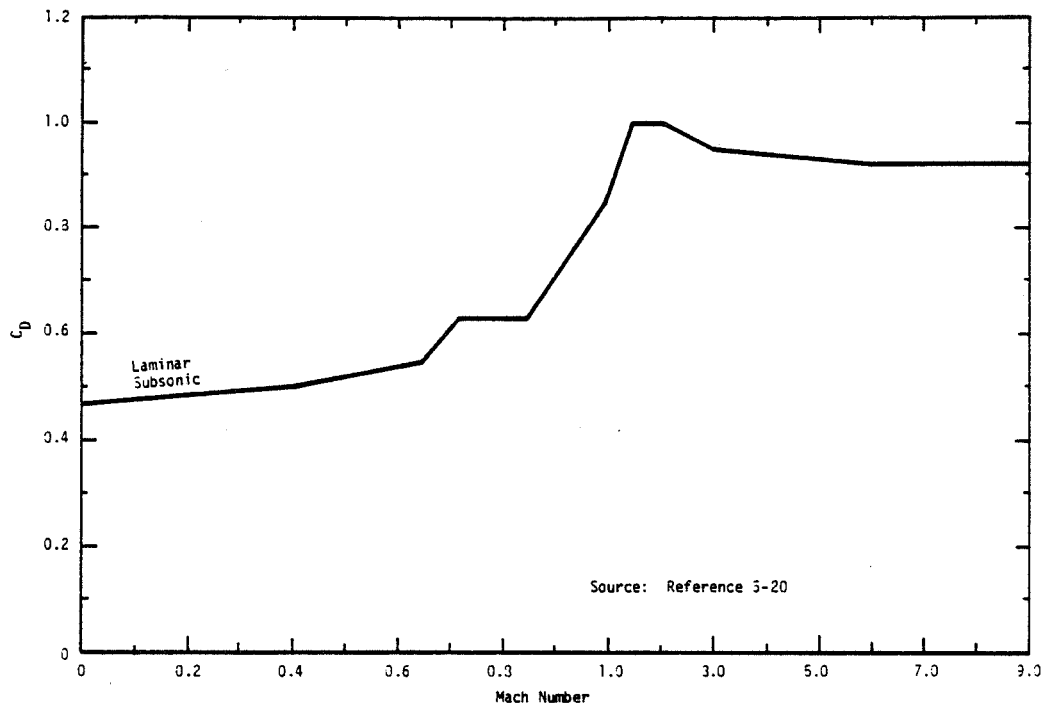


FIGURE 5-22. DRAG COEFFICIENT FOR A SPHERE AS A FUNCTION OF MACH NUMBER

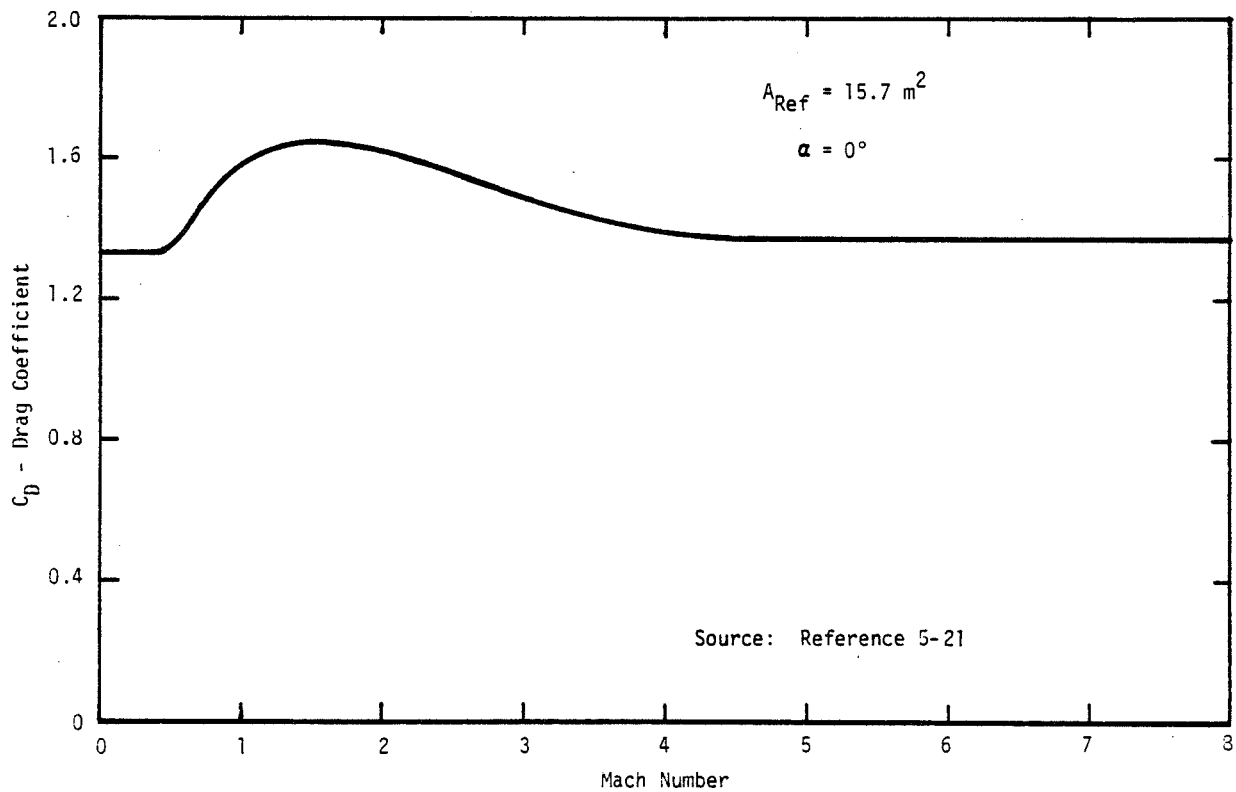


FIGURE 5-23. DRAG COEFFICIENT FOR REENTRY SYSTEM AS A FUNCTION OF MACH NUMBER

TABLE 5-4. INPUT AND ASSUMPTIONS FOR THE REENTRY ENVIRONMENT ANALYSIS

Parameter	Payload Configuration		
	Unprotected Container		Reentry System
	Steep Reentry	Shallow Reentry	
Mass, kg	6270	6270	19492
Cross Sectional Area, m <sup>2</sup>	1.97	1.97	15.68
Nose Diameter, m	1.59	1.59	2.13
Initial Velocity, m/s	3660	7600	7818
Initial Altitude, km	333	333	91.4
Initial Flight Path Angle, degrees	0	0	0
Mass/Area Ratio, kg/m <sup>2</sup>	3183	3183	1243
Drag Curve	see Figure 5-22		see Figure 5-23

NOTE: See Figures 2-5 and 3-6 for description of payload configurations.  
Reentry system data were obtained from NASA/MSFC in-house studies.

The results of the reentry calculations for the three cases indicated in Table 5-4 are presented in Figures 5-24 through 5-38, where various parameters are plotted as a function of altitude. The parameters are time, velocity, stagnation heating rate, stagnation pressure and stagnation temperature. These environments were used in the thermal response analysis as discussed in Section 3.4.3.2.



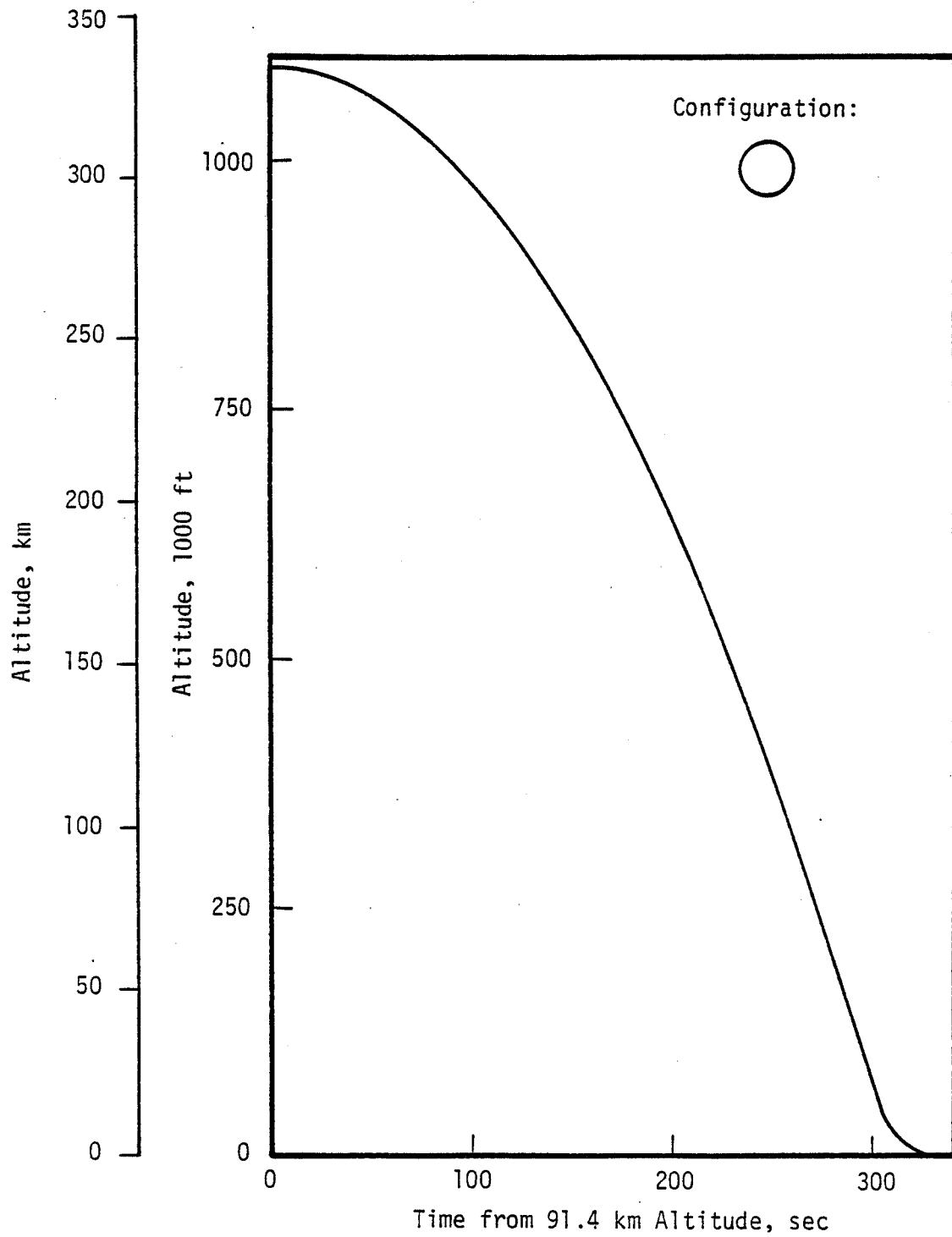


FIGURE 5-24. TIME AS A FUNCTION OF ALTITUDE FOR STEEP REENTRY OF UNPROTECTED CONTAINER

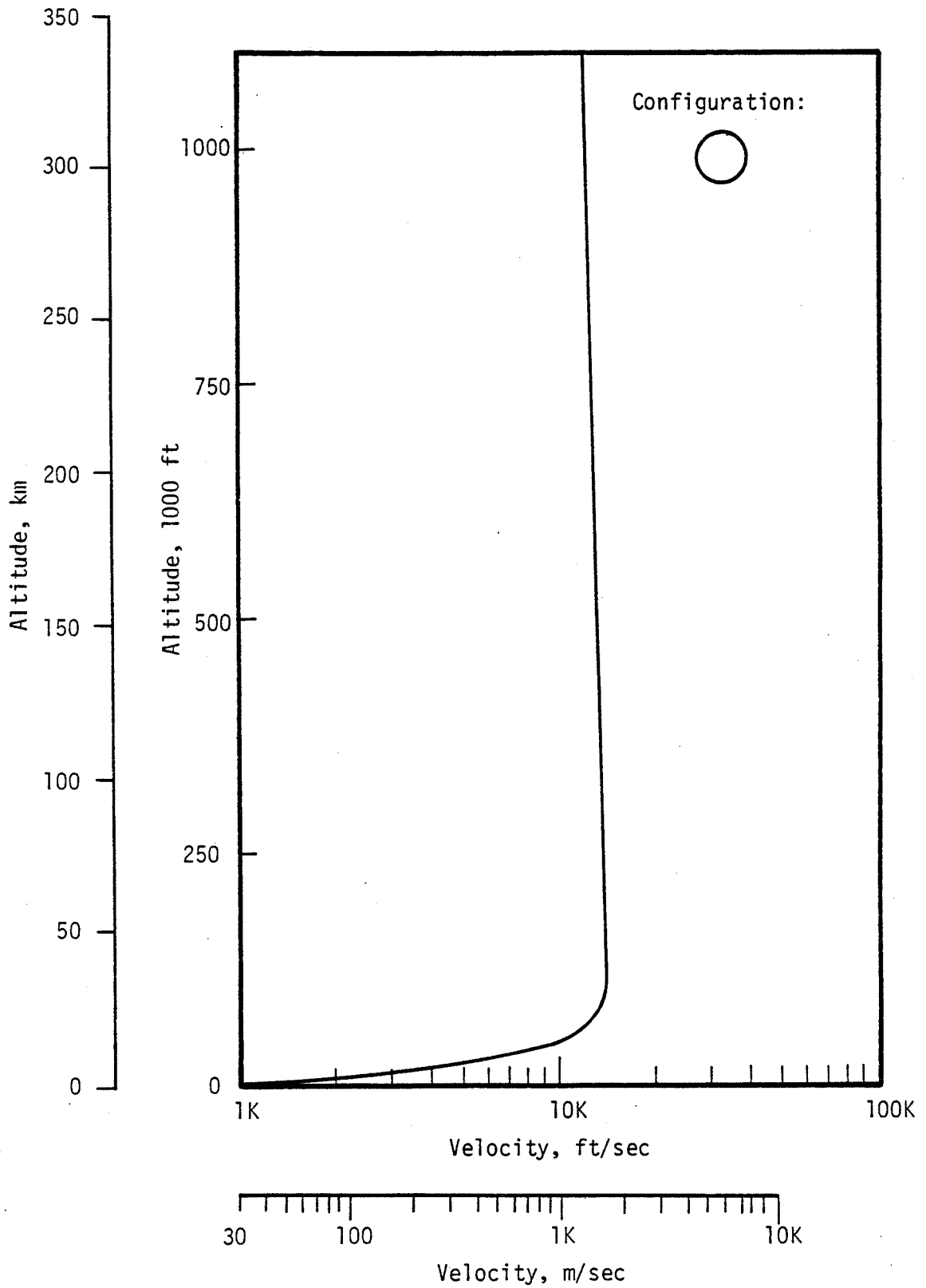


FIGURE 5-25. VELOCITY AS A FUNCTION OF ALTITUDE FOR STEEP REENTRY OF UNPROTECTED CONTAINER

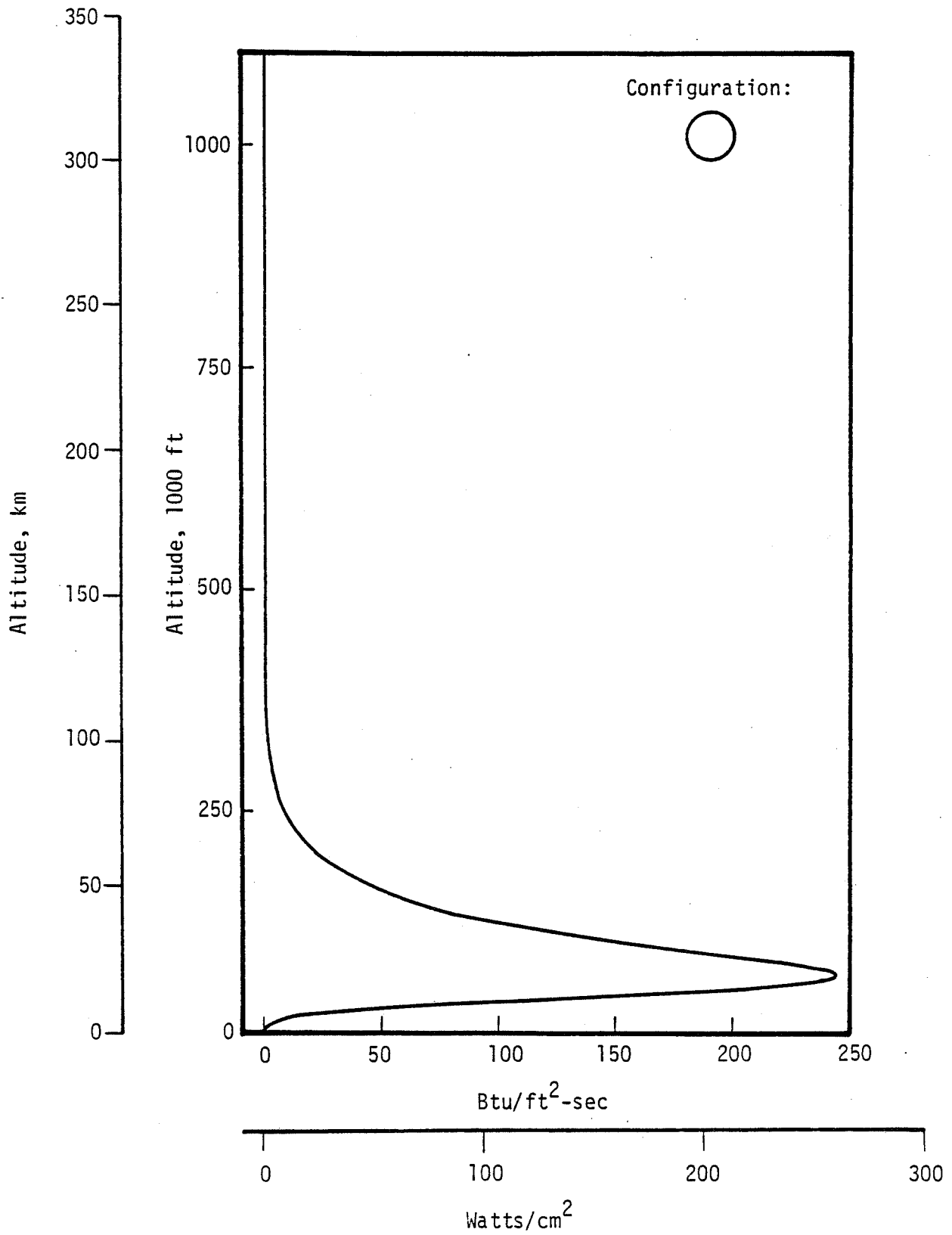


FIGURE 5-26. STAGNATION POINT HEATING RATE AS A FUNCTION OF ALTITUDE FOR STEEP REENTRY OF UNPROTECTED CONTAINER

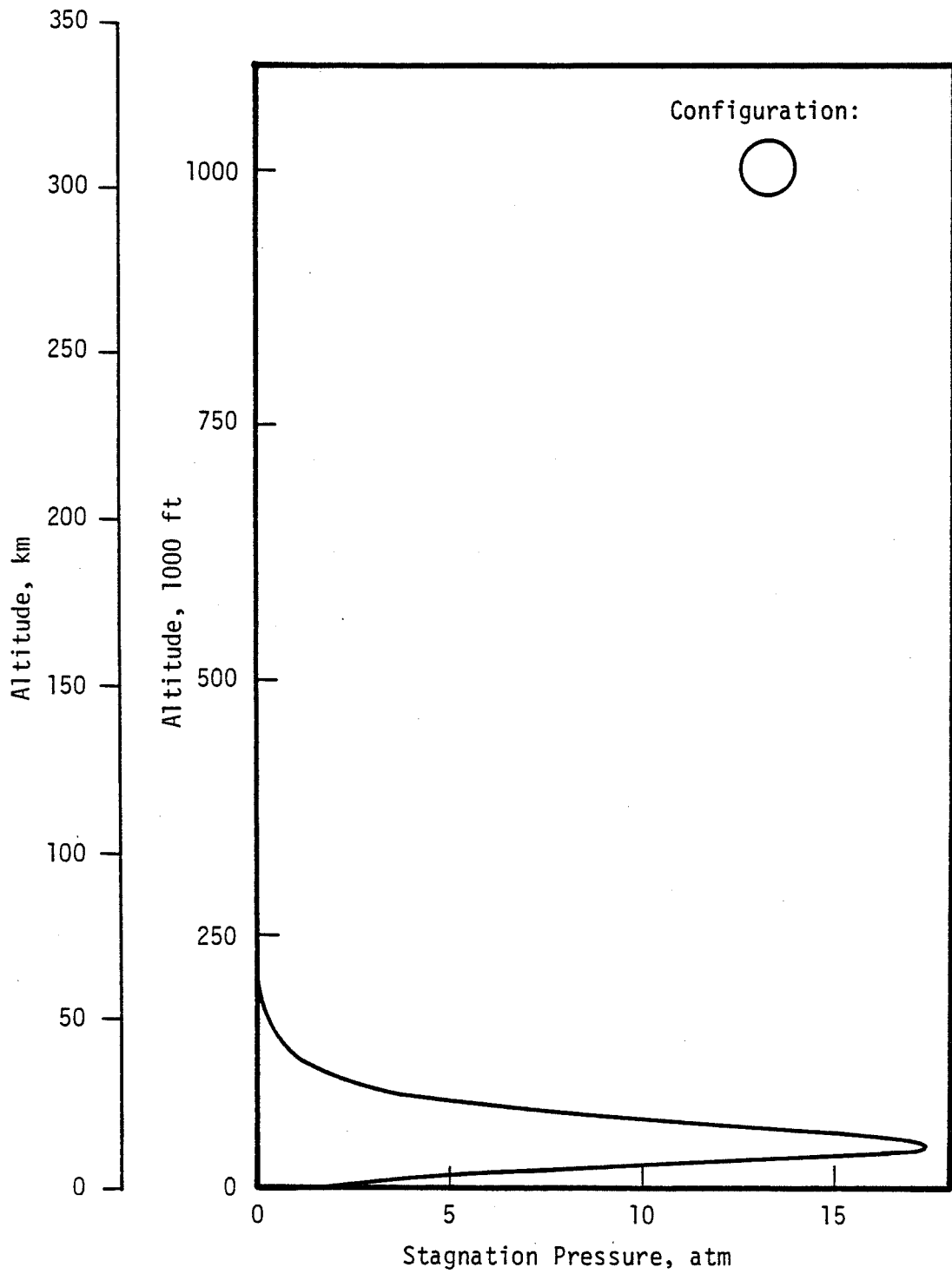


FIGURE 5-27. STAGNATION PRESSURE AS A FUNCTION OF ALTITUDE FOR STEEP REENTRY OF UNPROTECTED CONTAINER

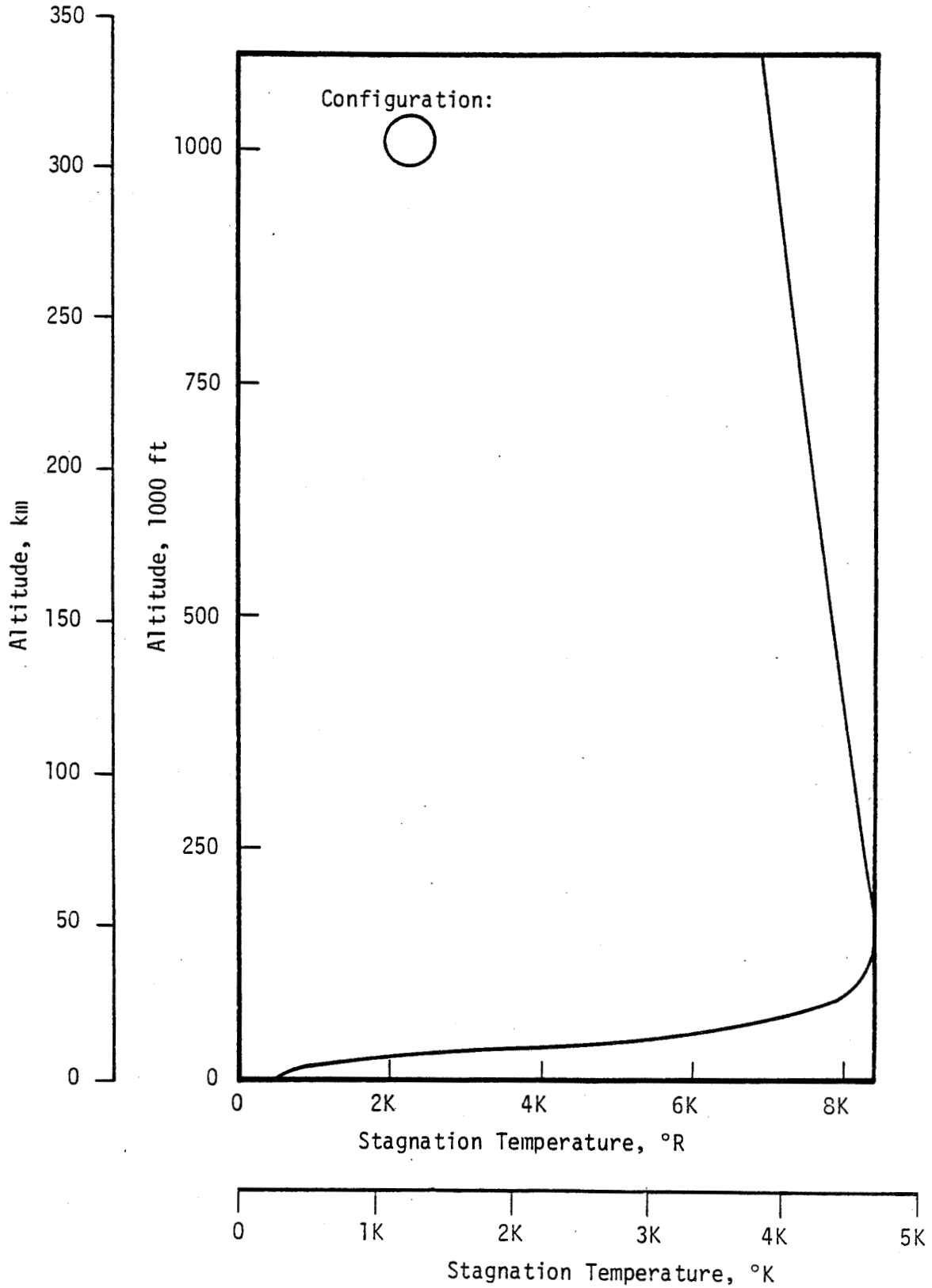


FIGURE 5-28. STAGNATION TEMPERATURE AS A FUNCTION OF ALTITUDE FOR STEEP REENTRY OF UNPROTECTED CONTAINER

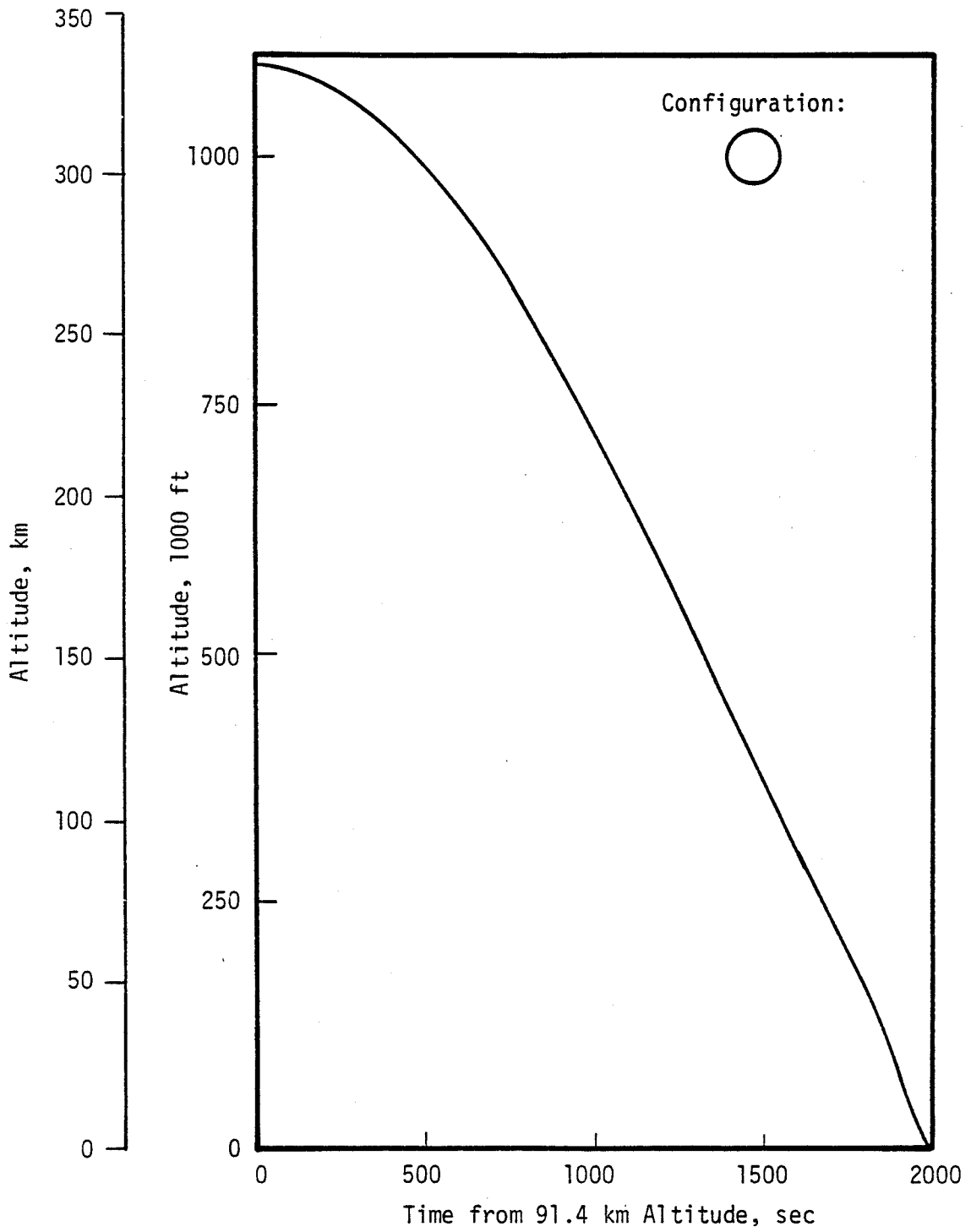


FIGURE 5-29. TIME AS A FUNCTION OF ALTITUDE FOR SHALLOW REENTRY OF UNPROTECTED CONTAINER

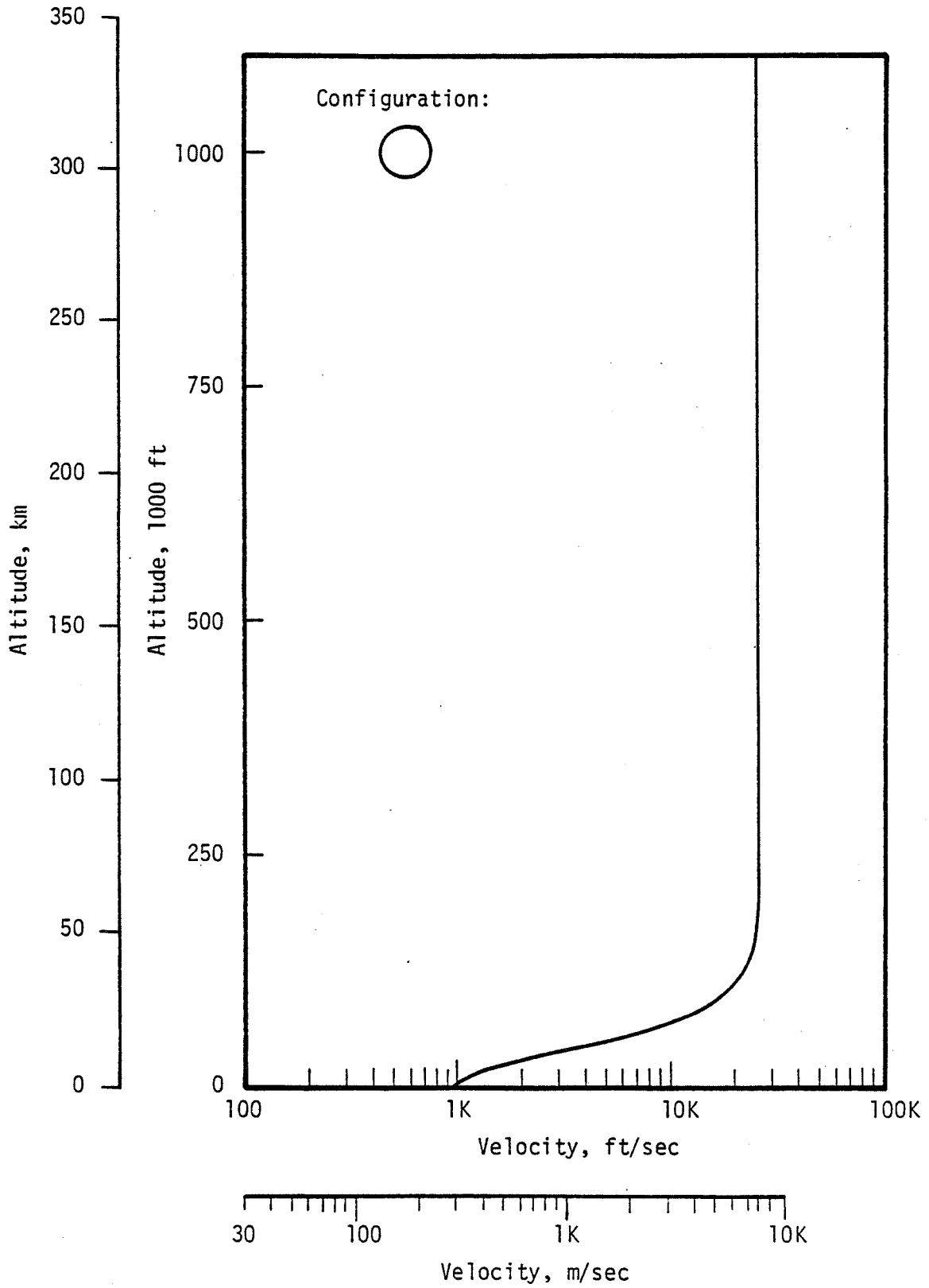


FIGURE 5-30. VELOCITY AS A FUNCTION OF ALTITUDE FOR SHALLOW REENTRY OF UNPROTECTED CONTAINER

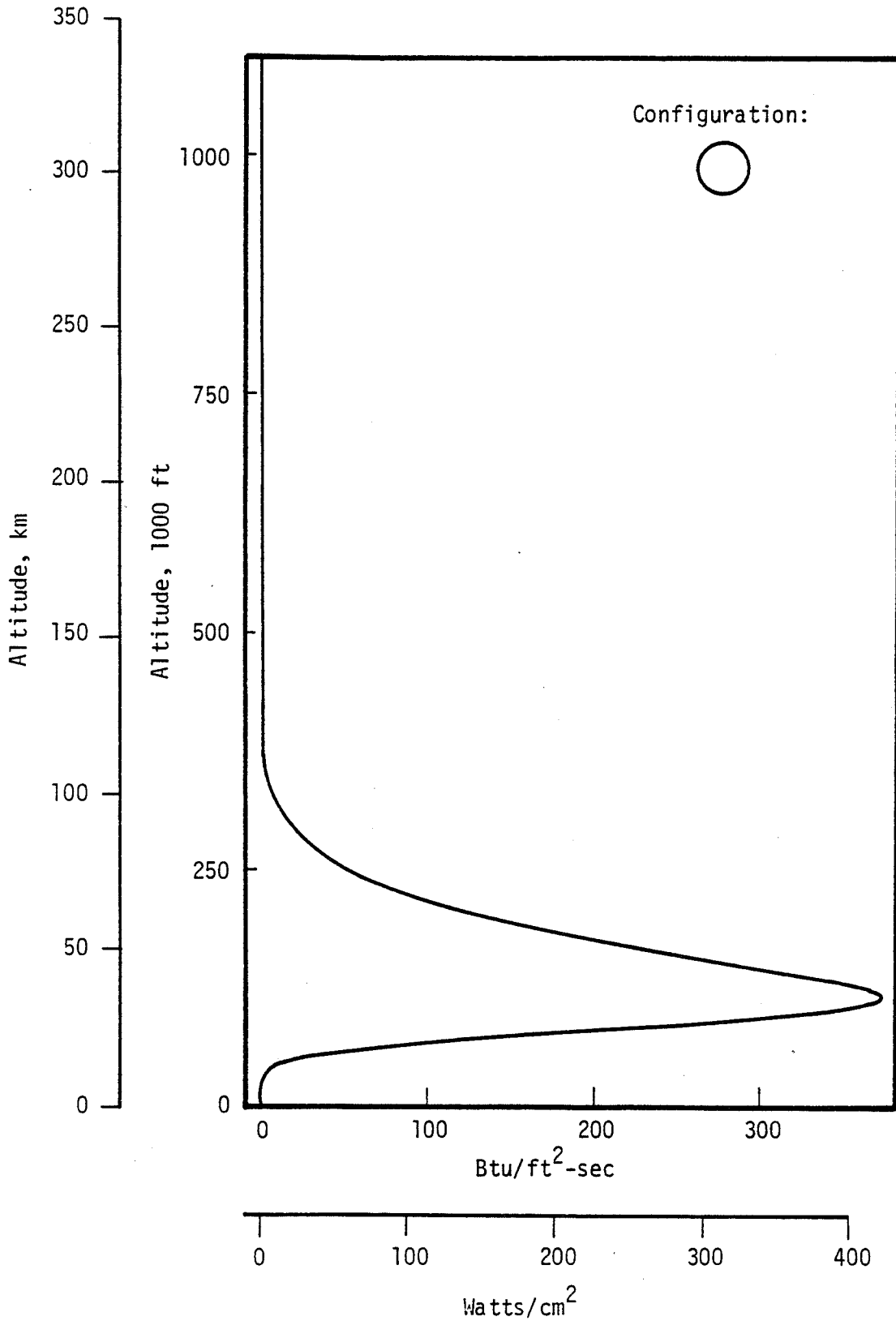


FIGURE 5-31. STAGNATION POINT HEATING RATE AS A FUNCTION OF ALTITUDE FOR SHALLOW REENTRY OF UNPROTECTED CONTAINER



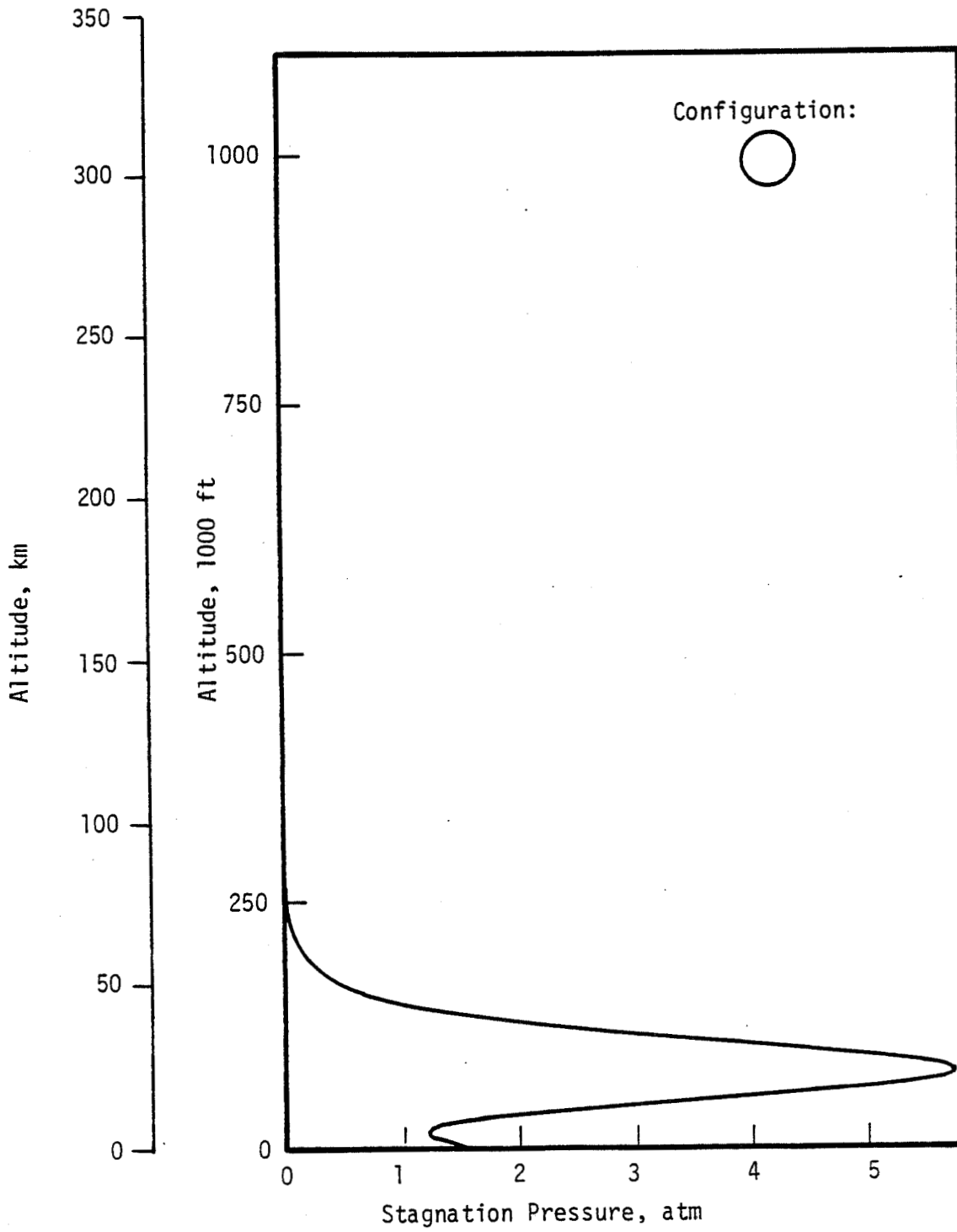


FIGURE 5-32. STAGNATION PRESSURE AS A FUNCTION OF ALTITUDE FOR SHALLOW REENTRY OF UNPROTECTED CONTAINER

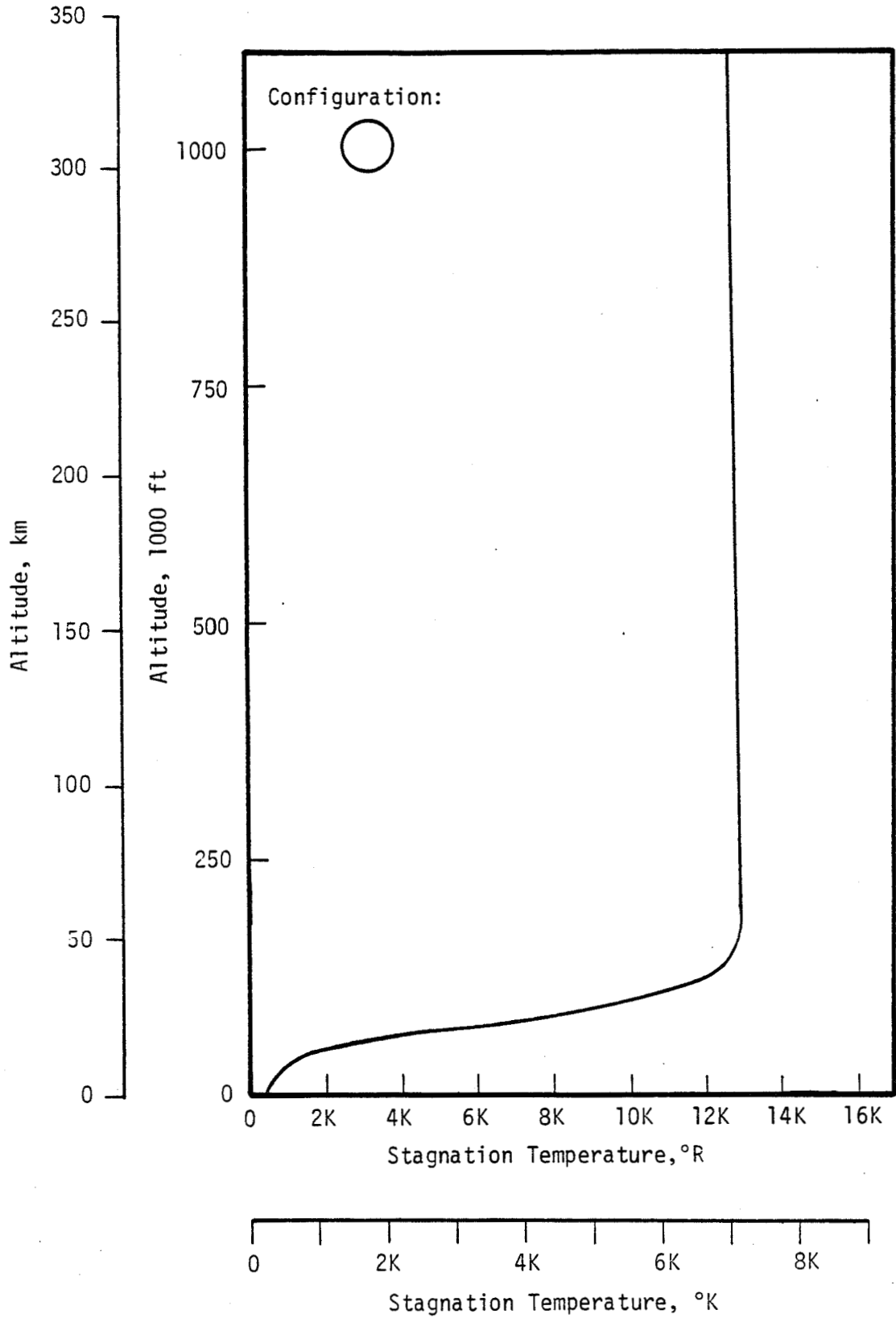


FIGURE 5-33. STAGNATION TEMPERATURE AS A FUNCTION OF ALTITUDE FOR SHALLOW REENTRY OF UNPROTECTED CONTAINER

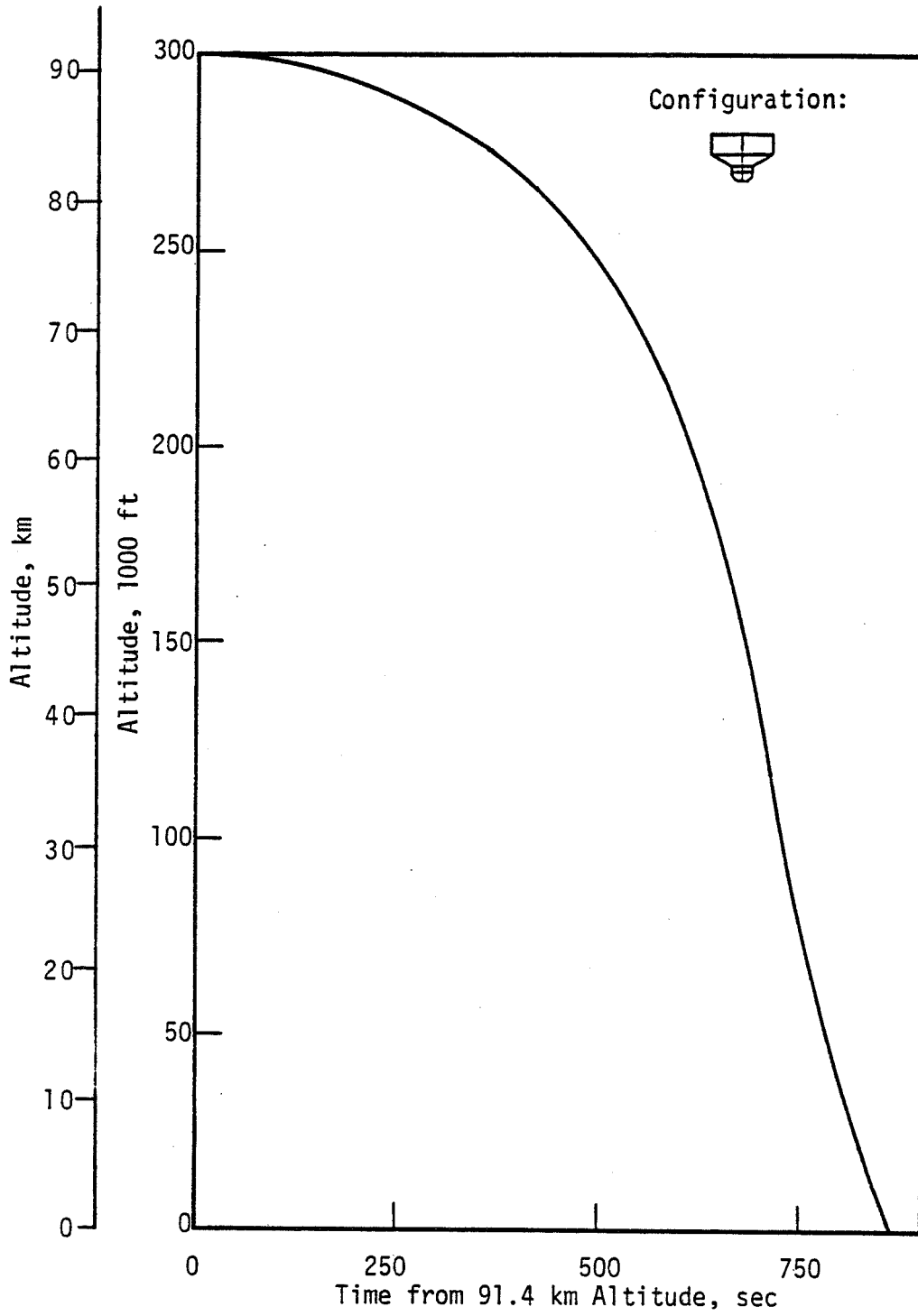


FIGURE 5-34. TIME AS A FUNCTION OF ALTITUDE FOR REENTRY OF REENTRY SYSTEM

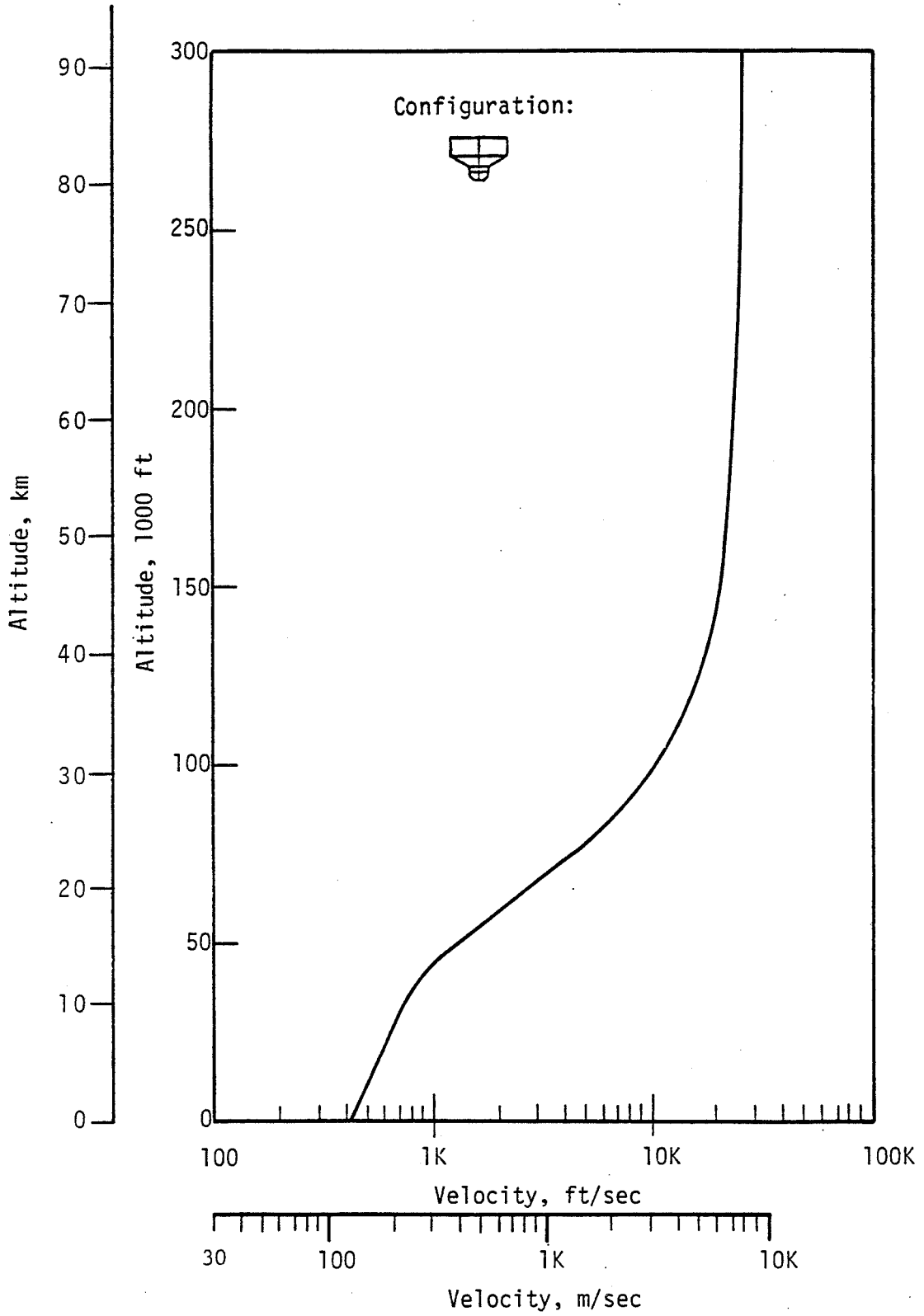


FIGURE 5-35. VELOCITY AS A FUNCTION OF ALTITUDE FOR REENTRY OF REENTRY SYSTEM

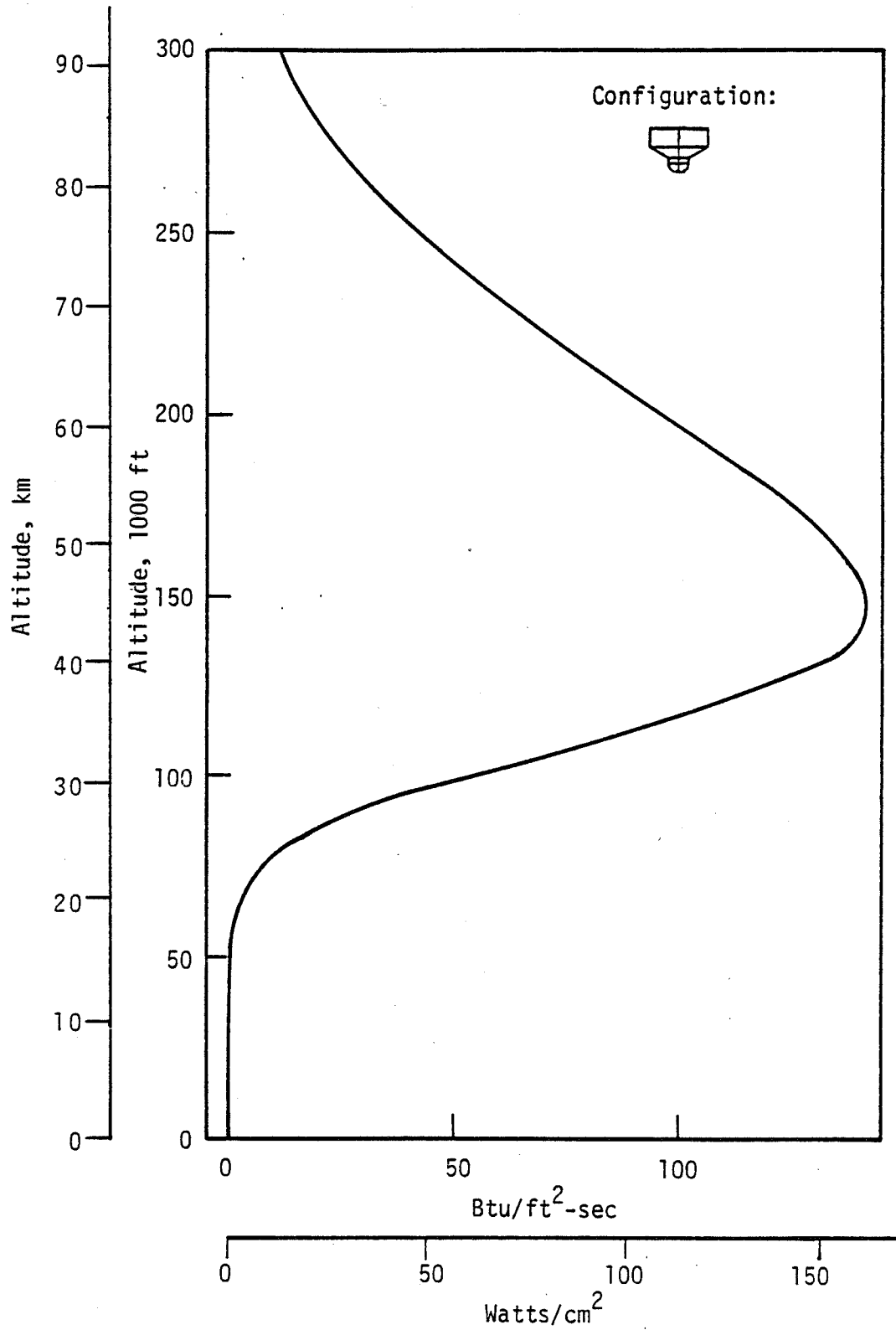


FIGURE 5-36. STAGNATION POINT HEATING RATE AS A FUNCTION OF ALTITUDE FOR REENTRY OF REENTRY SYSTEM

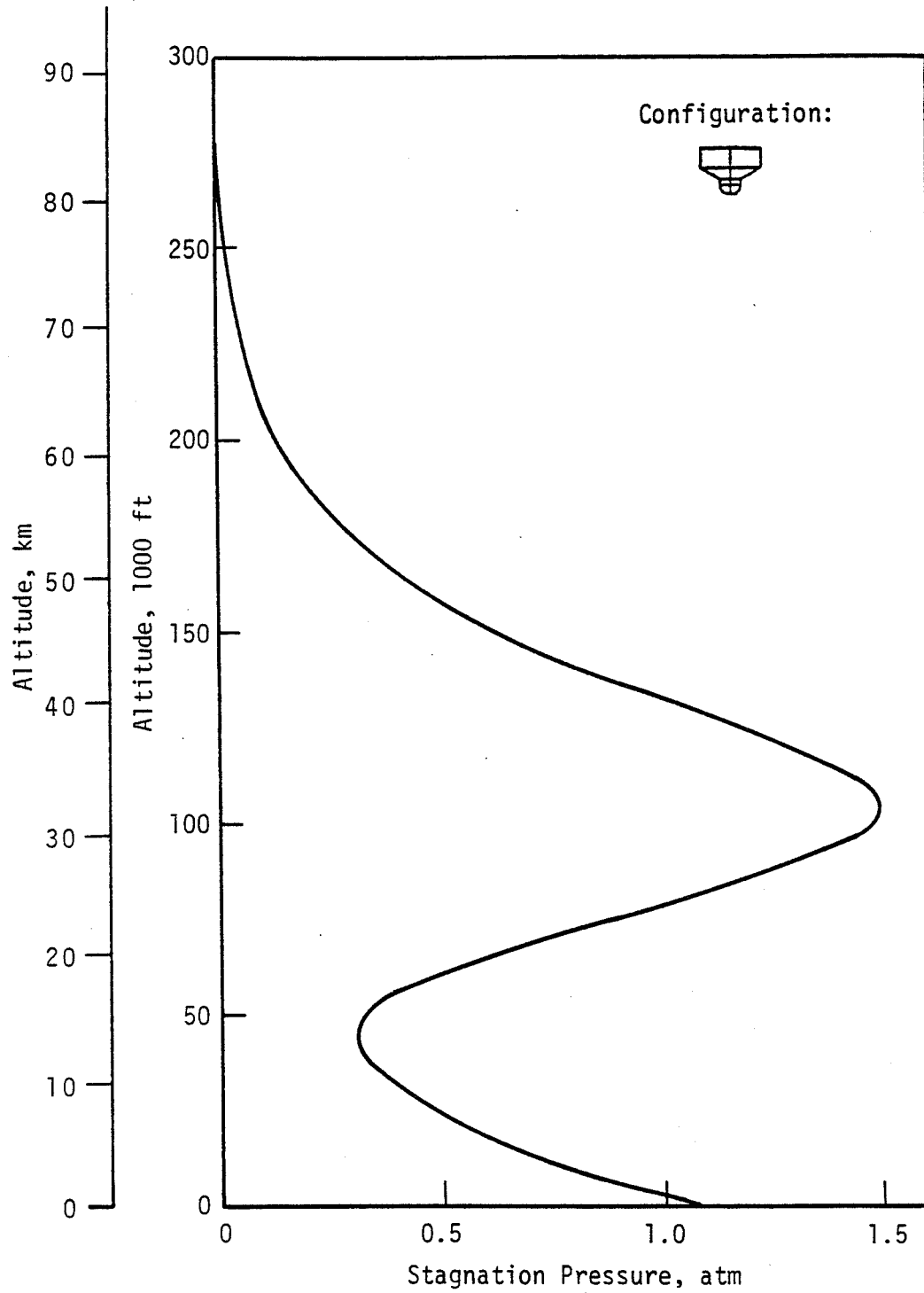


FIGURE 5-37. STAGNATION PRESSURE AS A FUNCTION OF ALTITUDE FOR REENTRY OF REENTRY SYSTEM

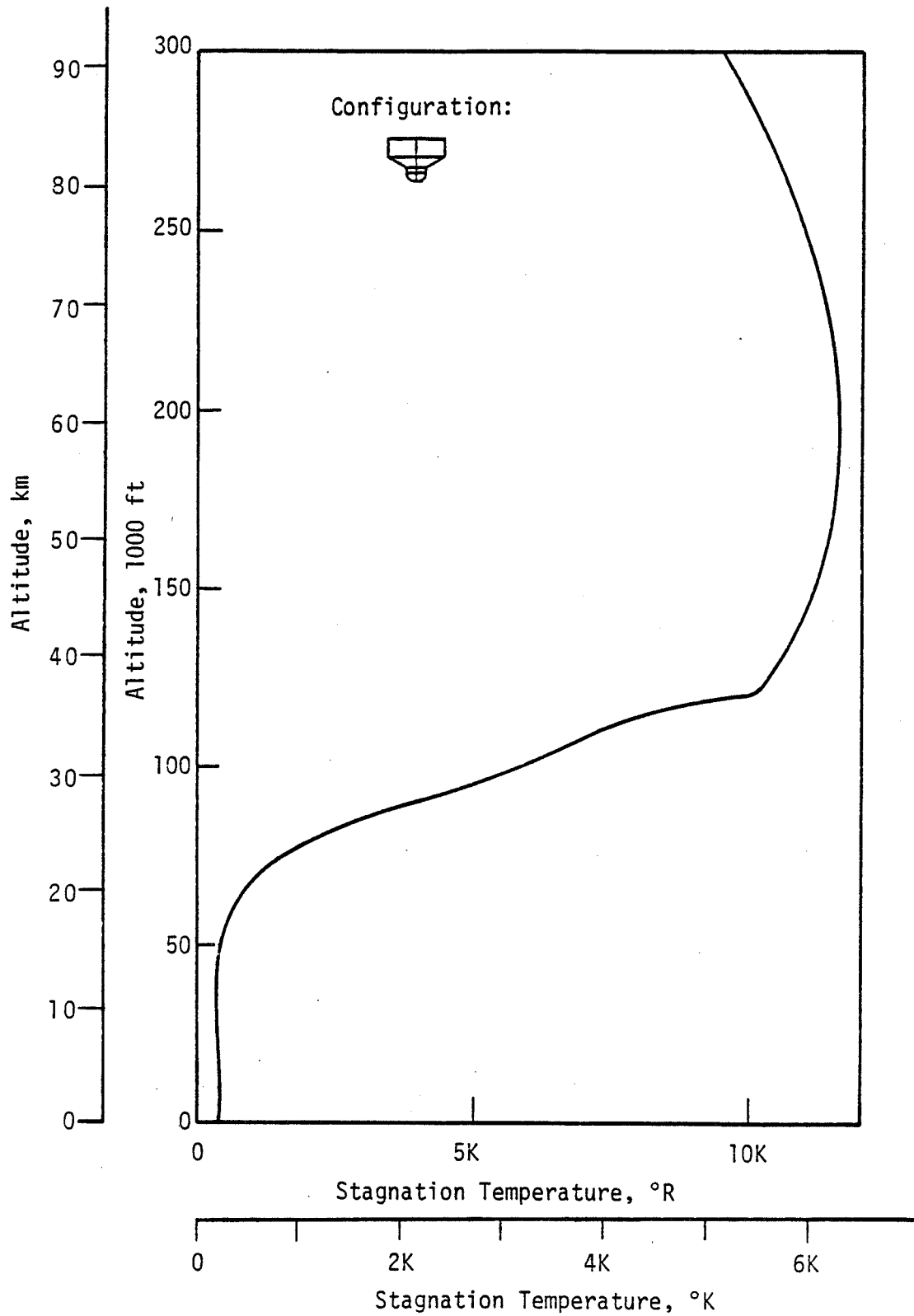


FIGURE 5-38. STAGNATION TEMPERATURE AS A FUNCTION OF ALTITUDE FOR REENTRY OF REENTRY SYSTEM

### 5.1.3 Payload Entry into Deep Ocean

The reentry of a protected container would likely result in an ocean landing. Should the flotation system fail, the reentry system with the loaded container would sink to the ocean floor. The most severe immediate environment that the payload would see would be the very high external pressure exerted on the payload. Problems related to the eventual saltwater corrosion and waste overheating as a result of poor heat transfer characteristics, assuming the payload is buried in ocean sediment, are believed to be more of a long-time problem. General characteristics of seawater and the ocean floor are reviewed in Reference 5-22 and are not reported here.

The relationship between the fraction of ocean depth greater than a certain value as a function of ocean depth pressure for ground track resulting in a 38 degree inclination orbit (first pass assumed - KSC launch) has been approximated. The ground track trajectory was superimposed on a world map containing ocean depth data to obtain the relationship. Figure 5-39 presents the results. The average ocean depth (considering all three major oceans) is roughly 4 km. For the orbital pass assumed here for ocean impact and random reentry, the payload would fall into the ocean at depths greater than 4 km about 73% of the time, or depth greater than 6 km only 7% of the time.



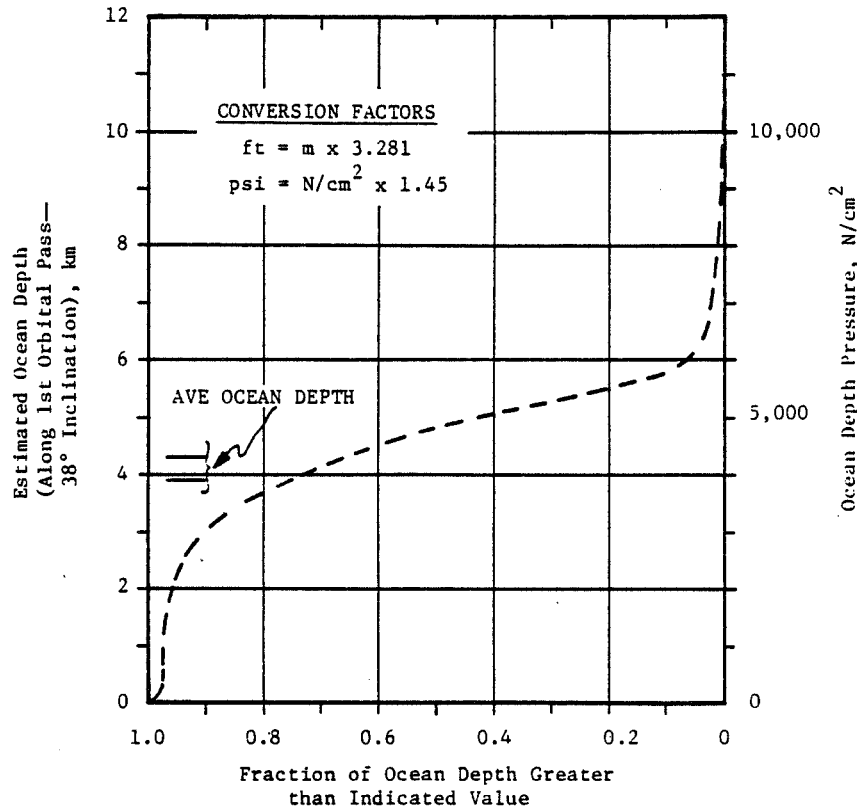


FIGURE 5-39. DISTRIBUTION OF OCEAN DEPTH (PRESSURE) FOR A 38° INCLINATION SPACE DISPOSAL ORBIT (1st ORBITAL PASS)

The ocean pressures resulting from these various assumed depths are indicated in Figure 5-39. The maximum ocean depth and pressure possible are 10.9 km and 11,000 N/cm<sup>2</sup> (16,000 psi), respectively. These types of data should be useful in future container design and in risk analysis, once the consequences of certain accidents are determined.

## 5.2 Preliminary Hazard Analysis

A preliminary hazard analysis was conducted to identify those events and sequences of events most likely to lead to a release of radioactive waste. This preliminary analysis was considered to be the first in a series of steps that, over a period of several years, would result in a final estimate of risk associated with space disposal of nuclear waste. As a first step, the results achieved in the current effort are qualitative rather than quantitative. The results are, nonetheless, valuable as indications of those portions of the conceptualized system that should be studied more thoroughly to delineate significant risks involved in the disposal of nuclear waste in space.

This section is divided into three subsections to facilitate discussion. The first subsection breaks the mission down into phases that differ from one another in the hazards and accident environments that would likely be encountered. Then, the status of failure and probability data is discussed. Finally, elementary fault trees for each mission phase are presented and discussed. The more significant failure paths are outlined, and a sensitivity as to the likelihood of occurrence of the more hazardous events is developed.

### 5.2.1 Mission Phase Definition

To facilitate the presentation of fault tree information in Section 5.2.3, the baseline mission has been partitioned into a number of phases, as shown in Table 5.5. These phases are not identical to those discussed in the baseline mission profile in Section 2.3, but have been chosen to separate the baseline mission into portions in which the hazards can be clearly defined. A short description of the significant events occurring in each phase is contained in the following subsections of this report.

TABLE 5-5. DEFINITION OF MISSION PHASES

Phase Number	Description of Phase
1	Payload Processing and Storage at Launch Site
2	On-Pad, Prelaunch Operations
3	Ignition to Clearing of Tower
4	Clearing of Tower to SRB Burnout
5	SRB Burnout to ET Drop
6	ET Drop to Achieving Orbit
7	Achieving Orbit to Rendezvous
8	Rendezvous and Docking with OTV/SOIS
9	OTV Ignition to Burnout
10	OTV Jettison to SOIS Ignition
11	SOIS Burn
12	Stay in Planned Orbit

#### 5.2.1.1 Phase 1: Payload Processing and Storage at Launch Site

Before its arrival at the launch site, the nuclear waste payload would be the responsibility of the Department of Energy. This responsibility would include payload treatment, fabrication and transportation to the launch site. Once it has arrived at the launch site, responsibility for safety of the payload package and its contents would be transferred to NASA. In Phase 1, these operations would include unloading and storage of the shielded waste container in the Nuclear Payload Preparation Facility (NPPF); cooling, inspection and monitoring of the waste containers; and insertion of the waste container into the reentry system. The loaded reentry system would then be mated with cooling, ejection and docking systems, mounted on a pallet and prepared for transfer to the Payload Changeout Room (PCR). A special-purpose transporter would be used to move the assembled payload/reentry/docking assembly to the launch pad area.

#### 5.2.1.2 Phase 2: On-Pad, Prelaunch Operations

In this phase, the loaded reentry system would be removed from its transporter, elevated and placed in the PCR; in the PCR, an auxiliary cooling system would be attached and the total package then inserted into the Orbiter's payload bay. While in the payload bay the waste payload would remain attached

to the auxiliary cooling equipment that would be required through the next several phases of the mission (until shortly before the payload/reentry/docking assembly was removed from the Orbiter's payload bay in low Earth orbit). Since detailed mission timelines have not been developed yet, it has not been determined whether Shuttle ET fueling would take place before the waste payload was inserted or after. In any event, there would be some period of time during which the payload would be mounted near both the loaded ET and the two SRBs. Before launch, a final systems checkout procedure would be accomplished.

#### **5.2.1.3 Phase 3: Ignition to Clearing of Tower**

This phase of the mission contains those events that occur from Space Shuttle ignition until the SRB nozzles have cleared the launch tower. This is a very short phase of the mission, but one which contains several unique hazards. Nominally, the Shuttle engines and SRBs would ignite, and the Shuttle would rise vertically and build up speed during this initial phase of the flight.

#### **5.2.1.4 Phase 4: Clearing of Tower to SRB Burnout**

After the Shuttle clears the launch tower, it would turn downrange and proceed until the SRBs burn out at about 120 seconds into the flight.

#### **5.2.1.5 Phase 5: SRB Burnout to ET Drop**

During Phase 5 of the mission, the SRBs would be jettisoned a few seconds after their burnout, and the Shuttle would continue under the thrust provided by the SSMEs. About 480 seconds into the flight, the ET would run out of propellant and oxidizer. Several seconds later, ET staging would occur.

#### **5.2.1.6 Phase 6: ET Drop to Achieving Orbit and Phase 7: Achieving Orbit to Rendezvous**

After the ET is dropped, the Shuttle Orbiter would continue into its planned orbit by using on-board propellants. Prior to launch of the Shuttle with the nuclear waste payload on-board, the OTV/SOIS combination would have been

launched on a separate Shuttle, checked out and released into the rendezvous orbit. The Shuttle with the nuclear payload would conduct required phasing and orbit adjustment maneuvers using the Orbital Maneuvering System (OMS) to rendezvous with the OTV/SOIS.

#### **5.2.1.7 Phase 8: Rendezvous and Docking with OTV/SOIS**

When the Orbiter containing the nuclear waste payload has approached the OTV/SOIS, the payload/reentry/docking assembly would be checked out, removed from the Orbiter payload bay with the remote manipulator system and released. Auxiliary cooling might still be required from this point in time until the payload container is removed from the reentry system. The OTV/SOIS would maneuver to perform the actual closing and docking operations with the payload/reentry/docking assembly. The payload docking system would contain a remotely operated arm that would:

- Remove the rear reentry shield wall
- Remove the payload container from the reentry system and attach it to the SOIS payload adapter
- Replace the rear reentry shield wall.

Following this sequence of events, the OTV/SOIS would back away from the reentry/docking assembly, carrying the waste container attached to the payload adapter. The docking process is a complicated one, with a number of points at which potential mishaps could occur. These are discussed in Section 5.2.3.8.

#### **5.2.1.8 Phase 9: OTV Ignition and Burn**

Once the docking maneuver had been performed, the OTV attitude control system would position the OTV/SOIS/payload for OTV firing. The OTV would then be ignited and perform a propulsive burn that would place the SOIS/payload onto an Earth-escape trajectory.

#### **5.2.1.9 Phase 10: OTV Jettison to SOIS Ignition**

When the OTV propulsive burn had been terminated, the SOIS/payload assembly would be released to travel to the proper perihelion, and the OTV

would return to the Shuttle orbit for capture and return to the Earth for refurbishment. The SOIS/payload would coast for 163 days to arrive at a perihelion of 0.86 a.u.

#### 5.2.1.10 Phase 11: SOIS Burn

When the SOIS/payload reached perihelion, the 3-axis attitude control system carried by the SOIS would align and stabilize the SOIS/payload assembly prior to firing. The SOIS burn would reduce the aphelion of the SOIS/payload to 0.86 a.u. to place the payload in its nominal, circular disposal orbit of 0.86 a.u. This orbit is planned to be inclined at least 1 degree to the ecliptic plane.

#### 5.2.1.11 Phase 12: Stay in Planned Orbit

The final mission phase would consist of the payload circling the Sun at 0.86 a.u., and being exposed for an indefinite period of time to the space environment.

### 5.2.2 Failure Probability Data

None of the launch systems (e.g., Shuttle, OTV, and SOIS) for initial and follow-on nuclear waste disposal missions have been flown. Thus, there are no demonstrated reliability data available. However, historical data on unmanned and manned expendable launch vehicles, preliminary projections on Space Shuttle reliability and safety, and information about stages similar to the OTV and kickstage do exist.

Historically, unmanned expendable boosters (Scout, Delta, Atlas-Centaur, Titan, etc.) have exhibited about a 90 percent success rate. This success rate is acceptable for the types of payloads being launched by these vehicles, but it would not be acceptable for nuclear waste payloads. On the other hand, the expendable launch vehicles for manned missions were designed for much higher reliability. The flight of Apollo 13 demonstrated the ability of man to safely recover and land a vehicle that had sustained potentially catastrophic damage. After four or five years of operation of the Shuttle, the necessary data base should exist to assess its reliability.

It is known that critical items lists and failure mode and effects analyses have been developed for some of the Space Shuttle systems. However, to date the required overall Space Shuttle reliability data have not been calculated by either NASA or the Space Shuttle contractors.

The projected OTV and SOIS are both stages that rely on proven technology. The OTV is a hydrogen-oxygen upper stage that has the benefit of over a decade of Centaur and Saturn experience to draw upon. The SOIS employs technology similar to the Titan Transtage and the Space Shuttle Orbital Maneuvering and Reaction Control Systems components (e.g., tanks, engines, etc.). This technology is quite reliable and available now. There should be little difficulty in designing, developing, and demonstrating safe, reliable upper stages for the space disposal mission.

Design of the waste container, reentry and docking systems is at such a preliminary conceptual level that estimation of system reliabilities are not appropriate at this time. As these designs mature, generation of reliability data will become more feasible.

### 5.2.3 Fault Trees

To obtain a qualitative feel for the relative importance of various potential system failures, preliminary fault trees were constructed and analyzed for each phase of the mission. The methodology and symbology used follows that presented in Reference 5-23. Because of reasons previously discussed in Section 5.2.2, it is not feasible, presently, to assign probabilities to each fault event. Additionally, for those phases involving Space Shuttle elements, the fault trees were terminated when a Shuttle element failure was encountered. Analysis below this level is correctly being conducted by the Shuttle prime contractor.

Table 5-6 shows the fault tree symbols used in this section and defines the meaning of each symbol. In one case, the similarity transfer, additional explanation is needed. This symbol is used to avoid unnecessary clutter in the diagrams. Its meaning, as used in this report, can be explained by examining Figure 5-41. In this figure, there is an OR gate with the numeral 1 in it, leading into event number 11. There are also three similarity transfer symbols, one leading into event number 13 - the others into events 15 and 17, and identified with the numeral 1. This means that the same outputs operating from







the OR gate numbered 1 are also operating as outputs of the similarity transfer symbols shown as .

TABLE 5-6. FAULT TREE SYMBOLS

Symbol	Meaning
	Rectangle: A Fault Event
Output  Inputs	OR Gate: Output Exists If At Least One Input Is Present
Output  Inputs	AND Gate: Coexistence Of All Inputs Is Needed To Produce An Output
	Triangle: A Connecting Or Transfer Symbol
	Inverted Triangle: Similarity Transfer

Each of the fault trees for the 12 mission phases shown in the following subsections has been examined for those single-point and multiple-point failures considered most likely to lead to catastrophic results --- the release of nuclear waste from containment. Elementary criteria have been used in choosing these most likely failure paths. For example, a path that involves only two failure events has been considered more likely to occur than one that requires five or six failure events to occur sequentially. In most cases, careful study of the fault tree was sufficient to eliminate all but two or three of the potential



event sequences. These "critical paths" are indicated (where identified) on the fault tree figures included in the remainder of this section.

Once the most likely event sequences were determined, potential ways of avoiding these paths (or of decreasing the possibility of their occurring) were examined. Possible workarounds were suggested for reducing the possibility of nuclear waste release. The feasibility of these workarounds was not examined in any detail. More detailed study and analysis of workaround feasibility and practicability in terms of cost, payload impact and incremental safety achieved is required downstream of the current effort.

### 5.2.3.1 Phase I Fault Tree

During Phase I, the risks do not appear to be critically large, and those risks that do exist seem to be amenable to relatively simple workarounds. The fault tree for this phase is given in Figure 5-40.

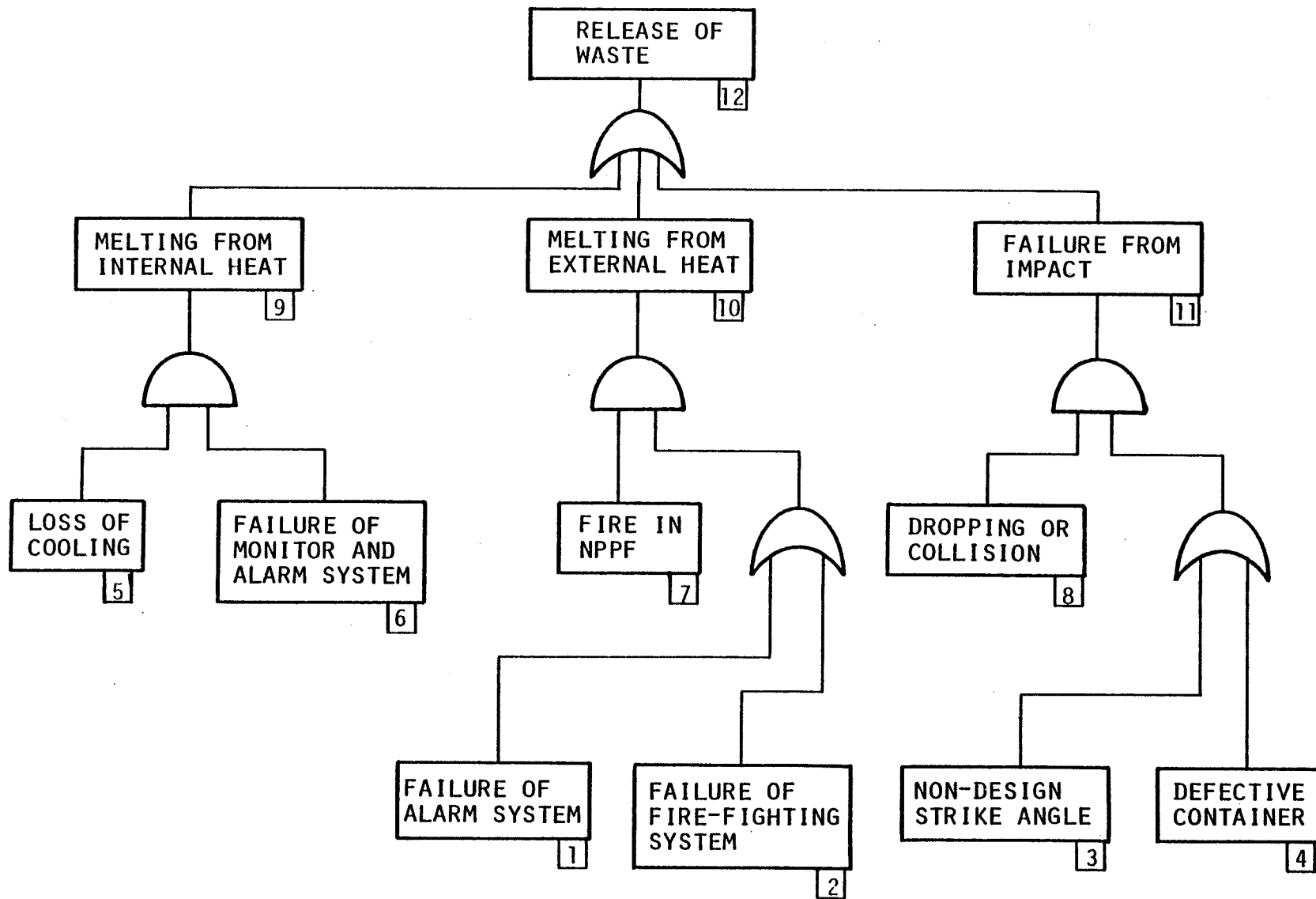
Any path that leads to Blocks 9, 10 or 11 results in release of waste (Block 12). In this phase, the paths are as follows:

- (a) 6 given 5 leads to 9 after a certain time
- (b) 7 given 1 or 2 leads to 10 after a certain time
- (c) 8 given 3 or 4 leads to 11 immediately.

No one of these paths stands out as being more critical than the others, so workarounds are given for all three paths.

**Path (a).** Loss of cooling can be worked around by providing: (1) redundant prime cooling systems, (2) redundant prime movers for these systems, and (3) self-contained, backup cooling systems.

Failure of the monitor and alarm system can be worked around by providing: (1) independent, redundant temperature sensors based on different principles, (2) different transmission paths to the alarm system, (3) voting logic (fail-operational, fail-safe) at the monitor/alarm console, (4) periodic temperature sensing by a man with a portable sensor, and (5) redundant paths to the emergency station.



5-67

FIGURE 5-40. PHASE I FAULT TREE (PAYLOAD PROCESSING AT LAUNCH SITE)

**Path (b).** Fire in the NPPF can be worked around by: (1) using fireproof principles in designing and constructing the NPPF, (2) limiting use and storage of flammable materials, and (3) using fireproof vaults for storing flammable materials in an area away from the waste containment area. Waste containers and the containment area should be designed so that a fire will not breach a container.

Possible failure of the alarm system has previously been discussed.

Failure of the fire-fighting system can be worked around by providing: (1) mobile fire-fighting equipment at two locations on the base, (2) separate means of access from the fire stations to the NPPF in case one should become blocked, and (3) redundant, independent water sources in the vicinity of the NPPF.

**Path (c).** The possibility of dropping or collision while a container is in the NPPF can be minimized by following stringent procedures and exercising safety discipline.

If there is an angle (non-design strike angle) at which a container impact suffered in the NPPF could lead to a breach, the workaround would be to change the design of the container.

A defective container can be eliminated by meticulous design, fabrication, testing and inspection.

#### **5.2.3.2 Phase 2 Fault Tree**

Starting with this phase, the potentially catastrophic consequences resulting from an explosion of the External Tank contents and the ensuing fire (possibly including burning SRB fragments) must be considered. The fault tree for Phase 2 is shown in Figure 5-41.

Any path that leads to Blocks 14-18 represents a sequence of events that could result in release of waste. From preliminary analyses of event consequences, paths that lead through Block 11 appear to be most critical with respect to potential for breaching the waste containment system and releasing waste products.

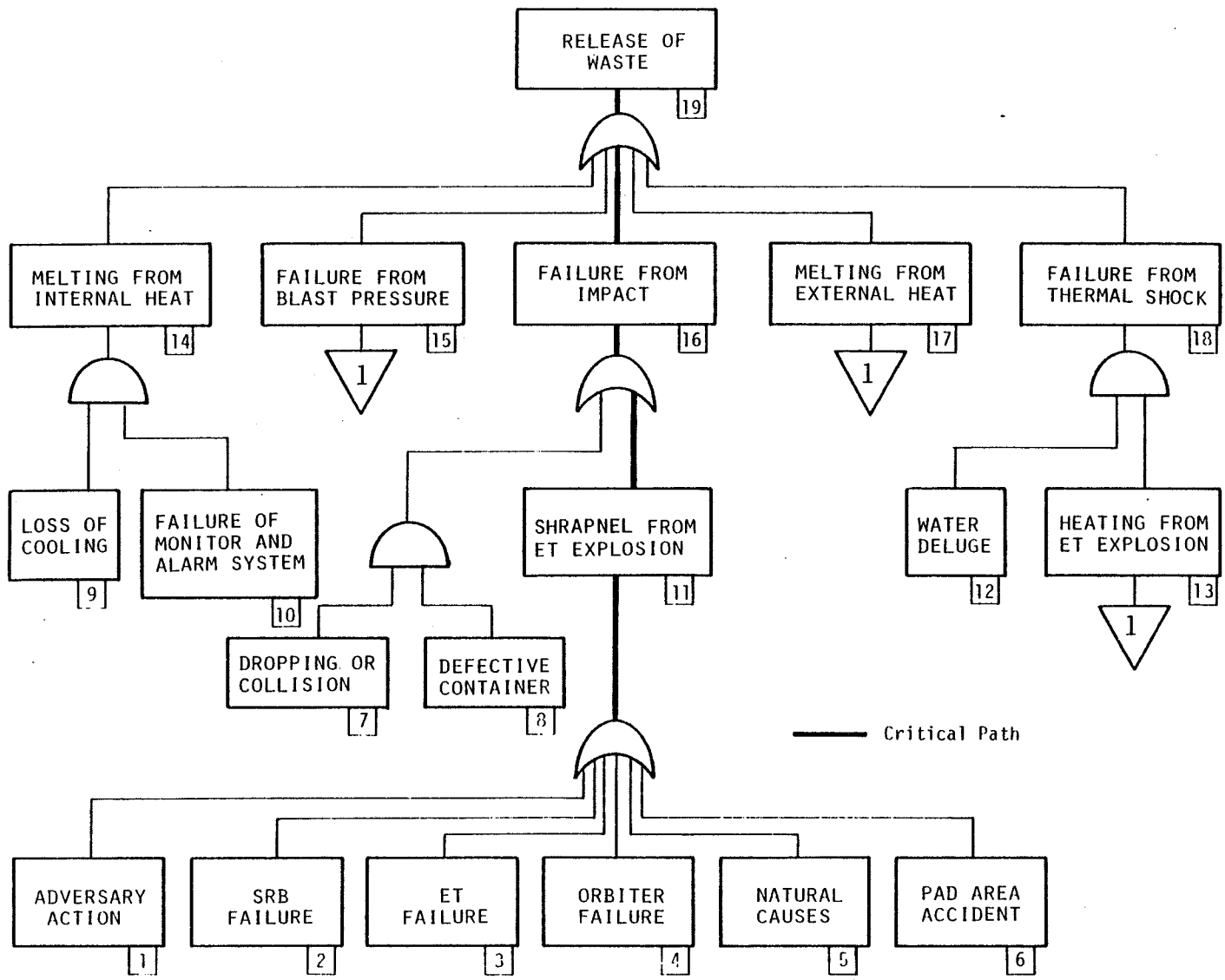


FIGURE 5-41. PHASE 2 FAULT TREE (ON-PAD, PRELAUNCH OPERATIONS)

Blocks 7, 8, 9 and 10 have been covered in the discussion of the Phase I fault tree, and are not considered to pose a serious risk of container breach as long as appropriate measures are taken.

In like manner, it should be possible to design against failure from thermal shock (Block 18). In fact, if detailed analyses show low probability of melting due to external heat applied by an ET explosion followed by exposure to fire from an SRB fragment, a deluge system could be dispensed with for this phase of operations.

The current container concept appears to be more vulnerable to shrapnel fragments from the ET explosion than to the associated heat or overpressure. Workarounds for the fragment problem can be of two types. First, minimize the chances of the fragment-producing explosion occurring; second, minimize the effect of the fragments on the waste container.

There are two ways in which the effects of an ET explosion on a container in the Orbiter cargo bay could be mitigated. The ET itself might be designed in such a way that the effects of a blast would be directed away from the Orbiter. The second way would involve placement of energy-absorbing and/or fragment-deflecting material and structure between the waste container and the ET. Such an addition could be made on the floor of Orbiters built specially for the nuclear waste disposal mission - this would likely create less weight penalty than trying to add such additional structure to an existing general purpose Orbiter.

To examine ways to minimize the probability of an ET explosion occurring, it is necessary to develop Orbiter, SRB and ET fault trees. Fault trees of this type are currently under development by the Space Shuttle contractor and subcontractors.

Other sources of events that might lead to an ET explosion are shown in Blocks 1, 5, and 6. Stringent security, similar to that found at Strategic Air Command sites, would be prudent. Protection from natural causes would be provided by procedures (no operations in high winds or when they are predicted) and by the best lightning protection that could be devised. The major pad area accident to be guarded against in Phase 2 is explosion of the cryogenic storage tanks. A workaround would be to ensure that these tanks are located far enough from the pad (or shielded well enough) that a worst-case, accidental blast could not damage the assembled Shuttle to the extent of leading to an ET explosion.

The ultimate workaround to ensure no release of waste products would be to design and build the waste container so that it could withstand any possible hazard environment or credible combination of them. At this point in the study, it is not clear that this could be done without reducing the waste loading of the payload below acceptable levels.

#### 5.2.3.3 Phase 3 Fault Tree

During this phase, the events that could happen are largely the same as those in Phase 2, with two exceptions. During ascent of the Shuttle, it could collide with the tower - this would likely lead to an uncontrollable crash with a resultant ET explosion. The Phase 3 fault tree is included as Figure 5-42. Another major difference is that the SRBs and SSMEs have been ignited and the Shuttle is moving. This increases the number of things that could go wrong. For example, at commanded ignition one of the SRBs could fail to ignite - this would result in a large overturning moment and likely rupture of the ET, leading to an  $H_2/O_2$  explosion. The same result could be achieved by a sidewall burnout of an SRB, or a malfunction of the Orbiter control system.

Until more information is available about Shuttle hardware fault trees, it is not possible to do much in the way of suggesting workarounds. Again, as suggested in the discussion under Phase 2, protection of the waste container from shrapnel could be effected by redesign of the Orbiter on the side facing the ET to provide fragment deflection and/or energy absorption. Another possible workaround would be to design the ET in such a manner that the effects of an explosion would focus away from the Orbiter and waste package. This might be done by use of "blowout panels" incorporated into the ET on the side away from the Orbiter.

#### 5.2.3.4 Phase 4 Fault Tree

In Phase 4, the Shuttle achieves sufficient altitude that an emergency landing is possible during portions of this phase. As a result, some failures (Blocks 7, 8 and 9 of Figure 5-43) could result in an attempt at an emergency Orbiter landing rather than an inevitable Shuttle crash with the resultant explosion. One outcome of an attempt at an emergency landing is to crash the

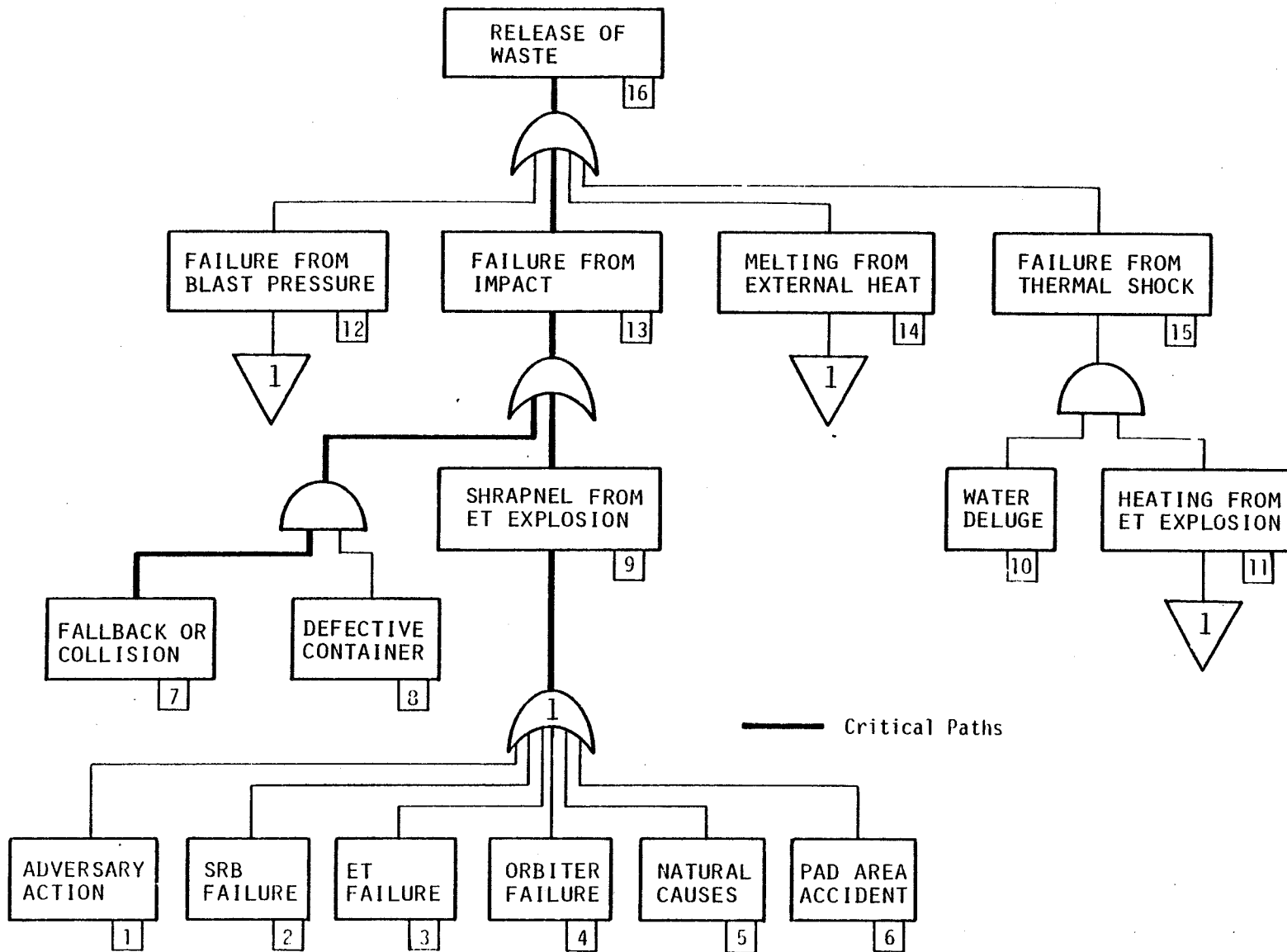


FIGURE 5-42. PHASE 3 FAULT TREE (IGNITION TO CLEARING OF TOWER)

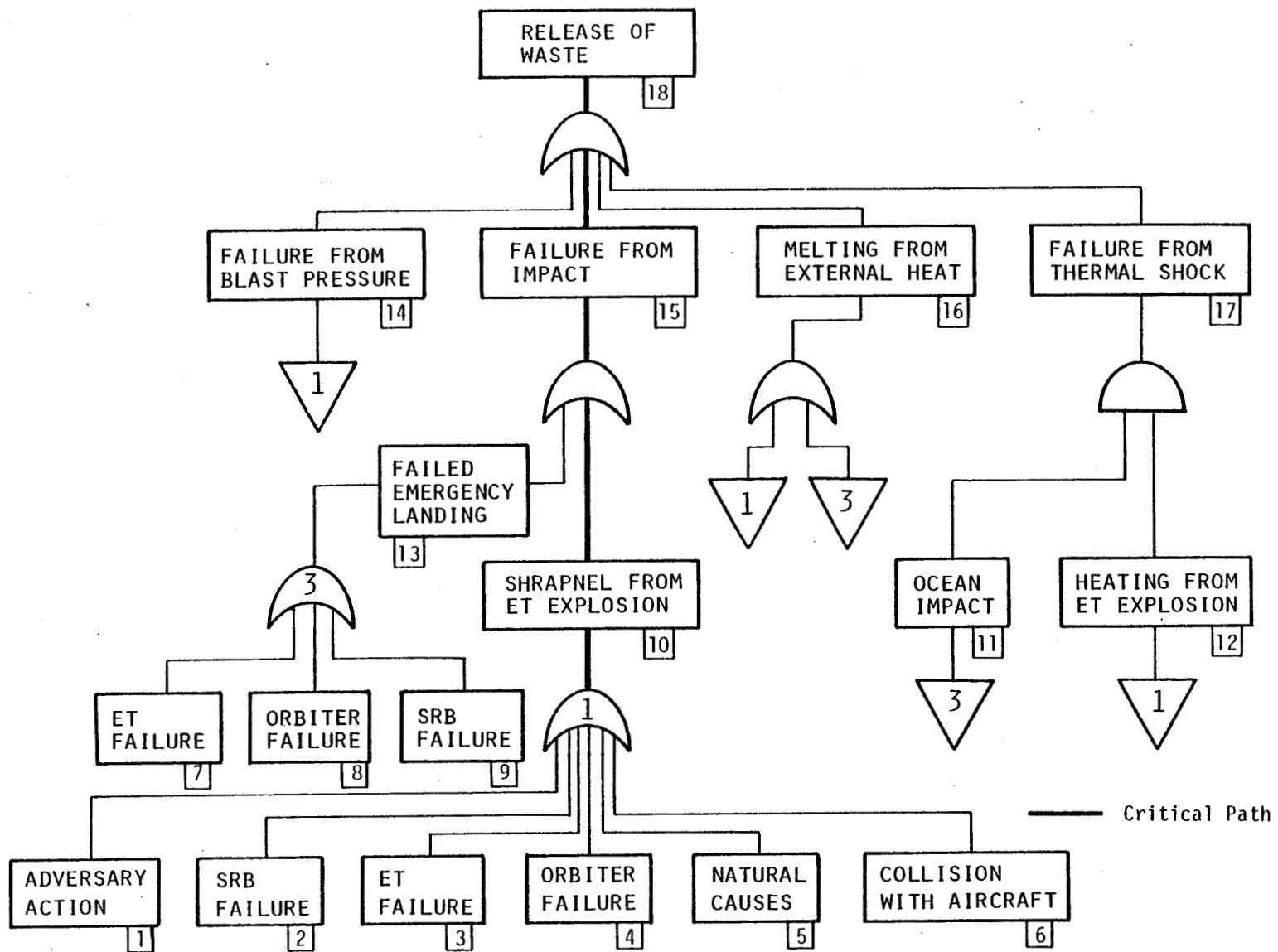


FIGURE 5-43. PHASE 4 FAULT TREE (CLEARING OF TOWER TO SRB BURNOUT)



Orbiter (Block 13), which could lead to an impact failure of the waste container (Block 15). A workaround that might lessen the probability of a crash from a low-altitude abort would be to provide the waste-disposal Orbiter with a propulsive capability that would give the pilot a better chance to make a successful emergency landing. This propulsive capability could consist of small auxiliary rocket motors designed for operation in the atmosphere and using OMS fuel. They could be designed to be jettisoned once a "safe" altitude had been reached. An alternative approach would be to provide a system for emergency ejection of the payload.

Block 6, Collision with Aircraft, is a low-probability event since every effort will be made to keep aircraft from intruding into the launch area during a launch. Since such a collision would be highly likely to lead to an ET explosion, however, it is suggested that a system be implemented that scans the surrounding airspace, projects any vectors with a reasonable probability of intruding into the launch zone, and automatically holds the countdown until such time as the potential danger is past.

During this phase, the danger from an ET explosion could be most severe. Although some of the cryogenic fuel has been used up, the explosive yield of the remaining fuel and oxidizer could be greater than for an on-pad failure if the vehicle nosed over and power dived into the ground or ocean. Again a possible workaround to avoid exposing the waste container to the worst of such an explosion would be to use an ejection system that would be armed at lift-off and would be activated if the Orbiter attitude should exceed tolerances that would be precursors of a powered crash.

#### 5.2.3.5 Phase 5 Fault Tree

The fault tree for Phase 5 is given in Figure 5-44. The only major change between this phase and Phase 4 is the hazard introduced if an SRB doesn't separate when it is supposed to (Block 8). If this happens, the Orbiter should be separated and an emergency landing attempted. Since the emergency landing attempt would be initiated from a higher altitude than in Phase 4, its probability of success could be expected to be higher. Use of auxiliary propulsion units (as discussed in Phase 4) could increase this probability of success.

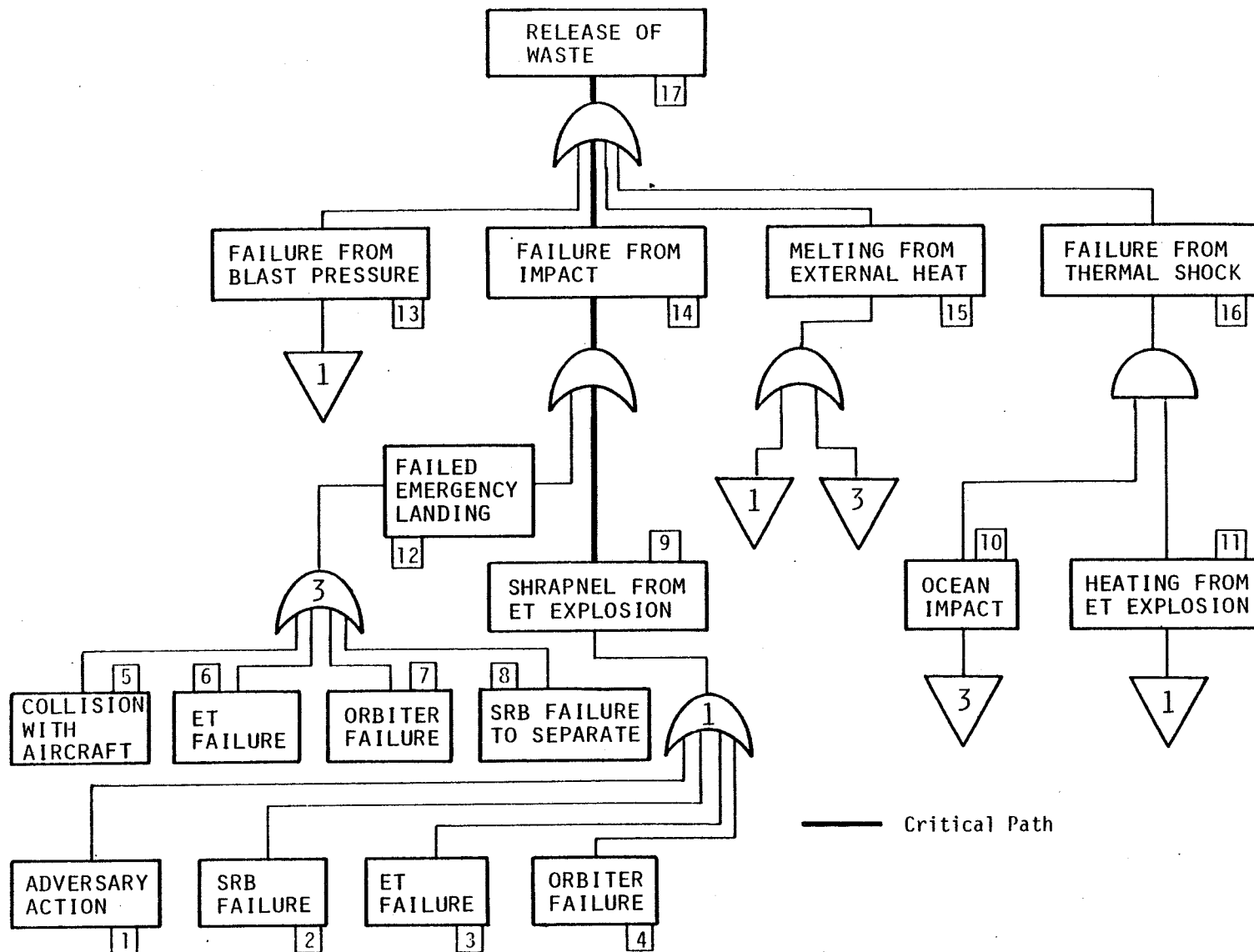


FIGURE 5-44. PHASE 5 FAULT TREE (SRB BURNOUT TO ET DROP)

#### 5.2.3.6 Phase 6 Fault Tree

The most immediate path to release of waste in this phase is an Orbiter explosion (Box 11 of Figure 5-45) that produces shrapnel (Box 6) of sufficient energy to penetrate the waste container (Box 14). No analyses have been done to predict what the likelihood of such an incident would be. It is believed that all other paths in this tree are less likely to occur than the one just described.

#### 5.2.3.7 Phase 7 Fault Tree

In this phase, since the Orbiter with the waste package is in a stable orbit, there are only two things that can go wrong (see Figure 5-46). First the Orbiter could be stranded in orbit, unable to maneuver (Block 5). This is considered highly unlikely, but if it happened the waste package could eventually breach due to heat and pressure buildup (Block 9). Another unlikely event would be explosion of the Orbiter (Block 7). If this happened, the container might be ruptured (Block 10), but it would still be in its reentry shield, making the probability of rupture quite low.

In case of reentry of either the container after an explosion, or the Orbiter after orbital decay, events in Boxes 1, 3, and 11 could occur, all with potential for release of waste. The obvious workaround to prevent reentry of the waste package is a rescue vehicle that could retrieve the container and return it safely to Earth. The package could also be protected from an explosion by a shield between the OMS fuel and oxidizer and the waste container if the probability of such an event were non-negligible.

#### 5.2.3.8 Phase 8 Fault Tree

There are close to 100 separate paths possible in the Phase 8 fault tree (included as Figure 5-47). Analysis of the diagram shows that the most significant paths are the following: 1-27, 6-11-28, and 2-27.

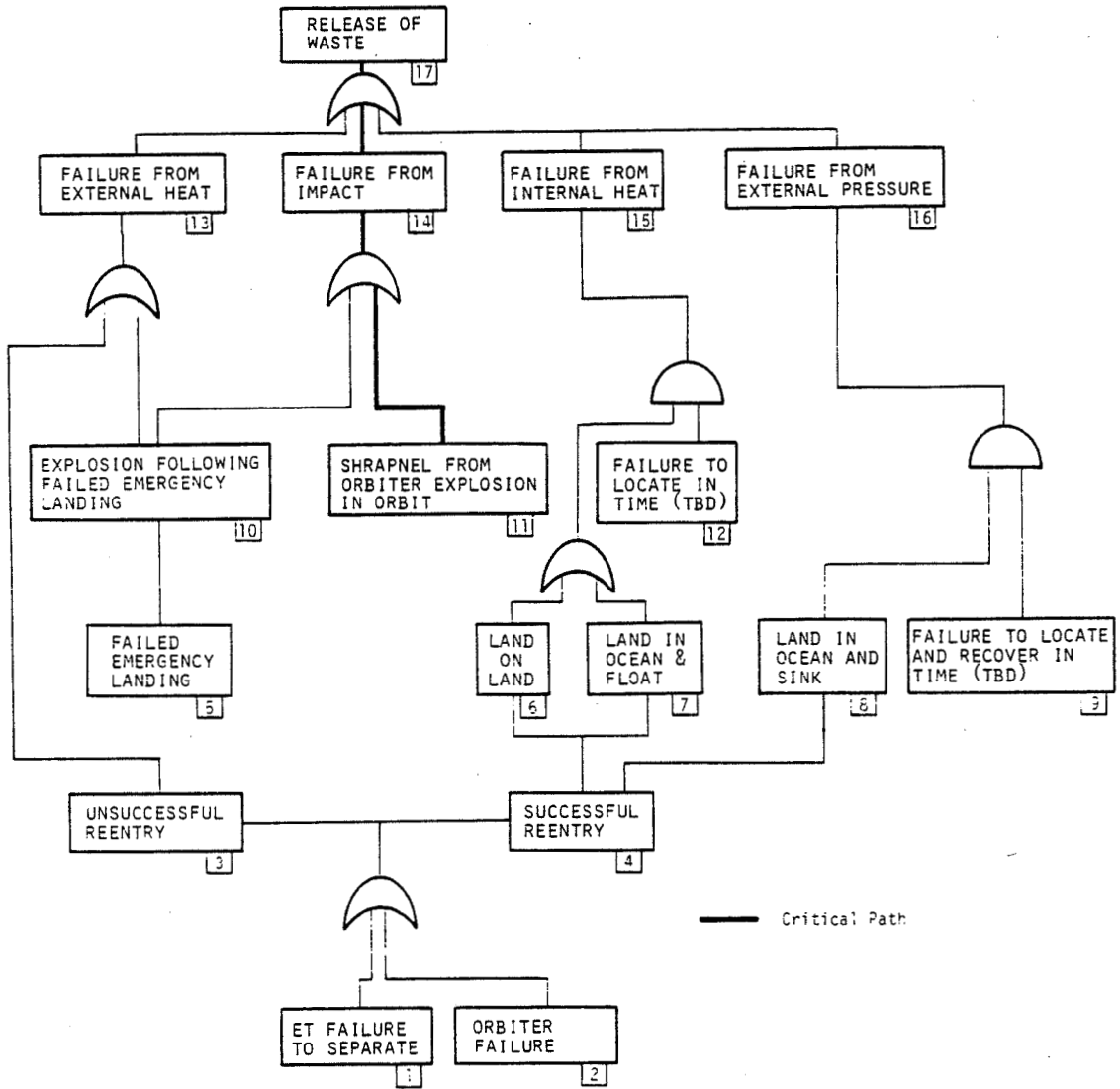


FIGURE 5-45. PHASE 6 FAULT TREE (ET DROP TO ACHIEVE ORBIT)

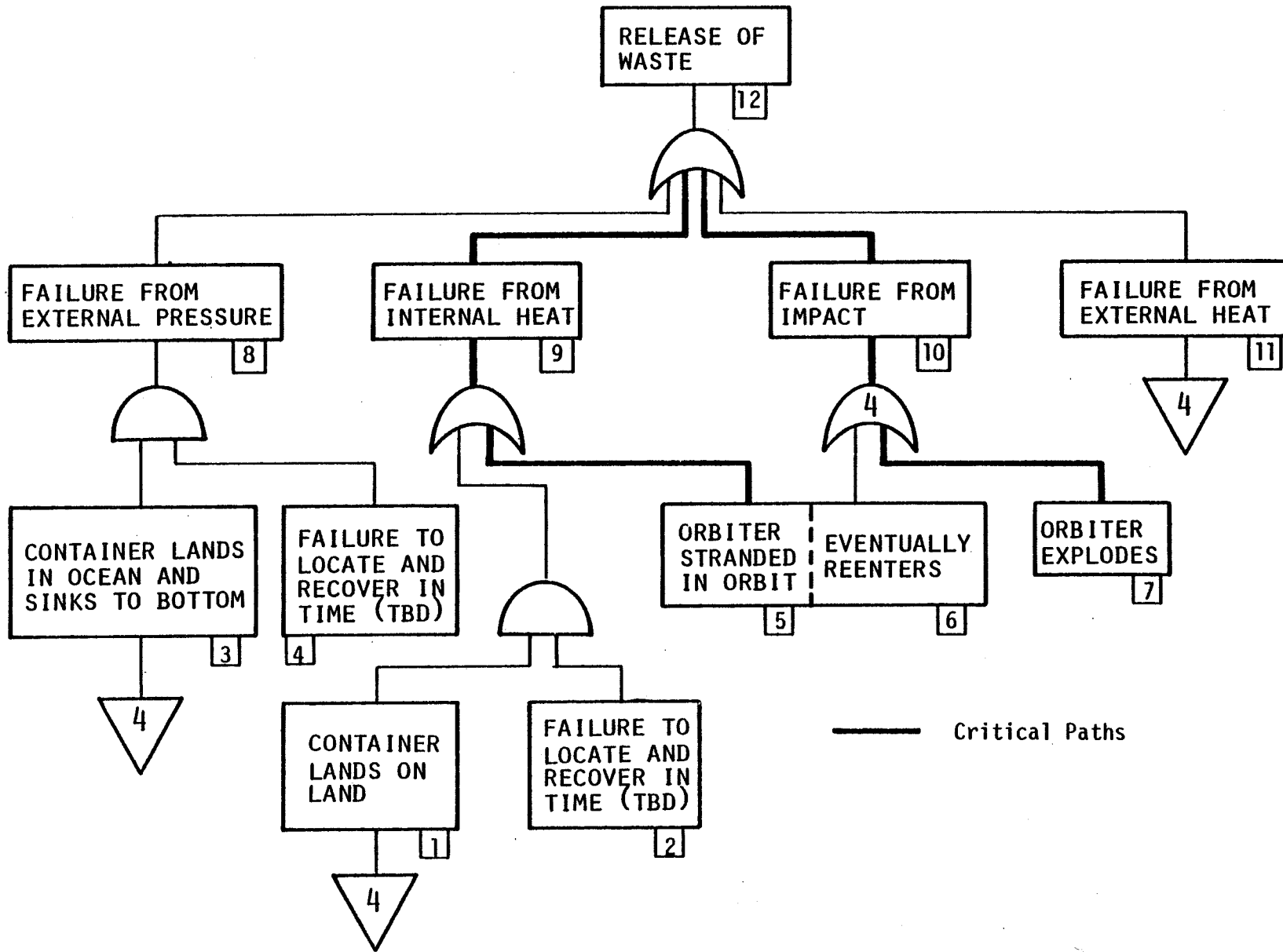


FIGURE 5-46. PHASE 7 FAULT TREE (ACHIEVING ORBIT TO RENDEZVOUS)



Paths 1-27 and 2-27. If the Orbiter or OTV should explode in the vicinity of the waste container, there is a chance of immediate breaching of the waste container due to shrapnel puncturing it with a resultant release of waste products. Obvious workarounds are to make these vehicles as explosion-proof as possible. Since this is likely to be a design requirement in any event, the concern is with explosions that might occur despite design efforts. The waste container probably could be designed to withstand an Orbiter or OTV explosion. This is an area in which further analysis and trade-offs are needed.

In case of a breach in orbit (Box 27), a special purpose rescue vehicle could be used to attempt to recover the ruptured container in order to minimize the effects of the breach.

Path 6-11-28. This path requires that the combination OTV/SOIS/container package does not check out after it has been assembled in orbit and that undocking of the container cannot be effected. There are several workarounds that could be attempted in the case of a recalcitrant undocking attempt. First, a manual backup undocking mode could be designed into the mechanism and could be actuated by an EVA. Second, a brute force technique involving an EVA with a cutting torch or bolt cutters could be effective. The objective would be to release the container so that it could be recaptured by its Orbiter or by a rescue vehicle before it re-entered with potentially disastrous effect.

#### 5.2.3.9 Phase 9 Fault Tree

Like the Phase 8 fault tree, Phase 9 has a multitude of paths as shown in Figure 5-48. Examination of the tree shows that the ones of greatest concern are: 1-29 and 1-14-24-30.

Path 1-29. Path 1-29 is the same as Path 2-27 in Phase 8, and is discussed there.

Path 1-14-24-30. If the OTV explodes and the waste container is not ruptured, but driven Earthwards so that neither an on-orbit Orbiter nor a rescue vehicle could retrieve it, it would re-enter and likely burn up since the reentry

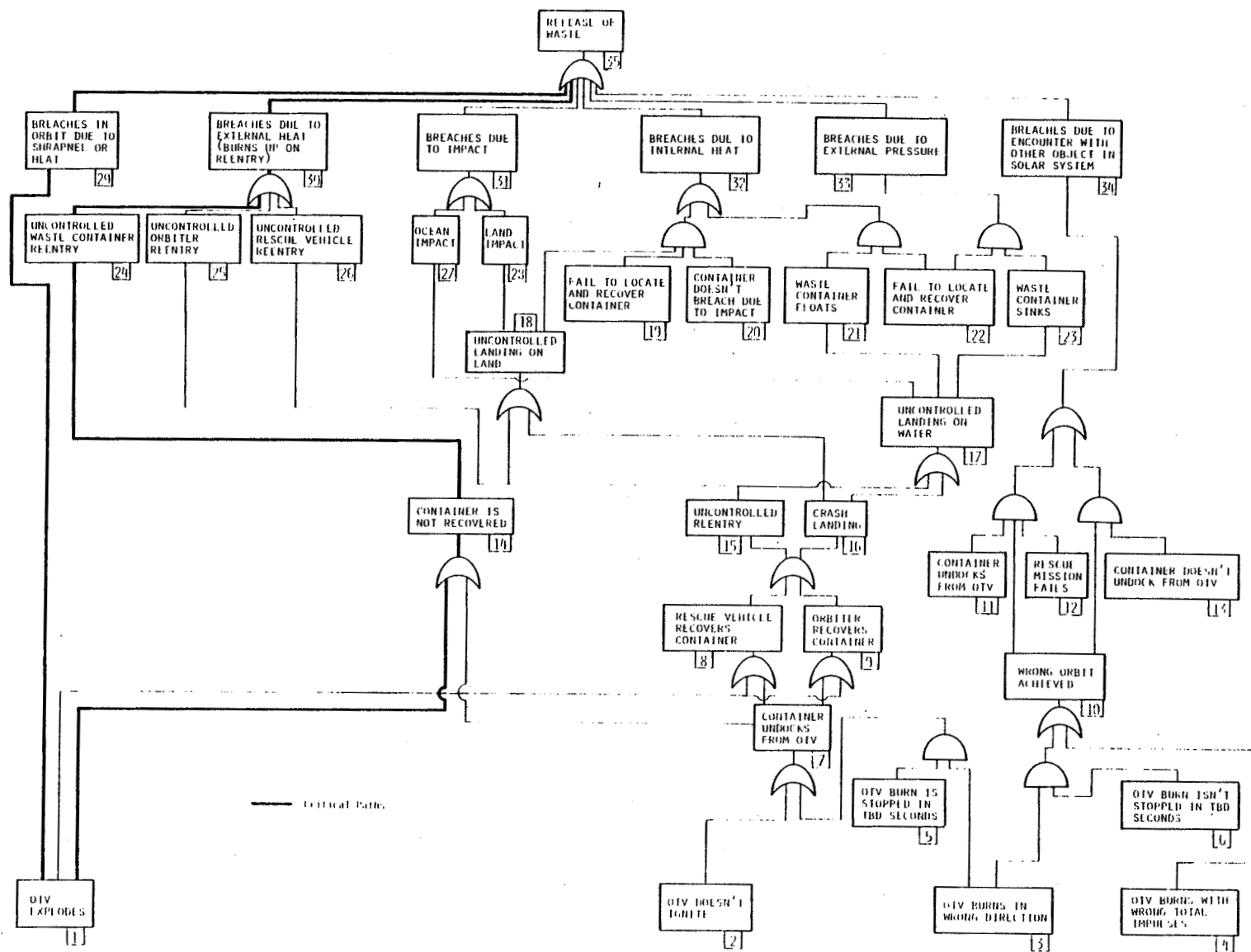


FIGURE 5-48. PHASE 9 FAULT TREE (OTV IGNITION AND BURN)



shield has been removed in a previous operation. This would scatter waste products in the upper atmosphere.

The best workaround would be one that rendered the probability of an OTV explosion negligible. An approach to this would be to design the OTV so that the chance of hydrogen and oxygen mixing in space in flammable amounts was negligible. Design and procedures should be such as to ensure that no sparks occur during and after docking. An alternative approach would be to add a layer of non-reusable thermal protection (e.g., an ablative) to the container to allow it to survive an inadvertent reentry.

#### 5.2.3.10 Phase 10 Fault Tree

All possible paths in this fault tree (Figure 5-49) are of the same length: 1 given 2, 3; 1 given 2, 4; and 1 given 2, 5. The second path is the one most likely to occur, however, since the reentry shield has been removed from the waste container prior to the OTV burn. In any event, the most effective (and least costly) place to attack these potential problems is in Block 2.

Attempts should be made to make the primary OTV release mechanism as reliable as possible. In addition, a possible workaround would be to incorporate a backup release mechanism that could be activated in case the primary mechanism jammed.

The highly elliptical orbit of the payload at this point in the mission should provide enough lifetime to permit several rescue attempts. A workaround for Block 4 would be the addition of thermal protection to the container, as discussed under Phase 9.

#### 5.2.3.11 Phase 11 Fault Tree

In this phase of operations, only one thing can go wrong: the SOIS malfunctions as it attempts to circularize the final disposal orbit at 0.86 a.u. It can fail to ignite, burn in the wrong direction or burn for the wrong length of time (see Figure 5-50). The first workaround for any of these conditions (Boxes 1, 2 and 3) is to attempt a rescue mission to: (1) retrieve the waste package, or (2) correct the orbit of the package. The most critical event would be one in

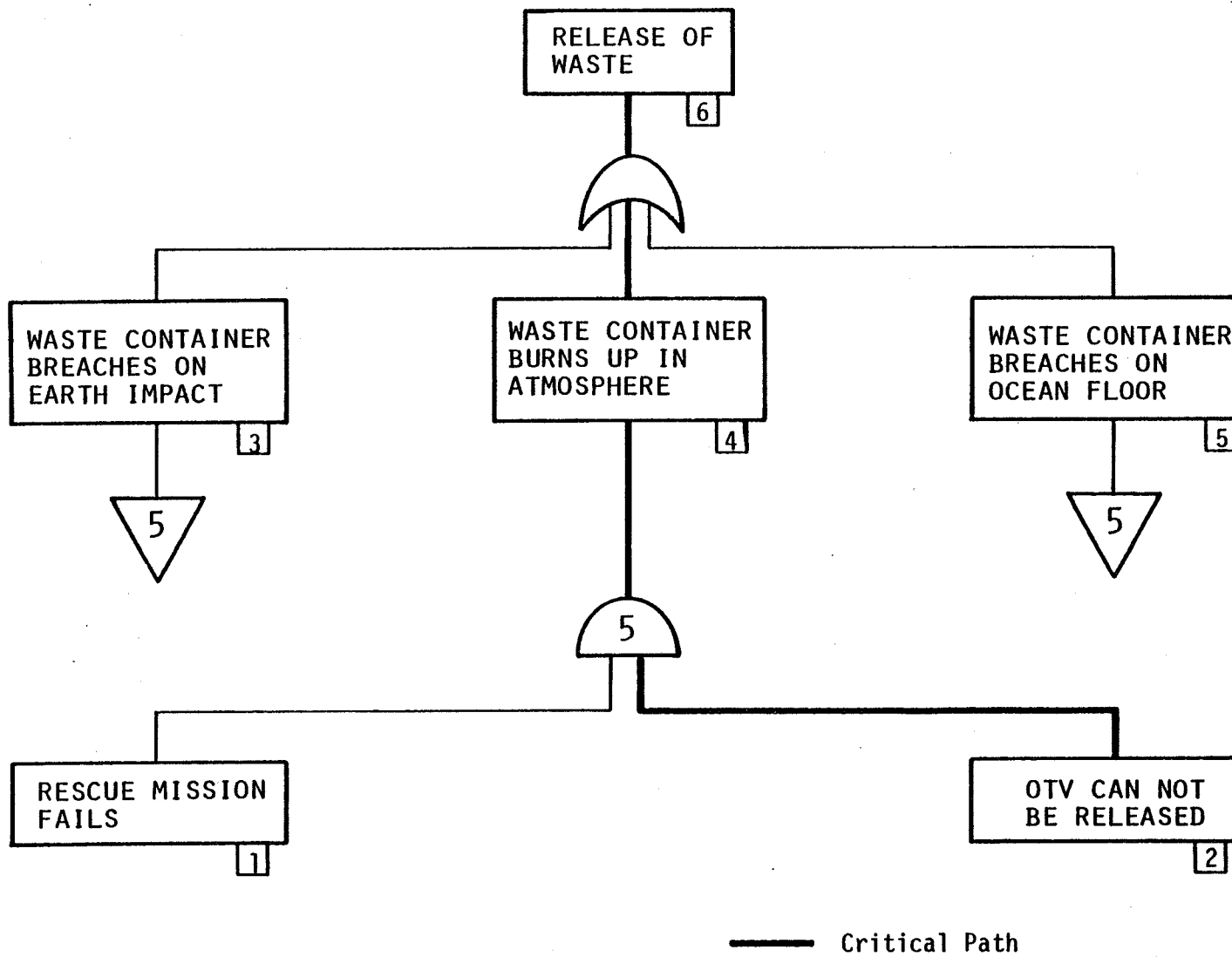


FIGURE 5-49. PHASE 10 FAULT TREE (OTV JETTISON TO SOIS IGNITION)

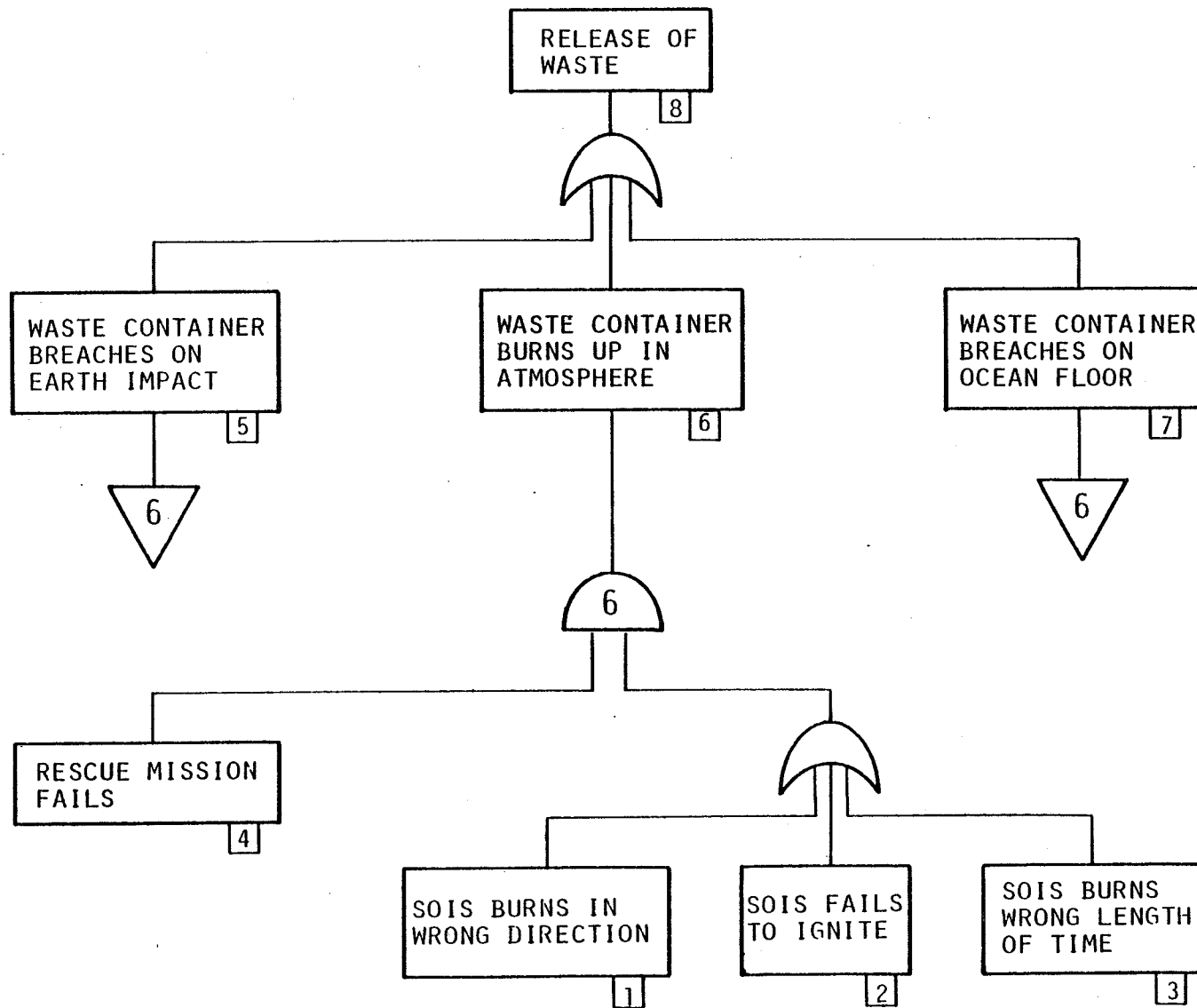


FIGURE 5-50. PHASE II FAULT TREE (SOIS BURN)

which the SOIS would burn in such a fashion as to place the waste package on an immediate Earth reentry trajectory. In this case, there might only be time to attempt one rescue mission. In all other cases, there would be ample time to attempt numerous rescues.

Event 6 is most likely to happen in case of a reentry since the container will have been removed from its reentry shield prior to kickstage firing. Again, a possible workaround would be to design the waste container to withstand reentry, as discussed in Phase 9. Because of the greater reentry velocity for return from heliocentric orbit as compared to low Earth orbit, the amount of protection required would be greater and might significantly reduce the amount of waste that could be carried. Since Earth reentry from heliocentric orbit is a highly unlikely event, trade-off analyses are needed here.

#### 5.2.3.12 Phase 12 Fault Tree

There is little known at the present time about how well a container could resist being breached eventually by exposure to the space environment at 0.86 a.u. for millions of years. Block 5 of Figure 5-51, Effect of Waste on Container, might be the one event in this phase most amenable to workarounds to ameliorate the effects of possible chemical, heat and pressure reactions over long periods of time. Even if breaching of the container should occur, it is expected that any escaping particles would be swept out of the solar system by the solar wind.

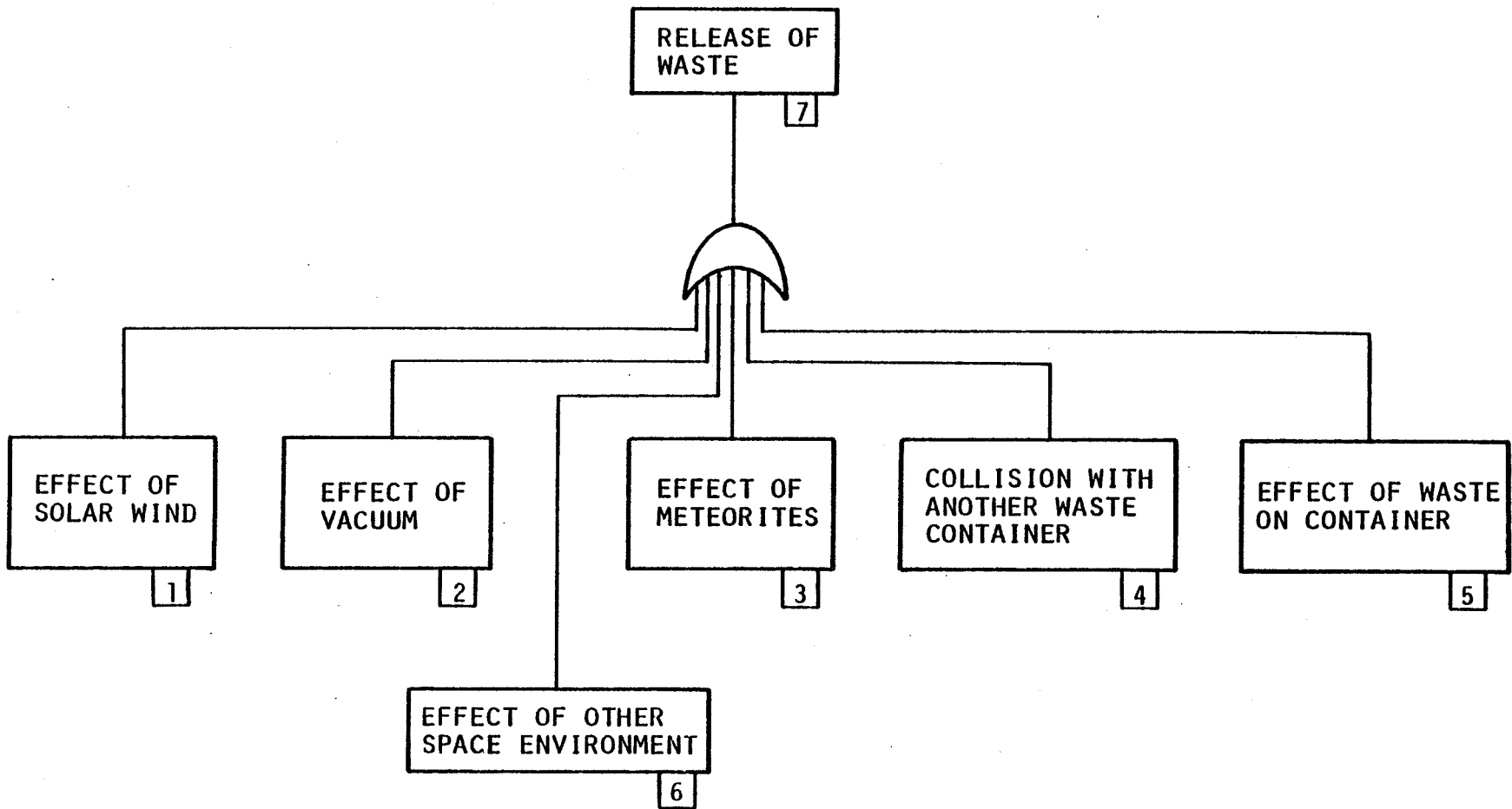


FIGURE 5-51. PHASE 12 FAULT TREE (STAY IN PLANNED ORBIT)

### 5.3 System Modification Requirements

As the design of a system for disposing of nuclear waste in space matures, modifications to enhance the safety, efficiency and economy of the disposal system will be advanced and considered. This section summarizes some proposed modifications that are suggested as a result of defining and analyzing the baseline waste disposal mission and its associated hardware and operations. These proposed modifications need to be investigated in more detail in follow-on activities to determine their efficacy and applicability. The discussion of possible modifications has been divided into subsections dealing with ground, payload, Shuttle and upper stage systems.

#### 5.3.1 Ground Systems

Ground systems include the NPPF, ground transporter and the route it travels from the NPPF to the launch pad. A number of design considerations for the NPPF have been identified as being critical from a safety point of view. These include:

- Establishing the NPPF in a secure area in order to protect against sabotage and other intrusive acts
- Providing the NPPF with adequate radiation containment, including portable shields if necessary
- Keeping fuels/oxidizers isolated from the container storage area
- Providing adequate, redundant radiation and temperature monitoring devices
- Providing alternative cooling equipment and independent emergency power supplies for them in case of primary power failure
- Providing rapid and redundant access to the NPPF for firefighting equipment
- Minimizing payload handling heights within the NPPF
- Eliminating sharp appendages from all areas through which or over which a payload might be moved.

The ground transporter required to move the nuclear waste payload from the NPPF to the launch complex area should be designed to minimize chance of breakdown during transit (e.g., redundant tires, backup prime motor).

It should also be built to include redundant payload cooling systems and be accompanied on its loaded trips by firefighting equipment and personnel. All reasonable care should be taken to eliminate any grade-level railroad crossings along its route. If this is not possible, positive procedures should be developed to guarantee no movement of rail traffic in the vicinity of the transporter route while it is carrying a waste payload.

Once the payload has reached the launch complex, procedures and equipment must be such that the payload has negligible chance of being dropped while being transferred from its transporter to the PCR. As an added factor of safety, the area to which the payload might fall should be cleared of all sharp appendages.

Both standard and non-standard reentry shields should be available at the launch site in case a rescue mission is needed to recover an unshielded payload from orbit. An oversized, non-standard shield could be needed in the case of a payload container that was deformed due to an accident.

A final ground system consideration is the location of the NPPF and launch complex for the nuclear waste mission. Although the likelihood of a launch site catastrophic failure is deemed to be very small, there is a finite possibility that such an accident could contaminate significant areas of KSC and put our nation's space-launch program in serious jeopardy. Thus, significant effort should be devoted to dealing with the questions of launch and NPPF site selection.

### 5.3.2 Payload Systems

As described in Section 3.4.3, the baseline payload system is potentially vulnerable to inadvertent reentry and Shuttle explosion fragment environments. In addition, it is called upon to perform a complicated automated maneuver in low Earth orbit -- removing the rear of the reentry system, using a manipulator arm to extract the payload from the reentry system, then replacing the rear of the reentry system. This portion of the payload system must be designed to ensure that the payload will not hang up during the process of being withdrawn from the reentry system. For example, in Section 5.2.3.8, the possibility of the OTV/SOIS/container package not checking out after orbital assembly combined with an inability to undock from the OTV is discussed. This

situation could lead to inadvertent reentry of the entire OTV/SOIS/container. Inclusion of a backup undocking mode involving EVA or pyrotechnic devices is recommended for consideration, and is typical of the types of backup approaches that need to be considered in the final design of the automated docking and assembly sequence.

As indicated in Section 6, upper atmosphere release of nuclear waste due to inadvertent reentry of an unprotected waste container could have serious environmental effects. The reentry thermal analysis (Section 3.4.3.2) indicates that the unprotected container is not likely to survive reentry without breaching. It is possible that the container could easily survive reentry burnup if some reentry protection were added to the container wall. This protection might take the form of a layer of non-reusable material such as insulation or an ablative covering the outside of the container. Use of a non-reusable material can be considered due to the expected low probability of inadvertent reentry and might not add excessive weight to the payload. Thermal problems (heat transfer to outside) with an insulated container would have to be analyzed and designed for.

Another approach of minimizing the chance for release is to select a waste form that will resist dispersion and/or minimize the amount of inhalable particles produced in an accident environment. This will be a major payload design choice and will influence the feasibility/desirability of other possible modifications such as the addition of additional reentry protection as described above.

### 5.3.3 Space Shuttle Systems

There are several significant modifications that may need to be made to the Space Shuttle system to decrease the hazards associated with the boost phase of placing nuclear waste payloads into space. These modifications could probably best be carried out on Shuttle vehicles designed and built specifically for the nuclear waste disposal mission, but the current line of Shuttles could probably be modified, through the use of removable kits, to supply the additional protection.

One potential modification is placement of an energy and fragment absorbing shield between the payload and the likely locus of the External Tank explosion. Section 3.4.3.1 of this report indicates that the baseline payload



design is currently vulnerable to such an explosion occurring on the ground. A shield could have the effect of slowing down or stopping the high-speed fragments. Design studies are required to determine the optimum configuration and materials of a shield that would be both performance and weight effective.

Presently anticipated licensing requirements may require that the payload demonstrate accident environment survival without credit due to environment mitigation by the presence of the Orbiter. In this case, the energy and fragment absorbing shielding would have to be added to the payload rather than the Orbiter.

Another possible modification would be the proposed incorporation of a payload ejection device, that would eject the nuclear waste package from the Shuttle Orbiter bay prior to a catastrophic event. The sensor system for such a payload ejection system could be either a tilt or rate sensor that would compare actual vehicle angles or angular rates with those commanded, and require payload ejection if preset limits were exceeded. Some details of this approach, such as required ejection velocity and waste package stability, and impact conditions, have been examined. However, additional details such as the ejection distance needed for payload safety, speed of response required and design of the actual payload expulsion system to meet these needs are tasks that should be investigated in the follow-on to this study. Again, a weight penalty would be involved and would have to be evaluated in terms of the overall mission and the additional cost involved.

#### 5.3.4 Upper Stage Systems

The upper stages (OTV and SOIS) envisioned for the nuclear waste disposal mission remain conceptual at this point in time. It is appropriate, however, to suggest that they exhibit certain safety features including:

- Multiple redundant communications and control systems (particularly on the SOIS)
- Communications links that would permit remote manual control and operation of upper stages in cases where checkout shows a problem exists, or there is reason to doubt the ability of a stage to function properly in the automatic mode

- A system to monitor the OTV injection burn and detect and terminate grossly misdirected burns.

The need for a rescue vehicle has also been identified. This would be an upper stage (possibly a modified OTV) that could be used to retrieve the waste payload in case of an accident or malfunction in low Earth or transfer orbit. Such a vehicle would have to be able to rendezvous and dock with a payload that possibly has been deformed by a collision or explosion. It might have to capture a payload with part or all of its reentry system (or other debris) adhering to it. At present, the requirements for a rescue vehicle and its associated equipment and capabilities have not been fully delineated. This is a task that should be done in a later phase of the total effort. In the end, a manned rescue vehicle may be decided upon because of the need for certain operations that could most reliably be performed by a manned EVA (such as detaching a payload from a malfunctioning OTV that will not automatically release the payload).

#### 5.4 References

- 5-1. Bader, B. E., Donaldson, A. B., and Hardee, H. C., "Liquid-Propellant Rocket Abort Fire Model", AIAA Journal of Spacecraft, Vol. 8, No. 12 (December 1971).
- 5-2. Van Nice, L. J., and Carpenter, H. J., "Thermal Radiation from Saturn Fireballs", NAS 9-4810, TRW Systems, Redondo Beach, California (December 1965).
- 5-3. High, R. W., and Fletcher, R. F., "Estimation of Fireball from Saturn Vehicles Following Failure on Launch Pad", 1181, NASA (August 1965).
- 5-4. Gayle, J. B., and Bransford, J. W., "Size and Duration of Fireballs from Propellant Explosions", TM X-53314, NASA (August 1965).
- 5-5. Pesante, R. E., Nishibayashi, et al., "Blast and Fireball Comparison of Cryogenic and Hypergolic Propellants", 0822-01(01)FP, Aerojet-General Corporation, Downey, California (June 1964).
- 5-6. Kite, F. D., Webb, D. M., and Bader, B. E., "Launch Hazards Assessment Program, Report on Atlas/Centaur Abort", SC-RR-65-333, Sandia Laboratories, Albuquerque, New Mexico (October 1965).
- 5-7. Mansfield, J. A., "Heat Transfer Hazards of Liquid Propellant Explosions", URS 706-5, URS Research Company, Burlingame, California (February 1969).
- 5-8. Kite, F. D., and Bader, B. E., "Pad-Abort Thermal Flux Model for Liquid Rocket Propellants", SC-RR-65-577, Sandia Laboratories, Albuquerque, New Mexico (November 1966).
- 5-9. Rowe, J. R., "Properties and Performance of Liquid Rocket Propellants", Aerojet Liquid Rocket Company, Sacramento, California (May 1975).
- 5-10. McBride, B. J., Heimel, S., Ehlers, J. G., and Gordon, S., "Thermodynamic Properties to 6000°K for 210 Substances Involving the First 18 Elements", NASA SP-3001, NASA/Lewis Research Center, Cleveland, Ohio (1963).
- 5-11. Srinivas, V., a letter transmitting data on the maximum fireball diameter, TES-VS-1435, Teledyne Energy Systems, Timonium, Maryland (June 13, 1978).
- 5-12. McAdams, W. H., Heat Transmission, 3rd Edition, McGraw-Hill (1954).
- 5-13. "Minutes of the Interagency Nuclear Safety Review Panel Shuttle (STS) Data Meeting, October 26-27, 1977", Department of Energy (November 22, 1977).

- 5-14. "Space Shuttle Transportation System - Shuttle Model Information", PUB 2547-V-3, Space Division, Rockwell International, Downey, California (December 1976).
- 5-15. "Joint Activities Review - Nuclear Waste Management (Space Option)", NASA's Marshall Space Flight Center, Huntsville, Alabama (April 1978).
- 5-16. "Hazards of Chemical Rockets and Propellants Handbook, Volume 1, General Safety Engineering Design Criteria", CPIA/194, Chemical Propulsion Information Agency, Silver Spring, Maryland (May 1972).
- 5-17. Olsen, T., "Fragment Environment and Response for SSS", Memorandum, Teledyne Energy Systems (August 23, 1977).
- 5-18. Keller, L., "Launch Pad Abort Environments, A Status Report (Rough Draft)" (December 30, 1969).
- 5-19. Jeffers, S. L., "Fragment Velocity Measurements from Three Project Pyro Experiments", SC-DR-69-329 (June 1969).
- 5-20. Unpublished memorandum from Gale Whitacre of Battelle's Columbus Laboratories, Columbus, Ohio (1978).
- 5-21. Unpublished Marshall Space Flight Center memorandum transmitted by the MSFC In-House Study Team (1978).
- 5-22. Myers, J. J., Holm, C. H., and McAllister, R. F., Handbook of Ocean and Underwater Engineering, McGraw Hill Book Co., New York (1969).
- 5-23. "Risk Analysis Using the Fault Tree Technique", Flow Research Inc., Kent, Washington (1973).

## 6.0 ENVIRONMENTAL IMPACT ASSESSMENT

The purpose of this environmental impact assessment of the nuclear waste disposal in space program was to concentrate on those critical areas identified during a previous effort.<sup>(6-1)</sup> The specific objective of the current assessment was to study, in more detail, the health consequences posed by two accidents which are believed to be potentially the most hazardous and to identify how adverse consequences might be mitigated and/or eliminated. The two major accidents treated here are: (1) the on- or near-pad catastrophic Space Shuttle failure with a breach of defense nuclear waste containment, and (2) the reentry and upper atmospheric burnup of a defense waste payload. Analysis was performed for both Savannah River and Hanford waste, assuming the baseline given in Section 2.0 and radionuclide data provided in Tables 3-5 and 3-6. Radionuclide data for Idaho are unavailable at the present time.

An in-depth "credible" environmental assessment of the baseline disposal concept is not possible until more work is done related to the response of designed containment systems to various accident environments. However, the analysis presented here, concerning the two accidents chosen for study, should be useful in choosing among containment designs and concepts, waste forms, and operational procedures.

The following sections describe the work that was accomplished concerning the environmental impact assessment of both the on- or near-pad Space Shuttle failure and the high-altitude atmospheric burnup of a defense nuclear waste payload.

### 6.1 On- or Near-Pad Catastrophic Space Shuttle Failure with Release of Defense Nuclear Waste Material

The on- or near-pad catastrophic Space Shuttle failure could result in the release of defense nuclear waste (see Section 5.0). The purpose of this section is to provide an assessment of the impact of such an accident on human health. The assessment presented here is based upon the use of the NASA/MSFC Multilayer Diffusion Model<sup>(6-2)</sup> to provide time-integrated doses to individuals downwind from the event and BNWL's DACRIN Code<sup>(6-3)</sup>, which provided the dose factors. Other principal assumptions, upon which human health effects were based, are summarized as follows:

- All of the Space Shuttle solid propellant is consumed. The burn time for the Shuttle solid propellant is assumed to be 450 seconds (see Section 5.1.1.2).
- A release of 55 kg of defense nuclear waste is assumed for the purposes of the calculation (~1% of the 5500-kg waste for each payload). This estimate is considered conservative based upon the design features of the protection systems. However, health effects results are presented parametrically for 1, 10 and 100% releases.
- Isotopic compositions employed for the Savannah River and Hanford defense wastes are those shown in Tables 3-5 and 3-6 (see Section 3.2.2).
- Three different meteorologies have been assumed: Sea Breeze, Fall and Spring.<sup>(6-4)</sup>
- The activity median aerodynamic diameters (AMAD) for the radioactive particles were chosen as 0.2, 1.0 and 5.0  $\mu\text{m}$ .
- The area used to calculate the population dose is limited to 100 km from the Kennedy Space Center, Florida, launch pad (Launch Complex 39). Population data were obtained from Reference 6-5. Dose contributions outside this area are neglected.
- 70-year dose commitments were calculated based upon only inhalation of particulate matter. External doses due to submersion in contaminated air and radiation from particles deposited on environmental surfaces were ignored.
- Inhalation of resuspended particles and ingestion of contaminated food and water was ignored.

- Health risk factors are based upon those used in the Draft Environmental Impact Statement for Management of Commercially Generated Radioactive Waste.<sup>(6-6)</sup>
- Organs assumed in the calculations include total body, kidneys, liver, bone, lungs and thyroid.

### 6.1.1 Model Descriptions

Three different computer codes have been used to calculate the consequences of an on- or near-pad catastrophic Space Shuttle failure: the NASA/MSFC Multilayer Diffusion Model<sup>(6-2)</sup>, DACRIN<sup>(6-3)</sup>, and an in-house code which combines outputs from the MSFC code and DACRIN. The first two are described below. The last is described in Appendix F.

#### 6.1.1.1 The NASA/MSFC Multilayer Diffusion Model

The NASA/MSFC Multilayer Diffusion Model<sup>(6-2)</sup> has been employed extensively by NASA and the USAF to predict the downwind concentrations of potentially toxic rocket exhaust effluents (e.g., HCl and Al<sub>2</sub>O<sub>3</sub>). Predictions for ground level concentrations as a result of normal launches of expendable launch vehicles (e.g., Delta and Titan III) have been compared to ground-based measurements and found to be somewhat conservative (i.e., model overpredicts by a factor of 2 or more). The recent Space Shuttle Program Environmental Impact Statement<sup>(6-7)</sup> also employed this model, exclusively. Although no effluent measurements are available for on-pad catastrophic failures of launch vehicles, the models developed to handle these scenarios are believed to be adequate. The reader is referred to Reference 6-2 for the use of Model Number 3 and discussion of the on-pad slow burn scenario. The most recent Space Shuttle on-board propellant data were employed and the slow burn was assumed to occur over 7.5 minutes, or 450 seconds (see Section 5.1.1.2), as compared to a value of 5 minutes, or 300 seconds, that was used previously. Also, since the Space Shuttle SRB propellant combustion appears to provide the worst thermal environment, the short-term hydrogen/oxygen fireball (duration, ~10 seconds) was ignored as a carrier of waste particles in the diffusion model. If waste is to be released, it is likely that the longer term solid propellant fire will

contribute to the breach of containment and provide the air transport mechanism for the waste material. (See Section 5.1.1 for Shuttle accident environments.)

The MSFC Multilayer Diffusion Model (MLDM) was modified to provide concentration and time-integrated concentration data for the nuclear waste material out to a distance of 100 km. For the purposes of the calculations it was assumed that a 55 kg of waste (1% of 5500 kg) would be released. Three previously used meteorological cases (Spring, Fall, and Sea Breeze)<sup>(6-4)</sup> were employed to estimate individual and population dose data.

The peak downwind waste concentrations for any waste mix as a function of meteorological conditions and distance from the launch pad are shown in Table 6-1. Table 6-2 provides the peak downwind waste time-integrated concentrations also as a function of meteorology and distance from the launch pad. Figures 6-1 through 6-3 display isopleth data for time-integrated concentrations (in  $\mu\text{g}\cdot\text{s}/\text{m}^3$ ) as a result of nuclear waste released during the three meteorology cases. Also shown in the figures are population data, as provided by Reference 6-5. When the time-integrated concentration data are combined with population data, assuming an average inhalation rate of  $2.315 \text{ E-}4 \text{ m}^3/\text{sec}$  ( $20 \text{ m}^3/\text{day}$ ), a population dose in terms of  $\mu\text{g}\cdot\text{man}$  results. Appendix F describes this procedure. The above data when combined with dose factors for the various organs, particle sizes, and waste mixes of interest, provide the population dosage data in terms of man-rems (see following discussions).



TABLE 6-1. PEAK DOWNWIND INSTANTANEOUS CONCENTRATIONS OF NUCLEAR WASTE AS A FUNCTION OF DISTANCE

Distance, km	----- Meteorological Case -----		
	Fall	Spring	Sea Breeze
	----- $\mu\text{g}/\text{m}^3$ -----		
5	0.160	0.000	0.125
10	0.766	0.260	0.046
15	0.460	0.530	0.013
20	0.292	0.547	0.006
30	0.144	0.378	0.003
40	0.084	0.244	0.002
50	0.054	0.167	0.002
60	0.038	0.120	0.001
70	0.028	0.090	0.001
80	0.021	0.070	-
90	0.016	0.054	-
100	0.012	0.041	-

NOTE: Based on 55-kg release of waste.

TABLE 6-2. PEAK DOWNWIND TIME-INTEGRATED CONCENTRATIONS OF NUCLEAR WASTE AS A FUNCTION OF DISTANCE

Distance, km	----- Meteorological Case -----		
	Fall	Spring	Sea Breeze
	----- $\mu\text{g-s}/\text{m}^3$ -----		
5	23.4	0.06	12.29
10	123.2	43.9	6.73
15	85.4	92.5	4.57
20	63.6	100.3	3.52
30	42.1	78.8	2.40
40	31.4	58.6	1.82
50	25.0	46.1	1.46
60	20.8	38.0	1.22
70	17.8	32.3	1.05
80	15.6	28.1	0.92
90	13.8	23.7	0.81
100	12.0	20.3	0.72

NOTE: Based on 55-kg release of waste.

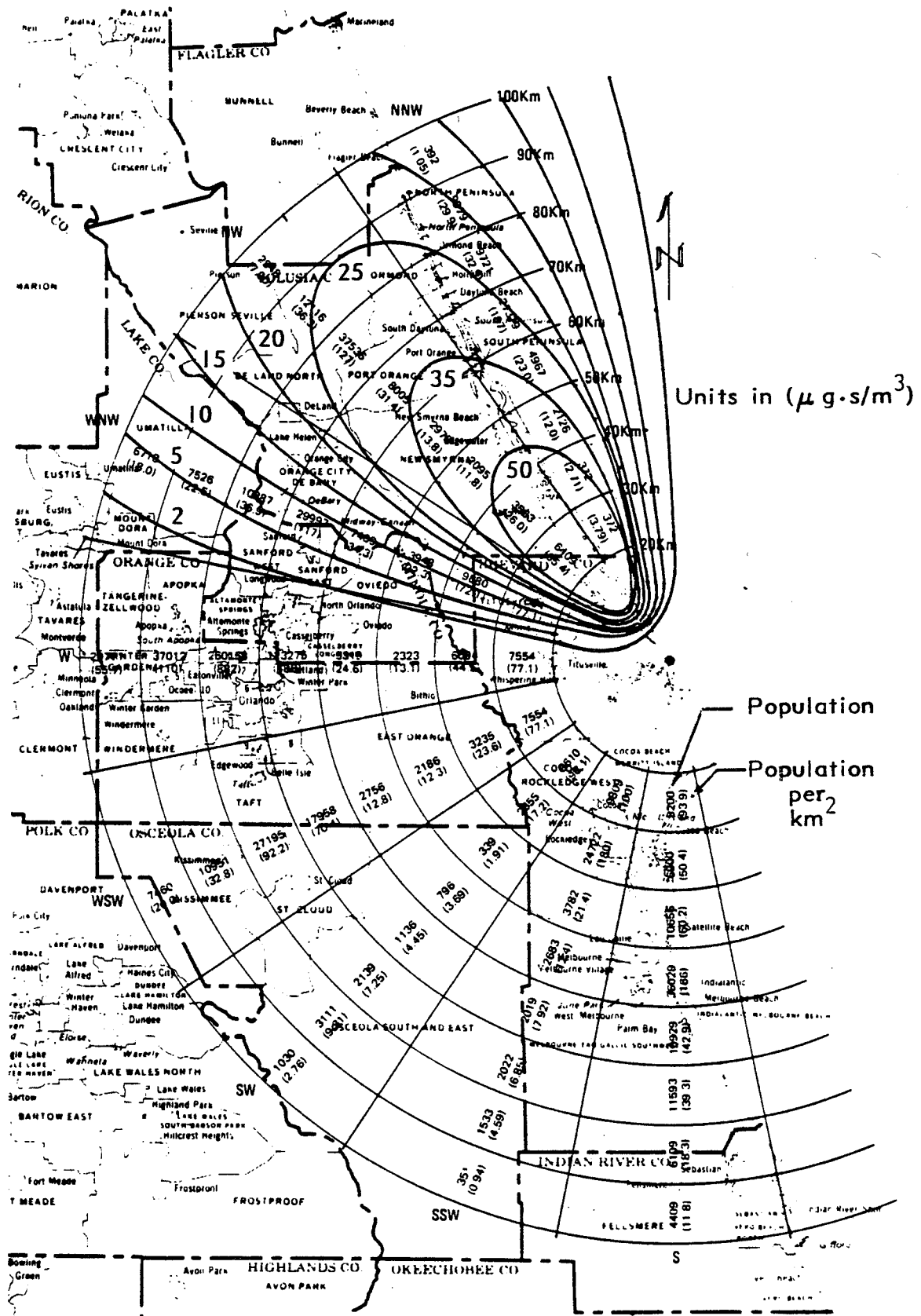


FIGURE 6-1. ISOPLETHS FOR ASSUMED 55-KG RELEASE OF WASTE PAYLOAD DURING SPRING METEOROLOGICAL CONDITION

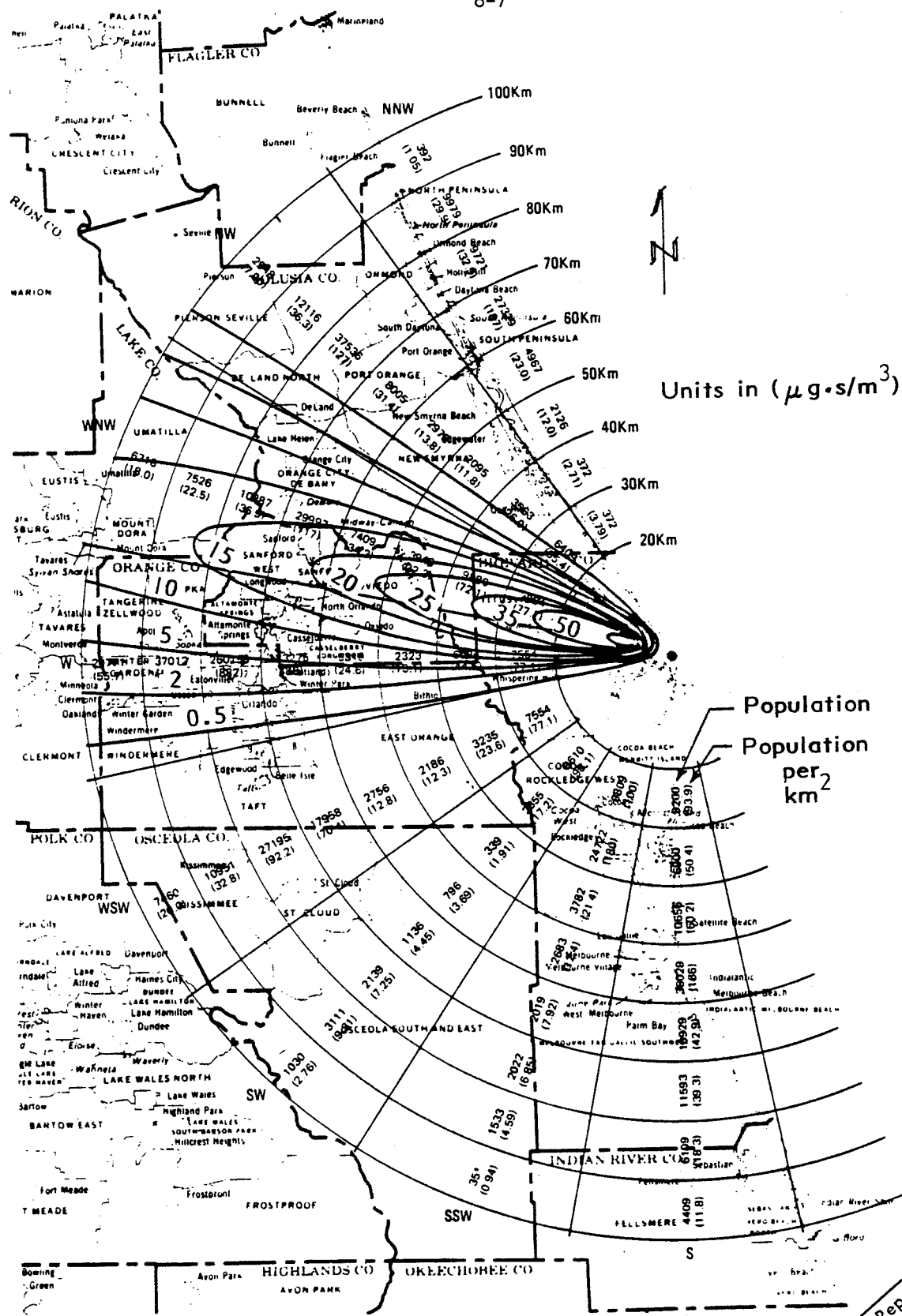


FIGURE 6-2. ISOPLETHS FOR ASSUMED 55-KG RELEASE OF WASTE PAYLOAD DURING FALL METEOROLOGICAL CONDITION

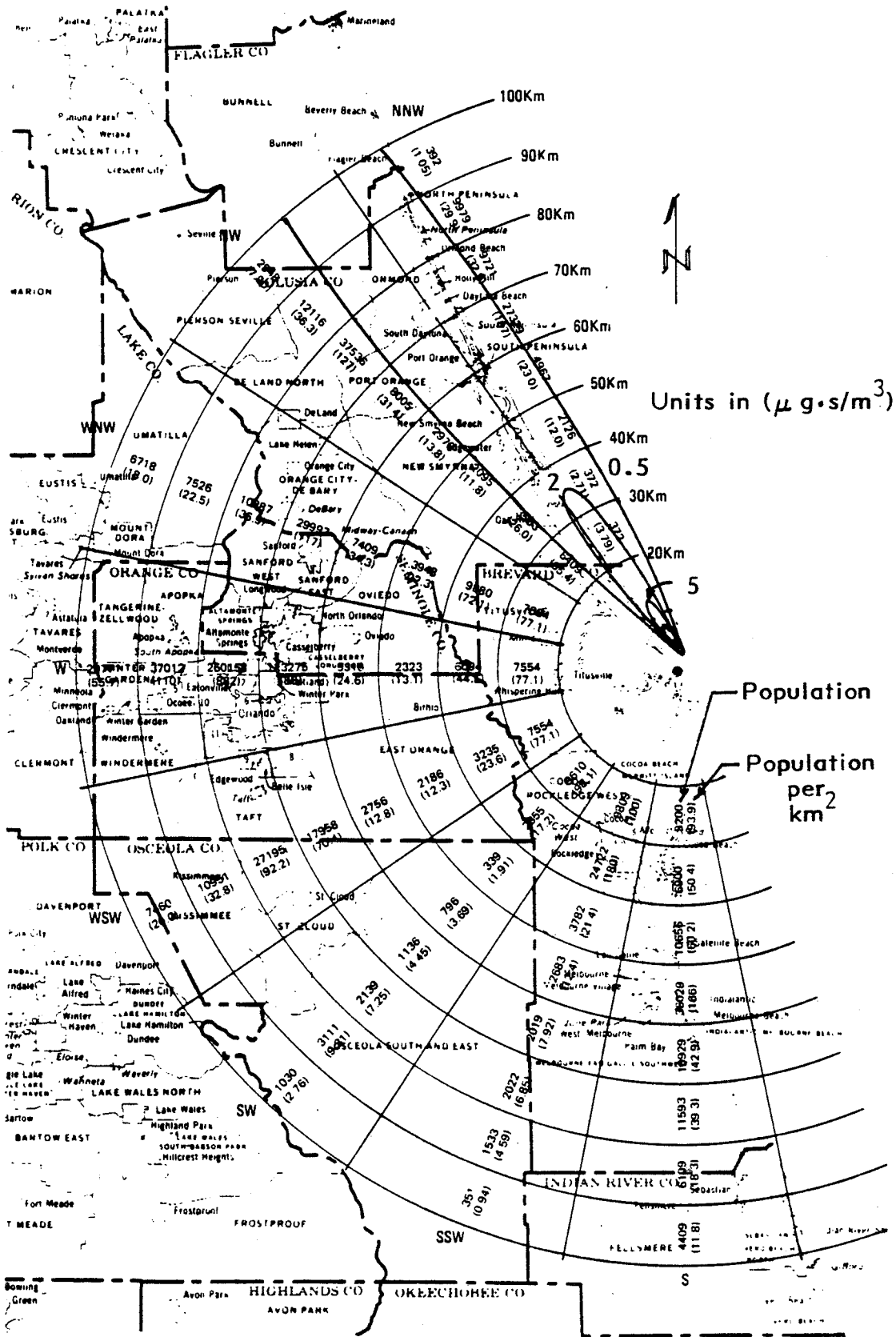


FIGURE 6-3. ISOPLETHS FOR ASSUMED 55-KG RELEASE OF WASTE PAYLOAD DURING SEA BREEZE METEOROLOGICAL CONDITION

### 6.1.1.2 DACRIN Model and Dose Factors

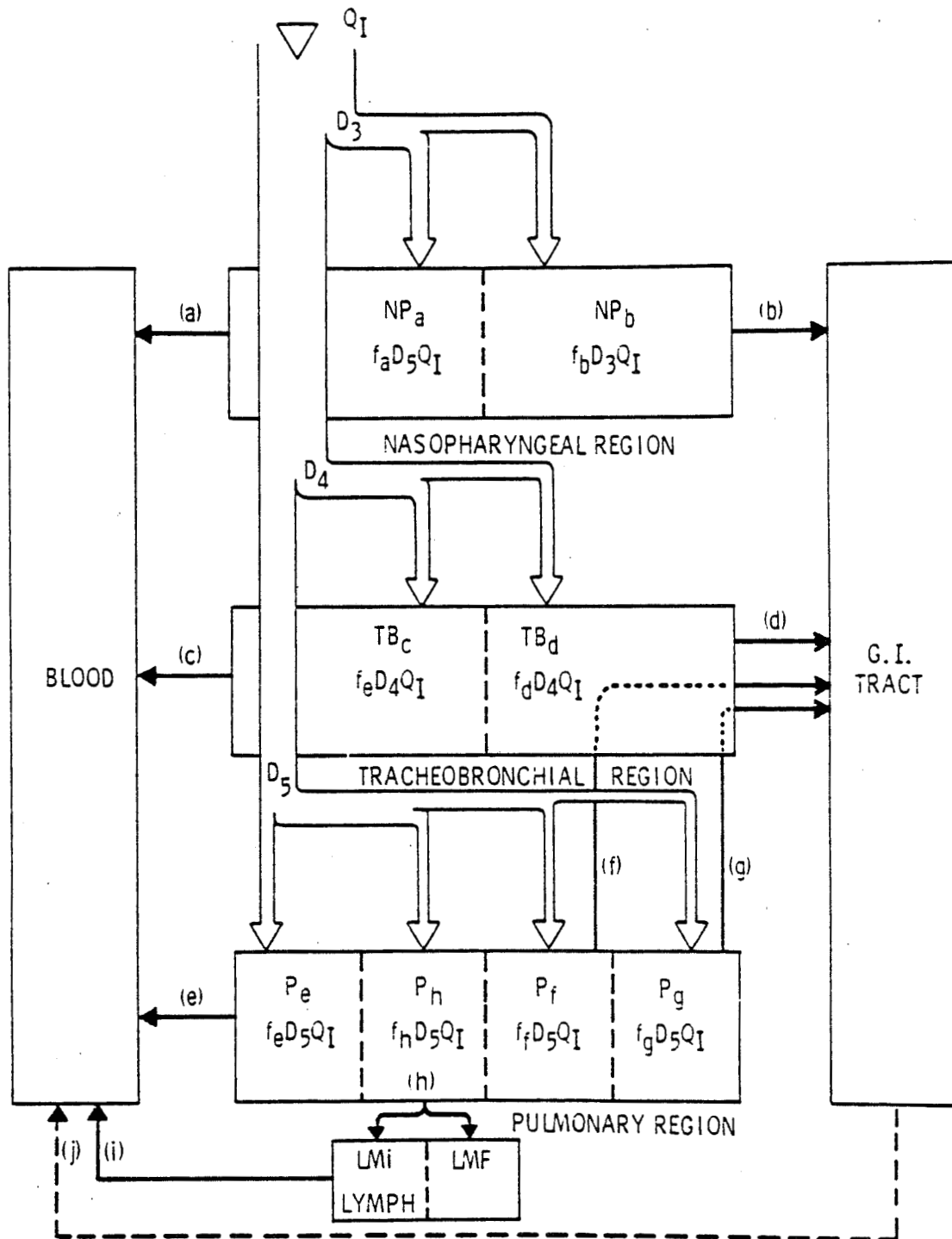
The DACRIN computer program<sup>(6-3)</sup>, permits rapid and consistent estimates of the effective radiation dose to the human respiratory tract and other organs resulting from the inhalation of radioactive aerosols. The program is an outgrowth of the development of a mathematical model for the organ dose following the basic precepts of the ICRP Task Group on Lung Dynamics<sup>(6-8)</sup> and a simple exponential model for retention by an organ of interest.

The program calculates the effective radiation dose to any of 23 organs and tissues from inhalation of any one or combination of radionuclides considered by the ICRP (see Table 6-3). A maximum of 10 organs can be selected for any one case (run). In addition, up to five multiple intake intervals and 10 time intervals measured from the last intake, may be selected for each case. Organ doses from inhalation are calculated by specifying the quantity of a radionuclide inhaled.

TABLE 6-3. DACRIN ORGAN LIST

<u>Organs Included in DACRIN</u>		
Total Body	Adrenals	Pancreas
Body Water	Testes	Heart
Kidneys	Ovaries	G.I. Tract
Liver	Skin	Stomach
Spleen	Brain	Small Intestine
Bone	Muscle	Upper Large Intestine
Fat	Prostrate	Lower Large Intestine
Lungs	Thyroid	

The model of the respiratory tract adopted by the Task Group on Lung Dynamics forms the general basis for the mathematical models developed to calculate the dose from the inhalation of radionuclides.<sup>(6-8)</sup> In this model, the respiratory tract is divided into three regions, the nasopharyngeal (NP), the tracheobronchial (TB), and the pulmonary (P). The schematic representation of the respiratory tract used in the development of the mathematical model for the deposition and clearance of inhaled radionuclides is shown in Figure 6-4. Deposition into each region is assumed to vary with the aerodynamic properties of the aerosol distribution and is described by the three parameters  $D_3$ ,  $D_4$ , and



Source: Reference 6-3.

FIGURE 6-4. SCHEMATIC DIAGRAM OF THE TASK GROUP LUNG MODEL

$D_5$  (see Figure 6-4). These parameters represent the fraction of the inhaled material,  $Q_1$ , initially deposited in the NP, TB, and P regions, respectively. Each of the three regions of deposition is further subdivided into two or more subcompartments. Each subcompartment represents the fraction of material initially in a compartment that is subject to a particular clearance process. This fraction is represented by  $f_k$ , where  $k$  indicates the clearance pathway. The quantity of material in the TB region, for example, cleared by process (c) is then represented by the product  $f_c D_4 Q_1$ . Values of the ( $f_k$ ) and the clearance half-times for each clearance process for the three solubility classes of aerosols used in the code are those suggested by the ICRP<sup>(6-9)</sup> (see Appendix G, Tables G-2 and G-3). Values of the deposition fractions  $D_3$ ,  $D_4$ , and  $D_5$  as a function of activity median aerodynamic diameter (AMAD) as used in DACRIN are shown in Table 6-4.

For other details concerning the DACRIN model, the reader is referred to References 6-3 and 6-9.

TABLE 6-4. FRACTION OF INHALED PARTICLES DEPOSITED IN THE RESPIRATORY SYSTEM VS PARTICLE DIAMETER, AS EMPLOYED BY DACRIN

Particle Size, AMAD micrometers	Fraction of Inhaled Quantity Retained		
	Nasopharyngeal Region, $D_3$	Tracheobronchial Region, $D_4$	Pulmonary Region, $D_5$
0.2	0.031	0.08	0.414
0.6	0.165	0.08	0.286
1.0	0.288	0.08	0.234
2.0	0.500	0.08	0.173
3.0	0.628	0.08	0.142
5.0	0.770	0.08	0.109

Source: DACRIN Model.

Dose factors (rem/  $\mu\text{g}$ ) for the Savannah River and Hanford waste payloads as a function of time after the initial dose and activity median aerodynamic diameter (AMAD) were calculated using DACRIN. Data in Tables 3-5 and 3-6 were converted to values of  $C_i$  for a given radionuclide per  $\mu\text{g}$  of waste. Table G-3 was used to determine the solubility class for each oxide. Also, a 10-minute uptake time was assumed. These data provided the input to the DACRIN code. The dose commitment factors in rem/  $\mu\text{g}$  waste have been

calculated for three AMAD values (0.2, 1.0 and 5  $\mu\text{m}$ ), two mixes (Hanford and Savannah River), and various organs. These data are presented in Tables 6-5 through 6-10. The bottom line in these tables represents 70-year dose commitment factors used to calculate the population doses as discussed in the next section.

### 6.1.2 Results

Individual and population dose commitments due to an accidental release of radioactive material from a waste payload during an on- or near-pad catastrophic Space Shuttle failure are presented below. Dosage data developed are based upon 1% releases (55 kg of defense waste) and upon results previously developed in Section 6.1.1. Dose and risk data for other release scenarios (either higher or lower than the assumed 1% release) may be obtained by multiplying the dose and risk data by the appropriate ratio.

Dose commitments to individuals as a result of releases of Hanford and Savannah River wastes are shown in Figures 6-5 and 6-6 as a function of years after release. Doses to total body, bone, lung, liver and kidney are presented for activity median aerodynamic diameter (AMAD) particles of 1  $\mu\text{m}$  and the Spring meteorological case. These data are for an individual 20 km downwind, at a location such that he inhales air containing the highest concentration of radionuclides that have dispersed to the ground level. In general, Figures 6-5 and 6-6 indicate that the Savannah River waste presents the highest hazard of the two mixes. The 70-year lung dose commitment is a factor of 100 greater than for Hanford. However, the 70-year bone dose commitment is only a factor of 4 greater than that of Hanford. It can be seen from Figures 6-5 and 6-6 that the lung dose is delivered during the first 5 years following accidental release, whereas doses to other organs continue to rise as the radionuclides are transported through the body. The highest lifetime dose commitment shown is 300 millirem for the lung (see Figure 6-5).

The relationships among particle sizes, meteorological cases and doses as they occur in the total body, lung and bone are shown in Figures 6-7, 6-8 and 6-9. Variations in assumed particle sizes have more of an effect on lung doses than any other organ. The lung doses increase with decreasing particle size and doses to other organs decrease with decreasing particle size. Doses



TABLE 6-5. DOSE COMMITMENT FACTORS (rem/  $\mu\text{g}$  WASTE) FOR HANFORD WASTE, WITH AMAD VALUE OF 0.2  $\mu\text{m}$

Dose Time (Years)	Total Body	Kidneys	Liver	Bone	Lungs
1	5.64 E-03	1.02 E-03	2.79 E-03	1.91 E-02	1.23 E-01
5	2.47 E-02	2.60 E-03	6.87 E-03	9.52 E-02	1.85 E-01
10	4.46 E-02	6.16 E-03	1.56 E-02	1.80 E-01	1.94 E-01
20	7.40 E-02	1.42 E-02	3.44 E-02	3.15 E-01	1.94 E-01
30	9.33 E-02	2.18 E-02	5.08 E-02	4.13 E-01	1.94 E-01
40	1.06 E-01	2.86 E-02	6.44 E-02	4.85 E-01	1.94 E-01
50	1.15 E-01	3.48 E-02	7.58 E-02	5.39 E-01	1.94 E-01
60	1.21 E-01	4.04 E-02	8.52 E-02	5.80 E-01	1.94 E-01
70	1.25 E-01	4.55 E-02	9.31 E-02	6.11 E-01	1.94 E-01

TABLE 6-6. DOSE COMMITMENT FACTORS (rem/  $\mu\text{g}$  WASTE) FOR HANFORD WASTE, WITH AMAD VALUE OF 1.0  $\mu\text{m}$

Dose Time (Years)	Total Body	Kidneys	Liver	Bone	Lungs
1	6.40 E-03	1.16 E-03	3.18 E-03	2.17 E-02	6.97 E-02
5	2.66 E-02	2.20 E-03	5.95 E-03	1.10 E-01	1.05 E-01
10	4.75 E-02	4.39 E-03	1.13 E-02	1.87 E-01	1.10 E-01
20	7.81 E-02	9.29 E-03	2.27 E-02	3.21 E-01	1.10 E-01
30	9.82 E-02	1.39 E-02	3.26 E-02	4.16 E-01	1.10 E-01
40	1.11 E-01	1.80 E-02	4.08 E-02	4.84 E-01	1.10 E-01
50	1.20 E-01	2.17 E-02	4.76 E-02	5.33 E-01	1.10 E-01
60	1.26 E-01	2.51 E-02	5.33 E-02	5.69 E-01	1.10 E-01
70	1.30 E-01	2.82 E-02	5.81 E-02	5.96 E-01	1.10 E-01

TABLE 6-7. DOSE COMMITMENT FACTORS (rem/  $\mu\text{g}$  WASTE) FOR HANFORD WASTE, WITH AMAD VALUE OF 5.0  $\mu\text{m}$

Dose Time (Years)	Total Body	Kidneys	Liver	Bone	Lungs
1	9.93 E-03	1.84 E-03	5.04 E-03	3.35 E-02	3.28 E-02
5	3.95 E-02	2.66 E-03	7.35 E-03	1.48 E-01	4.93 E-02
10	7.00 E-02	4.07 E-03	1.08 E-02	2.70 E-01	5.16 E-02
20	1.14 E-01	7.06 E-03	1.77 E-02	4.56 E-01	5.18 E-02
30	1.43 E-01	9.83 E-03	2.36 E-02	5.85 E-01	5.18 E-02
40	1.62 E-01	1.23 E-02	2.85 E-02	6.75 E-01	5.18 E-02
50	1.74 E-01	1.46 E-02	3.27 E-02	7.38 E-01	5.18 E-02
60	1.82 E-01	1.66 E-02	3.61 E-02	7.83 E-01	5.18 E-02
70	1.87 E-01	1.85 E-02	3.89 E-02	8.15 E-01	5.18 E-02

**TABLE 6-8. DOSE COMMITMENT FACTORS (rem/  $\mu\text{g}$  WASTE) FOR SAVANNAH RIVER WASTE, WITH AMAD VALUE OF 0.2  $\mu\text{m}$**

Dose Time (Years)	Total Body	Kidneys	Liver	Bone	Lungs
1	4.17 E-02	7.59 E-02	8.56 E-02	2.23 E-01	1.73 E+01
5	9.90 E-02	1.29 E-01	1.80 E-01	6.19 E-01	2.23 E+01
10	1.50 E-01	1.46 E-01	2.37 E-01	8.83 E-01	2.24 E+01
20	2.25 E-01	1.80 E-01	3.51 E-01	1.31 E+00	2.24 E+01
30	2.76 E-01	2.10 E-01	4.43 E-01	1.63 E+00	2.24 E+01
40	3.10 E-01	2.36 E-01	5.15 E-01	1.87 E+00	2.24 E+01
50	3.34 E-01	2.58 E-01	5.71 E-01	2.06 E+00	2.24 E+01
60	3.50 E-01	2.76 E-01	6.15 E-01	2.20 E+00	2.24 E+01
70	3.62 E-01	2.93 E-01	6.49 E-01	2.32 E+00	2.24 E+01

**TABLE 6-9. DOSE COMMITMENT FACTORS (rem/  $\mu\text{g}$  WASTE) FOR SAVANNAH RIVER WASTE, WITH AMAD VALUE OF 1.0  $\mu\text{m}$**

Dose Time (Years)	Total Body	Kidneys	Liver	Bone	Lungs
1	4.64 E-02	8.26 E-02	9.27 E-02	2.50 E-01	9.80 E+00
5	1.03 E-01	1.18 E-01	1.54 E-01	5.87 E-01	1.26 E+01
10	1.55 E-01	1.28 E-01	1.89 E-01	8.32 E-01	1.27 E+01
20	2.32 E-01	1.49 E-01	2.57 E-01	1.22 E+00	1.27 E+01
30	2.83 E-01	1.67 E-01	3.13 E-01	1.50 E+00	1.27 E+01
40	3.17 E-01	1.83 E-01	3.57 E-01	1.70 E+00	1.27 E+01
50	3.40 E-01	1.96 E-01	3.90 E-01	1.86 E+00	1.27 E+01
60	3.55 E-01	2.07 E-01	4.17 E-01	1.97 E+00	1.27 E+01
70	3.66 E-01	2.17 E-01	4.37 E-01	2.06 E+00	1.27 E+01

**TABLE 6-10. DOSE COMMITMENT FACTORS (rem/  $\mu\text{g}$  WASTE) FOR SAVANNAH RIVER WASTE, WITH AMAD VALUE OF 5.0  $\mu\text{m}$**

Dose Time (Years)	Total Body	Kidneys	Liver	Bone	Lungs
1	6.83 E-02	1.19 E-01	1.37 E-01	3.77 E-01	4.57 E+00
5	1.46 E-01	1.47 E-01	1.82 E-01	7.79 E-01	5.88 E+00
10	2.21 E-01	1.53 E-01	2.04 E-01	1.10 E+00	5.90 E+00
20	3.31 E-01	1.66 E-01	2.46 E-01	1.59 E+00	5.90 E+00
30	4.02 E-01	1.77 E-01	2.79 E-01	1.93 E+00	5.90 E+00
40	4.49 E-01	1.86 E-01	3.05 E-01	2.17 E+00	5.90 E+00
50	4.80 E-01	1.94 E-01	3.25 E-01	2.35 E+00	5.90 E+00
60	5.00 E-01	2.01 E-01	3.41 E-01	2.47 E+00	5.90 E+00
70	5.13 E-01	2.07 E-01	3.54 E-01	2.56 E+00	5.90 E+00

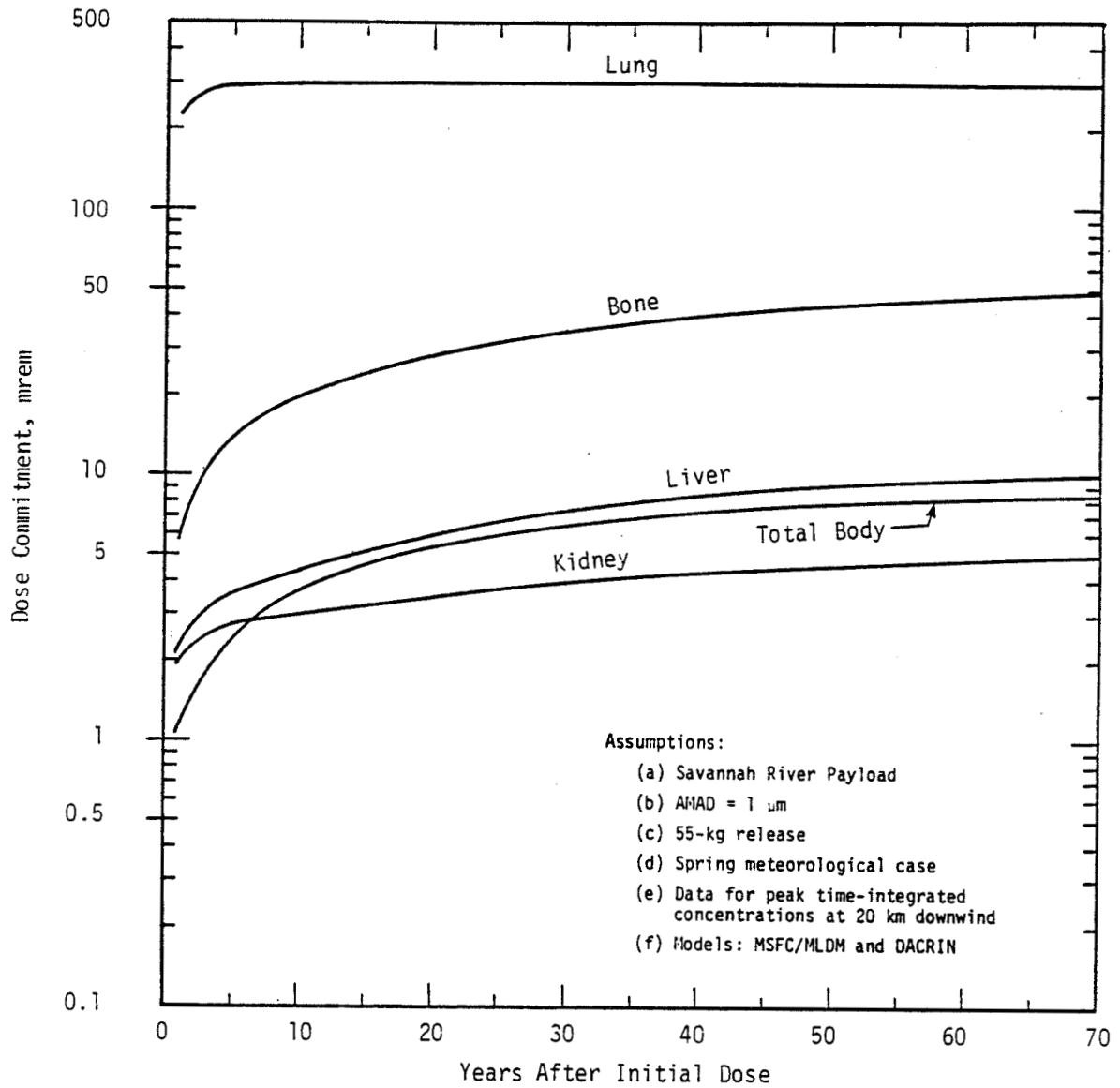


FIGURE 6-5. INDIVIDUAL DOSE COMMITMENTS FOR RELEASE OF SAVANNAH RIVER RADIOACTIVE WASTE AS A RESULT OF ON- OR NEAR-PAD SPACE SHUTTLE CATASTROPHIC ACCIDENT

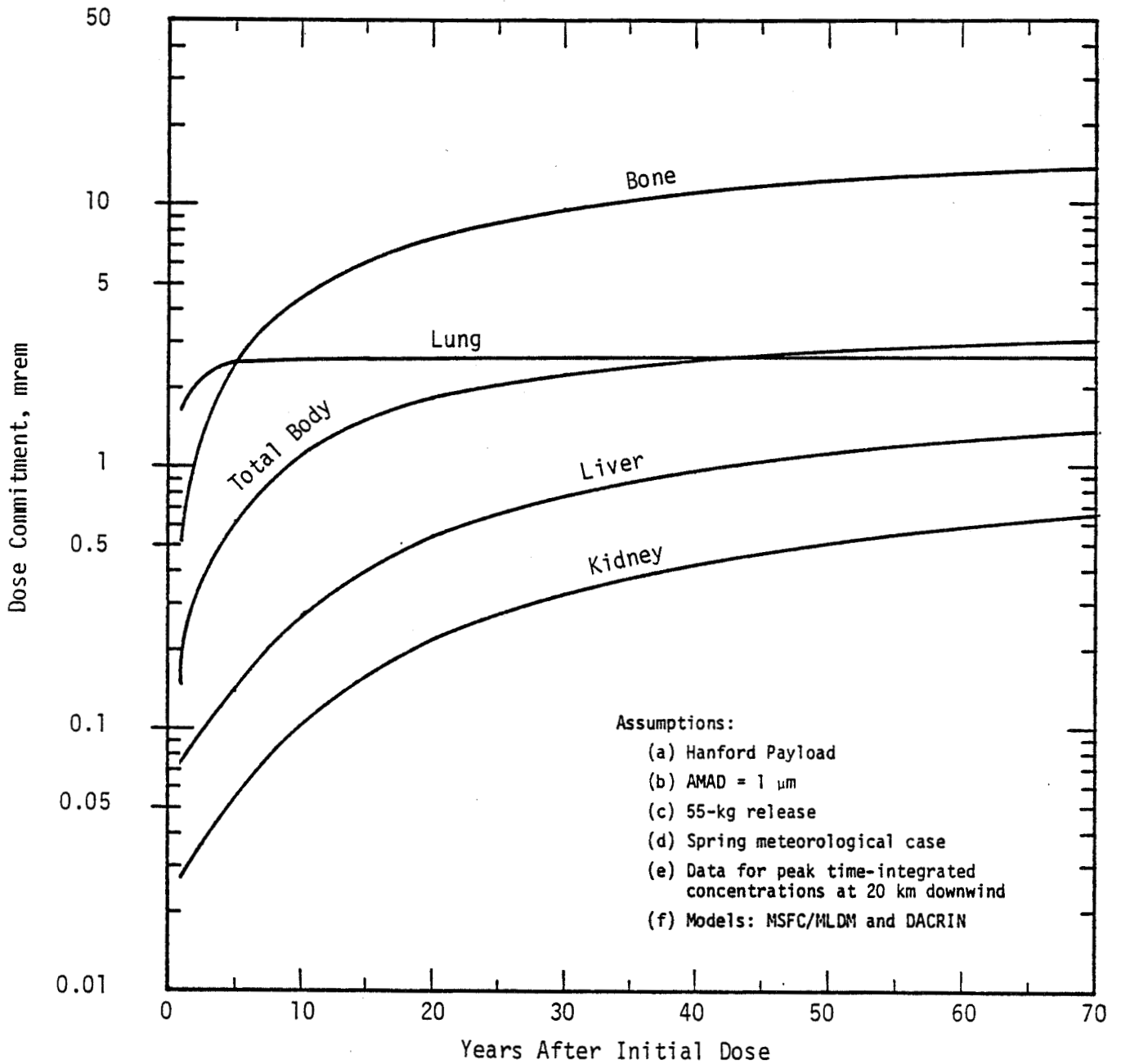


FIGURE 6-6. INDIVIDUAL DOSE COMMITMENTS FOR RELEASE OF HANFORD RADIOACTIVE WASTE AS A RESULT OF ON-OR NEAR-PAD SPACE SHUTTLE CATASTROPHIC ACCIDENT

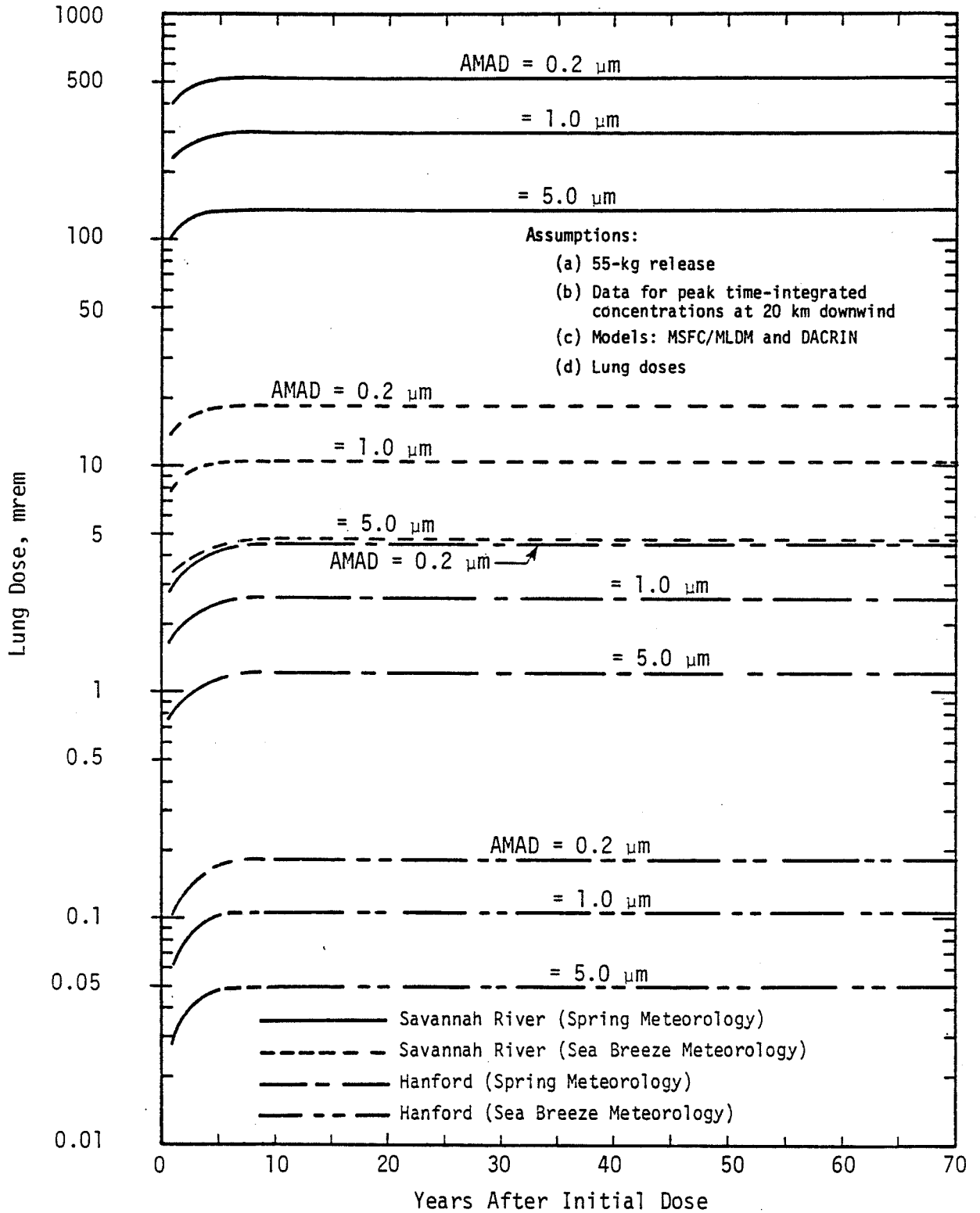


FIGURE 6-7. INDIVIDUAL LUNG DOSE COMMITMENTS FOR RELEASE OF RADIOACTIVE WASTE RESULTING FROM ON- OR NEAR-PAD SPACE SHUTTLE CATASTROPHIC ACCIDENT AS A FUNCTION OF AMAD, WASTE MIX, AND METEOROLOGICAL CASE

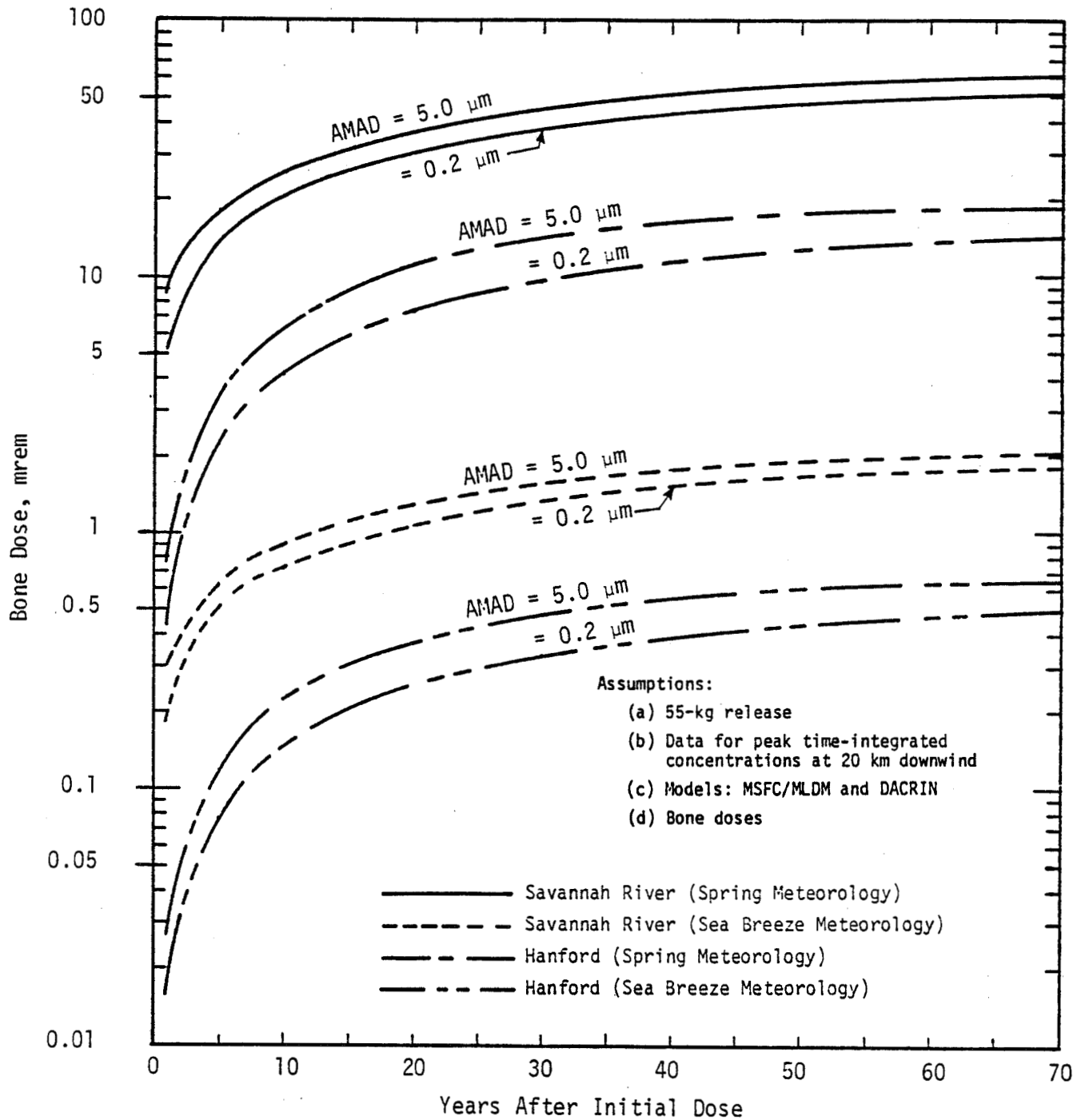


FIGURE 6-8. INDIVIDUAL BONE DOSE COMMITMENTS FOR RELEASE OF RADIOACTIVE WASTE RESULTING FROM ON- OR NEAR-PAD SPACE SHUTTLE CATASTROPHIC ACCIDENT AS A FUNCTION OF AMAD, WASTE MIX, AND METEOROLOGICAL CASE

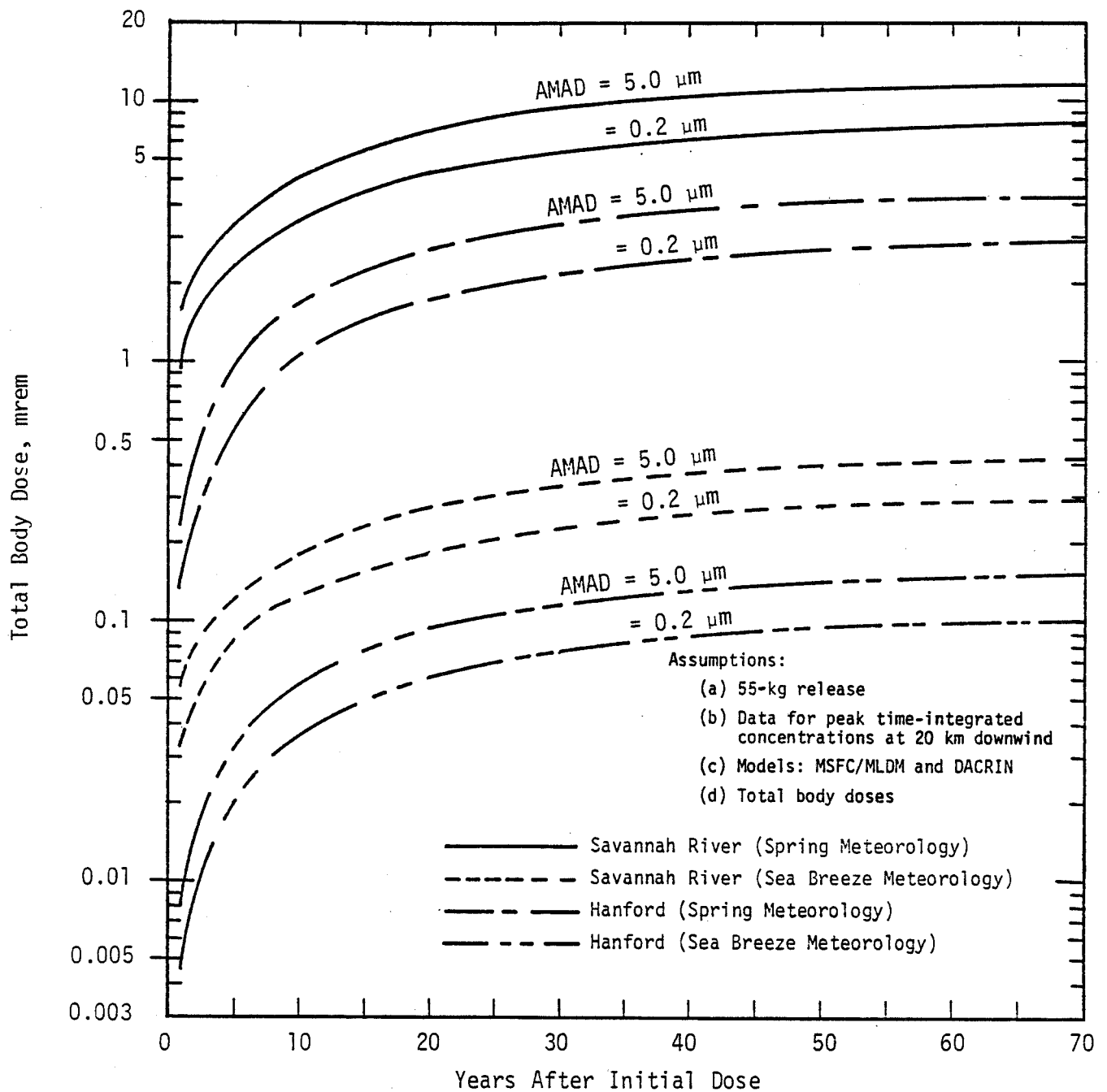


FIGURE 6-9. INDIVIDUAL TOTAL BODY DOSE COMMITMENTS FOR RELEASE OF RADIOACTIVE WASTE RESULTING FROM ON- OR NEAR-PAD SPACE SHUTTLE CATASTROPHIC ACCIDENT AS A FUNCTION OF AMAD, WASTE MIX, AND METEOROLOGICAL CASE

obviously could be reduced by choosing a waste form that would not allow the formation of small respirable particles. Doses also could be significantly reduced by employing launch constraints dealing with meteorological conditions (see differences between Sea Breeze and Spring cases). The most important parameter would be wind direction. For example, if wind is from the west, radioactive fallout from an on-pad accident would be transported out over the Atlantic, avoiding an acute exposure to local populations.

Population doses were calculated from isopleth data for time-integrated concentrations and population data (see Section 6.1.1 and Appendix F for details). The range was limited to 100 km because of the following three reasons: (1) the MSFC/MLDM, when used beyond 100 km, would create considerable uncertainty, (2) population data were available only out to 100 km, and (3) isopleth data (see Figures 6-1, 6-2 and 6-3) indicate that most of the acute dose would be expected inside the 100-km distance. Calculation of the population dose at distances greater than 100 km should be considered in future studies. However, the analysis provided below is believed to provide reasonable results.

Table 6-11 provides the 70-year population dose commitments in man-rems, calculated for Hanford and Savannah River wastes, for organs and tissues such as total body, kidneys, liver, bone and lung for three meteorological conditions, and for three particle sizes.



TABLE 6-11. POPULATION DOSE COMMITMENTS (70-YEAR) FOR DIFFERENT CONDITIONS AS A RESULT OF A 55-KG RELEASE (1%) OF WASTE PAYLOAD, DURING ON-PAD SPACE SHUTTLE ACCIDENT

Condition/ Waste	AMAD Value ( $\mu\text{m}$ )	Lung	Bone	Total Body man-rems	Kidneys	Liver
<u>Spring Meteorology Case</u>						
Savannah River	0.2	23,000	2,400	370	300	660
	1.0	13,000	2,100	370	220	440
	5.0	6,000	2,600	520	210	360
Hanford	0.2	200	620	130	46	95
	1.0	110	610	130	29	59
	5.0	53	830	190	19	40
<u>Fall Meteorology Case</u>						
Savannah River	0.2	20,000	2,100	330	270	590
	1.0	12,000	1,900	330	200	400
	5.0	5,400	2,300	470	190	320
Hanford	0.2	180	560	110	42	85
	1.0	100	550	120	26	53
	5.0	47	750	170	17	36
<u>Sea Breeze Meteorology Case</u>						
Savannah River	0.2	260	27	4.2	3.4	7.6
	1.0	150	24	4.3	2.5	5.1
	5.0	69	30	6.0	2.4	4.1
Hanford	0.2	2.3	7.2	1.5	0.53	1.1
	1.0	1.3	7.0	1.5	0.33	0.68
	5.0	0.61	9.5	2.2	0.22	0.46

To determine the level of risk for the above scenarios, linear, non-threshold, health effects risk factors developed in Table G.3 of the Draft Environmental Impact Statement for Management of Commercially Generated Radioactive Waste<sup>(6-6)</sup> were employed. Table 6-12 provides these data.

TABLE 6-12. HEALTH EFFECTS RISK FACTORS

<u>Type of Risk</u>	<u>Predicted Incidence per 10<sup>6</sup> Man-Rem</u>
Cancer deaths from:	
Total body exposure	50
Lung exposure	5
Bone exposure	2
Thyroid exposure	3
Specific genetic effects to all generations from:	
Total body exposure	50

Source: Reference 6-6.

The range of health effects for a given organ or tissue (Savannah River highest) were then determined from the population doses listed in Table 6-11. Combined with the health risk factors of Table 6-12, these data were used to determine ranges of health effects for different release percentages, meteorological conditions and waste mix, as shown below in Table 6-13.

TABLE 6-13. RANGES OF EXPECTED HEALTH EFFECTS FOR ON-PAD SHUTTLE FAILURE WITH RELEASE OF DEFENSE NUCLEAR WASTE MATERIAL

<u>Type of Risk</u>	<u>Ranges of Expected Health Effects*</u>		
	<u>Percent Release</u>		
	1	10	100
Cancer deaths from:			
Total body exposure	0-1	0-1	0-3
Lung exposure	0-1	0-2	0-12
Bone exposure	0-1	0-1	0-1
Specific genetic effects to all generations from:			
Total body exposure	0-1	0-1	0-3

\*NOTE: Data have been rounded off to nearest whole number; for accurate values, multiply appropriate data in Tables 6-11 and 6-12.

The on-pad Space Shuttle failure and postulated release of 55-kg of respirable-sized particles of defense nuclear waste, dispersed by a slow burn of the Space Shuttle SRB propellant, would be expected to result in less than one eventual cancer death and less than one eventual genetic defect to individuals outside of the launch site area based on the assumptions and analysis herein. For the worst case release assumption (this would not be a credible accident), it could be assumed that 100 percent of the waste payload would be released. This implies that cancer deaths that would result would be  $\sim 3$  from whole body exposure,  $\sim 12$  from lung exposure and  $\sim 1$  from bone exposure. Less than 3 genetic defects would be expected.

### 6.1.3 Conclusions

The analysis performed to date regarding the on-pad Space Shuttle catastrophic accident indicates that large credible-type releases, such as 1%, do not pose a significant health risk to the general public. However, more research is required to calculate population doses outside of the immediate 100 km radius. The effects of resuspension and ingestion also need to be determined. Studies evaluating resuspension and ingestion would allow an assessment of whether the populations in certain areas would have to be relocated. More work is required to assess the impact to the immediate KSC area and its workers. The use of launch constraints coupled with highly reliable container systems, and use of a non-dispersable waste form would greatly enhance safety. Also, a more realistic definition of the Savannah River waste for space disposal may alter, to some degree, the results shown here (see Section 3.2.2.2 and Table 3-6). Specific conclusions are as follows:

- The Savannah River waste, as defined for space disposal, is considerably more hazardous than that from Hanford
- The smaller the particle size (within the 0.2-5.0  $\mu\text{m}$  range), the higher the dose to the respiratory system
- The larger the particle size (within the 0.2-5.0  $\mu\text{m}$  range), the higher the dose to other organs
- Meteorological conditions have a profound effect on predicted exposures

- The maximum number of health effects expected from a 1% release under the various conditions presented here is less than 1
- Launch constraints concerning wind direction should be employed during waste payload launches.

## 6.2 Reentry and Burnup of Defense Nuclear Waste Payload

Reentry and burnup of a nuclear waste payload in the upper atmosphere would result in the worldwide distribution of small radioactive particles. The purpose of this section is to provide an assessment of the impact of such an accident on world health. The assessment is based on a model designed to provide estimates of world population doses due to inhalation of radioactive particles injected into the upper atmosphere by the reentry and burnup of a defense nuclear waste payload. The principal assumptions, upon which the world population dose model is based, are summarized as follows:

- Reentry and burnup of a defense nuclear waste payload takes place in the upper atmosphere at altitudes greater than 21 km (HASL model requirement).
- For the purpose of the calculation, the entire nuclear waste payload (100% of the radioactive waste) was assumed to be converted to radioactive particles less than 10  $\mu\text{m}$  diameter (see Section 3.4.3.2 for discussion of reentry analysis). However, health effects results are presented parametrically for 1, 10 and 100% releases.
- The contribution of particles greater than 10  $\mu\text{m}$  to inhalation dose is assumed to be negligible.
- The activity median aerodynamic diameters (AMAD) for the radioactive particles were chosen as 0.2, 1.0, or 5.0  $\mu\text{m}$ .
- Isotopic compositions employed for the Savannah River and Hanford defense wastes are those shown in Tables 3-5 and 3-6 (see Section 3.2.2).
- The latitudinal distribution of particles moving from the upper atmosphere to the Earth's surface is a function of the injection latitude (i.e., the latitude at which reentry and burnup occurs), as given by Reference 6-5.
- The general kinetics of small particle transfer from the upper atmosphere to the Earth's surface are adequately described by the HASL model of atmospheric transport (References 6-10 and 6-11), ignoring the interhemispheric exchange rate.
- Inhalation of radioactive particles descending into surface air will account for the principal component of world population dose due

to a reentry and burnup accident. External dose due to submersion in contaminated air and to radiation from particles deposited on environmental surfaces was ignored. The internal doses due to inhalation of resuspended particles and ingestion of contaminated food and water were also ignored.

- The model proposed by the ICRP Task Group on Lung Dynamics<sup>(6-8)</sup> as modified by ICRP Publication 19,<sup>(6-12)</sup> provides the best available basis for estimating internal radiation doses to human organs and tissues due to the inhalation of radioactive dust particles.

Because it is assumed that the entire defense nuclear waste payload is converted to small, radioactive particles, the model will provide worst case estimates of world population doses. The world population dose estimates given for Savannah River and Hanford wastes may be reduced if only a fraction of the waste payload is converted into small radioactive particles and if only a fraction of the particles are less than 10  $\mu\text{m}$  in diameter. If, for example, only 20% of the payload were converted to small particles and 50% of these particles were converted to particles less than 10  $\mu\text{m}$  in diameter, the health risk data given in this section should be multiplied by  $0.2 \times 0.5 = 0.1$ . This would reduce each value by an order of magnitude.

If we assume that accurate adjustments could be made for partial burnup and that the particle size could be established, the adjusted predictions for world population doses might actually be lower than the real case. This would be due to the dose contributions from exposure pathways ignored by the model. It is believed that the total lifetime dose for all exposure pathways that have been ignored could be as much as 20% higher than the dose due only to direct inhalation of fallout particles. For the case of 20% burnup with 50% of the radioactivity in particles  $< 10 \mu\text{m}$ , the recommended adjustment factor would then be  $0.2 \times 0.5 \times 1.2 \times W_n$ , where  $W_n$  is a world population dose estimate given in this section in terms of man-rem to a given organ, n.

### 6.2.1 Model Description

The world population dose to organ n,  $W_n$ , from the injection of radionuclide mixture X, into the upper atmosphere of latitude band i, is given by

$$W_n = \left( \sum_{r=1}^{r=x} D_{nrk} A_{ir} \right) \left( \sum_{k=1}^{k=20} f_{ik} P_k \right) \quad (1)$$

where:

$W_n$  is the world population dose (man-rems) to organ n, due to the injection of radionuclide mixture X into the upper atmosphere (> 21 km) of latitude band i;

x is the total number of radionuclides in mixture X;

$D_{nrk}$  is the lifetime (70-year) radiation dose (rem) to organ n of an individual member of the population ( $P_k$ ) of equal-area latitude band k per  $\mu\text{Ci}$  of radionuclide r falling in band k, based on inhalation of radioactive particles passing through surface air (the model used to calculate these dose factors is described in Appendix G);

$A_{ir}$  is the amount ( $\mu\text{Ci}$ ) of radionuclide r initially injected in latitude band i (see Tables 3-4 and 3-5 for compositions);

$f_{ik}$  is the fraction of radioactive material (particles  $\leq 4 \mu\text{m}$ ) injected in latitude band i, which falls in equal area latitude band k (see Table 6-14);

and

$P_k$  is the population (number of people) of band k (see Table 6-8).

The parameter values for substitution in Equation (1) are listed in Tables 3-5, 3-6, and 6-14 through 6-18. The results,  $W_n$ , are given in Tables 6-19 and 6-20 for: two postulated radionuclide mixtures (Savannah River and Hanford), seven different injection latitude bands (see Table 6-14), 9 organs, and the total body.

The  $A_{ir}$  values are taken from Tables 3-5 and 3-6 which list the amounts of radionuclides contained in each of the two types of postulated waste payloads. Note that the units of  $A_{ir}$  are in micro-Curies ( $\mu\text{Ci}$ ).

The  $f_{ik}$  values given in Table 6-14 were calculated according to the LOPAR subroutine of the RISK II computer program which is described in

TABLE 6-14. FRACTION  $f_{ik}$  OF SOURCE (A.) INJECTED IN LATITUDE BANK  $i$  WHICH FALLS IN EQUAL AREA LATITUDE BAND  $k$  AND TOTAL POPULATION ( $P_k$ ) OF BAND  $k$

Equal Area Latitude Band k	Lat.*	Injection Latitude Band										$P_k$ Total Population	
		i Lat.	1 85-90°N	2 75-85°N	3 65-75°N	4 55-65°N	5 45-55°N	6 35-45°N	7 25-35°N	8 15-25°N	9 5-15°N		10 5°N-5°S
1	64-90°N		0.0727	0.0727	0.0725	0.0718	0.0700	0.0672	0.0636	0.0588	0.0524	0.0437	30,469,587
2	54-64°N		0.1478	0.1477	0.1473	0.1450	0.1398	0.1317	0.1208	0.1064	0.0876	0.0622	161,300,755
3	44-54°N		0.1787	0.1787	0.1782	0.1753	0.1687	0.1584	0.1445	0.1263	0.1024	0.0703	432,222,025
4	36-44°N		0.1745	0.1745	0.1741	0.1712	0.1648	0.1548	0.1413	0.1236	0.1004	0.0691	543,074,832
5	30-36°N		0.1606	0.1606	0.1602	0.1576	0.1518	0.1428	0.1305	0.1145	0.0935	0.0652	691,722,558
6	24-30°N		0.1109	0.1109	0.1107	0.1091	0.1055	0.1001	0.0927	0.0830	0.0703	0.0532	605,118,210
7	17-24°N		0.0823	0.0823	0.0822	0.0812	0.0789	0.0754	0.0707	0.0644	0.0563	0.0453	387,278,363
8	11-17°N		0.0474	0.0474	0.0474	0.0471	0.0464	0.0454	0.0439	0.0421	0.0397	0.0363	199,943,660
9	6-11°N		0.0178	0.0178	0.0179	0.0182	0.0188	0.0199	0.0213	0.0231	0.0255	0.0288	203,931,205
10	0-6°N		0.0074	0.0074	0.0075	0.0080	0.0091	0.0108	0.0133	0.0164	0.0205	0.0260	78,887,239
11	0-6°S		0.0000	0.0000	0.0001	0.0008	0.0024	0.0049	0.0082	0.0126	0.0183	0.0260	69,355,336
12	6-11°S		0.0000	0.0000	0.0000	0.0009	0.0027	0.0060	0.0091	0.0139	0.0202	0.0288	132,699,175
13	11-17°S		0.0000	0.0000	0.0002	0.0011	0.0034	0.0068	0.0115	0.0176	0.0256	0.0363	43,233,315
14	17-24°S		0.0000	0.0000	0.0002	0.0014	0.0042	0.0085	0.0143	0.0219	0.0319	0.0453	58,286,844
15	24-30°S		0.0000	0.0000	0.0002	0.0017	0.0049	0.0100	0.0168	0.0257	0.0374	0.0532	44,606,711
16	30-36°S		0.0000	0.0000	0.0003	0.0021	0.0060	0.0122	0.0205	0.0315	0.0458	0.0652	37,873,258
17	36-44°S		0.0000	0.0000	0.0003	0.0022	0.0064	0.0129	0.0218	0.0333	0.0486	0.0691	7,566,457
18	44-54°S		0.0000	0.0000	0.0003	0.0022	0.0065	0.0131	0.0221	0.0339	0.0494	0.0703	828,162
19	54-64°S		0.0000	0.0000	0.0003	0.0019	0.0058	0.0116	0.0196	0.0300	0.0437	0.0622	56,392
20	64-90°S		0.0000	0.0000	0.0000	0.0013	0.0041	0.0082	0.0138	0.0211	0.0307	0.0437	449

Equal Area Latitude Band k	Lat.*	Injection Latitude Band										$P_k$ Total Population	
		i Lat.	11 5-15°S	12 15-25°S	13 25-35°S	14 35-45°S	15 45-55°S	16 55-65°S	17 65-75°S	18 75-85°S	19 85-90°S		
1	64-90°N		0.0307	0.0211	0.0138	0.0082	0.0041	0.0013	0.0000	0.0000	0.0000	0.0000	30,469,587
2	54-64°N		0.0437	0.0300	0.0196	0.0116	0.0058	0.0019	0.0003	0.0000	0.0000	0.0000	161,300,755
3	44-54°N		0.0494	0.0339	0.0221	0.0131	0.0065	0.0022	0.0003	0.0000	0.0000	0.0000	432,222,025
4	36-44°N		0.0486	0.0333	0.0218	0.0129	0.0064	0.0022	0.0003	0.0000	0.0000	0.0000	543,074,832
5	30-36°N		0.0458	0.0315	0.0205	0.0122	0.0060	0.0021	0.0003	0.0000	0.0000	0.0000	691,722,558
6	24-30°N		0.0374	0.0257	0.0168	0.0100	0.0049	0.0017	0.0002	0.0000	0.0000	0.0000	605,118,210
7	17-24°N		0.0319	0.0219	0.0143	0.0085	0.0042	0.0014	0.0002	0.0000	0.0000	0.0000	387,278,363
8	11-17°N		0.0256	0.0176	0.0115	0.0068	0.0034	0.0011	0.0002	0.0000	0.0000	0.0000	199,943,660
9	6-11°N		0.0202	0.0139	0.0091	0.0060	0.0027	0.0009	0.0000	0.0000	0.0000	0.0000	203,931,205
10	0-6°N		0.0183	0.0126	0.0082	0.0049	0.0024	0.0008	0.0001	0.0000	0.0000	0.0000	78,887,239
11	0-6°S		0.0205	0.0164	0.0133	0.0108	0.0091	0.0080	0.0075	0.0074	0.0074	0.0074	69,355,336
12	6-11°S		0.0255	0.0231	0.0213	0.0199	0.0188	0.0182	0.0179	0.0178	0.0178	0.0178	132,699,175
13	11-17°S		0.0397	0.0421	0.0439	0.0454	0.0464	0.0471	0.0474	0.0474	0.0474	0.0474	43,233,315
14	17-24°S		0.0563	0.0644	0.0707	0.0754	0.0789	0.0812	0.0822	0.0823	0.0823	0.0823	58,286,844
15	24-30°S		0.0703	0.0830	0.0927	0.1001	0.1055	0.1091	0.1107	0.1109	0.1109	0.1109	44,606,711
16	30-36°S		0.0935	0.1145	0.1305	0.1428	0.1518	0.1576	0.1602	0.1606	0.1606	0.1606	37,873,258
17	36-44°S		0.1004	0.1236	0.1413	0.1548	0.1648	0.1712	0.1741	0.1745	0.1745	0.1745	7,566,457
18	44-54°S		0.1024	0.1263	0.1445	0.1584	0.1687	0.1753	0.1782	0.1787	0.1787	0.1787	828,162
19	54-64°S		0.0876	0.1064	0.1208	0.1317	0.1398	0.1450	0.1473	0.1477	0.1478	0.1478	56,392
20	64-90°S		0.0524	0.0588	0.0636	0.0672	0.0700	0.0718	0.0725	0.0727	0.0727	0.0727	449

\*Boundaries are approximate.

Source: Reference 6-5.



Reference 6-5. While LOPAR applies to particles having diameters less than 4  $\mu\text{m}$ , we assume, for present purposes, that it also applies to particle populations for which the AMAD values are less than 5  $\mu\text{m}$ . The relationship between injection latitude (i) and deposition latitude (k) is shown graphically in Figure 6-10. This figure and the data in Table 6-14, including the population data, were extracted from Reference 6-5.

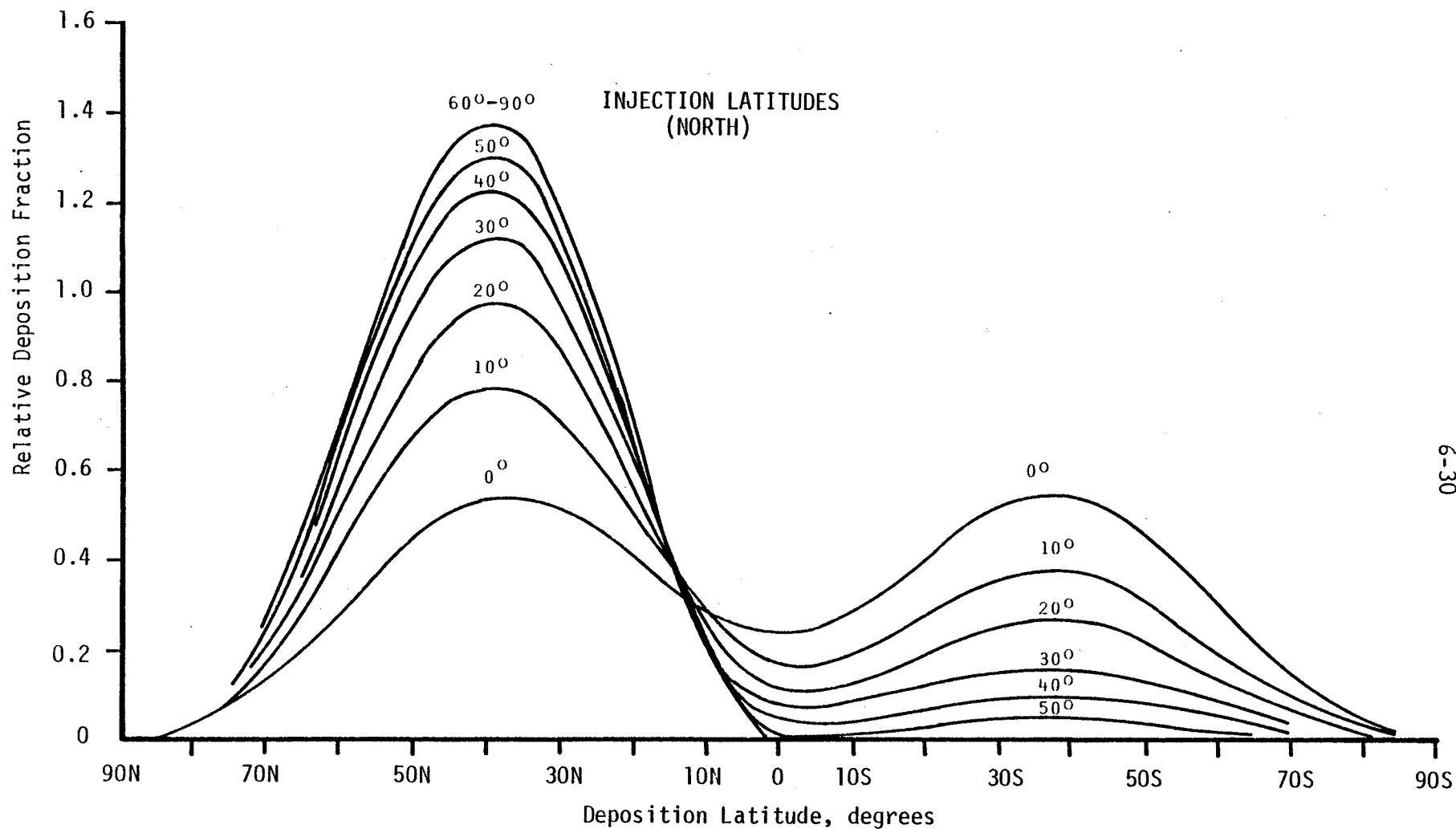
Table 6-15 gives, for each injection band i, the sums indicated in Equation (1) by  $\sum_{k=1}^{k=20} f_{ik} P_k$ . The sums in Table 6-15 reflect two facts, also observable in Table 6-14: (a) the population of the northern hemisphere is greater than the population of the southern hemisphere, and (b) the farther north injection occurs the larger the total deposition in the northern hemisphere. In other words, the farther north the injection latitude, the greater the world population dose estimate will be for any postulated mixture of radionuclides.

TABLE 6-15. SUMMATION OF POPULATION FACTORS FOR EACH INJECTION BAND

Injection Latitude Band (i)	$\sum_{k=1}^{k=20} (f_{ik} P_k)_i$	Injection Latitude Band (i)	$\sum_{k=1}^{k=20} (f_{ik} P_k)_i$
1 (85-90°N)	4.21822 E+08	11 (5-15°S)	1.50421 E+08
2 (75-85°N)	4.21806 E+08	12 (15-25°S)	1.10250 E+08
3 (65-75°N)	4.20944 E+08	13 (25-35°S)	7.9700 E+07
4 (55-65°N)	4.15038 E+08	14 (35-45°S)	5.64713 E+07
5 (45-55°N)	4.20939 E+08	15 (45-55°S)	3.90881 E+07
6 (35-45°N)	3.81304 E+08	16 (55-65°S)	2.80052 E+07
7 (25-35°N)	3.53348 E+08	17 (65-75°S)	2.30093 E+07
8 (15-25°N)	3.16835 E+08	18 (75-85°S)	2.22276 E+07
9 (5-15°N)	2.69197 E+08	19 (85-90°S)	2.22276 E+07
10 (5°N-5°S)	2.04556 E+08	-	-

Source: Based on data from Reference 6-5, and as given in Table 6-14.

The individual lifetime dose factors per unit ( $\mu\text{Ci}$ ) input to band k,  $D_{nrk}$  of Equation (1), are listed for three postulated particle populations (AMAD = 0.2, 1.0, or 5.0  $\mu\text{m}$ ) in Tables 6-16, 6-17 and 6-18, respectively, for 41 radionuclides and 10 organs. The next to last column "BODY DOSE" gives dose factors for the total body. As the dose to an organ is determined by the energy deposited per gram of tissue, the "BODY DOSE" is not the sum of doses to the organs of the body. The zero values listed in these three tables mean that the



6-30

FIGURE 6-10. DEPOSITION OF SMALL PARTICLES ( $< 4 \mu m$ )  
RELEASED AT HIGH ALTITUDE AS A  
FUNCTION OF INJECTION LATITUDE

TABLE 6-16. DOSE FACTORS (REM/ $\mu$  CI FOR EACH NUCLIDE) FOR AMAD OF 0.2 MICRONS

Radio-nuclide	Class	Organ									
		NP	TB	P	LM	GIT	Bone	Liver	Kidney	Total Body	Thy-roid
CO-060	W	8.727E-16	4.828E-18	2.643E-15	7.057E-15	4.502E-17	0.	4.751E-19	0.	4.840E-19	0.
SE-079	W	6.577E-17	3.663E-19	2.044E-16	5.602E-16	5.611E-18	0.	3.893E-18	9.008E-15	6.190E-19	0.
SR-089	W	1.659E-17	6.021E-20	2.624E-17	3.566E-17	1.124E-18	3.941E-18	0.	0.	2.578E-19	0.
SR-090	W	1.637E-15	9.104E-18	5.061E-15	1.380E-14	2.661E-17	2.011E-13	0.	0.	3.807E-15	0.
Y-091	Y	2.568E-17	1.537E-19	7.556E-17	6.856E-17	1.467E-18	3.182E-19	0.	0.	8.625E-21	0.
ZR-093	W	2.975E-17	1.657E-19	5.245E-17	2.534E-16	2.539E-18	1.192E-16	1.719E-17	5.301E-16	2.981E-18	0.
NB-095	W	3.617E-18	1.701E-20	4.715E-18	5.224E-18	1.437E-19	8.520E-20	5.802E-20	2.927E-20	3.058E-20	0.
ZR-095	W	2.440E-17	1.200E-19	4.280E-17	6.487E-17	7.851E-19	1.656E-18	6.824E-19	4.772E-19	4.287E-19	0.
TC-099	W	1.472E-16	8.198E-19	4.574E-16	1.254E-15	1.256E-17	2.113E-19	3.133E-19	3.384E-16	8.453E-20	0.
RU-103	Y	5.803E-18	3.452E-20	1.251E-17	8.101E-18	1.692E-19	2.270E-21	0.	8.369E-20	1.084E-21	0.
RU-106	Y	8.074E-16	5.179E-18	9.552E-15	4.396E-14	5.050E-17	1.959E-18	0.	2.721E-16	2.463E-19	0.
PD-107	Y	1.529E-17	1.100E-19	4.279E-16	1.330E-14	1.315E-18	0.	2.872E-19	1.257E-15	2.039E-20	0.
CD-113M	Y	2.864E-16	2.029E-18	7.301E-15	1.512E-13	2.381E-17	0.	1.711E-16	1.713E-15	5.542E-18	0.
SB-125	W	1.953E-16	1.072E-18	5.746E-16	1.489E-15	1.009E-17	5.459E-18	1.368E-19	0.	3.402E-18	8.627E-21
SN-126	W	1.722E-15	9.594E-18	5.352E-15	1.467E-14	5.077E-17	1.079E-15	2.851E-17	0.	4.092E-17	8.372E-18
TE-127M	W	3.641E-17	1.855E-19	7.713E-17	1.423E-16	2.019E-18	1.148E-18	5.600E-19	9.996E-18	1.530E-19	3.171E-19
TE-129M	W	1.314E-17	4.745E-20	1.277E-17	1.365E-17	5.084E-19	1.431E-19	8.488E-20	6.644E-19	3.586E-20	5.320E-20
I-129	D	3.557E-18	6.242E-20	7.183E-18	8.750E-17	4.691E-19	3.979E-17	4.113E-18	1.791E-14	1.781E-17	1.429E-14
CS-134	D	1.439E-17	2.526E-19	2.905E-17	3.535E-16	1.421E-18	4.008E-17	1.127E-16	3.802E-16	5.995E-17	0.
CS-135	D	7.808E-18	1.370E-19	1.577E-17	1.921E-16	1.093E-18	6.577E-17	6.771E-17	1.047E-14	2.132E-17	0.
CS-137	D	1.696E-17	2.979E-19	3.428E-17	4.176E-16	2.086E-18	1.072E-16	1.460E-16	6.963E-15	5.660E-17	0.
CE-141	Y	2.252E-18	1.339E-20	3.869E-18	1.962E-18	1.186E-19	3.829E-21	2.689E-21	6.760E-22	3.198E-22	0.
CE-144	Y	6.056E-16	3.840E-18	6.235E-15	2.395E-14	3.972E-17	4.593E-17	1.951E-17	8.797E-18	2.488E-18	0.
PM-147	Y	7.197E-17	4.635E-19	1.306E-15	1.136E-14	5.372E-18	3.737E-17	3.492E-16	7.924E-18	1.414E-18	0.
SM-151	Y	7.116E-17	5.105E-19	1.965E-15	7.261E-14	5.945E-18	1.345E-16	2.309E-18	4.239E-16	5.500E-18	0.
EU-152	Y	1.046E-15	7.739E-18	2.772E-14	5.530E-13	9.085E-17	1.812E-15	1.379E-16	1.790E-15	7.512E-17	0.
EU-154	Y	1.354E-15	9.593E-18	3.489E-14	7.637E-13	9.066E-17	1.879E-15	1.785E-16	2.492E-15	1.207E-16	0.
EU-155	Y	8.072E-17	5.321E-19	1.253E-15	8.475E-15	4.564E-18	1.480E-17	3.447E-18	6.030E-18	1.679E-18	0.
TB-160	Y	3.219E-17	1.937E-19	1.158E-16	1.309E-16	1.320E-18	2.066E-19	0.	4.702E-20	2.574E-20	0.
U-233	Y	8.591E-14	6.176E-16	2.404E-12	1.028E-10	7.241E-17	1.182E-13	0.	3.095E-11	7.164E-15	0.
U-235	Y	7.903E-14	5.684E-16	2.212E-12	9.459E-11	7.685E-17	1.630E-14	0.	4.050E-12	9.876E-16	0.
NP-237	Y	8.419E-14	6.059E-16	2.356E-12	1.008E-10	7.241E-17	2.423E-11	2.090E-12	8.274E-12	4.596E-13	0.
PJ-238	Y	9.642E-14	6.919E-16	2.658E-12	9.662E-11	7.957E-17	2.680E-12	1.726E-12	5.548E-13	1.318E-13	0.
U-238	Y	7.368E-14	5.313E-16	2.068E-12	8.841E-11	6.355E-17	1.559E-14	0.	3.736E-12	9.232E-16	0.
PU-239	Y	8.965E-14	6.429E-16	2.471E-12	8.984E-11	7.523E-17	2.584E-12	1.607E-12	5.159E-13	1.225E-13	0.
PU-240	Y	8.965E-14	6.429E-16	2.471E-12	8.984E-11	7.523E-17	2.584E-12	1.607E-12	5.158E-13	1.225E-13	0.
AM-241	Y	9.764E-14	7.018E-16	2.724E-12	1.127E-10	6.241E-17	2.041E-12	2.141E-12	1.235E-12	1.279E-13	0.
PU-241	Y	8.365E-17	6.429E-16	2.471E-12	8.984E-11	7.668E-20	1.340E-13	3.032E-14	2.433E-14	5.317E-15	0.
PU-242	Y	8.730E-14	6.274E-16	2.434E-12	9.997E-11	7.205E-17	2.927E-12	1.855E-12	7.208E-13	1.450E-13	0.
AM-243	Y	9.276E-14	6.671E-16	2.596E-12	1.103E-10	7.979E-17	1.658E-12	2.132E-12	1.289E-12	1.270E-13	0.
GM-244	Y	9.556E-14	6.783E-16	2.489E-12	5.791E-11	7.738E-17	8.607E-13	3.441E-13	1.564E-13	5.036E-14	0.

Class = Translocation Class

D = Day

W = Week

Y = Year

NOTE: NP = Nasopharyngeal Region

TB = Tracheobronchial Region

P = Pulmonary Lung Region

LM = Thoracic Lymph

GIT = Large Intestine

TABLE 6-17. DOSE FACTORS (REM/ $\mu$  CI FOR EACH NUCLIDE) FOR AMAD OF 1.0 MICRONS

Radio-nuclide	Class	Organ									
		NP	TB	P	LM	GIT	Bone	Liver	Kidney	Total Body	Thy-roid
CO-060	W	8.436E-15	3.711E-18	1.483E-15	3.959E-15	5.560E-17	0.	5.122E-19	0.	5.218E-19	0.
SE-079	W	6.357E-16	2.811E-19	1.146E-16	3.143E-16	6.890E-18	0.	4.468E-18	1.035E-14	7.105E-19	0.
SR-089	W	1.604E-16	6.406E-20	1.472E-17	2.001E-17	1.574E-18	5.033E-18	0.	0.	3.292E-19	0.
SR-090	W	1.582E-14	6.988E-16	2.839E-15	7.743E-15	3.270E-17	2.155E-13	0.	0.	4.079E-15	0.
Y-091	Y	2.443E-16	1.370E-19	4.239E-17	3.846E-17	2.366E-18	4.569E-19	0.	0.	1.238E-20	0.
ZR-093	W	2.876E-16	1.272E-19	5.186E-17	1.422E-16	3.117E-18	1.097E-16	1.581E-17	4.882E-16	2.743E-18	0.
NU-095	W	3.497E-17	1.370E-20	2.645E-18	2.931E-18	2.073E-19	1.012E-19	6.892E-20	3.476E-20	3.632E-20	0.
ZR-095	W	2.359E-16	9.536E-20	2.401E-17	3.639E-17	1.061E-18	1.818E-18	7.493E-19	5.239E-19	4.707E-19	0.
TC-099	W	1.423E-15	6.291E-19	2.566E-16	7.033E-16	1.542E-17	2.343E-19	3.473E-19	3.754E-16	9.371E-20	0.
RU-103	Y	5.610E-17	3.083E-20	7.016E-18	4.545E-18	2.757E-19	3.716E-21	0.	1.170E-19	1.775E-21	0.
RU-106	Y	7.805E-15	4.501E-18	5.358E-15	2.467E-14	7.338E-17	2.012E-18	0.	2.795E-16	2.530E-19	0.
PU-107	Y	1.478E-16	9.191E-20	2.401E-16	1.027E-14	1.657E-18	0.	2.731E-19	1.216E-15	1.940E-20	0.
CU-113M	Y	2.768E-15	1.702E-18	4.996E-15	8.482E-14	3.056E-17	0.	1.045E-16	1.047E-15	3.385E-18	0.
SB-125	W	1.888E-15	8.261E-19	3.224E-16	8.354E-16	1.254E-17	5.260E-18	1.318E-19	0.	3.278E-18	8.313E-21
SN-126	W	1.665E-14	7.361E-16	3.003E-15	8.231E-15	6.234E-17	1.196E-15	3.161E-17	0.	4.536E-17	9.281E-18
TE-127M	W	3.520E-16	1.459E-19	4.327E-17	7.985E-17	2.686E-18	1.351E-18	6.595E-19	1.177E-17	1.802E-19	3.734E-19
TE-129M	W	9.799E-17	3.827E-20	7.165E-18	7.657E-18	7.369E-19	1.697E-19	1.126E-19	8.811E-19	4.755E-20	7.054E-20
I-129	D	3.438E-17	6.242E-20	4.648E-18	4.908E-17	3.679E-18	4.591E-17	4.745E-18	2.067E-14	2.055E-17	1.649E-14
CS-134	D	1.391E-16	2.526E-19	1.880E-17	1.983E-16	1.115E-17	4.626E-17	1.300E-16	4.389E-16	6.920E-17	0.
CS-135	D	7.547E-17	1.370E-19	1.020E-17	1.076E-16	8.568E-18	7.589E-17	7.812E-17	1.208E-14	2.459E-17	0.
CS-137	D	1.641E-16	2.979E-19	2.218E-17	2.343E-16	1.636E-17	1.236E-16	1.685E-16	6.034E-15	6.554E-17	0.
CE-141	Y	2.177E-17	1.194E-20	2.170E-18	1.101E-18	1.943E-19	7.016E-21	4.926E-21	1.239E-21	5.859E-22	0.
CF-144	Y	5.854E-15	3.351E-18	3.498E-15	1.344E-14	5.867E-17	3.659E-17	1.554E-17	7.008E-18	1.982E-18	0.
PH-147	Y	6.957E-16	4.134E-19	7.325E-16	6.375E-15	7.338E-18	2.465E-17	2.303E-18	5.226E-18	9.323E-19	0.
SM-151	Y	6.879E-16	4.270E-19	1.102E-15	4.073E-14	7.509E-18	8.104E-17	1.392E-18	2.600E-16	3.345E-18	0.
EU-152	Y	1.059E-14	6.507E-18	1.555E-14	3.102E-13	1.168E-16	1.109E-15	8.442E-17	1.030E-15	4.598E-17	0.
FU-154	Y	1.309E-14	5.057E-18	1.957E-14	4.284E-13	1.161E-16	1.146E-15	1.089E-16	1.521E-15	7.362E-17	0.
EJ-155	Y	7.803E-16	4.580E-19	7.028E-16	4.754E-15	6.389E-18	1.020E-17	2.377E-18	4.158E-18	1.158E-18	0.
TJ-160	Y	3.112E-16	1.723E-19	6.437E-17	7.344E-17	2.111E-18	2.688E-19	0.	6.118E-20	3.350E-20	0.
U-233	Y	8.304E-13	5.163E-16	1.349E-12	5.767E-11	9.121E-17	1.372E-13	0.	3.632E-11	9.317E-15	0.
U-235	Y	7.640E-13	4.750E-16	1.241E-12	5.306E-11	9.679E-17	9.800E-15	0.	2.448E-12	5.940E-16	0.
NP-237	Y	8.138E-13	5.060E-16	1.322E-12	5.652E-11	9.121E-17	2.840E-11	2.445E-12	9.709E-12	1.124E-12	0.
PU-238	Y	9.370E-13	5.784E-16	1.491E-12	5.420E-11	1.005E-16	1.620E-12	1.044E-12	3.353E-13	7.968E-14	0.
U-238	Y	7.142E-13	4.441E-16	1.160E-12	4.960E-11	8.004E-17	9.374E-15	0.	2.289E-12	5.552E-16	0.
PU-239	Y	8.666E-13	5.378E-16	1.386E-12	5.040E-11	9.505E-17	1.562E-12	9.702E-13	3.118E-13	7.409E-14	0.
PU-240	Y	8.666E-13	5.378E-16	1.386E-12	5.040E-11	9.505E-17	1.562E-12	9.702E-13	3.118E-13	7.409E-14	0.
AM-241	Y	9.448E-13	5.866E-16	1.528E-12	6.320E-11	1.039E-16	1.233E-12	1.293E-12	7.467E-13	7.718E-14	0.
PU-241	Y	8.666E-13	5.378E-16	1.386E-12	5.040E-11	9.505E-17	1.562E-12	9.702E-13	3.118E-13	7.409E-14	0.
PU-242	Y	8.449E-13	5.245E-16	1.366E-12	5.608E-11	9.082E-17	1.767E-12	1.119E-12	4.455E-13	8.760E-14	0.
AM-243	Y	8.916E-13	5.579E-16	1.456E-12	6.214E-11	1.005E-16	1.001E-12	1.297E-12	7.791E-13	7.665E-14	0.
CM-244	Y	5.238E-13	5.694E-16	1.396E-12	3.240E-11	9.892E-17	5.246E-13	2.095E-13	9.521E-14	3.069E-14	0.

Class = Translocation Class

D = Day  
W = Week  
Y = Year

NOTE: NP = Nasopharyngeal Region  
TB = Tracheobronchial Region  
P = Pulmonary Lung Region  
LM = Thoracic Lymph  
GIT = Large Intestine

TABLE 6-18. DOSE FACTORS (REM/ $\mu$ CI FOR EACH NUCLIDE) FOR AMAD OF 5.0 MICRONS

Radio-nuclide	Class	Organ									Total Body	Thy-roid
		NP	TB	P	LM	GIT	Bone	Liver	Kidney			
CO-060	W	2.240E-14	2.967E-18	7.092E-16	1.894E-15	9.445E-17	0.	7.619E-19	0.	7.762E-19	0.	
SE-079	W	1.688E-15	2.242E-19	5.483E-17	1.503E-16	1.166E-17	0.	7.112E-18	1.648E-14	1.131E-18	0.	
SR-089	W	4.257E-16	5.329E-20	7.039E-18	9.571E-18	2.863E-18	8.343E-18	0.	0.	5.457E-19	0.	
SR-090	W	4.201E-14	5.578E-18	1.358E-15	3.703E-15	5.540E-17	3.191E-13	0.	0.	6.041E-15	0.	
Y-091	Y	6.592E-16	1.258E-19	2.027E-17	1.839E-17	4.501E-18	0.262E-19	0.	0.	2.239E-20	0.	
ZR-093	W	7.636E-16	1.015E-19	2.480E-17	6.799E-17	5.276E-18	1.326E-16	1.912E-17	5.307E-16	3.316E-18	0.	
NB-095	W	5.284E-17	1.149E-20	1.265E-18	1.402E-18	3.824E-19	1.484E-19	1.011E-19	5.097E-20	5.326E-20	0.	
ZR-095	W	6.262E-16	7.893E-20	1.148E-17	1.740E-17	1.950E-18	2.534E-18	1.045E-18	7.304E-19	6.562E-19	0.	
TC-099	W	3.778E-15	5.019E-19	1.227E-16	3.364E-16	2.610E-17	3.601E-19	5.338E-19	5.774E-16	1.440E-19	0.	
RU-103	Y	1.490E-16	2.837E-20	3.356E-18	2.174E-18	5.266E-19	7.110E-21	0.	2.622E-19	3.396E-21	0.	
RU-106	Y	2.072E-14	4.049E-18	2.563E-15	1.80E-14	1.334E-16	2.956E-18	0.	4.107E-16	3.716E-19	0.	
PO-107	Y	3.925E-16	7.987E-20	1.148E-16	4.10E-15	2.798E-18	0.	3.753E-19	1.696E-15	2.665E-20	0.	
CO-113M	Y	7.351E-15	1.487E-18	1.959E-15	4.056E-14	5.218E-17	0.	6.864E-17	6.873E-16	2.223E-18	0.	
SB-125	W	5.013E-15	6.618E-19	1.542E-16	3.995E-16	2.138E-17	6.750E-18	1.692E-19	0.	4.206E-18	1.067E-20	
SN-126	W	4.421E-14	5.873E-18	1.436E-15	3.936E-15	1.055E-16	1.839E-15	4.858E-17	0.	6.972E-17	1.427E-17	
TE-127M	W	9.346E-16	1.195E-19	2.069E-17	3.819E-17	4.760E-18	2.124E-19	1.037E-18	1.851E-17	2.832E-19	5.870E-19	
TE-129M	W	2.602E-16	3.214E-20	3.427E-18	3.662E-18	1.362E-18	3.192E-19	1.894E-19	1.483E-18	9.001E-20	1.187E-19	
I-129	D	9.123E-17	6.742E-20	2.958E-18	2.340E-17	9.605E-18	7.346E-17	7.592E-18	3.307E-14	3.288E-17	2.638E-14	
CS-134	C	3.694E-16	2.526E-19	1.196E-17	9.484E-17	2.910E-17	7.404E-17	2.081E-16	7.023E-16	1.107E-16	0.	
CS-135	D	2.004E-16	1.370E-19	6.493E-18	5.153E-17	2.237E-17	1.214E-16	1.250E-16	1.933E-14	3.935E-17	0.	
CS-137	U	4.357E-16	2.979E-19	1.412E-17	1.120E-16	4.270E-17	1.978E-16	2.696E-16	1.286E-14	1.049E-16	0.	
CE-141	Y	5.779E-17	1.100E-20	1.038E-18	5.265E-19	3.719E-19	1.396E-20	9.819E-21	2.469E-21	1.168E-21	0.	
CE-144	Y	1.554E-14	3.025E-18	1.673E-15	6.426E-15	1.075E-16	4.113E-17	1.747E-17	7.878E-18	2.228E-18	0.	
PH-147	Y	1.847E-15	3.667E-19	3.503E-16	3.049E-15	1.295E-17	1.983E-17	1.853E-18	4.204E-18	7.500E-19	0.	
SM-151	Y	1.827E-15	3.713E-19	5.272E-16	1.948E-14	1.270E-17	5.102E-17	8.760E-19	1.653E-16	2.106E-18	0.	
EU-152	Y	2.813E-14	5.689E-18	7.437E-15	1.484E-13	1.996E-16	7.325E-16	5.576E-17	7.199E-16	3.037E-17	0.	
EU-154	Y	3.475E-14	7.033E-18	9.360E-15	2.049E-13	1.981E-16	7.494E-16	7.118E-17	9.945E-16	4.814E-17	0.	
EU-155	Y	2.072E-15	4.006E-19	3.361E-16	2.274E-15	1.142E-17	9.032E-18	2.104E-18	3.693E-18	1.025E-18	0.	
TD-160	Y	8.263E-16	1.580E-19	3.107E-17	3.512E-17	4.001E-18	4.625E-19	0.	1.053E-19	5.763E-20	0.	
U-233	Y	2.205E-12	4.487E-16	6.450E-13	2.758E-11	1.541E-16	2.205E-13	0.	5.876E-11	1.336E-14	0.	
U-235	Y	2.029E-12	4.128E-16	5.934E-13	2.536E-11	1.635E-16	6.126E-15	0.	1.556E-12	3.713E-16	0.	
NP-237	Y	2.161E-12	4.397E-16	6.321E-13	2.703E-11	1.541E-16	4.592E-11	3.959E-12	1.571E-11	1.816E-12	0.	
PU-238	Y	2.475E-12	5.031E-16	7.131E-13	2.592E-11	1.701E-16	1.029E-12	6.609E-13	2.130E-13	5.069E-14	0.	
U-238	Y	1.896E-12	3.859E-16	5.547E-13	2.372E-11	1.352E-16	5.859E-15	0.	1.454E-12	3.470E-16	0.	
PU-239	Y	2.301E-12	4.674E-16	6.831E-13	2.410E-11	1.608E-16	9.927E-13	6.145E-13	1.981E-13	4.713E-14	0.	
PU-240	Y	2.331E-12	4.678E-16	6.631E-13	2.410E-11	1.608E-16	9.927E-13	6.145E-13	1.981E-13	4.713E-14	0.	
AM-241	Y	2.506E-12	5.099E-16	7.309E-13	3.023E-11	1.755E-16	7.828E-13	8.196E-13	4.745E-13	4.881E-14	0.	
PU-241	Y	2.301E-12	4.674E-16	6.831E-13	2.410E-11	1.608E-16	9.927E-13	6.145E-13	1.981E-13	4.713E-14	0.	
PU-242	Y	2.241E-12	4.559E-16	6.531E-13	2.682E-11	1.535E-16	1.119E-12	7.055E-13	2.763E-13	5.553E-14	0.	
AM-243	Y	2.311E-12	4.845E-16	6.964E-13	2.972E-11	1.697E-16	6.352E-13	8.152E-13	4.950E-13	4.843E-14	0.	
CH-244	Y	2.453E-12	4.967E-16	6.677E-13	1.593E-11	1.685E-16	3.421E-13	1.362E-13	6.192E-14	1.999E-14	0.	

Class = Translocation Class

D = Day

W = Week

Y = Year

NOTE: NP = Nasopharyngeal Region

TB = Tracheobronchial Region

P = Pulmonary Lung Region

LM = Thoracic Lymph

GIT = Large Intestine

metabolic data needed to calculate the dose factor were not available. The model used to calculate dose factors,  $D_{nrk}$ , is fully described in Appendix G.

## 6.2.2 Results

### 6.2.2.1 Maximum Doses to Individuals

The world population dose estimates summarized in Tables 6-19 and 6-20 were calculated according to the formula indicated by Equation (1), i.e., by successively substituting the values given in Tables 3-5 and 3-6 for the  $A_{ir}$  terms of Equation (1), values from Table 6-15 for  $\sum f_{ik} P_k$ , and values from Tables 6-16 through 6-18 for  $D_{nrk}$ . Then, for each organ, injection band, AMAD, and mix, the dose terms were summed.

Maximum lifetime organs doses (70-year) can be estimated as three times the mean lifetime organ dose to an individual in the equal area latitude band receiving the largest fraction of the radioactivity injected into the upper atmosphere by reentry burnup of a nuclear waste payload, i.e.,

$$D(70)_{\max} = 3f_{ik\max}W_n/\sum f_{ik}P_k \quad (2)$$

where:

$f_{ik\max} = 0.1787$  is the maximum value of  $f_{ik}$ , Table 6-14,

and

$W_n/\sum f_{ik}P_k = \sum D_{nrk}A_{ir}$  is the dose factor sum, which is constant for a radionuclide mix, AMAD, and organ.

For example, the highest estimated world population for lung is the first value given for lung in Table 6-19. Based on this value and Equation (1), the estimated maximum individual lifetime lung dose is

$$\begin{aligned} D(70)_{\text{LUNG MAX}} &= 3(0.1787) (7.52 \text{ E}+07/4.15 \text{ E}+08) \\ &= 0.097 \text{ rem}; 0.0014 \text{ rem/yr} \end{aligned} \quad (3)$$

As lifetime doses are integrated over a 70-year interval the preceding estimate implies a mean annual dose rate of  $0.097/70 = 0.0014 \text{ rem/yr}$ .

TABLE 6-19. WORLD POPULATION DOSE SUMMARY FOR TOTAL BURNUP OF SAVANNAH RIVER DEFENSE WASTE PAYLOAD ABOVE 21 KM

World Population Doses (man-rems) Organs*											
Injection Latitude Band	AMAD Value ( $\mu\text{m}$ )	NP	TB	P	LM	GIT	Bone	Liver	Kidney	Total Body	Thy-roid
4	0.2 ↓	7.65E+06	4.79E+04	7.52E+07	4.46E+08	4.49E+05	8.75E+07	3.12E+06	4.04E+06	1.83E+06	1.04E+02
6		7.03E+06	4.40E+04	6.91E+07	4.10E+08	4.13E+05	8.04E+07	2.86E+06	3.71E+06	1.69E+06	9.51E+01
8		5.84E+06	3.66E+04	5.74E+07	3.40E+08	3.43E+05	6.68E+07	2.38E+06	3.08E+06	1.40E+06	7.91E+01
10		3.77E+06	2.36E+04	3.71E+07	2.20E+08	2.21E+05	4.31E+07	1.54E+06	1.99E+06	9.04E+05	5.10E+01
12		2.03E+06	1.27E+04	2.00E+07	1.18E+08	1.19E+05	2.32E+07	8.28E+05	1.07E+06	4.87E+05	2.75E+01
14		1.04E+06	6.52E+03	1.02E+07	6.07E+07	6.11E+04	1.19E+07	4.24E+05	5.50E+05	2.50E+05	1.41E+01
16		5.16E+05	3.23E+03	5.08E+06	3.01E+07	3.03E+04	5.91E+06	2.10E+05	2.73E+05	1.24E+05	6.99E+00
4	1.0 ↓	7.40E+07	4.13E+04	4.22E+07	2.50E+08	6.65E+05	9.16E+07	1.95E+06	4.05E+06	1.86E+06	1.24E+02
6		6.79E+07	3.79E+04	3.88E+07	2.30E+08	6.11E+05	8.42E+07	1.79E+06	3.73E+06	1.71E+06	1.14E+02
8		5.65E+07	3.15E+04	3.22E+07	1.91E+08	5.08E+05	6.99E+07	1.49E+06	3.10E+06	1.42E+06	9.47E+01
10		3.65E+07	2.04E+04	2.08E+07	1.23E+08	3.28E+05	4.52E+07	9.63E+05	2.00E+06	9.16E+05	6.12E+01
12		1.96E+07	1.10E+04	1.12E+07	6.64E+07	1.77E+05	2.43E+07	5.19E+05	1.08E+06	4.94E+05	3.30E+01
14		1.01E+07	5.62E+03	5.74E+06	3.40E+07	9.05E+04	1.25E+07	2.66E+05	5.52E+05	2.53E+05	1.69E+01
16		4.99E+06	2.79E+03	2.85E+06	1.63E+07	4.49E+04	6.18E+06	1.32E+05	2.74E+05	1.25E+05	8.37E+00
4	5.0 ↓	1.96E+08	3.69E+04	2.02E+07	1.20E+08	1.22E+06	1.33E+08	1.38E+06	5.84E+06	2.64E+06	1.97E+02
6		1.80E+08	3.39E+04	1.85E+07	1.10E+08	1.12E+06	1.22E+08	1.27E+06	5.37E+06	2.42E+06	1.81E+02
8		1.50E+08	2.82E+04	1.54E+07	9.13E+07	9.32E+05	1.02E+08	1.06E+06	4.46E+06	2.01E+06	1.51E+02
10		9.68E+07	1.82E+04	9.95E+06	5.89E+07	6.02E+05	6.57E+07	6.81E+05	2.88E+06	1.30E+06	9.72E+01
12		5.22E+07	9.80E+03	5.36E+06	3.14E+07	3.24E+05	3.54E+07	3.67E+05	1.55E+06	7.00E+05	5.24E+01
14		2.67E+07	5.02E+03	2.75E+06	1.63E+07	1.66E+05	1.81E+07	1.89E+05	7.95E+05	3.59E+05	2.68E+01
16		1.33E+07	2.44E+03	1.36E+06	8.07E+06	8.24E+04	9.00E+06	9.33E+04	3.94E+05	1.78E+05	1.33E+01

\* NOTE: NP = Nasopharyngeal Region  
 TB = Tracheobronchial Region  
 P = Pulmonary Lung Region  
 LM = Thoracic Lymph  
 GIT = Large Intestine

TABLE 6-20. WORLD POPULATION DOSE SUMMARY FOR TOTAL BURNUP OF HANFORD DEFENSE WASTE PAYLOAD ABOVE 21 KM

Injection Latitude Band	AMAD Value ( $\mu\text{m}$ )	World Population Doses (man-rems) Organs*									
		NP	TB	P	LM	GIT	Bone	Liver	Kidney	Total Body	Thy-roid
4	0.2	3.10E+05	1.79E+03	1.67E+06	3.41E+07	4.86E+03	3.43E+07	6.01E+05	1.06E+06	6.93E+05	2.55E+00
6		2.84E+05	1.65E+03	1.54E+06	3.13E+07	4.47E+03	3.21E+07	5.52E+05	9.70E+05	6.37E+05	2.35E+00
8		2.36E+05	1.37E+03	1.28E+06	2.60E+07	3.71E+03	2.67E+07	4.54E+05	8.06E+05	5.29E+05	1.95E+00
10		1.53E+05	8.83E+02	8.25E+05	1.68E+07	2.40E+03	1.72E+07	2.96E+05	5.20E+05	3.41E+05	1.26E+00
12		8.22E+04	4.76E+02	4.44E+05	9.05E+06	1.29E+03	9.28E+06	1.60E+05	2.80E+05	1.84E+05	6.78E-01
14		4.21E+04	2.44E+02	2.28E+05	4.64E+06	6.61E+02	4.75E+06	8.18E+04	1.44E+05	9.44E+04	3.47E-01
16		2.09E+04	1.21E+02	1.13E+05	2.30E+06	3.28E+02	2.36E+06	4.06E+04	7.12E+04	4.68E+04	1.72E-01
4	1.0	2.53E+06	1.40E+03	9.39E+05	1.91E+07	7.47E+03	3.71E+07	3.72E+05	1.05E+06	7.25E+05	2.95E+00
6		2.75E+06	1.2E+03	8.63E+05	1.76E+07	6.86E+03	3.41E+07	3.42E+05	9.69E+05	6.66E+05	2.71E+00
8		2.28E+06	1.07E+03	7.17E+05	1.46E+07	5.70E+03	2.83E+07	2.84E+05	8.05E+05	5.53E+05	2.25E+00
10		1.47E+06	6.8E+02	4.63E+05	9.42E+06	3.68E+03	1.83E+07	1.83E+05	5.20E+05	3.57E+05	1.45E+00
12		7.95E+05	3.71E+02	2.49E+05	5.08E+06	1.98E+03	9.86E+06	9.88E+04	2.80E+05	1.93E+05	7.82E-01
14		4.07E+05	1.50E+02	1.28E+05	2.60E+06	1.02E+03	5.05E+06	5.06E+04	1.43E+05	9.86E+04	4.01E-01
16		2.02E+05	9.43E+01	6.34E+04	1.29E+06	5.04E+02	2.50E+06	2.51E+04	7.11E+04	4.89E+04	1.99E-01
4	5.0	7.95E+06	1.13E+03	4.49E+05	9.14E+06	1.43E+04	5.46E+07	2.54E+05	1.51E+06	1.05E+06	4.71E+00
6		7.30E+06	1.04E+03	4.13E+05	8.40E+06	1.31E+04	5.02E+07	2.34E+05	1.39E+06	3.63E+05	4.33E+00
8		6.07E+06	8.66E+02	3.43E+05	6.36E+06	1.09E+04	4.17E+07	1.94E+05	1.15E+06	8.05E+05	3.60E+00
10		3.92E+06	5.59E+02	2.21E+05	4.51E+06	7.03E+03	2.69E+07	1.25E+05	7.46E+05	5.20E+05	2.32E+00
12		2.11E+06	3.01E+02	1.19E+05	2.43E+06	3.79E+03	1.45E+07	6.76E+04	4.02E+05	2.80E+05	1.25E+00
14		1.04E+06	1.54E+02	6.11E+04	1.24E+06	1.94E+03	7.43E+06	3.46E+04	2.06E+05	1.44E+05	6.41E-01
16		5.36E+05	7.65E+01	3.33E+04	6.17E+05	6.63E+02	3.69E+06	1.72E+04	1.02E+05	7.12E+04	3.18E-01

\*NOTE: NP = Nasopharyngeal Region  
 TB = Tracheobronchial Region  
 P = Pulmonary Lung Region  
 LM = Thoracic Lymph  
 GIT = Large Intestine



The highest estimated world population dose for any organ is the estimate in Table 6-19 for Savannah River Waste. AMAD = 5.0  $\mu$ m, and injection band 4, i.e., 1.33 E+08 man-rem to bone. Substituting this value in Equation (2),

$$\begin{aligned} D(70)_{\text{BONE MAX}} &= 3(0.1787) (1.33 \text{ E}+08/4.15 \text{ E}+08) \\ &= 0.14 \text{ rem}; 0.002 \text{ rem/yr} \end{aligned} \quad (4)$$

Current ICRP recommendations<sup>(6-13)</sup> concerning "dose limits for individual members of the public" indicate that the dose to lungs should not exceed "1.5 rems in a year" while the dose to bone should not exceed "3 rems in a year". Although the mean annual maximum individual dose rates estimated above, Equations (3) and (4), are not precisely comparable to the ICRP limits, the differences seem to justify the conclusion that even the worst postulated reentry burnup accident would not expose any individual to a lifetime dose greater than the lifetime dose indicated by current recommendations concerning dose limits.

### 6.2.2.2 Worldwide Health Effects

To estimate the possible impact of a reentry burnup accident on world health, the principal objective of this section, it was decided to rely upon the linear, non-threshold health effects risk factors employed in Reference 6-6 rather than recommendations concerning maximum permissible doses (or dose rates) to individuals. The factors listed in Table G.3 (page G.8) of Reference 6-6 are given in Table 6-12.

Considerations leading to adoption of the risk factors listed in Table 6-12 are discussed at length in Appendix G of Reference 6-6. It should be noted that there are many uncertainties regarding the relationship between dose (or population dose) and health effects which may be due to radiation exposure or to other unspecified causes. In applying the risk factors listed in Table 6-12 to the world population dose estimates listed in Tables 6-19 and 6-20, additional uncertainties may arise due to differences in the methods employed for estimating population doses. Unfortunately, in the absence of clear, firm evidence concerning dose/health effects relationships (evidence which would

eradicate the considerable difference of opinion expressed in the recent, voluminous literature on the subject) these certainties cannot be resolved.

Table 6-21 gives the range of health effects expected from the maximum and minimum estimates of world population doses presented in Tables 6-19 and 6-20. These ranges reflect the different types of waste (Hanford and Savannah River), the different particle sizes, and the different injection latitudes that are possible. A more realistic definition of the Savannah River waste for space disposal may alter, to some degree, the results obtained here (see Section 3.2.2.2 and Table 3-6). Future work should include additional evaluation of the health risk of Savannah River waste payloads as a result of a burnup event.

**TABLE 6-21. RANGES OF EXPECTED HEALTH EFFECTS FOR PAYLOAD REENTRY BURNUP**

Type of Risk	Ranges of Expected Health Effects		
	Percent Release		
	1	10	100
<b>Cancer from:</b>			
Total body exposure	0-2	0-14	2-132
Lung exposure	0-4	0-38	0-376
Bone exposure	0-3	0-27	4-266
<b>Specific genetic effects to all generations from:</b>			
Total body exposure	0-2	0-14	2-132

### 6.2.3 Conclusions

The results described in the preceding section support the following conclusions:

- Savannah River waste, as defined for space disposal, is considerably more of a health problem than is the waste from Hanford.
- For any radionuclide mix, world population dose estimates increase as the latitude of injection increases in the northern hemisphere or decreases in the southern hemisphere, i.e., the farther north the injection latitude, the greater the expected world population dose.

- The most hazardous accident considered in this assessment involves the reentry and burnup of a Savannah River waste payload, north of  $55^{\circ}$  N latitude. The least hazardous involves the reentry burnup of a Hanford waste payload, south of  $55^{\circ}$  S latitude.
- Even the worst postulated burnup accident would not be expected to expose any individual to a lifetime organ or total body dose greater than the lifetime dose indicated by current ICRP recommendations<sup>(6-13)</sup> concerning "dose limits for individual members of the public".
- With respect to expected numbers of health effects due to the reentry and burnup of a nuclear waste payload (Table 6-21), lung and bone appear to be the critical organs. The expected number of cancers due to lung exposure, based on the minimum and the maximum population dose estimate, is between 0 and 376 lung cancers, and between 4 and 266 bone cancers in a world population of about 3.34 billion.
- While the magnitude of the expected health effects indicated by this assessment is not catastrophic, the careful consideration of measures which would prevent or significantly reduce the burnup in the upper atmosphere and the production of particles less than  $10\ \mu\text{m}$  diameter is extremely desirable. Any measure which would reduce the burnup fraction and/or the particle fraction, as defined for Equation (1), would have a proportional effect in reducing world population dose estimates and expected numbers of health effects.

### 6.3 References

- 6-1. Pardue, W. M., et al., "Preliminary Evaluation of the Space Disposal of Nuclear Waste", 8-32391(100), Battelle Memorial Institute, Columbus, Ohio (August 1977).
- 6-2. Dumbould, R. K., and Bjorklund, J. R., "NASA/MSFC Multilayer Diffusion Models and Computer Programs - Version 5", NASA CR-2631, H. E. Cramer Company, Salt Lake City, Utah (December 1975).
- 6-3. Houston, J. R., Strenge, D. L., and Watson, E. C., "DACRIN - A Computer Program for Calculating Organ Dose from Acute or Chronic Radionuclide Inhalation", BNWL-B-389, UC-41, Battelle-Northwest Laboratories, Richland, Washington (December 1974).
- 6-4. Stephens, J. B., and Susko, M., "Baseline Meteorological Soundings for Parametric Environmental Investigations at Kennedy Space Center and Vandenberg Air Force Base", NASA TMX-64986, NASA/Marshall Space Flight Center, Huntsville, Alabama (February 1976).
- 6-5. "Overall Safety Manual", prepared by NUS Corporation, Rockville, Maryland, for U.S. Atomic Energy Commission, Space Nuclear Systems Division (June 1975).
- 6-6. "Draft Environmental Impact Statement for the Management of Commercially Generated Radioactive Waste - Working Papers for Review", Battelle-Northwest Laboratories, Richland, Washington (December 1977).
- 6-7. "Final Environmental Impact Statement for the Space Shuttle Program", National Aeronautics and Space Administration, Headquarters, Washington, D.C. (April 1978).
- 6-8. "Task Group on Lung Dynamics for Committee II of the International Commission on Radiological Protection", Health Physics, 12, 173 (1966).
- 6-9. Strenge, D. L., "DACRIN - A Computer Program for Calculating Organ Dose from Acute or Chronic Radionuclide Inhalation: Modification for Gastrointestinal Tract Dose", BNWL-B-389-Supp, UC-41, Battelle-Northwest Laboratories, Richland, Washington (February 1975).
- 6-10. Krey, P. W., and Krajewski, B., "HASL Model of Atmospheric Transport", U.S. Atomic Energy Commission Report, HASL-25 (1969).
- 6-11. Krey, P. W., and Krajewski, B., "Comparison of Atmospheric Transport Model with Observations of Radioactive Debris", Journal of Geophysics Res., 75(15) (1970).
- 6-12. "The Metabolism of Compounds of Plutonium and Other Actinides", International Commission on Radiological Protection, ICRP Publication Number 19, Pergamon Press (1972).
- 6-13. "Recommendations of the International Commission on Radiological Protection", ICRP Publication 9, Pergamon Press (September 1965).

## 7.0 CONCLUSIONS

Based on the analysis presented in Sections 3 through 6, the following final conclusions have been reached:

- The mass of defense wastes stored at the three repositories is large ( $10^6$ - $10^7$  kg each, following preliminary preparation).
- The Hanford wastes exist in several forms, while the Savannah River and Idaho wastes are more uniform.
- The data on Hanford and Savannah River wastes are more complete than for Idaho. For space disposal purposes, the Hanford and Savannah River wastes are expected to be roughly similar.
- Chemical processes for concentration of defense wastes have been postulated but the supporting data base is limited and is generally based on laboratory experiments.
- The postulated concentration processes would reduce the number of required Shuttle flights to a manageable level ( $\sim 100$  to 400 flights for disposing of the projected year 2000 inventory).
- There are a number of waste forms that would be suitable for space disposal. Based on the study results to date, it appears that minimizing waste release under accident conditions will be a major consideration in waste form selection.
- Development of a suitable container appears to be feasible. Thermal control and shielding are manageable and not a major design problem. Minimizing waste release under credible accident conditions must be a major consideration.
- Of the various accident conditions examined, the fragments due to External Tank explosion and the thermal environment during reentry of an unprotected container present the greatest problems. Provision of sufficient additional protection to ensure container survival under these two conditions will be necessary and is probably feasible but has not been examined in detail.
- Recovery of a payload following an incomplete or misdirected OTV insertion burn is feasible provided that the perigee of the resulting orbit is high enough to allow time to conduct the rescue mission with a second OTV. This condition can be met if grossly

misoriented (off by 30° error or more) OTV burns can be avoided or terminated early. Under some conditions the failed OTV and the SOIS can be returned also. Under extreme conditions, boosting of the payload to a higher Earth orbit for later recovery is feasible even when Shuttle orbit return is not.

- Many of the failure modes identified have one or more potential workarounds in terms of backup systems, design changes or approaches, and procedures. In particular, workarounds for both the inadvertent reentry and ET explosion have been identified. Future detailed design activities may well uncover additional workarounds.
- The environmental impacts for two credible accidents has been examined in detail. The health risk from release of nuclear waste material in the upper atmosphere is greater than that from on-pad failure. The on-pad risk can be reduced further by imposing launch constraints based on meteorological conditions.
- The imposition of launch constraints based on meteorological conditions could result in delays of the launch of the Shuttle carrying the nuclear waste payload. If this Shuttle is launched second (as in the current baseline), this delay could significantly affect the chances of mission success.
- Under the worst case postulated conditions, a total release of a nuclear waste payload in the upper atmosphere would be a significant accident. The consequences would be spread worldwide. Measures to reduce the percentage release or the percentage of inhalable particles would mitigate expected adverse effects.

## 8.0 RECOMMENDATIONS

Prior to any development or implementation decision on space disposal of nuclear waste, certain critical problems will have to be addressed by NASA and DOE. The general areas requiring effort are defined in Section 2.7 of this volume and in Volume III. Some specific recommendations concerning the technical areas discussed in this volume of the report are summarized below:

- Further definition of the defense nuclear waste radionuclide composition (particularly for Idaho calcine) is needed (DOE)\*
- Definition and demonstration of nuclear waste concentration methods are required for all three waste sources (DOE)
- The characteristics and behavior of calcine and alternative waste forms under credible accident conditions as a means for reducing radionuclide release need to be examined further (DOE)
- The behavior of the waste container in the blast fragment environment and potential means of additional protection needs to be studied in more detail (NASA)
- The possibility of protecting the unshielded container during inadvertent reentry by addition of a layer of ablative material to the outer wall should be considered (NASA)
- Methods for detecting and terminating a critically misdirected OTV Earth escape insertion burn and payload safety or rescue need to be developed (NASA)
- Failure modes potentially leading to External Tank explosion need to be examined further and any potential workarounds or mitigation measures defined (NASA)
- Quantitative reliability data need to be developed for all elements of the space disposal mission (NASA)
- Methods for reducing the number of inhalable particles produced during an on-pad accident or inadvertent reentry need to be examined (DOE)
- The health effects from particle resuspension and ingestion require further study (NASA)
- The effect on overall mission probability of success and safety of launching the waste payload first rather than second needs to be evaluated (NASA).

---

\*Parenthetical notation after each recommendation indicates prime agency responsibility.

**APPENDIX A**  
**ACRONYMS AND ABBREVIATIONS**

A-1



APPENDIX A  
ACRONYMS AND ABBREVIATIONS

a.u.	astronomical unit
AMAD	activity median aerodynamic diameter
ASME	American Society of Mechanical Engineers
atm	atmospheres
ATO	abort-to-orbit
ATOA	abort-to-once-around
BNWL	Battelle-Northwest Laboratories
B.R.	burn rate
C	degrees centigrade
C <sub>3</sub>	twice the energy per unit mass
cal	calories
CANDU	Canadian deuterium uranium reactor
cc	cubic centimeters (cm <sup>3</sup> )
c.g.	center of gravity
CFR	Code of Federal Regulations
Ci	Curies
μ Ci	micro-Curies
cm	centimeters
COE	center of explosion
CPIA	Chemical Propulsion Information Agency
DOE	U.S. Department of Energy
DOT	U.S. Department of Transportation
EIS	environmental impact statement
ERDA	U.S. Energy Research and Development Administration
ET	Space Shuttle's External Tank
EVA	extravehicular activity in space
g	grams
gal	gallons (U.S.)
G.I.	gastrointestinal (tract)
HLW	high-level waste
H <sub>2</sub> /O <sub>2</sub>	hydrogen-oxygen
HTGR	high-temperature gas-cooled reactor

ICRP	International Commission on Radiological Protection
JSC	NASA's Johnson Space Center, Houston
kg	kilogram
km	kilometer
KS	kickstage
KSC	Kennedy Space Center, Florida
kW	kilowatt
L	lymph
LeRC	NASA's Lewis Research Center, Cleveland
LH <sub>2</sub>	liquid hydrogen
LO <sub>2</sub>	liquid oxygen
LM	thoracic lymph
LMFBR	liquid metal fast breeder reactor
LWR	light water reactor
m	meters
μ m	micrometers
m/s	meters per second
<u>M</u>	molar
MT	metric tons
Mev	million electron volts
MLDM	Multilayer Diffusion Model (MSFC's)
MMH	monomethyl hydrazine
MSFC	NASA's Marshall Space Flight Center, Huntsville, Alabama
N	Newtons
N/cm <sup>2</sup>	Newtons per square centimeter
N <sub>2</sub> O <sub>4</sub>	nitrogen tetroxide
NASA	National Aeronautics and Space Administration
NEP	nuclear electric propulsion
NP	nasopharyngeal
NPPF	Nuclear Payload Preparation Facility
NRC	Nuclear Regulatory Commission
O/F	oxidizer to fuel ratio
OMS	Orbital Maneuvering System (Shuttle)
OTV	Orbit Transfer Vehicle
P	pulmonary

PCR	Payload Changeout Room
PL	payload
rem	roentgen equivalent, man
R&D	research and development
RCS	Reaction Control System (Shuttle)
RETAC	Reentry Thermal Analysis Code
RS	Reentry System
RTG	radioisotope thermal generator
RTLS	return-to-landing-site
SEP	solar electric propulsion
SOIS	Solar Orbit Insertion Stage
SRB	Solid Rocket Booster (Shuttle)
SRM	Solid Rocket Motor (Shuttle)
SS	Space Shuttle
SSME	Space Shuttle Main Engine
SSP	solar sail propulsion
STS	Space Transportation System
$\Delta T$	change in temperature
TB	tracheobronchial
TBD	to be determined
TBP	tributyl phosphate
USAF	U.S. Air Force
$\Delta V$	change in velocity
W	Watt
WCF	waste concentration factor

**APPENDIX B**  
**METRIC/ENGLISH CONVERSION FACTORS**

B-1

APPENDIX B  
METRIC/ENGLISH CONVERSION FACTORS

<u>To convert</u>	<u>into</u>	<u>multiply by</u>
atmospheres (atm) . . . . .	pounds per square inch (psi) . . . . .	14.70
atmospheres (atm) . . . . .	pounds per square ft (psf) . . . . .	2116.8
calories (cal) . . . . .	British thermal units (Btu) . . . . .	$3.9685 \times 10^{-3}$
calories per gram (cal/g) . . . . .	British thermal units per pound (Btu/lb) . . . . .	1.80
centimeters (cm) . . . . .	inches (in) . . . . .	0.3937
centimeters (cm) . . . . .	feet (ft) . . . . .	$3.281 \times 10^{-2}$
centimeters (cm) . . . . .	yards (yd) . . . . .	$1.094 \times 10^{-2}$
cubic centimeters (cm <sup>3</sup> ) . . . . .	cubic inches (in <sup>3</sup> ) . . . . .	0.0610
cubic meters (m <sup>3</sup> ) . . . . .	cubic feet (ft <sup>3</sup> ) . . . . .	35.32
cubic meters (m <sup>3</sup> ) . . . . .	gallons (gal) . . . . .	264.2
degrees Centigrade (°C) . . . . .	degrees Fahrenheit (°F) . . . . .	$1.8 C + 32^*$
degrees Kelvin (°K) . . . . .	degrees Rankine (°R) . . . . .	1.8
grams (g) . . . . .	pounds (lb) . . . . .	$2.205 \times 10^{-3}$
kilograms (kg) . . . . .	pounds (lb) . . . . .	2.205
kilometers (km) . . . . .	statute miles (mi) . . . . .	0.6214
kilometers (km) . . . . .	nautical miles (n.mi.) . . . . .	0.540
kilometers (km) . . . . .	feet (ft) . . . . .	3281
kilowatts (kW) . . . . .	Btu per hour (Btu/hr) . . . . .	3413
meters (m) . . . . .	inches (in) . . . . .	39.37
meters (m) . . . . .	feet (ft) . . . . .	3.281
meters (m) . . . . .	yards (yd) . . . . .	1.094

\*NOTE: Multiply by 1.8 and then add 32.

<u>To convert</u>	<u>into</u>	<u>multiply by</u>
meters per second (m/s) . . . . .	feet per second (ft/s) . . . . .	3.281
metric tons (MT) . . . . .	pounds (lb) . . . . .	2205
metric tons (MT) . . . . .	tons (T) . . . . .	1.102
micro-meters ( $\mu$ m) . . . . .	meters (m) . . . . .	$1.0 \times 10^{-6}$
Newtons (N) . . . . .	pounds force ( $lb_f$ ) . . . . .	0.2248
Newtons per $cm^2$ ( $N/cm^2$ ) . . . . .	pounds per square inch (psi) . . . . .	1.4504

APPENDIX C

WASTE MIX AND FORM DATA DEVELOPED FOR COMMERCIAL WASTE

C-1

## APPENDIX C

## WASTE MIX AND FORM DATA DEVELOPED FOR COMMERCIAL WASTE

Initially, Battelle's Columbus Laboratories was assigned the task of examining commercial high-level waste (HLW) to determine waste mixes and forms suitable for space disposal. Subsequently, this emphasis was changed to examine defense HLW rather than commercial HLW. This appendix deals with the initial efforts to develop data regarding commercial waste mixes and forms acceptable for space disposal. It also covers the effort on waste mixes and forms for commercial HLW submitted as input to the Commercial Nuclear Waste Management Generic Environmental Impact Statement (GEIS).

The previous study "Preliminary Evaluation of the Space Disposal of Nuclear Waste"<sup>(C-1)</sup>, examined several mixes for space disposal; these included:

- Mix 1: Spent fuel is leached and the entire dissolver solution is solidified and sent to space.
- Mix 2: 99.5% of U is separated from the spent fuel; the remainder of the dissolver solution (fission products, actinides, and Pu) is solidified and sent to space.
- Mix 3: 99.5% of U and Pu are separated from the spent fuel; the remaining waste products (fission products and actinides) are solidified and sent to space.
- Mix 4: 0.1% U and Pu, the actinides, and rare earth fission products except cerium are solidified and sent to space.
- Mix 5: 94% of the Tc is recovered from the dissolver solution, then solidified and sent to space.

Mix 3 was selected as the baseline case at that time, but because of plutonium safeguards and proliferation concerns, Mixes 2 and 3 were reevaluated in this study. In addition, an attempt was made to optimize Mix 2 by selective removal of specific nuclides in order to reduce mass, heat generation rate, and radiation dose rate. Results of this optimization effort would, in general, also apply to Mix 3. Finally, a total of eight waste mixes was examined for the Commercial Nuclear Waste Management GEIS. These included Mixes 1, 2, 3, and 5 of the previous study plus:

- Mix 4<sup>1</sup>: Lanthanides plus Am, Cm, and Np - This mix assumes extraction of U and Pu from the spent fuel dissolver



solution, followed by partitioning of the lanthanides plus Am, Cm, and Np, and solidification for space disposal. This replaces Mix 4 of the previous study.

- Mix 6: Iodine - Fission product iodine is collected via the reprocessing off-gas treatment system and solidified as  $Ba(IO_3)_2$  for space disposal.
- Mix 7: Carbon -  $^{14}C$  in the form of  $CO_2$  is collected via the reprocessing off-gas treatment system and solidified as solid  $CO_2$  or  $CaCO_3$ .
- Mix 8: Am and Cm - This mix is an extension of Mix 4' to separate Am and Cm, followed by solidification for space disposal.

### Mix 2 Optimization

Table C-1 presents the elements considered for removal from Mix 2 in order to optimize mass, heat generation rate and radiation dose rate. Pu removal yields significant improvement in mass and fair improvement in heat generation; however, this changes Mix 2 to Mix 3. Rare earth elements such as Nd, Ce, and Eu may be useful, but very difficult to separate. A large portion of the Zr and Mo could probably be removed from the liquid HLW by concentration precipitation. These elements are useful metals and do not constitute a disposal hazard if left on Earth. Cs-Ba and Sr-Y could possibly be removed by oxalate addition, which would cause precipitation of these elements, or ion exchange.

TABLE C-1. MIX 2 OPTIMIZATION

Mass		Heat Generation		Radiation Dose Rate	
Element	% Reduction	Element	% Reduction	Element	% Reduction
Pu	22.0	Pu	8	Eu	Not Significant
Nd	9.5	Cs-Ba	35-40	Cs	
Zr	9.0	Sr-Y	20-25		
Mo	8.7				
Cs	5-6				
Ce	6.6				

### Mix 2 Criticality

Since Mix 2 contains a significant amount of Pu, a series of calculations was performed to determine if a criticality problem existed. KENO<sup>(C-2)</sup>, a Monte Carlo criticality code, was used for all calculations. The result of a KENO calculation is an estimate of  $K_{eff}$ , the effective neutron multiplication factor. When  $K_{eff} \geq 1.0$ , criticality will occur. Table C-2 shows the results of the criticality analysis. The results clearly indicate that Mix 2 is not a viable option at projected payload masses of approximately 5 MT. Criticality can be prevented by the use of a neutron absorber such as boron which absorbs neutrons throughout the fission energy range. Resonance neutron absorbers, such as the majority of the fission products, have little poisoning effect.

TABLE C-2. MIX 2 CRITICALITY ANALYSIS

Case Number	Density, g/cc	Mass, kg	Shape	Chemical Composition	Reflector/Thickness, cm	$K_{eff}$
1	5.0	5000	cube	oxide	none	1.078
2	4.0	5000	sphere	oxide	Du/20	1.124
3	4.0	3600	sphere	oxide	Du/20	1.061
4	4.0	2100	sphere	oxide	Du/20	0.939
5	3.74	4670	sphere	boride	Du/20	0.631
6	3.42	5000	sphere	oxide-65% w/o Al-35% w/o	Du/20	0.858

NOTE: Results generated from KENO code.

### Mix 3

The exclusion of Pu as a waste constituent results in a waste payload without criticality problems. Furthermore, the Pu, which is a potentially valuable energy resource is saved for use. Mix 3 continues as the baseline for space disposal of commercial waste.

### Mix 4

Essentially all of the actinides and lanthanides in spent fuel are dissolved by nitric acid during fuel reprocessing. Under these conditions, the

actinides and lanthanides that do not extract into TBP as used in Purex are readily removed from the high-level liquid waste by solvent extraction with the bidentate, dihexyl-N, N-diethyl carbamylmethylene phosphonate.<sup>(C-3)</sup> The solvent extract may then be stripped and the actinides and lanthanides calcined to give the mixture shown in Table C-3. It should be realized, however, that these compositions are very approximate, and this flowsheet has never been demonstrated on a large scale. This waste mix would constitute approximately 2.7% of the dissolved spent fuel.

TABLE C-3. MIX 4' COMPOSITION

Compound	Percent
U <sub>3</sub> O <sub>8</sub>	21.10
NpO <sub>2</sub>	1.22
PuO <sub>2</sub>	0.78
Am <sub>2</sub> O <sub>3</sub>	3.55
Cm <sub>2</sub> O <sub>3</sub>	1.18
Ln <sub>2</sub> O <sub>3</sub>	70.30
ZrO <sub>2</sub>	0.01
Tc <sub>2</sub> O <sub>7</sub>	1.18
RuO <sub>2</sub>	0.19
PdO	<u>0.49</u>
	100.00

Since Am, Cm, Np, and Pu oxides make up approximately 6.8% of the mix, a criticality problem may exist. If this mix is ever considered as a serious candidate for space disposal, criticality experiments and calculations will have to be performed. One of the benefits of this mix is that essentially all long-lived radionuclides are removed from Earth using approximately 60% of the flights necessary for Mix 3.

#### Mix 6 (Iodine)

Spent fuel contains small quantities of <sup>129</sup>I, a radionuclide which has a half-life of 15.9 million years. Moreover, the chemistry of iodine favors the

migration of this element<sup>(C-4)</sup> and, under certain conditions, it might be released to man's environment in the distant future if it is placed in a geologic repository.<sup>(C-5 through C-7)</sup> Although somewhat speculative, concerns for possible iodine migration from a geologic repository in the distant future, coupled with the long half-life of  $^{129}\text{I}$ , have motivated the development of a space disposal alternative for this element.

Iodine forms volatile chemical species that tend to migrate to the dissolver off-gas system when spent fuel is dissolved in nitric acid during reprocessing. With proper air sparging of the dissolver solution, it is expected that approximately 99% of the iodine initially in the spent fuel will be volatilized and captured using silver zeolite adsorbent or possibly the Iodex scrubbing process.<sup>(C-8 through C-12)</sup> However, that small portion which does not volatilize will eventually report to the other reprocessing wastes or be lost to the environment. Captured iodine can be converted to  $\text{Ba}(\text{IO}_3)_2$ . This mix would constitute approximately 0.05% of the dissolved spent fuel.

### Mix 7 (Carbon)

Spent fuel contains small quantities of  $^{14}\text{C}$ , a radionuclide which has a half-life of 5730 years. This element tends to form gaseous carbon dioxide during fuel reprocessing. If the  $^{14}\text{C}$  is released into the environment, it will be inhaled or ingested as food by nearly all living organisms, including man. The chemistry of carbon is such that, under certain conditions, it may also migrate<sup>(C-5 and C-6)</sup> from a geologic repository eventually in the distant future. For these reasons  $^{14}\text{C}$  is considered as a candidate for partitioning and space disposal.

Carbon recovery conceptually takes place in a reprocessing plant dissolver off-gas system after iodine recovery. The process involves sorption of  $\text{CO}_2$  on molecular sieves, with prior removal of  $\text{NO}_x$  and  $\text{H}_2\text{O}$  being required for efficient  $\text{CO}_2$  recovery.  $\text{CO}_2$  is desorbed and captured by a slurry of  $\text{CaO}$  which forms  $\text{CaCO}_3$ .  $\text{CO}_2$ , as dry ice, could alternatively be formed. This mix would constitute approximately 0.13% of the dissolved spent fuel as  $\text{CaCO}_3$  or 0.06% as solid  $\text{CO}_2$ . The majority of this material (> 99%) is non-radioactive  $^{12}\text{C}$  compounds which are also formed during these processes.

**Mix 8 (Am and Cm)**

This mix can be quickly eliminated from consideration by an examination of criticality data. For example, the estimated fast critical mass for bare  $^{241}\text{Am}$  metal is 113.5 kg, and for  $^{245}\text{Cm}$  metal is 23.2 kg. (C-13) Clearly, 5 MT of Am and Cm must be ruled out as a possible mix, unless extreme dilution and neutron poisoning is used.

References

- C-1. Davis, D. K., Miller, N. E., Pardue, W. M., and Rice, E. E., "Preliminary Evaluation of the Space Disposal of Nuclear Waste", Report No. 8-32391(100), Battelle-Columbus Laboratories, Columbus, Ohio (August 30, 1977).
- C-2. Petrie, L. M., and Cross, N. F., "KENO-IV, An Improved Monte Carlo Criticality Program", ORNL-4938, Oak Ridge National Laboratory, Oak Ridge, Tennessee (November 1975).
- C-3. Tedder, D. W., and Blomeke, J. O., "Actinide Partitioning and Transmutation Program Progress Report", ORNL/TM-6056, Oak Ridge National Laboratory, Oak Ridge, Tennessee (October 1977).
- C-4. Wolfsberg, K., "Sorption-Desorption Studies of Nevada Test Site Alluvian and Leaching Studies of Nuclear Test Debris", LA-7216-MS, Los Alamos Scientific Laboratory of the University of California, Los Alamos, New Mexico (April 1978).
- C-5. Burkholder, H. C., et al., "Incentives for Partitioning High-Level Waste", BNWL-1927, Battelle-Northwest Laboratories, Richland, Washington (November 1975).
- C-6. Kubo, A. S., "Waste Management More Broadly", NR-CONF-001, proceedings of the Nuclear Regulatory Commission Workshop on the Management of Radioactive Waste: Waste Partitioning as an Alternative on June 8-10, 1976, at the Battelle-Seattle Research Center, Seattle, Washington, National Technical Information Service, Springfield, Virginia (June 1976).
- C-7. Fried, S., et al., "The Migration of Long-Lived Radioactive Processing Wastes in Selected Rocks", ANL-78-46, Argonne National Laboratory, Argonne, Illinois (April 1978).
- C-8. Campbell, D. O., and Buxton, S. R., "LWR Fuel Reprocessing and Recycle Program Quarterly Report", ORNL/TM-5547, Oak Ridge National Laboratory, Oak Ridge, Tennessee (July 1976).
- C-9. Campbell, D. O., "LWR Fuel Reprocessing and Recycle Program Quarterly Report", ORNL/TM-5660, Oak Ridge National Laboratory, Oak Ridge, Tennessee (November 1976).
- C-10. Campbell, D. O., et al., "LWR Fuel Reprocessing and Recycle Program Quarterly Report", ORNL/TM-5760, Oak Ridge National Laboratory, Oak Ridge, Tennessee (February 1977).
- C-11. Campbell, D. O., Buxton, S. R., and Pattison, W. L., "LWR Fuel Reprocessing and Recycle Program Quarterly Report", ORNL/TM-5987, Oak Ridge National Laboratory, Oak Ridge, Tennessee (August 1977).

- C-12. Davis, Wallace, Jr., "A Model of Iodine Transport and Reaction Kinetics in a Nuclear Fuel Reprocessing Plant", ORNL/NUREG-16, Oak Ridge National Laboratory, Oak Ridge, Tennessee (August 1977).
- C-13. Clayton, E. D., "Anomalies of Criticality", BNWL-SA-4868, Rev. 3, Battelle-Northwest Laboratories, Richland, Washington (April 1976).

APPENDIX D

REENTRY THERMAL ANALYSIS CODE (RETAC)



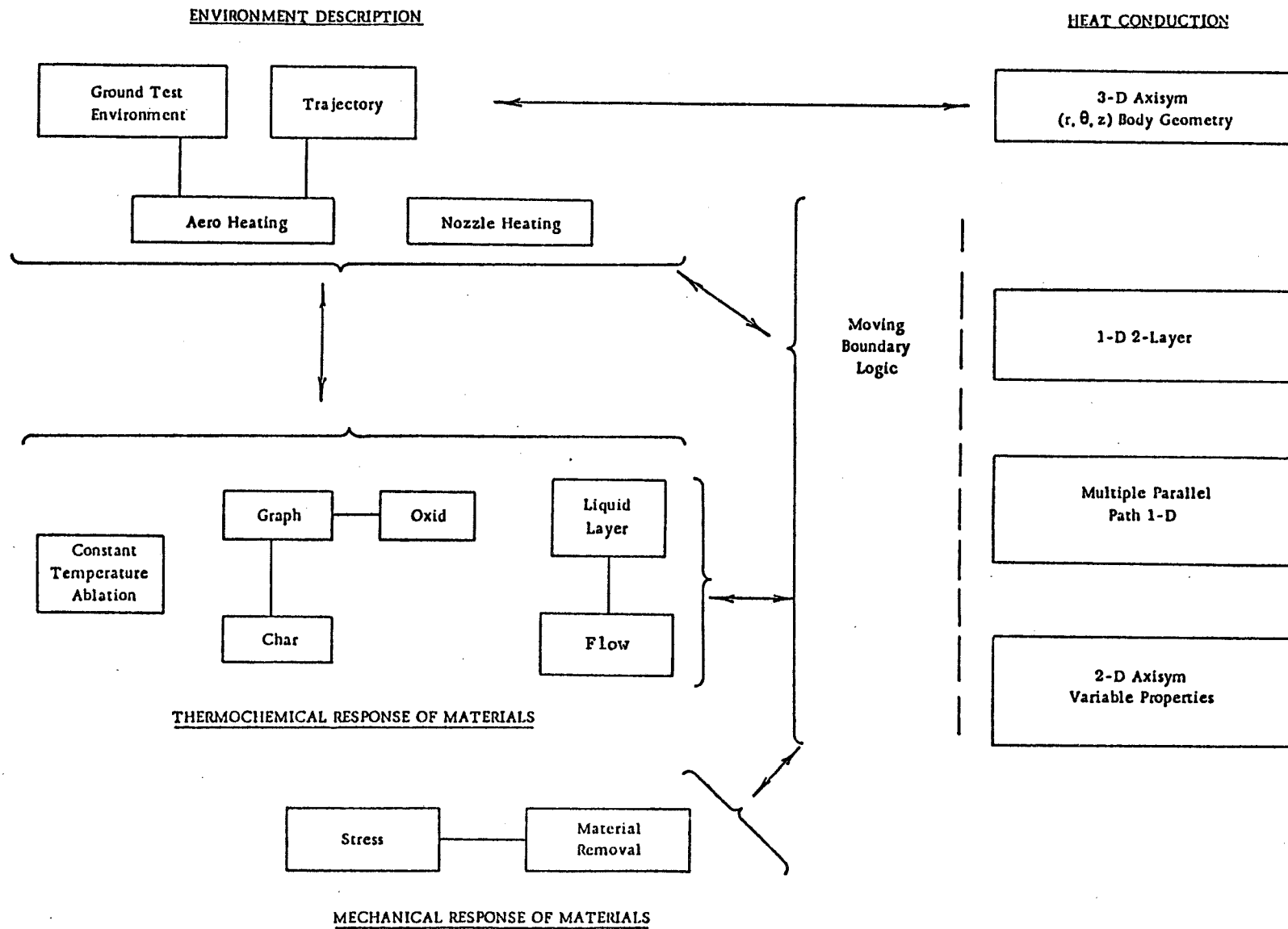
## APPENDIX D

## REENTRY THERMAL ANALYSIS CODE (RETAC)

The Reentry Thermal Analysis Code (RETAC) consists of a family of subprograms primarily directed toward reentry heating which can be combined in various ways to best simulate the specific problem under consideration. It is being upgraded almost continually both with improvements in existing subprograms and with the addition of new subprograms. Figure D-1 shows a general layout of the currently operational RETAC subprograms. They are, in general, divided into four areas: environment description, thermochemical response of materials, mechanical response of materials, and heat conduction. The heat conduction is coupled to the thermochemical and mechanical responses by moving boundary logic and a feedback of nose radius change and wall temperature to the aeroheating subroutine. Shape change feedback to the ground test environment and trajectory subprograms have been incorporated in certain cases. The link between the environment and material response includes gas boundary-layer blocking effects and surface temperature. In addition to the subprograms shown, a special subprogram can provide a simulation of internal vaporizing reservoirs with subsequent flow through a porous structure to the surface.

It should be noted that not all possible combinations of subprograms have been run to date; in fact, some programming changes are generally necessary when a new combination is first run. However, these changes generally are minor and, as experience has been gained in the use of RETAC on various problems, they are proceeding quite smoothly. This is in line with the basic philosophy of RETAC development which is to build a family of fairly simple subprograms which can then be combined in a flexible manner to fit the specific problem. As many direct interactions of pertinent phenomena as possible are incorporated. To remain flexible, an explicit finite difference method of solution is employed for the heat conduction equation.

Four alternate methods of calculating internal conduction are presently available. Multilayer, one-dimensional computations may be carried out with combined series-and-parallel heat flow paths to simulate certain two- and even three-dimensional effects. While these techniques are still used for certain



D-2

FIGURE D-1. GENERAL LAYOUT OF REENTRY THERMAL ANALYSIS CODE (RETAC)

problems, they have definite limitation. Therefore, alternate approaches have been developed which are a general two-dimensional axisymmetric subprogram and a three-dimensional  $(r, \theta, z)$  subprogram. A two-dimensional moving boundary scheme has been developed to remove material and predict shape change.

The aerodynamic heating subroutine is essentially the original subroutine developed for RTG reentry studies. Gas gap radiation has been added for superorbital conditions, however. The aerodynamic heating subroutine calculates heating to the reentry body on the basis of local properties (pressure, temperature), configuration, and reentry mode. Either existing internal (to the program) equations can be employed, or trajectory data supplied from the 3-degree-of-freedom or 6-degree-of-freedom computer program via punched-card input. In the aeroheating subprogram, heat transfer correlations covering free molecular theory, transition theory, and boundary layer theory are used. Coupling of the aeroheating calculations with the ablation and heat conduction analyses provides for calculation of the reentry shield surface temperature(s). Cooling of the reentry system during the latter portion of reentry is, therefore, automatically included in the analysis.

The GRAPH ablation subroutine essentially uses the general aerothermal model which includes the reaction rate-controlled regime, the diffusion-controlled regime, and sublimation regime. The model includes continuous transitions between the regimes and also predicts when the transition occurs. It has also been modified for other oxidation processes such as tungsten oxidation.

Another ablation model used in the program is a constant temperature phase change with mass removal. This can be used for surface melting or processes such as Teflon ablation. By allowing this model to simulate the pyrolysis boundary movement and gas evolution and combining it with subprogram GRAPH at the surface of the carbon char, CHAR, a subprogram for charring ablators, has also been developed and used. An alternate method for handling charring ablators is also available in which a pyrolysis zone is defined by specifying the properties including density as a function of temperature. The rate of gas evolution is obtained by determining the rate of change of the density of the material remaining. A time delay for the gases to reach the surface can also be included.

A generalized thermochemical response model can be used in which the subroutine OXID calculates the mass loss in the reaction rate- or diffusion-controlled regimes and the phase change ablation model takes over when a specified temperature is reached. This generalized model can ablate through layers of different materials. It can also be used in place of the GRAPH subroutine with sublimation handled in the phase change model.

The FLOW subroutine calculates the flow through a porous structure from an arbitrary number of internal reservoirs. The porosity between each reservoir and various surface locations is specified as input. The subroutine calculates the pressure within each reservoir by vapor pressure and continuity relationships and then obtains the pressure differences to the various surface locations using the external pressure distribution. The changing distances between the reservoirs and the surface locations are also recalculated as the surface recedes. The final result is a distribution of ejected flow along the surface. The heat transfer between the flowing fluid and the porous matrix can also be added to the energy equation in the conduction program.

The liquid layer subprogram provides a detailed description of the dynamics of a liquid layer on an axially symmetric reentry body surface. The liquid layer is coupled into the external flow by shear and surface vaporization. It is coupled to the solid body by the liquid injection rate and distribution, surface temperature distribution, and body shape. For parametric studies, this subprogram can be run separately from RETAC.

The mechanical response of materials is predicted by a subprogram STRESS in which any of a variety of models can be used. This is then coupled with material removal logic by some assumed failure criterion. This material removal is then linked to the heat conduction by the same moving boundary logic that is used for thermochemical material removal. At the present time, only one-dimensional stress subprograms have been linked directly with the heat conduction. However, two-dimensional thermal stress calculations have been made using two-dimensional temperature profiles generated by RETAC, so the extension to a two-dimensional linked model is relatively straightforward.

APPENDIX E

CALCULATION OF THE SPACE SHUTTLE EXTERNAL  
TANK FIREBALL TEMPERATURE AND HEAT FLUX

E-1

## APPENDIX E

CALCULATION OF THE SPACE SHUTTLE EXTERNAL  
TANK FIREBALL TEMPERATURE AND HEAT FLUX

This appendix describes the equations and data that were used to calculate the fireball temperature and surface heat flux (as a function of time) resulting from a postulated fireball of the Space Shuttle External Tank (ET). The results of these calculations and many of the assumptions are presented in Section 5.1.1.1. The Bader "Liquid-Propellant Rocket Abort Fire Model" (Reference E-1) were employed for this case, with modifications appropriate for the Space Shuttle vehicle. Solutions to the fireball energy equation for the two time regions of interest (the time from ignition,  $t = 0$ , until the time the liquid propellants have all been consumed,  $t = t_b$ , and the time,  $t = t_b$ , until the fireball stem lifts off the ground,  $t = 1.5 t_b$  -- see Figure 5-1) are presented below. Also, a discussion of fireball diameter is presented.

Temperature and Heat Flux Calculations for  $t \leq t_b$ 

The energy equation (Equation 10 of Reference E-1) for the fireball is derived by equating the rate of internal energy change and expansion work of the fireball to the difference between the rate of energy added by fuel (propellant) addition and the rate of energy loss by radiation, as shown below:

$$Rh_r - \epsilon\sigma AT^4 = \frac{d(W_h_p)}{dt} \quad (1)$$

where:

$R$  = Constant Rate of Fuel Addition

$h_r = h_{\text{reactants}}$  = Specific Enthalpy of Formation  
for Propellants (defined as  $h_{in}$  in Reference E-1)

$\epsilon$  = Fireball Emissivity

$\sigma$  = Stephan-Boltzmann constant

$A$  = Fireball Surface Area

$T$  = Fireball Temperature

$W$  = Mass of Fireball ( $W_b$  = total mass of propellants)

$h_p = h_{\text{products}}$  = Specific Enthalpy of Formation  
for Fireball (defined as  $h_{FB}$  in Reference E-1)

$t$  = time (defined as  $\tau$  in Reference E-1)

Equation (1) can be rearranged as:

$$Rh_r = \epsilon\sigma AT^4 + W \frac{dh_p}{dt} + h_p \frac{dW}{dt} , \quad (2)$$

but,  $\frac{dW}{dt}$  is equal to R, the constant rate of fuel addition. Thus, we can rewrite Equation (2) as:

$$R (h_r - h_p) = \epsilon\sigma AT^4 + W \frac{dh_p}{dT} \frac{dT}{dt} . \quad (3)$$

The surface area of the fireball, A, can be expressed in terms of the density,  $\rho$ , rate of fuel addition, R, and time, t. The surface area of the spherical fireball is defined as:

$$A = 4\pi r^2 , \quad (4)$$

where, r is the radius of the fireball. However, the density of the fireball at any given time can be expressed as:

$$\rho = \frac{\text{Mass}}{\text{Volume}} = \frac{W}{\frac{4}{3}\pi r^3} = \frac{Rt}{\frac{4}{3}\pi r^3} . \quad (5)$$

Therefore, the radius of the fireball can be expressed as:

$$r = \left( \frac{3Rt}{4\pi\rho} \right)^{1/3} ; \quad (6)$$

and, thus the surface area of the fireball is:

$$A = 4\pi \left( \frac{3Rt}{4\pi\rho} \right)^{2/3} . \quad (7)$$

Also, from the equation of state:

$$P = \rho RT , \quad (8)$$

where:

P = Pressure

R = Gas Constant

T = Temperature.

Equation (7) can be rewritten as:

$$A = 4\pi \left( \frac{3RtRT}{4\pi\rho} \right)^{2/3} . \quad (9)$$

Substituting Equation (7) into Equation (3) and noting that  $R = W/t$ , we arrive at a first order, non-linear differential equation:

$$\frac{dT}{dt} = \left[ (h_r - h_p) - St^{2/3} T^{14/3} \right] \left[ \frac{1}{t} \right] \left[ \frac{1}{dh_p/dT} \right], \quad (10)$$

where:

$$S = 4\pi\epsilon\sigma \left( \frac{3R}{4\pi p} \right)^{2/3} R^{-1/3}. \quad (11)$$

The relationship between  $h_p$  and  $T$  for the Space Shuttle cryogenic propellants was established and presented in Section 5.1.1.1 of this report. Table E-1, below, presents data calculated for  $h_p$  and  $T$ .

TABLE E-1. ENTHALPY OF PRODUCTS FOR VARIOUS VALUES OF TEMPERATURE FOR ET FIREBALL CASE

$T, ^\circ K$	$h_p, \text{ cal/g}$	$T, ^\circ K$	$h_p, \text{ cal/g}$
2100	-1844	2800	-836.4
2200	-1752	2900	-540.4
2300	-1653	3000	-178.8
2400	-1542	3050	26.27
2500	-1414	3100	251.9
2600	-1261	3200	739.6
2700	-1073		

NOTE: These data are plotted in Figure 5-2 of Section 5.1.1.1.

The data in Table E-1 were fitted to a fifth-order polynomial of the form:

$$h_p = B_0 + B_1 T + B_2 T^2 + B_3 T^3 + B_4 T^4 + B_5 T^5, \quad (12)$$

with,

$$\frac{dh_p}{dT} = B_1 + 2B_2 T + 3B_3 T^2 + 4B_4 T^3 + 5B_5 T^4. \quad (13)$$



For  $h_p$  in units of cal/g and T in  $^{\circ}\text{K}$ , the constants are as follows:

$$\begin{aligned} B_0 &= +1.615762 \text{ E}+05 \\ B_1 &= -3.309199 \text{ E}+02 \\ B_2 &= +2.645649 \text{ E}-01 \\ B_3 &= -1.044912 \text{ E}-04 \\ B_4 &= +2.036638 \text{ E}-08 \\ B_5 &= -1.557586 \text{ E}-12. \end{aligned}$$

The value of  $h_r$  was computed using the heats of formation as given in Reference E-2 for liquid hydrogen and liquid oxygen at their normal boiling points and the ratio of hydrogen to oxygen, as particular to the Space Shuttle ET. The value of  $h_r$  for these assumptions is -213 cal/g (-384 BTU/lb).

To obtain the value of S we must first define certain constants and determine the value of R, the constant rate of fuel (propellant) addition.

For a spherical fireball under the influence of atmospheric pressure ( $P = 1.0 \text{ atm}$ ), the average density of the gases at the time of liftoff ( $t = t_b$ ) can be approximated by assuming, for temperature, the value of  $2989^{\circ}\text{K}$  (see Section 5.1.1.1). From the equation of state, Equation (8), we have:

$$\rho = \frac{P}{RT} = \frac{(1.0 \text{ atm})}{\left(0.082 \frac{\text{m}^3\text{-atm}}{\text{kg-mole-}^{\circ}\text{K}}\right) \times \left(\frac{\text{kg-mole}}{14,006 \text{ kg}}\right) \times (2989^{\circ}\text{K})}$$

Thus,

$$\rho = 0.05714 \text{ kg/m}^3 \quad (0.003565 \text{ lb}_m/\text{ft}^3)$$

From Equation (6) and  $W = R \times t$ , the radius of the fireball at the time of liftoff ( $t = t_b$ ) is given as:

$$r_b = \left(\frac{3}{4\pi\rho}\right)^{1/3} W_b^{1/3} \quad (14)$$

$$r_b = 1.61 W_b^{1/3} \quad (\text{when } W_b \text{ is in kg})$$

or

$$[r_b = 4.063 W_b^{1/3} \quad (\text{when } W_b \text{ is in lb}_m)]$$

Reference E-1 defines the relationship between the time of liftoff,  $t_b$ , and the fireball radius at that time,  $r_b$ . This is given as:

$$t_b = \left( \frac{3r_b}{g} \right)^{1/2}, \quad (15)$$

where,  $g$  is the acceleration of gravity,  $9.8 \text{ m/s}^2$ . After substituting Equation (14) into the above relationship we arrive at:

$$t_b = 0.702 W_b^{1/6} \quad (\text{when } W_b \text{ is in kg}) \quad (16)$$

or

$$[t_b = 0.615 W_b^{1/6} \quad (\text{when } W_b \text{ is in lb}_m)]$$

Since the constant rate of fuel (propellant) addition,  $R$ , is given as:

$$R \text{ (kg/s)} = \frac{W}{t} = \frac{W_b}{t_b} = \frac{W_b}{0.702 W_b^{1/6}}$$

We have:

$$R = 1.425 W_b^{5/6} \quad (\text{when } W_b \text{ is in kg}) \quad (17)$$

or

$$[R = 1.626 W_b^{5/6} \quad (\text{when } W_b \text{ is in lb}_m)]$$

For the case of the Space Shuttle,  $W_b = 7.12 \text{ E}+05 \text{ kg}$  ( $1.57 \text{ E}+06 \text{ lb}_m$ ), we arrive at:

$$R = 1.074 \text{ E}+05 \text{ kg/s}$$

$$r_b = 144 \text{ m}$$

$$t_b = 6.63 \text{ s.}$$

Therefore, the fireball is expected to lift off the ground at 6.63 seconds after the initial fire; it is expected to have a diameter of 288 m. Reference E-1 indicates that the time of stem liftoff (see Figure 5-1) is given as  $1.5 \times t_b$ ; thus, the stem is expected to lift off the ground at 9.95 seconds after the initial fire.

The value of  $S$ , Equation (11), can now be determined from the following:

$$\epsilon = 1.0$$

$$\sigma = 1.3545 \text{ E}-08 \text{ cal}/(\text{m}^2 \cdot \text{K}^4 \cdot \text{s})$$

$$R = 5.855 \text{ E}-03 \text{ m}^3 \cdot \text{atm}/(\text{kg} \cdot \text{K})$$

$$P = 1.0 \text{ atm}$$

$$R = 1.074 \text{ E}+05 \text{ kg/s.}$$

We arrive at

$$S = 4.477 \text{ E-14} \left( \frac{\text{cal}}{\text{g}} \right) \left( \frac{1}{\text{°K}^{14/3}} \right) \left( \frac{1}{\text{s}^{2/3}} \right) .$$

Substituting in values for  $S$ ,  $h_r$  and using Equations (12) and (13) to substitute for  $h_p$  and  $(dh_p/dT)$ , Equation (10) was then integrated numerically by computer using the Runge-Kutta-Gill method. Battelle's IRKG and RKG Routines were employed. About one-third of the resulting data are shown in Table E-2. These data are plotted in Figures 5-3 and 5-4 of Section 5.1.1.1.

**TABLE E-2. RESULTS OF NUMERICAL INTEGRATION OF FIREBALL ENERGY EQUATION PRIOR TO FIREBALL LIFTOFF**

Time, sec	Temperature, °K	Radiant Flux, kW/m <sup>2</sup>
0.00	2989	4529
0.36	2938	4230
1.02	2879	3898
2.01	2815	3568
3.00	2763	3310
3.99	2718	3097
4.98	2678	2916
5.97	2641	2758
6.63	2618	2664

Temperature and Heat Flux Calculations for  $t_b < t < 1.5 t_b$

The energy equation used for  $t < t_b$  (see Equation 1) is modified by the assumption that there is no more chemical heat added and the mass of the fireball is constant ( $W = W_b$ ). This results in:

$$-\epsilon\sigma AT^4 = W_b \frac{dh_p}{dt} = W_b \frac{dh_p}{dT} \cdot \frac{dT}{dt} ; \quad (18)$$

rearranging, and substituting using Equation (9) for  $A$  we arrive at:

$$\frac{dT}{dt} = -S \cdot \left[ T^{14/3} \right] \left[ t^{2/3} \right] \left[ \frac{1}{dh_p/dT} \right] , \quad (19)$$

where:

$$S' = \frac{4\pi\epsilon\sigma}{W_b} \left( \frac{3R\dot{R}}{4\pi P} \right)^{2/3} \quad (20)$$

By employing Equation (13), giving the relationship between  $dh_p/dT$  and  $T$ , and evaluating  $S'$  to be:

$$S' = 6.751 \text{ E-15} \left( \frac{\text{cal}}{\text{g}} \right) \left( \frac{1}{^\circ\text{K}^{14/3}} \right) \left( \frac{1}{\text{s}^{5/3}} \right)$$

Equation (19) was then integrated numerically by computer using the Runge-Kutta-Gill method. About one-quarter of the resulting data are shown in Table E-3. These data are plotted in Figures 5-3 and 5-4 of Section 5.1.1.1.

**TABLE E-3. RESULTS OF NUMERICAL INTEGRATION OF FIREBALL ENERGY EQUATION BETWEEN THE TIMES OF FIREBALL AND STEM LIFTOFF**

Time, sec	Temperature, °K	Radiant Flux, kW/m <sup>2</sup>
6.796	2597	2581
7.128	2555	2417
8.124	2419	1944
9.120	2282	1540
9.950	2175	1270

### Fireball Diameter

The predicted fireball diameter as a function of time is shown in Figure 5-5 of Section 5.1.1.1. This relationship was generated by evaluating the following equation (also see Equation 6) which relates the diameter of the fireball to the density and the mass of the fireball:

$$d = 2xr = 2 \left( \frac{3W}{4\pi\rho} \right)^{1/3} \quad (21)$$

The values of density,  $\rho$ , and fireball mass,  $W$ , were calculated as a function of time and temperature. For values of time greater than  $t_b = 6.63$  seconds, a constant value of fireball mass was used,  $W_b = 7.12 \text{ E+05 kg}$ . The decrease in

fireball size for  $t > t_b$  is due to the large amount of radiation being emitted from the fireball, thus cooling it, and increasing its density.

Reference E-3 provides a relationship between the maximum fireball diameter and total propellant for the hydrogen/oxygen combination. This relationship was developed from experimental data.<sup>(E-3)</sup> The relationship, modified to reflect diameter in meters, is as follows:

$$d = 4.29 W_b^{0.306} \text{ (when } W_b \text{ is in kg)} \quad (22)$$

$$[d = 11.05 W_b^{0.306} \text{ (when } W_b \text{ is in lb)}]$$

For the Space Shuttle case,  $W_b = 7.12 \text{ E}+05 \text{ kg}$ , and the resulting maximum fireball diameter,  $d$ , is 265 m. This value is shown in Figure 5-5 in Section 5.1.1.1, and good agreement is observed.

References

- E-1. Bader, B. E., Donaldson, A. B., and Hardee, H. C., "Liquid-Propellant Rocket Abort Fire Model", AIAA Journal of Spacecraft, Vol. 8, No. 12 (December 1971).
- E-2. Rowe, J. R., "Properties and Performance of Liquid Rocket Propellants", Aerojet Liquid Rocket Company, Sacramento, California (May 1975).
- E-3. Srinivas, V., a letter transmitting data on the maximum fireball diameter, TES-VS-1435, Teledyne Energy Systems, Timonium, Maryland (June 13, 1978).

**APPENDIX F**

**POPULATION DOSE CALCULATION TECHNIQUE  
FOR ON-PAD SPACE SHUTTLE FAILURES**

## APPENDIX F

POPULATION DOSE CALCULATION TECHNIQUE  
FOR ON-PAD SPACE SHUTTLE FAILURES

To calculate the population doses from radiation exposure to the public downwind of a Space Shuttle accident during the launch of nuclear waste into space for disposal, a calculation technique was developed and a computer program written to perform the calculations. This program was developed to use output from both the MSFC Multilayer Diffusion Model and DACRIN. A summary of the scheme and computer program is presented below.

The input to the program consists of four types of data. The first is the population data\* surrounding the Kennedy Space Center launch site, a polar-coordinate grid composed of 64 individual areas having a certain population (see Figure F-1), starting at a distance 20 km from the launch complex and moving out in increments of 10 km. Second, two dose factor (rem/ $\mu$ g) arrays, for the specific waste mix dose factors (Hanford and Savannah River waste). Each array contained provisions for three particle sizes and six organs or body tissues (e.g., total body, lung, bone, kidney, liver, and thyroid). The dose factors (rem/ $\mu$ g) specific to a mix, particle size and organ were multiplied by a calculated  $\mu$ g-man value to provide the man-rem dose for a given set of conditions. Third, isopleth data for lines of equal time-integrated waste concentration ( $\mu$ g-s/ $m^3$ ) from the MSFC Multilayer Diffusion Model (MLDM) in the form of polar coordinates and specific to a certain meteorology condition (e.g., Spring, Fall, etc.) and were input from previous runs of the MLDM. Fourth, the inhalation rate assumed for a reference man of  $2.315 \times 10^{-4} m^3/s$ .

The program calculates an average value of time-integrated concentration ( $\mu$ g-s/ $m^3$ ) in each population area (see Figure F-1) by breaking up each area into eight regions having a center point, as shown by the illustration in Figure F-1, and employing a linear interpolation technique to estimate the value at each point between two isopleths (see Figure F-2). The time-integrated concentration was assumed to be zero for a point outside the isopleth for the

\*From: "Overall Safety Manual", prepared by NUS Corporation, Rockville, Maryland, for U.S. AEC, Space Nuclear Systems Division (June 1975).



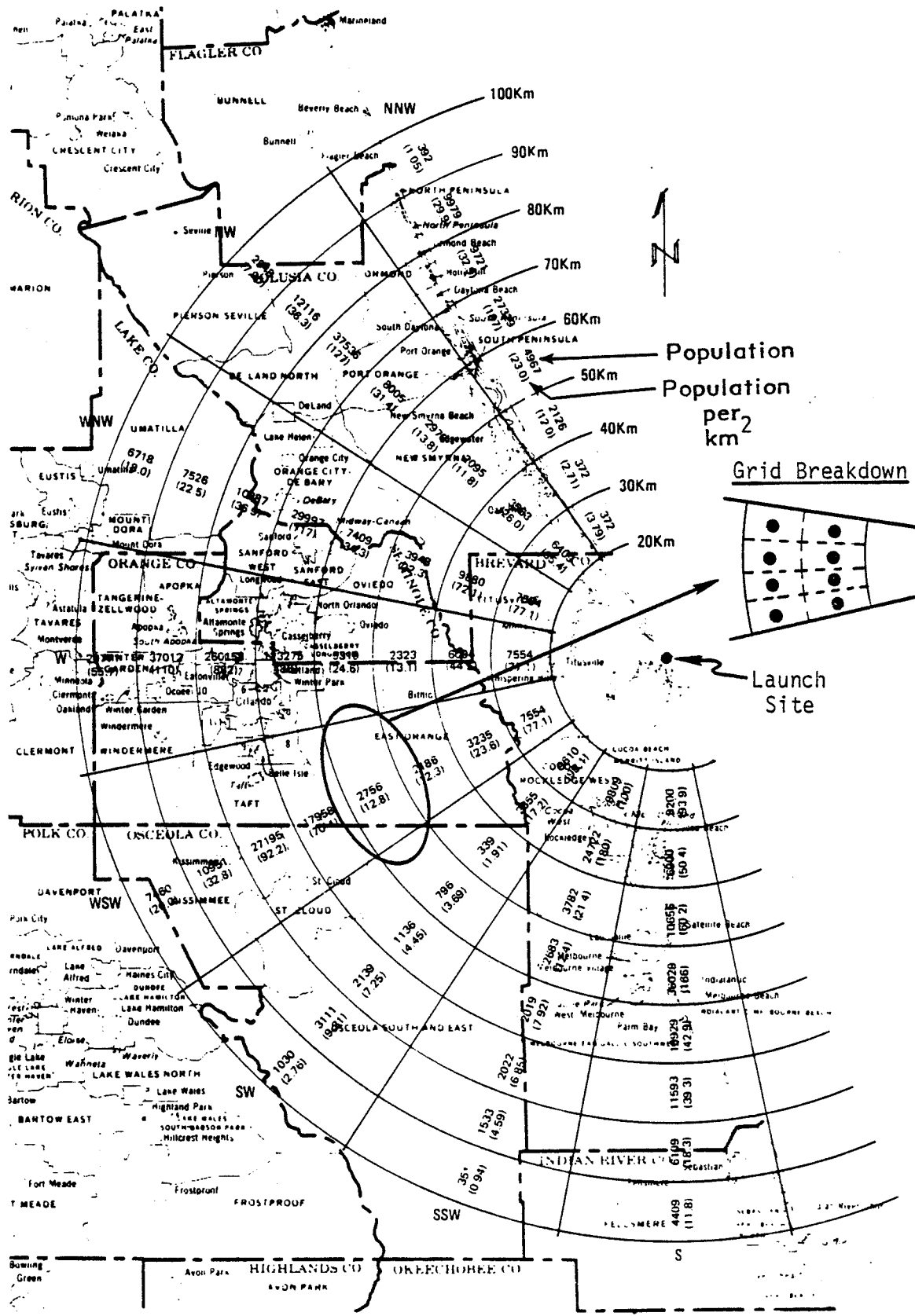


FIGURE F-1. POPULATION DISTRIBUTION SURROUNDING KSC LAUNCH SITE

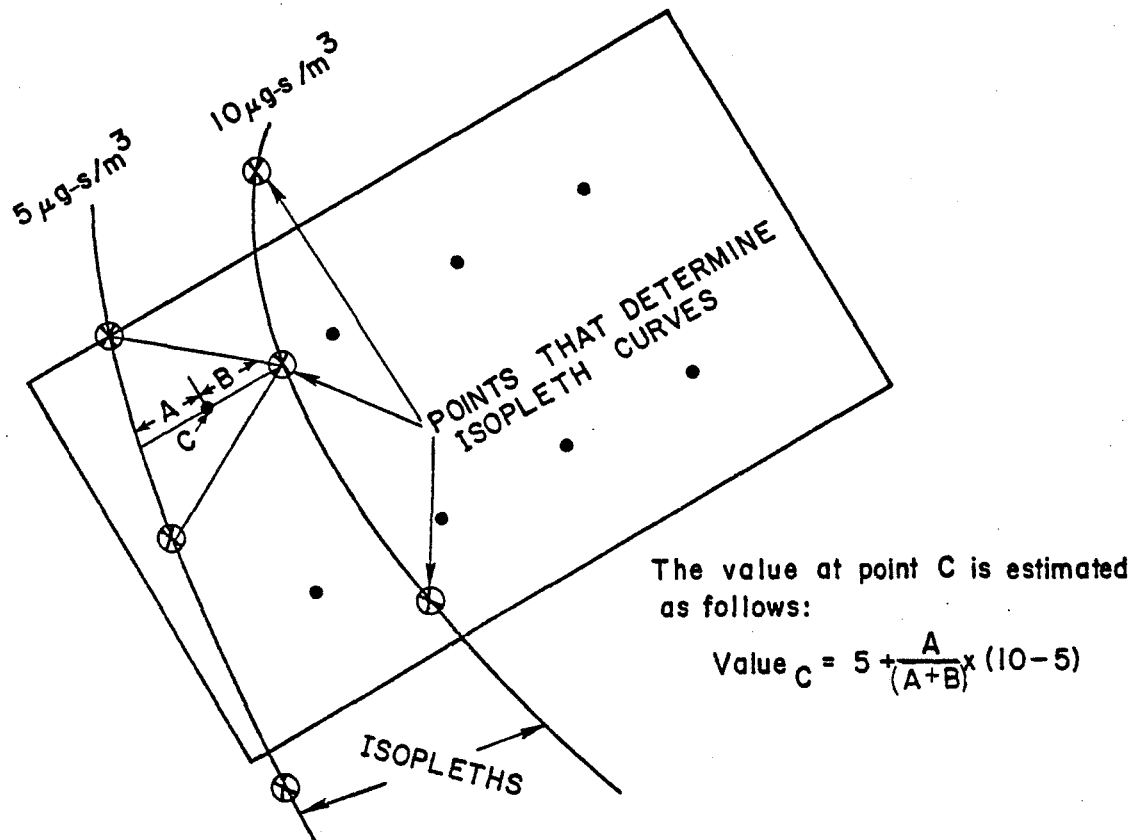


FIGURE F-2. ILLUSTRATION OF INTERPOLATION TECHNIQUE

smallest value. Once values for all eight points in a particular grid area were determined they were averaged and then multiplied by the population for that grid area to arrive at an average value of ( $\mu\text{g-s/m}^3$ ) - (man). The sum of all the values for each grid area was then multiplied by the inhalation rate and the dose conversion factor to obtain a value of man-rem for a given meteorological condition.

APPENDIX G

DOSE FACTOR MODEL FOR HIGH ALTITUDE BURNUP

G-1

## APPENDIX G

## DOSE FACTOR MODEL FOR HIGH ALTITUDE BURNUP

The world population dose model described by Equation (1) of Section 6.2 was used to estimate world population doses with respect to two radionuclide mixtures, three particle sizes, seven injection latitude bands, and ten organs (including total body). The results are tabulated in Section 6.2.1, and their implications with respect to the impact of a high altitude reentry burnup accident are discussed in Section 6.2.2. The purpose of this appendix is to explain how the dose factors,  $D_{nrk}$ , listed in the main body of this report (see Section 6.2, Tables 6-16, 6-17, and 6-18) were calculated.

The basic approach to development of the dose factor model is relatively simple. The amount of radioactive burnup material falling in an equal area latitude band  $k$  ( $k = 1, 2, \dots, 20$ ) is a function,  $f_{ik}$ , of the amount injected in latitude band  $i$  ( $i = 1, 2, \dots, 19$ ), as defined by Table 6-14 (see Section 6.2.1). The factor needed,  $D_{nrk}$ , is the dose to organ  $n$  of an individual in band  $k$  due to a unit injection of radionuclide  $r$  into the upper atmosphere of band  $k$ . In the model described below, a modified version of the atmospheric transport model developed by Krey and Krajewski<sup>(G-1, G-2)</sup> is used to estimate the radionuclide inhalation rate ( $\mu$  Ci/day) for an individual in band  $k$  as a function of time following an initial injection of  $1.0 \mu$  Ci of radionuclide  $r$  in the upper atmosphere. This inhalation rate is used as input for the internal dosimetry model proposed by the ICRP (International Commission on Radiological Protection) Task Group on Lung Dynamics<sup>(G-3)</sup> as modified by ICRP Publication 19.<sup>(G-4)</sup> The Task Group Lung Model and metabolic data from ICRP Publications 2 and 6<sup>(G-5, G-6)</sup> are used to calculate  $D_{nrk}$  for different particle sizes and different radionuclides.

**Atmospheric Transport Model**

The Krey-Krajewski model of atmospheric transport is a simple compartment model (see Figure G-1) based on first order kinetics. Disregarding radioactive decay, let  $A(o)$  be the amount of radioactive material injected in the northern hemisphere above 21 km, then

$$dA/dt = -\lambda_A A \quad (1)$$

$$dB/dt = \lambda_A A - \lambda_B B + kB' - kB \quad (2)$$

$$dC/dt = \lambda_A B - \lambda_C C \quad (3)$$

where:

$A(o)$  is the amount of material initially injected in A;  
 $A(t)$ ,  $B(t)$  and  $C(t)$  are the amounts present in A, B, and C  
 at time  $t$ ,

$$\lambda_A = \ln(2)/6 \text{ months}; \quad \lambda_B = \ln(2)/10 \text{ months}$$

$$k = \ln(2)/60 \text{ months}; \quad \lambda_C = \ln(2)/1 \text{ month.}$$

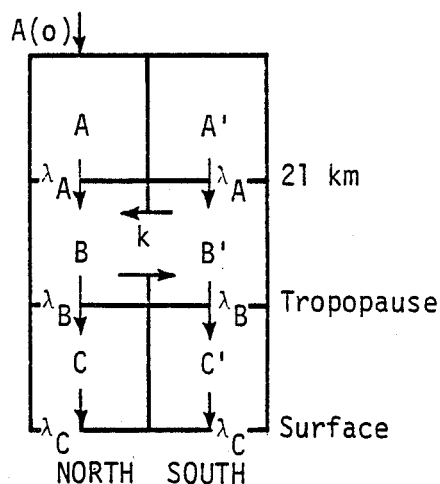


FIGURE G-1. KREY-KRAJEWSKI MODEL

For present purposes, we divide the atmosphere into three vertical layers corresponding to A, B, and C above, and we divide each hemisphere into 10 equal area latitude bands. The exchange between hemispheres indicated by  $k = \ln(2)/60$  months is ignored and replaced by the  $f_{ik}$  function defined by Table 6-14 (see Section 6.2.1).

Including consideration of radioactive decay, atmospheric transport in equal area latitude band  $k$  is represented in Figure G-2.

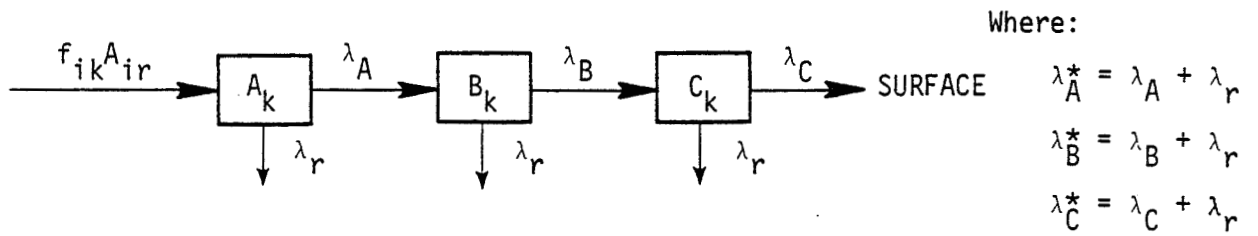


FIGURE G-2. SCHEMATIC DIAGRAM OF ATMOSPHERIC TRANSPORT

The differential equations for the model shown in Figure G-2 are:

$$dA_k/dt = -\lambda_A A_k \quad (4)$$

$$dB_k/dt = \lambda_A A_k - \lambda_B^* B_k \quad (5)$$

$$dC_k/dt = \lambda_B B_k - \lambda_C^* C_k \quad (6)$$

Taking Laplace transforms, indicated for  $A_k$  by  $\bar{A}_k$  and so on, the simultaneous solutions of Equations (4), (5), and (6) are given below for the following initial conditions:  $A_k(0) = f_{ik}A_{ir}$ ,  $B_k(0) = 0$ , and  $C_k(0) = 0$ .

$$s\bar{A}_k - A_k(0) = -\lambda_A^* \bar{A}_k \quad (7)$$

$$\bar{A}_k = A_k(0)/(s + \lambda_A^*) \quad (8)$$

$$A_k(t) = A_k(0) \exp(-\lambda_A^* t) \quad (9)$$

$$s\bar{B}_k - 0 = \lambda_A \bar{A}_k - \lambda_B^* \bar{B}_k \quad (10)$$

$$\bar{B}_k = \lambda_A \bar{A}_k / (s + \lambda_B^*) \quad (11)$$

$$= \lambda_A A_k(0) / (s + \lambda_A^*) (s + \lambda_B^*)$$

$$B_k(t) = \lambda_A A_k(0) \left[ \frac{\exp(-\lambda_A^* t)}{(\lambda_B^* - \lambda_A^*)} + \frac{\exp(-\lambda_B^* t)}{(\lambda_A^* - \lambda_B^*)} \right] \quad (12)$$

$$s\bar{C}_k - 0 = \lambda_B\bar{B}_k - \lambda_C^*\bar{C}_k \quad (13)$$

$$\begin{aligned} \bar{C}_k &= \lambda_B\bar{B}_k / (s + \lambda_C^*) \\ &= \lambda_A\lambda_B A_k(o) / (s + \lambda_A^*) (s + \lambda_B^*) (s + \lambda_C^*) \end{aligned} \quad (14)$$

$$\begin{aligned} C_k(t) &= \lambda_A\lambda_B A_k(o) \left[ \frac{\exp(-\lambda_A^*t)}{(\lambda_B^* - \lambda_A^*)(\lambda_C^* - \lambda_A^*)} + \frac{\exp(-\lambda_B^*t)}{(\lambda_A^* - \lambda_B^*)(\lambda_C^* - \lambda_B^*)} \right. \\ &\quad \left. + \frac{\exp(-\lambda_C^*t)}{(\lambda_A^* - \lambda_C^*)(\lambda_B^* - \lambda_C^*)} \right], \end{aligned} \quad (15)$$

where:

$A_k(o) = f_{ik} A_{ir} = 1.0 \mu\text{Ci}$  of radionuclide  $r$  falling in equal area latitude band  $k$ ,

$A_k(t)$ ,  $B_k(t)$ ,  $C_k(t)$  are the amounts ( $\mu\text{Ci}$ ) of radionuclide  $r$  in compartments,  $A_k$  (atmosphere above 21 km),  $B_k$  (between 21 km and the tropopause), and  $C_k$  (troposphere) of band  $k$  at time  $t$  (days),

$$\lambda_A = \ln(2)/182.5 \text{ days} \quad , \quad \lambda_A^* = \lambda_A + \lambda_r \quad ,$$

$$\lambda_B = \ln(2)/304.2 \text{ days} \quad , \quad \lambda_B^* = \lambda_B + \lambda_r \quad ,$$

$$\lambda_C = \ln(2)/30.42 \text{ days} \quad , \quad \lambda_C^* = \lambda_C + \lambda_r \quad ,$$

$$\lambda_r = \ln(2)/T_r \quad ,$$

$T_r$  is the half-life (days) of radionuclide  $r$ , and  $t = \text{days}$  after reentry burnup.

(N.B. Note that Equation (14) is the Laplace transform of  $dC_k/dt$  and Equation (15) is the inverse Laplace transform based on the Heaviside Expansion Theorem. (G-7))

Surface deposition,  $S_k(t)$ , also in  $\mu$  Ci of radionuclide  $r$ , is simply the integral of  $C_k(t)$ , Equation (15), i.e.,

$$S_k(t) = \lambda_C \int_0^t C_k(t) dt \quad (16)$$

$$S_k(t) = \lambda_A \lambda_B \lambda_C A_k(o) \left[ \frac{1 - \exp(-\lambda_A^* t)}{\lambda_A^* (\lambda_B^* - \lambda_A^*) (\lambda_C^* - \lambda_A^*)} + \frac{1 - \exp(-\lambda_B^* t)}{\lambda_B^* (\lambda_A^* - \lambda_B^*) (\lambda_C^* - \lambda_B^*)} + \frac{1 - \exp(-\lambda_C^* t)}{\lambda_C^* (\lambda_A^* - \lambda_C^*) (\lambda_B^* - \lambda_C^*)} \right] \quad (17)$$

Note that

$$\bar{S}_k = \lambda_A \lambda_B \lambda_C A_k(o) / s(s + \lambda_A^*) (s + \lambda_B^*) (s + \lambda_C^*) \quad (18)$$

from which it is obvious that

$$S_k(\infty) = \lambda_A \lambda_B \lambda_C A_k(o) / \lambda_A^* \lambda_B^* \lambda_C^* \quad (19)$$

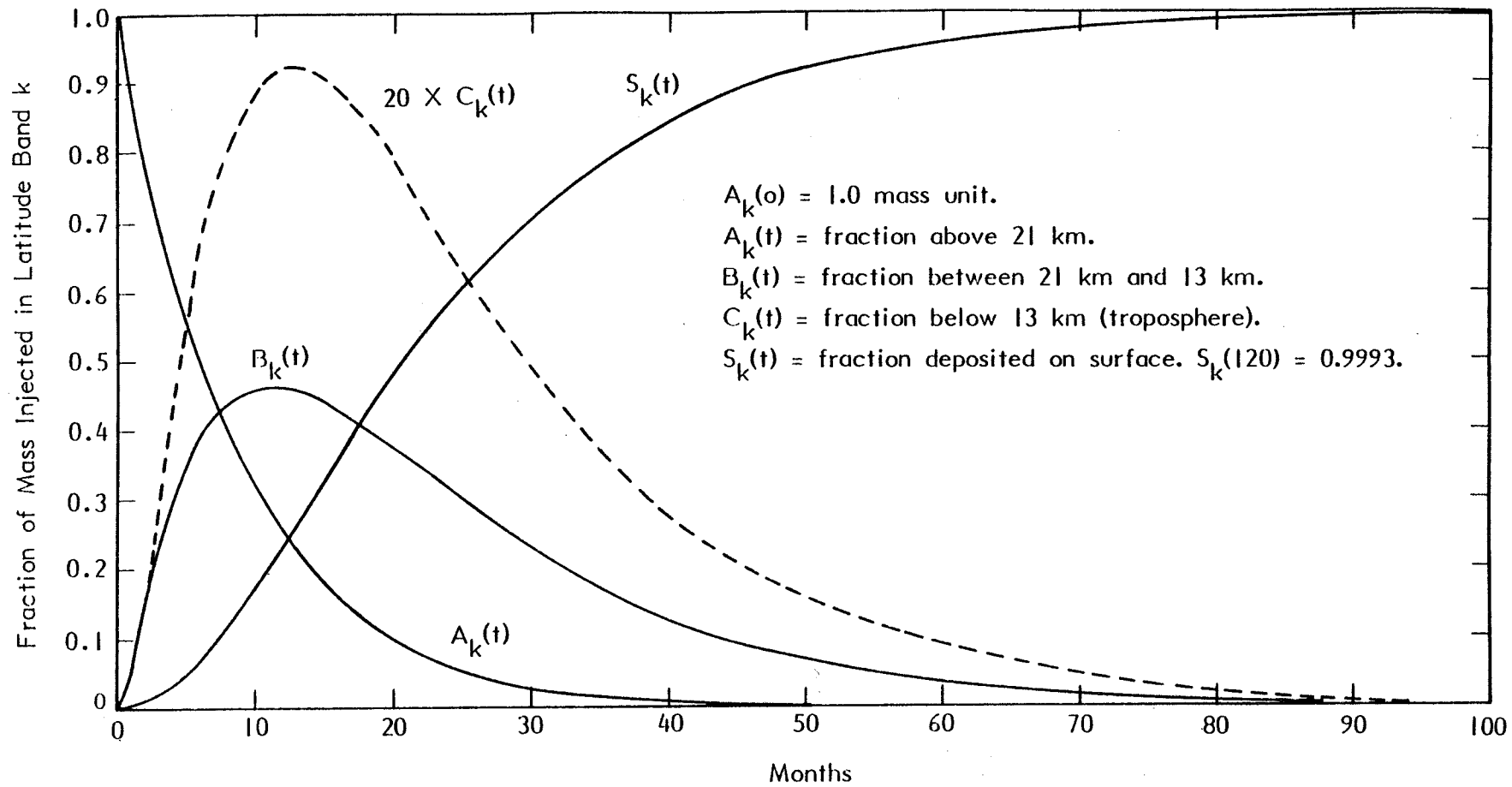
Disregarding radioactive decay,  $S_k(\infty) = A_k(o)$  and mass is conserved. Figure G-3 shows  $A_k(t)$ ,  $B_k(t)$ ,  $C_k(t)$  and  $S_k(t)$  based on  $A_k(o) = 1.0$  mass unit and no radioactive decay. Figure G-3 shows that following reentry and burnup (or any high altitude injection of small diameter particles,  $\leq 4 \mu\text{m}$  for example) fallout would occur over a period of several years with  $> 99\%$  of the mass being deposited within 7 years following injection,  $> 99.9\%$  within 10 years.

### Radionuclide Inhalation Rate

Equation (15) gives the total amount of radionuclide  $r$  in the tropospheric layer of the atmosphere of equal area latitude band  $k$ ,  $C_k(t)$ , as a function of time after injection (reentry burnup of a nuclear waste payload). According to ICRP<sup>(G-5)</sup>, Standard Man inhales  $20 \text{ m}^3$  (air)/day. His radionuclide inhalation rate ( $\mu$  Ci/day) will, therefore, be 20 times the radionuclide concentration ( $\mu$  Ci/ $\text{m}^3$ ) in surface air, i.e.,

$$Q_I(t) = C_k(t) 20F \quad (20)$$





G-6

FIGURE G-3. RESULTS FROM ATMOSPHERIC TRANSPORT MODEL

where:

$Q_i(t)$  is the radionuclide inhalation rate ( $\mu$  Ci/day) at time  $t$ ,  
 $C_k(t)$  is the amount of radionuclide ( $\mu$  Ci) in compartment  
 $C_k$  at time  $t$ ,  
 $20 \text{ m}^3$  (air)/day is Standard Man's inhalation (air) rate,

and

$F$  is a factor ( $\text{m}^{-3}$ ) relating the concentration of radionuclide in surface air ( $\mu \text{ Ci}/\text{m}^3$ ) to the amount of radionuclide in the tropospheric compartment of band  $k$ . See Equation (24).

If we assume that the radionuclide in compartment  $C_k$  is well mixed,  $F$  is simply the reciprocal of the volume ( $\text{m}^3$ ) of compartment  $C_k$ . It is known that the height of the tropopause varies from about 8 km at high latitudes to about 18 km near the equator. Assuming a mean tropospheric depth of 13 km and a mean Earth radius of 6371 km, the total volume of the troposphere,  $V_T$ , is estimated by

$$\begin{aligned} V_T &= 4/3 \pi (6384^3 - 6371^3) \times 10^9 \text{m}^3/\text{km}^3 \\ &= 6.644 \text{ E}+18 \text{ m}^3 \\ 1/V_T &= 1.51 \text{ E}-19 \text{ m}^{-3} \end{aligned} \quad (21)$$

Based on a worldwide network of air and fallout sampling stations, Krey and Krajewski<sup>(G-1,G-2)</sup> obtained empirical estimates of  $F$  (disregarding  $V_T$ ) by comparing mean monthly air concentrations (gross beta activity) with mean monthly deposition rates. Their results were reported as follows:

$$F_N = \frac{0.3 \text{ dpm}/1000 \text{ SCM}}{\text{kCi}} = \frac{\text{mean air concentration}}{\text{mean deposition}} \quad (22)$$

$$F_S = \frac{0.2 \text{ dpm}/1000 \text{ SCM}}{\text{kCi}} \quad (23)$$

where:

$F_N$  is based on sampling stations in the northern hemisphere,  
 $F_S$  is based on sampling stations in the southern hemisphere,

and

SCM = standard cubic meter of air.

Converting kCi (kilocuries) to dpm (2.22 E+15 dpm/kCi),  $F_N = 1.35 \text{ E-19 m}^{-3}$  and  $F_S = 9.01 \text{ E-20 m}^{-3}$ . These values, especially  $F_N$ , are comparable to the value,  $1/V_T$ , based on Equation (21), the latter being but 12% larger than the former. As there are 20 k-bands,  $V_k = V_T/20$ , and our estimate of the value of  $F$  in Equation (20) is

$$F = (V_T/20)^{-1} = 3.01 \text{ E-18 m}^{-3}. \quad (24)$$

### Model for Calculating Dose Factors

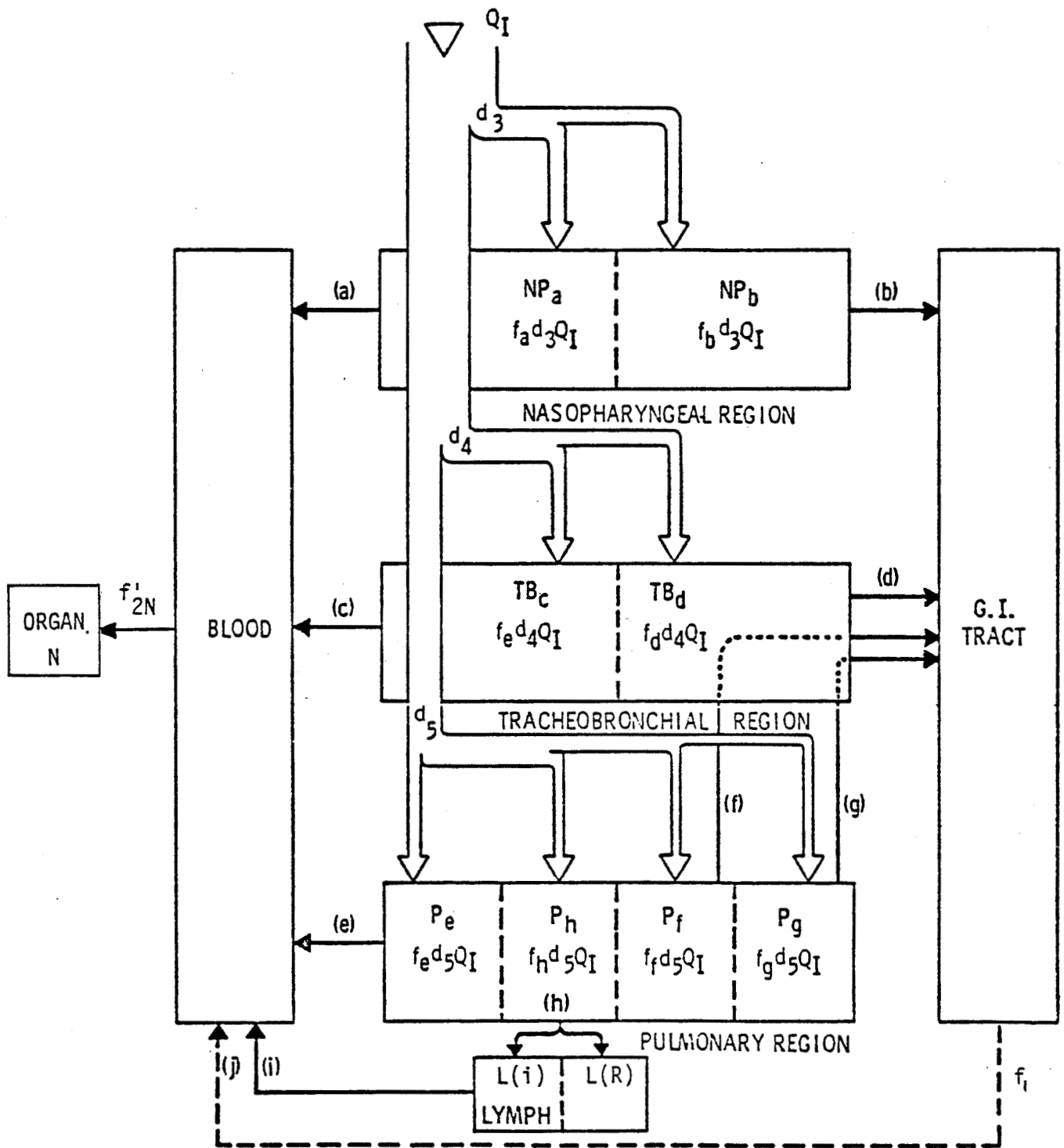
#### Comparison with DACRIN

Figure G-4 is a schematic diagram of the Task Group on Lung Dynamics model described by Morrow et al. <sup>(G-3)</sup> The DACRIN computer program <sup>(G-7)</sup> used in Section 6.1 is based on the same model, but the DACRIN equations require that  $Q_I$  (Figure G-4) be expressed as a pulse (acute inhalation) or a constant rate (chronic inhalation). In the present case, as shown by Equation (20) and its predecessors,  $Q_I(t)$  is a function of time; and, as shown by the graph of  $C_k(t)$  in Figure G-3, the fallout period is several years.

It is perhaps tempting to assume that  $Q_I(\infty)$  can be treated as a pulse input evaluated by

$$Q_I = 20 F \int_0^{\infty} C_k(t) dt \quad . \quad (25)$$

Then DACRIN or a similar program for calculating doses due to acute inhalation could be used directly. This approach would be appropriate if the fallout interval were very short (a few days or a few weeks). Since the fallout period is several years, the use of Equation (25) and DACRIN is not appropriate and would result in underestimates of lifetime organ doses.



Source: Reference G-3.

FIGURE G-4. SCHEMATIC DIAGRAM OF TASK GROUP LUNG MODEL

### Definitions and Data Sources

Symbols appearing in Figure G-4 and/or used in Equations (30) through (73), to follow, are defined below. Parameter values used in the dose factor model and their sources are given in Tables G-1 through G-4.

$Q_1(t)$  is the radionuclide inhalation rate ( $\mu$  Ci/day) as defined by Equation (18).

$d_3$ ,  $d_4$ , and  $d_5$  are the fractions of inhaled radionuclide initially deposited in the nasopharyngeal (NP), tracheobronchial (TB), and pulmonary (P) regions of the respiratory system. The fraction exhaled (not shown) is  $d_2$ ;  $d_1 = d_2 + d_3 + d_4 + d_5 = 1.0$  (Table G-1).

$$d_3 = (2\pi)^{-1/2} \int_{-\infty}^{X_L} \exp(-0.5 z^2) dz \quad (26)$$

$$X_L = [\log_{10}(\text{AMAD}) - \log_{10}(2.0)] / \log_{10}(3.45)$$

$$d_4 = 0.08 \quad (27)$$

$$d_5 = (2\pi)^{-1/2} \int_{-\infty}^{X_P} \exp(-0.5 z^2) dz$$

$$X_P = [\log_{10}(\text{AMAD}) - \log_{10}(0.1)] / \log_{10}(24) \quad (28)$$

AMAD = activity median aerodynamic diameter ( $\mu$  m)

- Sample values of  $d_3(\text{AMAD})$  and  $d_4(\text{AMAD})$  are listed in Table G-1.
- The clearance pathways for various parts of the respiratory system and the thoracic lymph are labeled  $j = a, b, \dots, i$  (Figure G-4).

$NP_a$ , for example, represents the quantity of material,  $t_a d_3 Q_1(t)$ , cleared from the nasopharyngeal region to blood via clearance pathway  $a$  (Figure G-4).

$f_j$  is the fraction of  $d_x Q_1(t)$  cleared via pathway  $j = a, b, \dots, i$  (Table G-2) from the G.I. tract to blood.

$f_1$  is the fraction of radionuclide  $r$  transferred from the G.I. tract to blood (Table G-4).

TABLE G-1. FRACTION OF INHALED PARTICLES DEPOSITED IN THE RESPIRATORY SYSTEM VERSUS PARTICLE DIAMETER

Particle Size AMAD Micrometers	Fraction of Inhaled Quantity Retained		
	Nasopharyngeal Region, $d_3$	Tracheobronchial Region, $d_4$	Pulmonary Region, $d_5$
0.05	0.001	0.08	0.59
0.1	0.008	0.08	0.50
0.3	0.063	0.08	0.36
0.5	0.13	0.08	0.31
1.0	0.29	0.08	0.23
2.0	0.50	0.08	0.17
5.0	0.77	0.08	0.11

Source: Reference G-7.

TABLE G-2. CLEARANCE PARAMETER VALUES

Compartment	j	Translocation Class					
		D (day)		W (week)		Y (year)	
		$T_j$	$f_j$	$T_j$	$f_j$	$T_j$	$f_j$
Nasopharyngeal (NP)	a	0.01	0.50	0.01	0.10	0.01	0.01
	b	0.01	0.50	0.40	0.90	0.40	0.99
Tracheobronchial (TB)	c	0.01	0.95	0.01	0.50	0.01	0.01
	d	0.20	0.05	0.20	0.50	0.20	0.99
Pulmonary (P)	e	0.50	0.80	50	0.15	500	0.05
	f	n.a.	n.a.	1	0.40	1	0.40
	g	n.a.	n.a.	50	0.40	500	0.40
	h	0.50	0.20	50	0.05	500	0.15
Lymph (L)	i	0.50*	1.00	50*	1.00	1000	0.90

\*NOTE: Values used for Equations (56) and (57) are 0.4999 and 49.99 days, respectively.

Source: Reference G-7.

TABLE G-3. PULMONARY CLEARANCE CLASSIFICATION OF INORGANIC COMPOUNDS

**Class Y—Avid retention: cleared slowly (years)**

Carbides—actinides, lanthanides, Zr, Y, Mn

Sulfides—none

Sulfates—none

Carbonates—none

Phosphates—none

Oxides and hydroxides—lanthanides, actinides Groups 8 (V and VI), 1b, 2b (IV and V), 3b except  $\text{Sc}^{3+}$ , and 6b.

Halides—lanthanide fluorides

Nitrates—none

**Class W—Moderate retention: intermediate clearance rates (weeks)**

Carbides—Cations of all Class W hydroxides except those listed as Class Y carbides.

Sulfides—Groups 2a (V + VI), 4a (IV-VI), 5a (IV-VI), 1b, 2b and 6b (V + VI).

Sulfates—Groups 2a (IV-VII), and 5a (IV-VI)

Carbonates—lanthanides,  $\text{Bi}^{3+}$  and Group 2a (IV-VII)Phosphates— $\text{Zn}^{2+}$ ,  $\text{Sn}^{2+}$ ,  $\text{Mg}^{2+}$ ,  $\text{Fe}^{3+}$ ,  $\text{Bi}^{3+}$  and lanthanidesOxides and hydroxides—Groups 2a (II-VII), 3a (III-VI), 4a (III-VI), 5a (IV-VI), 6a (IV-VI), 8, 2b (VI), 4b, 5b, and 7b  $\text{Sc}^{3+}$ 

Halides—lanthanides (except fluorides), Groups 2a, 3a (III-VI), 4a (IV-VI), 5a (IV-VI), 8, 1b, 2b, 3b (IV-V), 4b, 5b, 6b and 7b

Nitrates—all cations whose hydroxides are Class Y and W

**Class D—Minimal retention: rapid clearance (days)**

Carbides—see hydroxides

Sulfides—all except Class W

Sulfates—all except Class W

Carbonates—all except Class W

Phosphates—all except Class W

Oxides and Hydroxides—Groups 1a, 3a (II), 4a (II), 5a (II, III), 6a (III).

Halides—Groups 1a and 7a

Nitrates—all except Class W

Noble Gases—Group 0

Note: Where reference is made from one chemical form to another, it implies that an *in vivo* conversion occurs, e.g. hydrolysis reaction.

The following periodic table of the elements is used with the foregoing classification.

Group																		
Period	1a	2a	3b	4b	5b	6b	7b	8	1b	2b	3a	4a	5a	6a	7a	0		
I	H															He		
II	Li	Be									B	C	N	O	F	Ne		
III	Na	Mg									Al	Si	P	S	Cl	Ar		
IV	K	Ca	Sc	Ti	V	Cr	Mn	Fe	Co	Ni	Cu	Zn	Ga	Ge	As	Se	Br	Kr
V	Rb	Sr	Y	Zr	Nb	Mo	Tc	Ru	Rh	Pd	Ag	Cd	In	Sn	Sb	Te	I	Xe
VI	Cs	Ba	La*	Hf	Ta	W	Re	Os	Ir	Pt	Au	Hg	Tl	Pb	Bi	Po	At	Rn
VII	Fr	Ra	Act†															
* Lanthanides			Ce	Pr	Nd	Pm	Sm	Eu	Gd	Tb	Dy	Ho	Er	Tm	Yb	Lu		
† Actinides			Th	Pa	U	Np	Pu	Am	Cm	Bk	Cf	Es	Fm	Md	No	Lw		

Source: Reference G-3.

TABLE G-4. METABOLIC PARAMETERS FOR DOSE FACTOR CALCULATIONS<sup>(1)</sup>

Radionuclide	Co-60	Se-79*	Sr-89	Sr-90	Y-91	Zr-93	Zr-95	Nb-95	Tc-99	Ru-103	Ru-106	Pd-107*	Cd-113m*	Sn-121m	Sn-126*	
Trans. Class	W	W	W	W	Y	W	W	W	W	Y	Y	Y	Y	W	W	
$f_j$ (GIT → Blood)	0.3	0.9	0.3	0.3	10 <sup>-4</sup>	10 <sup>-4</sup>	10 <sup>-4</sup>	10 <sup>-4</sup>	0.5	0.03	0.03	0.2	2.5E-5	0.5	0.5	
Tr (days)	1900	(2.7E + 7)	50.5	10,000	58.0	4E + 8	63.3	35	7.7E + 7	41	365	(2.6E + 9)	5110	NDA	(3.65E + 7)	
$T_N$	Total Body	9.5	11.0	13,000	13,000	14,000	450	450	760	1	7.3	7.3	5	200	35	35
	Bone	0 <sup>(3)</sup>	0	18,000	18,000	18,000	1000	1000	1000	25	16.0	16.0	0	0	100	100
	Liver	9.5	24.0	0	0	0	900	900	845	30	0	0	19	200	70	70
	Kidney	0	11.0	0	0	0	900	900	760	20	2.5	2.5	30	300	0	0
	Thyroid	0	0	0	0	0	0	0	0	0	0	0	0	0	70	70
$I'_{2N}$	Total Body	1.0	1.0	1.0	1.0	1.0	1.0	1.0	1.0	1.0	1.0	1.0	1.0	1.0	1.0	1.0
	Bone	0	0	0.3	0.95	0.75	0.36	0.36	0.38	0.002	0.08	0.08	0	0	0.3	0.3
	Liver	0.04	0.07	0	0	0	0.07	0.07	0.09	0.003	0	0	0.09	0.75	0.01	0.01
	Kidney	0	0.04	0	0	0	0.02	0.02	0.02	0.001	0.2	0.2	0.08	0.10	0	0
	Thyroid	0	0	0	0	0	0	0	0	0	0	0	0	0	10 <sup>-4</sup>	10 <sup>-4</sup>
$\epsilon_N$	Total Body	0.099	(0.042)	0.55	1.1	0.59	0.019	1.1	0.51	0.094	0.44	1.4	(0.0089)	(0.184)	NDA	(1.3)
	Bone	0	0	2.8	5.5	2.9	0.095	1.1	0.37	0.47	0.62	6.5	0	0	NDA	(4.0)
	Liver	0.059	(0.042)	0	0	0	0.019	0.57	0.26	0.094	0	0	(0.0089)	(0.184)	NDA	(1.1)
	Kidney	0	(0.042)	0	0	0	0.019	0.46	0.2	0.094	0.22	1.3	(0.0089)	(0.184)	NDA	0
	Thyroid	0	0	0	0	0	0	0	0	0	0	0	0	0	NDA	(0.38)
$\epsilon_n$ (Resp. Syst.) <sup>(2)</sup>	0.72	(0.042)	0.55	1.1	0.59	0.019	0.52	0.26	0.094	0.27	1.4	(0.0089)	(0.184)	NDA	(1.1)	
$\epsilon_G$ (I.G. Intestine)	0.44	(0.042)	0.55	0.21	0.59	0.019	0.24	0.16	0.094	0.14	1.3	(0.0089)	(0.184)	NDA	(0.78)	

(1) Data extracted from References G-4 or G-5 unless otherwise indicated.

(2) Values used for NP, TB, P, and L are values listed by ICRP for "Lung".

(3) A zero, 0, simply indicates "no data listed by ICRP".

\*Isotope not listed in ICRP (1960) or ICRP (1964). Data in parentheses from DACRIN. Other data depend on element.

NDA = No Data Available.

G-13



TABLE G-4. METABOLIC PARAMETERS FOR DOSE FACTOR CALCULATIONS<sup>(1)</sup> (Continued)

Radionuclide	Sb-125	Te-127 m	Te-129 m	I-129	Cs-134	Cs-135	Cs-137	Ce-141	Ce-144	Pm-147	Sm-151	Eu-152	Eu-154	Eu-155	
Trans. Class	W	W	W	D	D	D	D	Y	Y	Y	Y	Y	Y	Y	
$f_j$ (GIT → Blood)	0.03	0.25	0.25	1.0	1.0	1.0	1.0	10 <sup>-4</sup>	10 <sup>-4</sup>	10 <sup>-4</sup>	10 <sup>-4</sup>	10 <sup>-4</sup>	10 <sup>-4</sup>	10 <sup>-4</sup>	
Tr (days)	877	105	33	6.3E + 9	840	1.1E + 9	11,000	32	290	920	37,000	4700	5800	621	
$T_N$	Total Body	38	15	15	138	70	70	70	563	563	656	656	635	635	635
	Bone	100	30	30	14	140	140	140	1500	1500	1500	1500	1500	1500	1500
	Liver	38	30	30	7	90	90	90	293	293	656	187	127	127	127
	Kidney	0(3)	30	30	7	42	42	42	563	563	656	656	1480	1480	1480
	Thyroid	4	9	9	138	0	0	0	0	0	0	0	0	0	0
$i_{2N}$	Total Body	1.0	1.0	1.0	1.0	1.0	1.0	1.0	1.0	1.0	1.0	1.0	1.0	1.0	
	Bone	0.1	0.09	0.09	0.07	0.04	0.04	0.04	0.3	0.3	0.35	0.35	0.36	0.36	
	Liver	0.002	0.05	0.05	0.12	0.07	0.07	0.07	0.25	0.25	0.06	0.35	0.25	0.25	
	Kidney	0	0.07	0.07	0.04	0.01	0.01	0.01	0.02	0.02	0.02	0.02	0.03	0.03	
	Thyroid	3E-5	0.001	0.001	0.3	0	0	0	0	0	0	0	0	0	
$\epsilon_N$	Total Body	0.43	0.32	1.1	0.089	1.1	0.066	0.59	0.21	1.3	0.069	0.042	0.88	1.3	0.16
	Bone	0.28	1.5	3.2	2.8	0.99	0.33	1.4	0.81	6.3	0.35	0.13	2.9	2.7	0.28
	Liver	0.21	0.32	0.83	0.082	0.57	0.066	0.41	0.18	1.3	0.069	0.042	0.71	0.86	0.095
	Kidney	0	0.32	0.78	0.077	0.46	0.066	0.41	0.18	1.3	0.069	0.042	0.71	0.76	0.083
	Thyroid	0.095	0.3	0.68	0.068	0	0	0	0	0	0	0	0	0	0
$\epsilon_H$ (Resp. Syst.) <sup>(2)</sup>	0.21	0.32	0.83	0.082	0.57	0.066	0.41	0.18	1.3	0.069	0.042	0.71	0.86	0.095	
$\epsilon_G$ (Lg. Intestine)	0.13	0.24	0.65	0.073	0.38	0.066	0.34	0.17	1.3	0.069	0.041	0.71	0.69	0.075	

(1) Data extracted from References G-4 or G-5 unless otherwise indicated.

(2) Values used for NP, TB, P, and L are values listed by ICRP for "Lung".

(3) A zero, 0, simply indicates "no data listed by ICRP".

TABLE G-4. METABOLIC PARAMETERS FOR DOSE FACTOR CALCULATIONS<sup>(1)</sup> (Continued)

Radionuclide	Tb-158	Tb-160	U-233	U-235	U-238	Np-237	Pu-238	Pu-239	Pu-240	Pu-241	Pu-242	Am-241	Am-243	Cm-244	
Trans. Class	Y	Y	Y	Y	Y	Y	Y	Y	Y	Y	Y	Y	Y	Y	
$f_i$ (GIT → Blood)	10 <sup>-4</sup>	10 <sup>-4</sup>	10 <sup>-4</sup>	10 <sup>-4</sup>	10 <sup>-4</sup>	1.0	3E-5	3E-5	3E-5	3E-5	3E-5	10 <sup>-4</sup>	10 <sup>-4</sup>	10 <sup>-4</sup>	
Tr (days)	NDA	73	5.9E + 7	2.6E + 11	1.7E + 12	8E + 8	33,000	8.6E + 6	2.4E + 6	4,800	1.4E + 8	1.7E + 5	2.9E + 6	6700	
$T_N$	Total Body	670	670	100	100	100	39,000	65,000	65,000	65,000	65,000	20,000	20,000	24,000	
	Bone	1000	1000	300	300	300	73,00	36,500(4)	36,500	36,500	36,500	73,000	73,000	73,000	
	Liver	0	0	0	0	0	54,000	14,600(4)	14,600	14,600	14,600	34,800	34,800	3,000	
	Kidney	700	700	15	15	15	64,000	32,000	32,000	32,000	32,000	27,000	27,000	2,400	
	Thyroid	0	0	0	0	0	0	0	0	0	0	0	0	0	
$i_{2N}$	Total Body	1.0	1.0	1.0	1.0	1.0	1.0	1.0	1.0	1.0	1.0	1.0	1.0	1.0	
	Bone	0.6	0.6	0.11	0.11	0.11	0.45	0.45(4)	0.45	0.45	0.45	0.25	0.25	0.3	
	Liver	0	0	0	0	0	0.05	0.45(4)	0.45	0.45	0.45	0.35	0.35	0.4	
	Kidney	0.03	0.03	0.11	0.11	0.11	0.03	0.02	0.02	0.02	0.02	0.03	0.03	0.02	
	Thyroid	0	0	0	0	0	0	0	0	0	0	0	0	0	
$\epsilon_N$	Total Body	NDA	(0.85)	50	46	43	49	57	53	53	2.3	51	57	54	60
	Bone	NDA	(1.1)	250	230	220	250	280	270	270	14.0	250	280	270	300
	Liver	NDA	0	0	0	0	49	57	53	53	1.0	51	57	54	60
	Kidney	NDA	(0.4)	50	46	43	49	57	53	53	2.5	51	57	54	60
	Thyroid	NDA	0	0	0	0	0	0	0	0	0	0	0	0	
$\epsilon_n$ (Resp. Syst.) <sup>(2)</sup>	NDA	(0.48)	50	46	43	49	57	53	53	0.053	51	57	54	60	
$\epsilon_G$ (Lg. Intestine)	NDA	(0.34)	0.49	0.52	0.43	0.49	0.52	0.52	0.52	(0.0005)	0.49	0.56	0.54	0.58	

G-15

(1) Data extracted from References G-4 or G-5 unless otherwise indicated.

(2) Values used for NP, TB, P, and L are values listed by ICRP for "Lung".

(3) A zero, 0, simply indicates "no data listed by ICRP".

(4) Based on ICRP (1972) recommendations for Pu.

\*Isotope not listed in ICRP (1960) or ICRP (1964). Data in parentheses from DACRIN. Other data depend on element.

NDA = No Data Available.

$f_{2N}^r$  is the fraction of radionuclide  $r$  entering blood which is transferred to organ  $N$  (Table G-4). See definition of  $n$ , below.

- Transfers from the G.I. Tract to blood and from blood to organ  $N$  are assumed to occur instantaneously.

$Q_n(t)$  is the quantity ( $\mu$  Ci) of radionuclide  $r$  in organ  $n$  at time  $t$ .

$D_n(t)$  is the cumulative dose (rem) delivered by radionuclide  $r$  to organ  $n$  from time zero to time  $t$ . See Equation (29) below.

$n = NP$  (nasopharyngeal region),  $L$  (thoracic lymph tissue),  $G$  (G.I. tract), and  $N$  (bone, liver, kidney, thyroid, total body).

- The relationship between  $Q_n(t)$  and  $D_n(t)$  is given by

$$D_n(t) = R_n \int_0^t Q_n(t) dt, \quad (29)$$

where:

$$R_n = 51.216 E_n/M_n \text{ (rem- } \mu\text{Ci}^{-1}\text{-day}^{-1}\text{)}$$

$E_n$  = effective energy deposited (MeV/dis) by radionuclide  $r$  in organ  $n$

and

$M_n$  = fresh weight (g) of organ  $n$ .

- The weights of the organs listed above (see definition of  $n$ ) are as follows:

$M_{NP}$	=	1.35	g (References G-8 and G-9)
$M_{TB}$	=	400	g (Reference G-10)
$M_P$	=	500	g (Reference G-10)
$M_L$	=	15	g (Reference G-10)
$M_{GIT}$	=	150	g (Reference G-5)
			(Refers to contents of large intestine)

$M_{\text{BONE}}$	=	7000	g (Reference G-5)
$M_{\text{LIVER}}$	=	1700	g (Reference G-5)
$M_{\text{KIDNEY}}$	=	300	g (Reference G-5)
$M_{\text{THYROID}}$	=	20	g (Reference G-5)
$M_{\text{TOT. BODY}}$	=	70,000	g (Reference G-5)

- Rate constants,  $\lambda$ , all have units of reciprocal days ( $\text{day}^{-1}$ ):

$T_r$  = half-life (days) of radionuclide  $r$  (Table G-4)

$T_j$  = biological half-time (days) for transfer via pathway  $j$   
(Table G-2)

$T_N$  = biological half-life (days) of radionuclide (element)  $r$   
in organ  $N$  (Table G-4). For  $N$ , see definition of  $n$ , above.

- Values of  $f_j$  and  $T_j$  are given for three Translocation Classes in Table G-2.
- The basis for determining the Translocation Classes for inorganic compounds is given in Table G-3 taken from Reference G-3.
- Table G-4 gives, for each radionuclide considered in the dose factor and world population models, the translocation class,  $f_j$ ,  $T_r$ ,  $T_N$ ,  $f_{2N}$ , and  $E_N$  and  $E_n$  for the regions of the respiratory tract (NP, TB, P, and L) and for the large intestine. The data given in Table G-4 are extracted from References G-5 or G-6.

### Equations for Dose Factor Model

The dose factors,  $D_{nrk}$ , given in Tables 6-16 through 6-18 in Section 6.2.1 of the main body of this report were calculated by means of a computer program which uses the matrix exponential function and a numerical procedure to solve systems of ordinary differential equations. For a description of this program see Reference G-11.

For any subcompartment,  $j$ , of the respiratory system (Table G-2) the differential equation for the radionuclide burden is

$$dQ_j/dt = f_k d_x Q_I - \lambda_j^* Q_j \quad (30)$$

To simplify the mathematical analysis, we note (Table G-2 and Figure G-4) that  $T_a$ ,  $T_b$ ,  $T_c$ ,  $T_d$ , and  $T_f$  are  $\leq 1.0$  day for all three translocation classes (D, W, and Y), and that the shortest half-time affecting  $Q_I$  is  $T_C = 30.42$  days. For  $T_j \leq 1.0$  day and  $t > 10 T_j$ ,  $dQ_j/dt \rightarrow 0$ , and

$$Q_j(t) \doteq (f_j d_x / \lambda_j^*) Q_I(t) \quad (31)$$

Based on the simplification indicated by Equation (31), and the definitions given previously, equations for organ burdens,  $Q_{nr}$ , and dose factors,  $D_{nrk}$ , are derived below.

**Nasopharyngeal Region.** Based on Equation (31), the simplified differential equation for  $Q_{NP}$  is

$$dQ_{NP}/dt = d_3 [(f_a/\lambda_a^*) + (f_b/\lambda_b^*)] Q_I(t) \quad (32)$$

$$\bar{Q}_{NP} = d_3 [(f_a/\lambda_a^*) + (f_b/\lambda_b^*)] \bar{Q}_I \quad (33)$$

Based on Equations (14) and (18),

$$\bar{Q}_I = 20 F \lambda_A \lambda_B A_k(o) / (s + \lambda_A^*) (s + \lambda_B^*) (s + \lambda_C^*) \quad (34)$$

Substituting Equation (34) in Equation (33), and taking the inverse Laplace transform,

$$Q_{NP}(t) = K_1 A_k(o) \left[ \frac{\exp(-\lambda_A^* t)}{(\lambda_B^* - \lambda_A^*)(\lambda_C^* - \lambda_A^*)} + \frac{\exp(-\lambda_B^* t)}{(\lambda_A^* - \lambda_B^*)(\lambda_C^* - \lambda_B^*)} + \frac{\exp(-\lambda_C^* t)}{(\lambda_A^* - \lambda_C^*)(\lambda_B^* - \lambda_C^*)} \right] \quad (35)$$

where:  $K_1 = 20 F \lambda_A \lambda_b d_3 (f_a/\lambda_a^*) + (f_b/\lambda_b^*)$  .

The integration indicated by Equation (29) yields

$$D_{NP}(t) = R_{NP} K_1 A_k(o) [(X_1/\lambda_A^*)(1-\exp(-\lambda_A^* t)) + (X_2/\lambda_B^*)(1-\exp(-\lambda_B^* t)) + (X_3/\lambda_C^*)(1-\exp(-\lambda_C^* t))] \quad (36)$$

where:

$$X_1 = 1/(\lambda_B^* - \lambda_A^*)(\lambda_C^* - \lambda_A^*) ,$$

$$X_2 = 1/(\lambda_A^* - \lambda_B^*)(\lambda_C^* - \lambda_B^*) ,$$

and

$$X_3 = 1/(\lambda_A^* - \lambda_B^*)(\lambda_B^* - \lambda_C^*) .$$

**Tracheobronchial Region.** As shown in Figure G-4, part of the dose to TB is due to materials initially deposited in TB and part is due to materials initially deposited in  $P_f$  and  $P_g$  and then cleared to the G.I. tract by way of the TB region. The time required for this material to pass through TB is assumed to be 1/24 day. <sup>(G-10)</sup> Note in Table G-2 that, for Class D compounds,  $f_f = f_g = 0$ .

$$dQ_{TB}/dt = [(f_c d_4/\lambda_c^*) + (f_d d_4/\lambda_d^*) + (\lambda_f f_f d_5/24 \lambda_f^*)] Q_I(t) + \lambda_g Q_g(t)/24 \quad (37)$$

where:

$$dQ_g/dt = f_g d_5 Q_I(t) - \lambda_g^* Q_g \quad (38)$$

$$\bar{Q}_{TB} = k_2 \bar{Q}_I + \lambda_g \bar{Q}_g/24 \quad (39)$$

$$k_2 = (f_c d_4/\lambda_c^*) + (f_d d_4/\lambda_d^*) + (\lambda_f f_f d_5/24 \lambda_f^*) \quad (40)$$

$$\bar{Q}_g = k_3 \bar{Q}_I / (s + \lambda_g)$$

$$\bar{Q}_{TB} = k_2 \bar{Q}_I + (k_3 \lambda_g/24) \bar{Q}_I / (s + \lambda_g^*)$$

$$k_3 = f_g d_5$$

Combining terms and changing the definition of  $\bar{Q}_I$ ,

$$\bar{Q}_{TB} = K_2 \bar{Q}_I + K_3 \bar{Q}_I / (s + \lambda_g^*) \quad (41)$$

where:  $K_2 = 20 F \lambda_A \lambda_B [(f_c d_4 / \lambda_c^*) + (f_d d_4 / \lambda_d^*) + (\lambda_f f_f d_5 / 24 \lambda_f^*)]$

$$K_3 = 20 F \lambda_A \lambda_B \lambda_g f_g d_5 / 24$$

and  $\bar{Q}_I = A_k(0) / (s + \lambda_A^*) (s + \lambda_B^*) (s + \lambda_C^*) \quad (42)$

(The only difference between Equation (42) and Equation (34) is that the constant factors of  $\bar{Q}_I$   $20F \lambda_A \lambda_B$ , have been transferred to the coefficients  $K_2$  and  $K_3$ . Note, following Equation (35) that  $K_1$  is of the same form as  $K_2$  and  $K_3$ .) Substituting  $\bar{Q}_I$  (as defined above) in Equation (41),

$$\bar{Q}_{TB} = A_k(0) \frac{K_2}{(s + \lambda_A^*) (s + \lambda_B^*) (s + \lambda_C^*)} + \frac{K_3}{(s + \lambda_A^*) (s + \lambda_B^*) (s + \lambda_C^*) (s + \lambda_g^*)} \quad (43)$$

(N.B. The Laplace transform equations for the pulmonary region and the gastrointestinal tract will have the same form as Equation (43). The corresponding equations for  $Q_{TB}$ ,  $D_{TB}$ ,  $Q_P$ ,  $D_P$ ,  $Q_G$  and  $D_G$  will also have the same general form.)

Taking the inverse Laplace transform of Equation (43), a process based on the Heaviside Expansion Theorem<sup>(G-12)</sup> but not collecting terms\*, the equations for  $Q_{TB}(t)$  and  $D_{TB}(t)$  are:

\* By not collecting terms, coefficients already calculated ( $X_1$ ,  $X_2$ , etc.) can be used again. Also note that since

the coefficients ( $X_1$ ,  $X_2, \dots, X_n$ ) are independent of radioactive decay rates. Equations (44) and (45) could be reduced, by collecting terms, to a more concise form, but the less concise form makes it easier to separate the parameters which vary with respect to translocation class, particle size (AMAD), and latitude.

$$\begin{aligned} \bar{Q}_{TB}(t) = A_k(o) \{ & K_2 [\chi_1 \exp(-\lambda_A^* t) + \chi_2 \exp(-\lambda_B^* t) + \chi_3 \exp(-\lambda_C^* t)] \\ & + K_3 [\chi_4 \exp(-\lambda_A^* t) + \chi_5 \exp(-\lambda_B^* t) + \chi_6 \exp(-\lambda_C^* t) + \chi_7 \exp(-\lambda_g^* t)] \} \end{aligned} \quad (44)$$

$$\begin{aligned} D_{TB}(t) = R_{TB} A_k(o) \{ & K_2 [(\chi_1/\lambda_A^*)(1-\exp(-\lambda_A^* t)) \\ & + (\chi_2/\lambda_B^*)(1-\exp(-\lambda_B^* t)) + (\chi_3/\lambda_C^*)(1-\exp(-\lambda_C^* t)) \\ & + K_3 [(\chi_4/\lambda_A^*)(1-\exp(-\lambda_A^* t)) + (\chi_5/\lambda_B^*)(1-\exp(-\lambda_B^* t)) \\ & + (\chi_6/\lambda_C^*)(1-\exp(-\lambda_C^* t)) + (\chi_7/\lambda_g^*)(1-\exp(-\lambda_g^* t))] \} \end{aligned} \quad (45)$$

where:

$$\begin{aligned} \chi_4 &= \chi_1/(\lambda_g^* - \lambda_A^*) \\ \chi_5 &= \chi_2/(\lambda_g^* - \lambda_B^*) \\ \chi_6 &= \chi_3/(\lambda_g^* - \lambda_C^*) \\ \chi_7 &= 1/(\lambda_A^* - \lambda_g^*)(\lambda_B^* - \lambda_g^*)(\lambda_C^* - \lambda_g^*) . \end{aligned}$$

**Pulmonary Region.** Following the procedure already demonstrated for the NP and TB regions, and noting that  $T_e = T_g = T_h$ , the Laplace transform equation for pulmonary burden is

$$\bar{Q}_p = (f_f d_5 / \lambda_f^*) \bar{Q}_I + (f_e + f_g + f_h) d_5 \bar{Q}_I / (s + \lambda_g^*) \quad (46)$$

Substituting Equation (43) in Equation (46) gives

$$\bar{Q}_p = A_k(o) \left\{ \frac{K_4}{(s + \lambda_A^*)(s + \lambda_B^*)(s + \lambda_C^*)} + \frac{K_5}{(s + \lambda_A^*)(s + \lambda_B^*)(s + \lambda_C^*)(s + \lambda_g^*)} \right\} , \quad (47)$$

where:  $K_4 = 20 F \lambda_A \lambda_B f_f d_5 / \lambda_f^*$  ,



$$\text{and } K_5 = 20 F \lambda_A \lambda_B (f_e + f_g + f_h) d_5 .$$

Comparing Equations (43) and (47), it is obvious that the equations for  $Q_p(t)$  and  $D_p(t)$  will have the same form as those for  $Q_{TB}(t)$  and  $D_{TB}(t)$ . The only changes required are to substitute  $K_4$  for  $K_2$ ,  $K_5$  for  $K_3$ , and  $R_p$  for  $R_{TB}$  in Equations (39) and (40).

**Lymph.** Figure G-4 and Table G-2 show the thoracic lymph system as two subcompartments L(i) and L(R) for Class Y compounds and as a single compartment for Class D and Class W compounds. The table of recommended clearance parameter values in ICRP (1972) showed  $T_h = T_i$  for Class D and Class W compounds. The values recommended for  $T_i$  in Table G-2 were slightly altered in order to avoid the special treatment required when  $T_h = T_i$  and to make the following equations applicable to all three translocation classes.

$$Q_L(t) = Q_{L(i)}(t) + Q_{L(R)}(t) \quad (48)$$

$$dQ_{L(i)}/dt = f_i \lambda_h Q_h - \lambda_i^* Q_{L(i)} \quad (49)$$

$$dQ_{L(R)}/dt = (1-f_i) \lambda_h Q_h - \lambda_r Q_{L(R)} \quad (50)$$

$$\bar{Q}_{L(i)} = f_i \lambda_h \bar{Q}_h / (s + \lambda_i^*) \quad (51)$$

$$\bar{Q}_{L(R)} = (1-f_i) \lambda_h \bar{Q}_h / (s + \lambda_r) \quad (52)$$

$$dQ_h/dt = f_h d_5 Q_I(t) - \lambda_h^* Q_h \quad (53)$$

$$\bar{Q}_h = f_h d_5 \bar{Q}_5 / (s + \lambda_h^*) \quad (54)$$

$$\bar{Q}_L = \frac{f_i \lambda_h f_h d_5 \bar{Q}_I}{(s + \lambda_h^*)(s + \lambda_i^*)} + \frac{(1-f_i) \lambda_h f_h d_5 \bar{Q}_I}{(s + \lambda_h^*)(s + \lambda_r)} \quad (55)$$

$$\bar{Q} = A(o) \left\{ \frac{K_6}{(s+\lambda_A^*)(s+\lambda_B^*)(s+\lambda_C^*)(s+\lambda_h^*)(s+\lambda_i^*)} + \frac{K_7}{(s+\lambda_A^*)(s+\lambda_B^*)(s+\lambda_C^*)(s+\lambda_h^*)(s+\lambda_r)} \right\}, \quad (56)$$

where:

$$K_6 = 20 F \lambda_A \lambda_B f_i \lambda_h f_h d_5,$$

and

$$K_7 = 20 F \lambda_A \lambda_B (1-f_i) \lambda_h f_h d_5 ; K_7 = 0 \text{ when } f_i = 1,$$

$$\begin{aligned} Q_L(t) = A_k(o) \{ & K_6 [X_8 \exp(-\lambda_A^* t) + X_9 \exp(-\lambda_B^* t) + X_{10} \exp(-\lambda_C^* t) \\ & + X_{11} \exp(-\lambda_h^* t) + X_{12} \exp(-\lambda_i^* t)] + K_7 [X_{13} \exp(-\lambda_A^* t) \\ & + X_{14} \exp(-\lambda_B^* t) + X_{15} \exp(-\lambda_C^* t) + X_{16} \exp(-\lambda_h^* t) \\ & + X_{17} \exp(-\lambda_r t)] \} \end{aligned} \quad (57)$$

$$\begin{aligned}
D_L(t) = R_L A_k(o) \{ & K_6[(X_8/\lambda_A^*)(1-\exp(-\lambda_A^*t)) + (X_9/\lambda_B^*)(1-\exp(-\lambda_B^*t))] \\
& + (X_{10}/\lambda_C^*)(1-\exp(-\lambda_C^*t)) + (X_{11}/\lambda_H^*)(1-\exp(-\lambda_H^*t)) \\
& + (X_{12}/\lambda_I^*)(1-\exp(-\lambda_I^*t)) + K_7[(X_{13}/\lambda_A^*)(1-\exp(-\lambda_A^*t)) \\
& + (X_{14}/\lambda_B^*)(1-\exp(-\lambda_B^*t)) + (X_{15}/\lambda_C^*)(1-\exp(-\lambda_C^*t)) \\
& + (X_{16}/\lambda_H^*)(1-\exp(-\lambda_H^*t)) + (X_{17}/\lambda_r)(1-\exp(-\lambda_r t))] \} , \quad (58)
\end{aligned}$$

where:

$$\begin{aligned}
X_8 &= X_4/(\lambda_i^* - \lambda_A^*) \quad , \quad X_9 = X_5/(\lambda_i^* - \lambda_B^*) \quad , \\
X_{10} &= X_6/(\lambda_i^* - \lambda_C^*) \quad , \quad X_{11} = X_7/(\lambda_i^* - \lambda_H^*) \quad , \\
X_{12} &= 1/(\lambda_A^* - \lambda_i^*)(\lambda_B^* - \lambda_i^*)(\lambda_C^* - \lambda_i^*)(\lambda_H^* - \lambda_i^*) \quad , \\
X_{13} &= X_4/(\lambda_r - \lambda_A^*) \quad , \quad X_{14} = X_5/(\lambda_r - \lambda_B^*) \quad , \\
X_{15} &= X_6/(\lambda_r - \lambda_C^*) \quad , \quad X_{16} = X_7/(\lambda_r - \lambda_H^*) \quad ,
\end{aligned}$$

and

$$X_{17} = 1/(\lambda_A^* - \lambda_r)(\lambda_B^* - \lambda_r)(\lambda_C^* - \lambda_r)(\lambda_H^* - \lambda_r) \quad .$$

**Gastrointestinal Tract.** The large intestine is assumed to be the critical organ of the G.I. tract. Based on Table II of Reference G-5, the contents of the large intestine weigh 150 g, and the average residence time is 18 hr = 0.75 day. The dose to the large intestine is assumed to be one-half the dose to its contents.

Based on Figure G-4 and the procedures described earlier, the Laplace transform equation for the amount of radionuclide ( $\bar{\mu}$  Ci) in the G.I. tract is:

$$\bar{Q}_G = K_8 \bar{Q}_I + K_9 \bar{Q}_I / (s + \lambda_g^*) \quad , \quad (59)$$

where:

$$K_8 = 20 F \lambda_A \lambda_B 0.75 (f_b d_3 + f_d d_4 + \lambda_f f_f d_s / \lambda_f^*)$$

and

$$K_g = 20 F \lambda_A \lambda_B 0.75 \lambda_g f_g d_5 .$$

To obtain the equation for  $Q_G(t)$ , substitute Equation (42) in Equation (59) and take the inverse Laplace transform of the result, using the procedure described for the tracheobronchial region. To obtain the equation for  $D_G(t)$ , multiply the integral of  $Q_G(t)$  by  $R_G$ . Note that  $R_G = (3/4 \times 1/2 \times 51.216/150) E_G$ , where  $E_G$  is the energy deposited by radionuclide  $r$  (MeV/dis) to the contents of the large intestine (Table G-4).

**Organs Receiving Radionuclides from Blood.** Organs identified (Figure G-4, Table G-4) by the subscript  $N$  ( $N$  = bone, liver, kidney, thyroid, ..., total body), receive inhaled radionuclides from the blood. The general equation for all these organs is

$$dQ_N/dt = f_{2N}' b - \lambda_N^* Q_N \quad (60)$$

$$\bar{Q}_N = f_{2N}' \bar{b} / (s + \lambda_N^*) \quad (61)$$

where:

$b$  is the rate at which radionuclide  $r$  enters blood from various parts of the respiratory system (NP, TB, P, and L(i)) and from the G.I. tract (Figure G-4).

and

$f_{2N}'$  is the fraction transferred from blood to organ  $N$  (Table G-4).

The rates of transfer from the G.I. tract to blood and from blood to organ  $N$  are "very fast" and assumed to be "instantaneous".

Based on Figure G-4, the general equation for  $b$  is

$$b = \lambda_a Q_a + \lambda_c Q_c + \lambda_e Q_e + f_1 (\lambda_b Q_b + \lambda_d Q_d + \lambda_f Q_f + \lambda_g Q_g) + \lambda_i Q_i \quad (62)$$

Separating the pathways for which  $T_j \leq 1.0$  day from those for which  $T_j > 1.0$  day, and noting that  $T_e = T_g = T_h$ :

$$b = kQ_I + \lambda_e Q_e + \lambda_g Q_g + \lambda_i Q_i \quad (63)$$

$$\bar{b} = k_{10} \bar{Q}_I + \lambda_e \bar{Q}_e + \lambda_g \bar{Q}_g + \lambda_i \bar{Q}_i \quad (64)$$

where:

$$k_{10} = 20 F \lambda_A \lambda_B \left\{ (\lambda_a f_a d_3 / \lambda_a^*) + (\lambda_c f_c d_4 / \lambda_c^*) + f_1 [(\lambda_b f_b d_3 / \lambda_b^*) + (\lambda_d f_d d_4 / \lambda_d^*) + (\lambda_f f_f d_5 / \lambda_f^*)] \right\} \quad (65)$$

(If  $T_r \gg T_j$ ,  $\lambda_j / \lambda_j^* \cong 1.0$ . The largest value of  $T_j$  in Equation (65), Table G-2, is 1.0 day, and the smallest value of  $T_r$ , Table G-4, is 32 days ( $^{141}\text{Ce}$ ). The smallest value of  $\lambda_j / \lambda_j^*$  is therefore 0.97 and the next smaller (for  $T_j = 0.4$ ) is 0.99. The error due to ignoring the  $\lambda_j / \lambda_j^*$  factors in Equation (65) is negligible for long-lived radionuclides, no more than 1% for  $T_r \geq 100$  days.)

Continuing, now, with the analysis of Equation (64),

$$dQ_e/dt = f_e d_5 - \lambda_e^* Q_e, \quad \bar{Q}_e = f_e d_5 / (s + \lambda_e^*) \quad (66)$$

$$dQ_g/dt = f_1 f_g d_5 - \lambda_g^* Q_g, \quad \bar{Q}_g = f_1 f_g d_5 / (s + \lambda_g^*) \quad (67)$$

Since  $T_e = T_g = T_h$ , Equations (66) and (68) can be combined as follows:

$$\bar{Q}_{eg} = (f_e + f_1 f_g) d_5 \bar{Q}_I / (s + \lambda_h^*) \quad (68)$$

$$dQ_i/dt = f_i \lambda_h Q_h - \lambda_i^* Q_i; \quad \bar{Q}_i = f_i \lambda_h \bar{Q}_h / (s + \lambda_i^*)$$

$$dQ_h/dt = f_h d_5 Q_I - \lambda_h^* Q_h; \quad \bar{Q}_h = f_h d_5 \bar{Q}_I / (s + \lambda_h^*) \quad (69)$$

Substituting Equation (69) in Equation (68),

$$Q_i = f_i \lambda_h f_h d_5 Q_I / (s + \lambda_h^*) (s + \lambda_i^*) \quad (70)$$

Equation (70) and Equation (68) → Equation (64),

$$\bar{b} = K_{10} \bar{Q}_I + \frac{K_{11} \bar{Q}_I}{(s + \lambda_h^*)} + \frac{K_{12} \bar{Q}_I}{(s + \lambda_h^*) (s + \lambda_i^*)} \quad (71)$$

Equation (71) → Equation (61),

$$\bar{Q}_N = f'_{2N} \left[ \frac{K_{10} \bar{Q}_I}{(s + \lambda_N^*)} + \frac{K_{11} \bar{Q}_I}{(s + \lambda_N^*) (s + \lambda_h^*)} + \frac{K_{12} \bar{Q}_I}{(s + \lambda_N^*) (s + \lambda_h^*) (s + \lambda_i^*)} \right] \quad (72)$$

Equation (43) → Equation (72),

$$\begin{aligned} \bar{Q}_N = f'_{2N} A_k(o) & \left[ \frac{K_{10}}{(s + \lambda_A^*) (s + \lambda_B^*) (s + \lambda_C^*) (s + \lambda_N^*)} \right. \\ & + \frac{K_{11}}{(s + \lambda_A^*) (s + \lambda_B^*) (s + \lambda_C^*) (s + \lambda_N^*) (s + \lambda_h^*)} \\ & \left. + \frac{K_{12}}{(s + \lambda_A^*) (s + \lambda_B^*) (s + \lambda_C^*) (s + \lambda_N^*) (s + \lambda_h^*) (s + \lambda_i^*)} \right] \quad (73) \end{aligned}$$

where:

$K_{10}$  is defined by Equation (65)

$$K_{11} = 20 F \lambda_A \lambda_B \lambda_h (f_e + f_1 f_g) d_5$$

and

$$K_{12} = 20 F \lambda_A \lambda_B \lambda_i f_i \lambda_h f_h d_5$$

Based on the Heaviside Expansion Theorem<sup>(G-12)</sup> and not collecting terms (in order to simplify the calculation of coefficients),

$$\begin{aligned}
 Q_N(t) = f'_{2N} A_k(0) \{ & K_{10} [X_{18} \exp(-\lambda_A^* t) + X_{19} \exp(-\lambda_B^* t) + X_{20} \exp(-\lambda_C^* t) \\
 & + X_{21} \exp(-\lambda_N^* t)] + K_{11} [X_{22} \exp(-\lambda_A^* t) + X_{23} \exp(-\lambda_B^* t) \\
 & + X_{24} \exp(-\lambda_C^* t) + X_{25} \exp(-\lambda_N^* t) + X_{26} \exp(-\lambda_h^* t)] \\
 & + K_{12} [X_{27} \exp(-\lambda_A^* t) + X_{28} \exp(-\lambda_B^* t) + X_{29} \exp(-\lambda_C^* t) \\
 & + X_{30} \exp(-\lambda_N^* t) + X_{31} \exp(-\lambda_h^* t) + X_{32} \exp(-\lambda_i^* t)] \} , \quad (74)
 \end{aligned}$$

$$\begin{aligned}
 D_N(t) = R_N f'_{2N} A_R(0) \{ & K_{10} [X_{18}/\lambda_A^* (1-\exp(-\lambda_A^* t)) + (X_{19}/\lambda_B^*) \\
 & \times (1-\exp(-\lambda_B^* t)) + (X_{20}/\lambda_C^*) (1-\exp(-\lambda_C^* t)) \\
 & + (X_{21}/\lambda_N^*) (1-\exp(-\lambda_N^* t))] + K_{11} [(X_{22}/\lambda_A^*) (1-\exp(-\lambda_A^* t)) \\
 & + (X_{23}/\lambda_B^*) (1-\exp(-\lambda_B^* t)) + (X_{24}/\lambda_C^*) (1-\exp(-\lambda_C^* t)) \\
 & + (X_{25}/\lambda_N^*) (1-\exp(-\lambda_N^* t)) + (X_{26}/\lambda_h^*) (1-\exp(-\lambda_h^* t))] \\
 & + K_{12} [(X_{27}/\lambda_A^*) (1-\exp(-\lambda_A^* t)) + (X_{28}/\lambda_B^*) (1-\exp(-\lambda_B^* t)) \\
 & + (X_{29}/\lambda_C^*) (1-\exp(-\lambda_C^* t)) + (X_{30}/\lambda_N^*) (1-\exp(-\lambda_N^* t)) \\
 & + (X_{31}/\lambda_h^*) (1-\exp(-\lambda_h^* t)) + (X_{32}/\lambda_i^*) (1-\exp(-\lambda_i^* t))] \} , \quad (75)
 \end{aligned}$$





References

- G-1. Krey, P. W., and Krajewski, B., "Comparison of Atmospheric Transport Model with Observations of Radioactive Debris", *Journal of Geophysics Res.*, 75(15) (1970).
- G-2. Krey, P. W., and Krajewski, B., "HASL Model of Atmospheric Transport", U.S. Atomic Energy Commission Report, HASL-25 (1969).
- G-3. "Task Group on Lung Dynamics for Committee II of the International Commission on Radiological Protection", *Health Physics*, 12, 173 (1966).
- G-4. "The Metabolism of Compounds of Plutonium and Other Actinides", International Commission on Radiological Protection, ICRP Publication Number 19, Pergamon Press (1972).
- G-5. "Recommendations of the International Commission on Radiological Protection: Report of Committee II on Permissible Dose for Internal Radiation", International Commission on Radiological Protection, ICRP Publication Number 2, Pergamon Press (1959); *Health Physics* (June, 1960).
- G-6. "Recommendations of the International Commission on Radiological Protection" (As amended 1959 and revised 1962), International Commission on Radiological Protection, ICRP Publication Number 6, Pergamon Press (1964).
- G-7. Houston, J. R., Strenge, D. L., and Watson, E. C., "DACRIN - A Computer Program for Calculating Organ Dose from Acute or Chronic Radionuclide Inhalation", BNWL-B-389, UC-41, Battelle-Northwest Laboratories, Richland, Washington (December 1974).
- G-8. Kotrappa, P., "Dose to Respiratory Tract from Continuous Inhalation of Radioactive Aerosol", U.S. AEC Rpt. UR-43-964 (1968).
- G-9. Kotrappa, P., "Calculation of the Burden and Dose to the Respiratory Tract from Continuous Inhalation of Radioactive Aerosol", *Health Physics*, 17 (1969).
- G-10. Snyder, W. S., "The Use of the Lung Model for Estimation of Dose", U.S. AEC Rpt. CONF-66108 (1967).
- G-11. Bloom, S. G., "Computer Model for the Mathematical Simulation of the Environmental Transport of Plutonium", Battelle-Columbus Laboratories, Columbus, Ohio, Report to U.S. EPA (1975).
- G-12. Abramowitz, M., and Stegun, I. A., Handbook of Mathematical Functions, National Bureau of Standards - Applied Math. Series 55, USGPO, Washington, D.C. (1964).